NATIONAL AERONAUTICS AND SPACE ADMINISTRATION

Technical Report 32-1526

Volume VIII

The Deep Space Network

Progress Report
For January and February 1972

JET PROPULSION LABORATORY
CALIFORNIA INSTITUTE OF TECHNOLOGY
PASADENA, CALIFORNIA

April 15, 1972

NATIONAL AERONAUTICS AND SPACE ADMINISTRATION

Technical Report 32-1526

Volume VIII

The Deep Space Network

Progress Report
For January and February 1972

JET PROPULSION LABORATORY
CALIFORNIA INSTITUTE OF TECHNOLOGY
PASADENA, CALIFORNIA

April 15, 1972

Preface

This report series presents progress on DSN supporting research and technology, advanced development and engineering, implementation, and operations which pertain to mission-independent or multiple-mission development as well as to support of flight projects. Each issue presents material in some, but not all, of the following categories in the order indicated.

Description of the DSN

Mission Support
- Interplanetary Flight Projects
- Planetary Flight Projects
- Manned Space Flight Project
- Advanced Flight Projects

Radio Science

Advanced Engineering
- Tracking and Navigational Accuracy Analysis
- Communications Systems Research
- Communications Elements Research
- Supporting Research and Technology

Development and Implementation
- Space Flight Operations Facility Development
- Ground Communications Facility Development
- Deep Space Instrumentation Facility Development
- DSN Projects and Systems Development

Operations and Facilities
- DSN Operations
- Space Flight Operations Facility Operations
- Ground Communications Facility Operations
- Deep Space Instrumentation Facility Operations
- Facility Engineering

In each issue, the part entitled "Description of the DSN" describes the functions and facilities of the DSN and may report the current configuration of one of the six DSN systems (tracking, telemetry, command, monitoring, simulation, and operations control).

The work described in this report series is either performed or managed by the Tracking and Data Acquisition organization of JPL for NASA.

Contents

Contents (contd)

Communications Elements Research

Supporting Research and Technology

DEVELOPMENT AND IMPLEMENTATION

DSIF Development

DSN Projects and Systems Development

Contents (contd)

OPERATIONS AND FACILITIES

DSN Operations

DSIF Operations

DSN Functions and Facilities

N. A. Renzetti
Mission Support Office

The objectives, functions, and organization of the Deep Space Network are summarized. The Deep Space Instrumentation Facility, the Ground Communications Facility, and the Space Flight Operations Facility are described.

The Deep Space Network (DSN), established by the NASA Office of Tracking and Data Acquisition under the system management and technical direction of JPL, is designed for two-way communications with unmanned spacecraft traveling approximately 16,000 km (10,000 mi) from Earth to planetary distances. It supports, or has supported, the following NASA deep space exploration projects: *Ranger, Surveyor, Mariner* Venus 1962, *Mariner* Mars 1964, *Mariner* Venus 67, *Mariner* Mars 1969, *Mariner* Mars 1971 (JPL); *Lunar Orbiter* and *Viking* (Langley Research Center); *Pioneer* (Ames Research Center); *Helios* (West Germany); and *Apollo* (Manned Spacecraft Center), to supplement the Manned Space Flight Network (MSFN).

The Deep Space Network is one of two NASA networks. The other, known as the Space Flight Tracking and Data Network, is under the system management and technical direction of the Goddard Space Flight Center. Its function is to support manned and unmanned Earth-orbiting and lunar scientific and communications satellites. Although the DSN was concerned with unmanned lunar spacecraft in its early years, its primary objective now and into the future is to continue its support of planetary and interplanetary flight projects. It has been a development objective that the network capability be kept at the state of the art of telecommunications and data handling and that it support as many flight projects as possible with a minimum of mission-dependent hardware and software. It provides direct support of each project through that project's tracking and data system. This management element, in concert with the telecommunications and mission operations personnel of the project, is responsible for the design and operation of the hardware and software which are required for the conduct of flight operation. The organization and procedures necessary to carry out these activities are described in Ref. 1.

The DSN function, in supporting a flight project by tracking the spacecraft, is characterized by six DSN systems:

(1) DSN Tracking System. Generates radio-metric data; i.e., angles, one- and two-way doppler and range.

(2) DSN Telemetry System. Receives, records, and retransmits engineering and scientific data generated in the spacecraft.

(3) DSN Command System. Sends coded signals to the spacecraft in order to initiate spacecraft functions in flight.

(4) DSN Monitor System. Instruments, transmits, records, and displays those parameters of the DSN that measure its performance.

(5) DSN Simulation System. Provides computer-based facilities in order to test and train network functions and assist the flight project in carrying out similar functions for its Mission Operations System.

(6) DSN Operations Control. Provides the hardware and software personnel, real-time and non-real-time operational direction of the network, and primary interface with the flight projects Mission Operations personnel.

The facilities needed to carry out these functions have evolved in three technical areas: (1) the deep space stations and the telecommunications interface through the RF link with the spacecraft is known as the Deep Space Instrumentation Facility (DSIF); (2) the Earth-based point-to-point voice and data communications from the stations to the control center is known as the Ground Communications Facility (GCF); (3) the control center, both for network control function and mission control support, is known as the Space Flight Operations Facility (SFOF).

I. Deep Space Instrumentation Facility

A. Tracking and Data Acquisition Facilities

A world-wide set of deep space stations (DSSs) with large antennas, low-noise phase-lock receiving systems, and high-power transmitters provide radio communications with spacecraft. The DSSs and the deep space communications complexes (DSCCs) they comprise are given in Table 1.

Radio contact with a spacecraft usually begins when the spacecraft is on the launch vehicle at Cape Kennedy, and it is maintained throughout the mission. The early part of the trajectory is covered by selected network stations of the Air Force Eastern Test Range (AFETR) and the MSFN of the Goddard Space Flight Center,[1] Normally, two-way communications are established between the spacecraft and the DSN within 30 min after the spacecraft has been injected into lunar, planetary, or interplanetary flight. A compatibility test station at Cape Kennedy (discussed later) monitors the spacecraft continuously during the launch phase until it passes over the local horizon. The deep space phase begins with acquisition by either DSS 51, 41, or 42. These and the remaining DSSs given in Table 1 provide radio communications to the end of the flight.

To enable continuous radio contact with spacecraft, the DSSs are located approximately 120 deg apart in longitude; thus, a spacecraft in deep space flight is always within the field-of-view of at least one DSS, and for several hours each day may be seen by two DSSs. Furthermore, since most spacecraft on deep space missions travel within 30 deg of the equatorial plane, the DSSs are located within latitudes of 45 deg north or south of the equator. All DSSs operate at S-band frequencies: 2110–2120 MHz for Earth-to-spacecraft transmission and 2290–2300 MHz for spacecraft-to-Earth transmission.

To provide sufficient tracking capability to enable useful data returns from around the planets and from the edge of the solar system, a 64-m (210-ft) diam antenna network will be required. Two additional 64-m (210-ft) diam antenna DSSs are under construction at Madrid and Canberra, which will operate in conjunction with DSS 14 to provide this capability. These stations are scheduled to be operational by the middle of 1973.

B. Compatibility Test Facilities

In 1959, a mobile L-band compatibility test station was established at Cape Kennedy to verify flight–spacecraft–DSN compatibility prior to the launch of the *Ranger* and *Mariner* Venus 1962 spacecraft. Experience revealed the need for a permanent facility at Cape Kennedy for this function. An S-band compatibility test station with a 1.2-m (4-ft) diam antenna became operational in 1965. In addition to supporting the preflight compatibility tests, this station monitors the spacecraft continuously during the launch phase until it passes over the local horizon.

Spacecraft telecommunications compatibility in the design and prototype development phases was formerly verified by tests at the Goldstone DSCC. To provide a more economical means for conducting such work and because of the increasing use of multiple-mission telemetry and command equipment by the DSN, a compatibility test area (CTA) was established at JPL in 1968. In all essential characteristics, the configuration of this facility is identical to that of the 26-m (85-ft) and 64-m (210-ft) diam antenna stations.

The JPL CTA is used during spacecraft system tests to establish the compatibility with the DSN of the proof test

[1]The 9-m (30-ft) diam antenna station established by the DSN on Ascension Island during 1965 to act in conjunction with the MSFN orbital support 9-m (30-ft) diam antenna station was transferred to the MSFN in July 1968.

model and development models of spacecraft, and the Cape Kennedy compatibility test station is used for final flight spacecraft compatibility validation testing prior to launch.

II. Ground Communications Facility

The GCF provides voice, high-speed data, wideband data, and teletype communications between the SFOF and the DSSs. In providing these capabilities, the GCF uses the facilities of the worldwide NASA Communications Network (NASCOM)[2] for all long distance circuits, except those between the SFOF and the Goldstone DSCC. Communications between the Goldstone DSCC and the SFOF are provided by a microwave link directly leased by the DSN from a common carrier.

Early missions were supported by voice and teletype circuits only, but increased data rates necessitated the use of high-speed circuits for all DSSs, plus wideband circuits for some stations.

[2]Managed and directed by the Goddard Space Flight Center.

III. Space Flight Operations Facility

Network and mission control functions are performed at the SFOF at JPL. The SFOF receives data from all DSSs and processes that information required by the flight project to conduct mission operations. The following functions are carried out: (1) real-time processing and display of radio metric data; (2) real-time and non-real-time processing and display of telemetry data; (3) simulation of flight operations; (4) near-real-time evaluation of DSN performance; (5) operations control, and status and operational data display; and (6) general support such as internal communications by telephone, intercom, public address, closed-circuit TV, documentation, and reproduction of data packages. Master data records of science data received from spacecraft are generated. Technical areas are provided for flight project personnel who analyze spacecraft performance, trajectories, and generation of commands.

Reference

1. *The Deep Space Network*, Space Programs Summary 37-50, Vol. II, pp. 15–17. Jet Propulsion Laboratory, Pasadena, Calif., Mar. 31, 1968.

Table 1. Tracking and data acquisition stations of the DSN

DSCC	Location	DSS	DSS serial designation	Antenna		Year of initial operation
				Diameter, m (ft)	Type of mounting	
Goldstone	California	Pioneer	11	26 (85)	Polar	1958
		Echo	12	26 (85)	Polar	1962
		(Venus)[a]	13	26 (85)	Az-El	1962
		Mars	14	64 (210)	Az-El	1966
—	Australia	Woomera	41	26 (85)	Polar	1960
Tidbinbilla	Australia	Weemala (formerly Tidbinbilla)	42	26 (85)	Polar	1965
		Ballima (formerly Booroomba)	43	64 (210)	Az-El	Under construction
—	South Africa	Johannesburg	51	26 (85)	Polar	1961
Madrid	Spain	Robledo	61	26 (85)	Polar	1965
		Cebreros	62	26 (85)	Polar	1967
		Robledo	63	64 (210)	Az-El	Under construction

[a]A research-and-development facility used to demonstrate the feasibility of new equipment and methods to be integrated into the operational network. Besides the 26-m (85-ft) diam az–el-mounted antenna, DSS 13 has a 9-m (30-ft) diam az–el-mounted antenna that is used for testing the design of new equipment and support of ground-based radio science.

DSN Tracking System: Operation With the Mutual Stations

W. D. Chaney and H. E. Nance
DSN Engineering and Operations Section

Two types of 26-m tracking stations are available to the Deep Space Network (DSN) for spacecraft tracking. Pioneer F will be supported primarily by the Mutual stations. This article describes in some detail the various functions performed by the Mutual station tracking system and compares its equipments and functions with those of the standard DSN tracking station. The operational capabilities and interfaces between the modules within the station are presented in the logical sequence, with the final output interfacing with the Ground Communications Facility and the Space Flight Operations Facility.

I. Introduction

The primary function of the DSN Tracking System is to provide precision radio-metric data to be used for the determination of the orbit of a spacecraft in deep space. Radio-metric data includes angle data, range data, and doppler data with associated status information, time, frequencies, data condition, and calibration data generated by the tracking station. The tracking system also provides tracking predictions (observables) for use in acquiring the spacecraft radio-frequency signal and for system data validation.

Two types of 26-m stations are available within the DSN for the acquisition of radio-metric data: the standard DSN station and the Mutual station (combined DSN and STDN equipment). The Mutual stations are DSSs 11, 42, and 61 and are committed to the support of the *Pioneer F* Mission and *Apollo* Missions. This article discusses the Mutual stations only.

II. Mutual Station Configuration

The tracking system at the Mutual stations is shown schematically in Fig. 1. As information, this configuration differs from the standard 26-m DSN station in that the STDN TDP (tracking data processor) replaces the DSN TDH (tracking and data handling subsystem) and the STDN APP (antenna position programmer) is added.

III. Radio-Metric Data

The TDP (tracking data processor), in conjunction with the APS (antenna-pointing subsystem), provides the Mutual station with the capability of transmitting radio-metric data to the SFOF via high-speed data lines (HSDL) or teletype circuits.

The high-speed data (HSD) is sent in a 1200-bit block, of which 1044 bits are available for data, with 156 bits being used for sync code, routing information, accounting

data, time tagging, and error detection. The sample rate of the data acquired is variable from 1/s to 1/60 s and a HSD block is transmitted when five samples are accumulated in the block. The rate of transmission of the HSDL is 4800 bits/s, requiring only one fourth of a second for transmission of the radio-metric data block. The rate of HSD block transmission is dependent on the sample rate of the data and varies from 1/5 s for 1-s data to 1/5 min for 60-s data.

The teletype data is sent directly from the TDP via the normal GCF teletype circuits. The sample rate of the data is likewise variable, being from 1/6 s to 1/10 min as well as a manual rate. There is only one format from the Mutual stations for the teletype data in contrast to the multiple formats available from the standard DSN stations.

A capability is provided for non-real time recovery of the radio-metric data. The HSD recovery is from the DSS original data record (ODR) by retransmission of any requested block or combination of blocks by block serial/sequence number or by the time of original transmission as indicated in the GCF header. The teletype recovery is from paper tape that is punched during data acquisition and requested recovery is by time only.

IV. Equipment Operation and Interfaces

The TDP samples and formats Greenwich Mean Time (GMT), doppler, range, angles, and partial status and outputs the sampled data to the APS for transmission via HSD or directly out to the GCF via teletype.

The APS also receives predictions generated in the SFOF and transmitted via HSDL or TTY to the station. The APS then interpolates these predictions to 1/s, and provides interpolated angles to the APP (antenna position programmer). A paper tape, to serve as a backup drive for the APP is punched on the APS computer high-speed tape punch at the same time. However, this tape only contains time-ordered antenna pointing information for every tenth point generated by the APS, or 1/10 sec. In addition, DSIF tracking system partial status information is transmitted to the DIS (digital instrumentation subsystem) by the APS.

The APP receives the 1/s predicted angular positions from the APS and further interpolates these angles to 50/s; it compares the 50/s predictions with the antenna angle readout and generates an error signal to the antenna servo subsystem. The antenna servo subsystem then drives the antenna to null this error signal, insuring smooth, accurate tracking of the spacecraft.

The DIS receives partial status and error alarms from the TDP for DSS operational control and DSN monitor functions. The DIS also receives predicts via HSDL from the SFOF and outputs page prints of the predicts for station spacecraft acquisition operations.

V. SFOF Operation

The SFOF has many internal operations in connection with the radio-metric data received from the Mutual station; however, only two prime interfaces will be discussed.

The SFOF tracking data input processor, TTY (TYDIP) provides data format identification, decommutation, data conversion, and reformatting. Alarms are generated for bad formats and data out of limits.

The SFOF high-speed data input processor (HYDIP) receives radio-metric data via HSDL and performs block error detection, data decommutation, conversion, and reformatting. Alarms are generated for HSD block transmission errors and data out of limits.

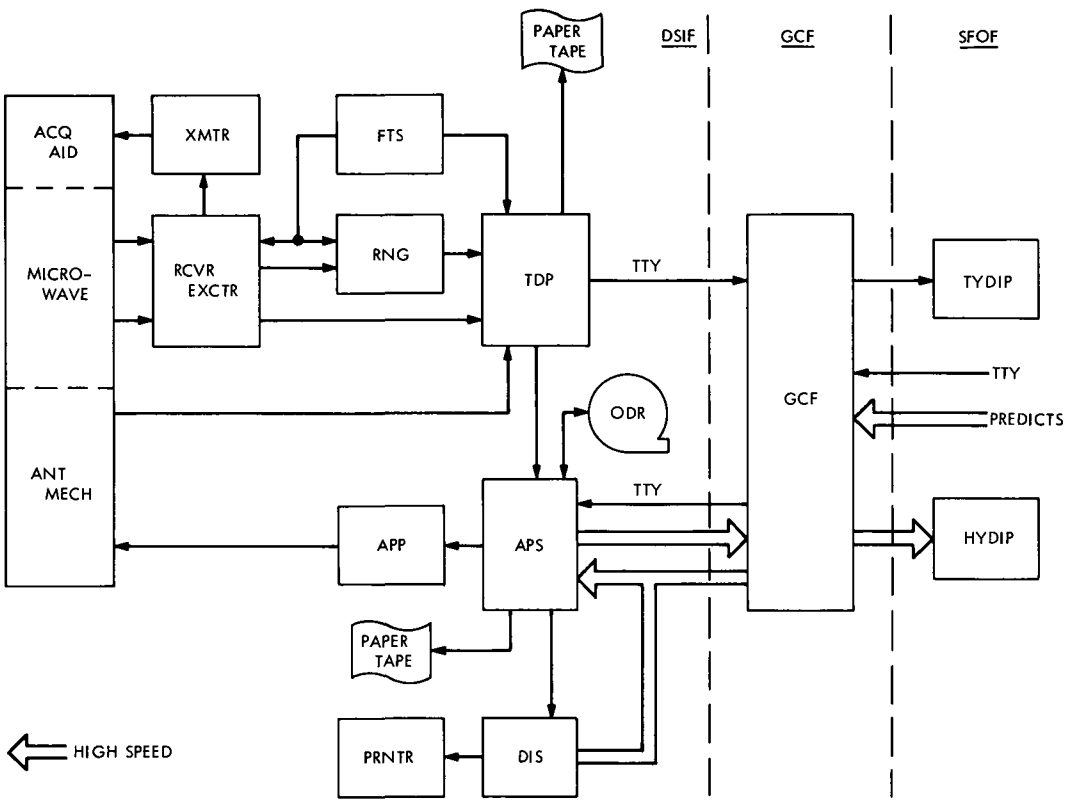

Fig. 1. Mutual station tracking system

Pioneer Mission Support

A. J. Siegmeth
Mission Support Office

The previous reports on the Jupiter-bound Pioneer F and G mission support delineated the mission description and the functional planning activities of the tracking and data system. Beginning with this current report, an account will be given of the actual management organization and engineering planning activities which were essential to assure an effective scientific data return and spacecraft control.

I. Introduction

The actual planning and implementation of the complex Deep Space Network's Mark III system was directed and controlled by a program management structure. After the specific *Pioneer F* and *G* flight support requirements were established, these requirements were merged with the network's standardized multimission "type capabilities" to assure cost-effective capabilities, which were compatible with both the *Pioneer* missions and most of the future NASA planetary and interplanetary missions. Specific management controls were applied to assure that the DSN Mark III system, as planned for *Pioneer F*, was ready for mission support, on time, within the budget, and with technical excellence. The actual management structure and techniques discussed in this report included the establishment of the appropriate level of detail for effective management control of subsystems, systems, network integration, and the optimization of all interfaces.

A description was given on the *Pioneer F* and *G* profiles, spacecraft design, and attitude control with special emphasis on tracking and data acquisition interfaces in Refs. 1–6. The last three reports described the DSN Mark III System and the *Pioneer F* and *G* Near-Earth/Deep Space Phase Support Plan.

II. Management Structure

A. Pioneer Project Management

The management structure of the *Pioneer F* and *G* project is shown in Fig. 1. The NASA Headquarters Office of Space Sciences is responsible for the planetary programs. The *Pioneer* Program Manager heads all *Pioneer* Project related activities. NASA's Ames Research Center (ARC) located at Moffett Field, California, is in charge of all management coordination and control aspects for the *Pioneer* missions. The *Pioneer* Project Office is headed by the *Pioneer* Project Manager who is supported by a Project staff. They assist him in the areas of management control, mission analysis, launch coordination, nuclear power, scientist coordination, contracts, magnetics, reliability, and quality assurance. In addition, seven government-sponsored organizations are supporting the *Pioneer F* and *G* missions with specific services. The Space Nuclear Systems Division of the Atomic Energy Commission controls the development and production of the Radioisotope Thermoelectric Generators (RTGs). Teledyne Isotopes is the prime contractor for these generators. The Experiment System, Spacecraft System, and Mission Operations System are supported by individual teams of the Ames Research Center. The spacecraft contractor was TRW

Systems Group, TRW, Inc. The Bendix Field Engineering Corporation provides the electronic data processing support for the Mission Operations System. The Jet Propulsion Laboratory is the tracking and data acquisition center of the *Pioneer* missions, and it plans, manages, and controls the support during the near-Earth and deep space phases of the missions. The Launch Vehicle System is managed by the Lewis Research Center, and the contractors are the Convair Division of General Dynamics and McDonnell Douglas. The Unmanned Launch Operations of the Kennedy Space Center was supported by the Convair Division of General Dynamics.

B. The Tracking and Data Acquisition Function

1. Definition. The major function of the Tracking and Data Acquisition System (TDS) is the acquisition and transmission of information necessary to determine space vehicle position, velocity and direction, system and subsystem performance, and experiment measurements, all with respect to a common time base.

2. Tracking and Data Acquisition Support Center. In accordance with sections of the NASA Management Instructions (NMI 8430.1) concerning tracking and data acquisition support for unmanned space flight projects, NASA Headquarters has designated JPL as the Tracking and Data Acquisition Support Center for the *Pioneer F* and *G* missions. JPL is responsible for overall achievement of the tracking and data acquisition objectives and functions.

3. Tracking and Data System Manager. As required by NASA Management Instruction 8430.1 the Director of the Tracking and Data Acquisition Support Center (JPL) has designated the Tracking and Data System Manager who shall be responsible for the tracking and data acquisition function, as defined above. Basically, he acts as the interface between the Project and the Tracking and Data System Support Agencies to match requirements with the capabilities of the support agencies to establish a compatible, integrated system of tracking and data acquisition resources. The resulting composite of supporting resources is identified as the "Tracking and Data System."

The TDS Manager reviews the NASA Support Instrumentation Requirements Document (SIRD), which is prepared by the *Pioneer* Project manager and approved by NASA Headquarters, Office of Space Sciences and Office of Tracking and Data Acquisition. It is also the TDS manager's function to identify any inconsistencies and to insure that all requirements are identified with the Department of Defence (DOD) or NASA organizations. He also assures the *Pioneer* Project that the NASA Network Support Plan (NSP) is prepared concurrently with the SIRD. He reviews the NSP and DOD Program Support Plan (PSP) to identify any conflicts, duplications, and possible omissions. He also certifies that all support planning is properly located and complete. The TDS Manager is accountable both to the *Pioneer* Project Manager to which he is assigned and to the assistant laboratory director for Tracking and Data Acquisition at JPL.

C. Tracking and Data System

1. General. The Tracking and Data System is an operationally unified collection of tracking and data acquisition resources. The required resources are provided by organizations under the Department of Defense, Goddard Space Flight Center (GSFC), and the Jet Propulsion Laboratory, herein referred to collectively as the Tracking and Data System Support Agencies. Although support agencies are not under the direct control of the Tracking and Data System manager, they are responsive to his needs through the systems of communication, coordination, and documentation.

2. Tracking and Data System support agencies

a. Department of Defense. Under the Department of Defense, the United States Air Force, Air Force Systems Command, manages the National Ranges: Air Force Eastern Test Range (AFETR) and Air Force Western Test Range (AFWTR). As lead range for the *Pioneer F* and *G* missions, the AFETR arranges for all support required from DOD resources.

b. Goddard Space Flight Center. NASA's Goddard Space Flight Center manages the Spaceflight Tracking and Data Network (STDN) network, and the NASA Communications System (NASCOM). Support required from these NASA resources is arranged through the appropriate organizational elements at GSFC.

c. Jet Propulsion Laboratory. The Jet Propulsion Laboratory is a NASA-owned installation, managed for NASA by the California Institute of Technology. With regard to the tracking and data acquisition function, JPL manages and operates the DSN. Support required from these resources is arranged through the JPL Office of Tracking and Data Acquisition.

3. Tracking and Data System configuration. Following is a general description of the Tracking and Data System. Because of support agencies' responsibilities and capabilities, the nature of project requirements, spacecraft

performance characteristics, and flight profiles, a major change in the required support configuration occurs naturally as the spacecraft proceeds from the near-Earth phase to the deep space phase of flight. Tracking and Data System preflight planning and flight operations support are oriented to coincide with these two phases. In effect, the Tracking and Data System manager established one system configuration for the near-Earth phase and another for the deep-space phase.

a. Near-Earth phase. The near-Earth phase begins with the launch countdown and ends when the spacecraft is in continuous view of the DSN stations. Normally, resources from all three support agencies comprise the configuration for the near-Earth phase. Data acquisition is provided by the AFETR land stations, ships, and aircraft; by STDN and by DSN stations in the near-Earth zone of operations. The John F. Kennedy Space Center (KSC), a field installation of NASA, manages certain instrumentation facilities available for TDA support. Support required from these sites is arranged through appropriate existing documentation. KSC is also the NASA single point-of-contact with the AFETR. Support required from the AFETR is contracted through the KSC.

For the near-Earth phase, the Tracking and Data System made available for *Pioneers F* and *G* the resources of the AFETR, KSC, the Spaceflight Tracking and Data System, the DSN, and the NASA Communications System.

b. Deep-space phase. The deep-space phase begins with deep space station continuous view and continues until the end of mission. Normally, the three facilities of the DSN are the only resources used to support data acquisition and processing requirements during this phase. The NASCOM and GCF resources are employed for data transmission. The support plan of the near-Earth and deep space phases of *Pioneer F* and *G* missions was reported in Ref. 6.

4. Tracking and Data System communication and coordination. The complexity of the Project and Tracking and Data System organization made it essential that a common means of communicating and coordinating tracking and data acquisition requirements, plans, procedures, reports, etc., existed between the Project and the Tracking and Data System, and also between support agencies. In addition to the frequent contacts which were made through the day-to-day business, two basic established methods provided the required information flow: (1) via standing committees and scheduled meetings, and (2) via formal documentation systems. Specific items under each of these categories are as follows:

a. Committees and meetings

(1) Planetary and Interplanetary Projects Tracking, Telemetry, and Communications Panel. This panel, chaired by the Tracking and Data System Office, meets approximately twice yearly, and its membership includes representatives of the *Pioneer* and other unmanned planetary and interplanetary projects, support agencies, launch vehicle agencies, and NASA Headquarters.

(2) Project/Tracking and Data System Quarterly Reviews. Project and Tracking and Data System personnel met quarterly with NASA Headquarters representatives, reviewed progress, and resolved problem areas.

(3) Ad Hoc Committees. The representation and frequency of meetings varied as required for the stated purposes.

b. Applicable documents. Support Agency and Tracking and Data System documents which were pertinent to the tracking and data acquisition function are only briefly discussed in this paragraph.

As separate entities supporting the Tracking and Data System, each support agency maintained its own internal documentation system. Without altering or controlling these internal documentation systems (e.g., DSN Documentation System, National Range Universal Documentation System, and Goddard Space Flight Center Documentation), the Tracking and Data System Manager has defined a Tracking and Data System documentation system which encompassed and supplemented the Support Agency documents. The Tracking and Data System Documentation System provided a comprehensive, unified description of the various documents produced in meeting the Project's tracking and data acquisition requirements. An outline of the documentation system is included here for general information:

(1) Tracking and Data System Standard Practices. These were prepared by the Tracking and Data System Manager. Of particular importance to the Project was the Tracking and Data System/Project Standard Technical Interface Document.

(2) Tracking and Data System Estimated Capabilities for the *Pioneer F* and *G* Missions. (607-96, dated December 15, 1969). This document was prepared by the Tracking and Data System Manager, based on inputs from the Near-Earth and Deep Space Support Agencies.

(3) Tracking and Data System Support Plan for the *Pioneer F* and *G* Missions. In actuality, this is comprised of the NASA Support Plan (NSP) and the Program Support Plan (PSP) for the *Pioneer F* and *G* Missions. It was prepared by the DSN Manager and by AFETR, respectively.

(4) Tracking and Data System Test Plan for the *Pioneer F* and *G* Missions. This document provided guidelines to and encompassed the near-Earth phase and the Deep Space Network test plans. It consisted of plans, procedures, and reports.

(5) Tracking and Data System Operation Plan for the *Pioneer F* and *G* Missions. This encompassed the near-Earth phase and Deep Space Network operations plans. Each plan contained numerous volumes regarding detailed commitments, interfaces, system descriptions, operational procedures, and directives. It included the Air Force Eastern Test Range Operations Directive and the Manned Space Flight Network Operations Plan.

(6) Tracking and Data System Support Reports for *Pioneer F* and *G*. These reports will be comprised of Tracking and Data System periodic progress reports and a final report.

D. TDS/Pioneer Project Planning Organization

The *Pioneer F* and *G* premission planning period spanned from project inception through operational readiness testing prior to launch.

The JPL Field Station, Air Force Eastern Test Range (JPL/ETR) organization operated by JPL Section 293, had the responsibility to plan and coordinate the required support by agencies involved in the support of the near-Earth phase of the *Pioneer F* and *G* missions. This organization advised the *Pioneer* Project on the long-term near-Earth TDS capabilities, and reviewed the TDA requirements and interface problems. They provided near-Earth phase assistance on the SIRD, NSP, Program Requirement Document (PRD), PSP, Operations Directive (OD), OR, Operations Plan (OP), and Tracking Instruction Manual (TIM). This organization planned and conducted the preflight compatibility verification and operational tests of the near-Earth system. They supported all interface reviews, analyzed plans and test results, and provided the required reports and documents. The near-Earth phase Project Engineer also acted collectively as an Assistant TDS Manager in matters related with the near-Earth function.

For the preparation and operation of the Deep Space Network a DSN/*Pioneer F* and *G* Operational Support and Planning Group was established. This organization consists of a DSN Manager, a DSN Project Engineer and a team of systems and facility-oriented project engineers.

Each position is devoted to supporting the *Pioneer F* and *G* Project. This organization is directly responsible to the Tracking and Data System Manager.

The DSN Manager is responsible for the planning and implementation of DSN support for the *Pioneer* Project. He was appointed for the *Pioneer* Project by the Jet Propulsion Laboratory. The DSN Manager is responsible for developing the support necessary to meet all flight project tracking and data acquisition requirements and for the operational readiness of the DSN. In addition, his functions will cover the flight operations to the end of the mission to be supported within the capabilities and resources of the DSN. The DSN Manager is responsible for the reviewing and clarification of the *Pioneer F* and *G* SIRD, for the preparation of the DSN portion of the NASA Network Support Plan, progress reports, and final report on implementation and readiness of the DSN for flight support. He conducts and documents pre- and post-flight operational readiness reviews and actual performance reviews of the network. He recommends changes to requirements and/or resources in order to meet mission objectives; observes and critiques the qualitative and quantitative performance of the DSN during flight operations, and terminates DSN support with approval of the flight project in a manner appropriate to the original commitment. He certifies to the TDS Manager the completion of task assignments and recommends actions in case of uncompleted tasks; prepares recommendations for improvements in flight project support, and provides the necessary interfaces between the Deep Space Network and other elements of the Tracking and Data System. The DSN Manager also functions as assistant TDS Manager, when requested.

The DSN project engineer is responsible for planning and coordinating all interface engineering. His function is to bring the DSN to a state of readiness and thus fulfill commitments which were made by DSN management in response to the particular *Pioneer* Project requirements. He is required to participate on the TDS planning team, under the TDS Manager and the DSN Manager during the early planning phases of the TDS DSN/Project activities. He assists in the definition of the data flow interfaces between the DSN and the other elements of the TDS. The DSN Project Engineer participated on the DSN Capabilities Planning Team and assisted the DSN Manager in defining DSN Systems Functional Specifications for *Pioneers F* and *G*. In response to the TDS and DSN milestone schedule, he produced and maintained a detailed implementation schedule reflecting the plan and status of DSN implementation, integration testing, training, documentation and operations. He coordinates the Interface Engineering Team; initiates actions necessary to complete events and tasks to meet the requirements of the NSP. He will evaluate the DSN performance by comparing actual

flight support with DSN commitments and Project requirements. The DSN Project Engineer is also responsible for assuring that scheduling inputs necessary for flight project support are submitted for the DSN Network Scheduling Office. He also participated in Mission Operations Working Group meetings established by the *Pioneer* Project. The DSN Project Engineer is accountable to the DSN Manager and to the Chief of *Pioneer* Mission Operations during all flight support activities.

The membership of the *Pioneer F* and *G* Interface Engineering Team consists of engineering representatives of the following organizations: DSIF Operations Engineering, DSIF Operations Planning, DSIF System Data Analysis, GCF Operations, SFOF/GCF Development, SFOF Data System, SFOF Data Processing, SFOF Support, DSN Simulation, and DSN System Engineering.

To assure that all Project/DSN interfaces are properly identified, the *Pioneer* Project was encouraged to participate in the team's activities. The Interface Team produced Volumes II through VIII of the DSN Operations Plan, DSN Test Plan, and Operations Reports. The team also performed detailed design functions pertaining to hardware/software and procedural interfaces. The team members are also performing advisory and operational roles during mission operations.

The efforts of the systems- and facility-oriented Project Engineers are coordinated by the DSN Project Engineer. Through this organization, talents available in the DSN can be applied to problems confronting the *Pioneer* planning organization. These people also support mission design teams, as follows:

(1) A Capability Planning Team staffed by DSN design personnel with a spacecraft telecommunication design and a mission operations representative from ARC. This team developed functional block diagrams and mission control interfaces of the DSN to a detail below that presented in this document.

(2) A Telecommunication Design Team chaired by ARC which consisted of spacecraft telecommunication engineers from ARC and TDS representatives from JPL.

(3) A Mission Operations Design Team chaired by ARC, with the DSN Project Engineer acting as a member of this team, for developing specific requirements for all elements of the ground system supporting the deep-space phase of these missions.

Figure 2 shows a part of JPL's organizational structure and identifies the Laboratory Divisions which support the major tracking and data acquisition functions for *Pioneers F* and *G*.

Under the Director of the Jet Propulsion Laboratory, the Assistant Laboratory Director for Tracking and Data Acquisition heads the system- and project-oriented functional organizations responsible for the Deep Space Network. The Engineering and Operations Section provides the System and Project Engineering functions and the DSN Operations Organization. The DSN Residents act as liaison between the DSN and the Deep Space Stations. The Mission Support Office is headed by the Tracking and Data System Manager. The DSN Managers provide the support for the specific current and future planetary and interplanetary missions. The DSN Systems Manager is responsible for the design of the DSN systems. The Tracking and Data Acquisition Program Control Office is engaged in the financial, budgeting and control functions.

Under the Assistant Laboratory Director for Technical Divisions, the Telecommunications Division is responsible for research, design, and implementation of the Deep Space Stations. The Mission Analysis Division is in charge of the space navigation and orbit determination functions. It assists DSN in the areas of research related to the radio metric tracking function. The Office of Computing and Information Systems heads the Data Systems Division which is responsible for the research, design, and implementation of the SFOF, and the Ground Communications Facility. The Facility System Engineers who handle the DSN Telemetry, Command, Tracking, Monitoring, Simulation, and Operations Control Systems are resident in the Telecommunications and Data Systems Divisions and interface with the corresponding DSN Systems engineers resident in the DSN Engineering and Operations Sections.

The JPL Systems Test and Launch Operations Section (not shown in Fig. 2) supports the JPL/ETR Station. This station was engaged in the Near-Earth Phase planning activities of the *Pioneer F* and *G* Missions.

References

1. Siegmeth, A. J., "Pioneer Mission Support," in *The Deep Space Network Progress Report*, Technical Report 32-1526, Vol. II, pp. 6–17. Jet Propulsion Laboratory, Pasadena, Calif., Apr. 15, 1971.

2. Siegmeth, A. J., "Pioneer Mission Support," in *The Deep Space Network Progress Report*, Technical Report 32-1526, Vol. III, pp. 7–19. Jet Propulsion Laboratory, Pasadena, Calif., June 15, 1971.

3. Siegmeth, A. J., "Pioneer Mission Support," in *The Deep Space Network Progress Report*, Technical Report 32-1526, Vol. IV, pp. 13–21. Jet Propulsion Laboratory, Pasadena, Calif., Aug. 15, 1971.

4. Siegmeth, A. J., "Pioneer Mission Support," in *The Deep Space Network Progress Report*, Technical Report 32-1526, Vol. V, pp. 4–16. Jet Propulsion Laboratory, Pasadena, Calif., Oct. 15, 1971.

5. Siegmeth, A. J., "Pioneer Mission Support," in *The Deep Space Network Progress Report*, Technical Report 32-1526, Vol. VI, pp. 13–24. Jet Propulsion Laboratory, Pasadena, Calif., Dec. 15, 1971.

6. Siegmeth, A. J., "Pioneer Mission Support," in *The Deep Space Network Progress Report*, Technical Report 32-1526, Vol. VII, pp. 5–16. Jet Propulsion Laboratory, Pasadena, Calif., Feb. 15, 1972.

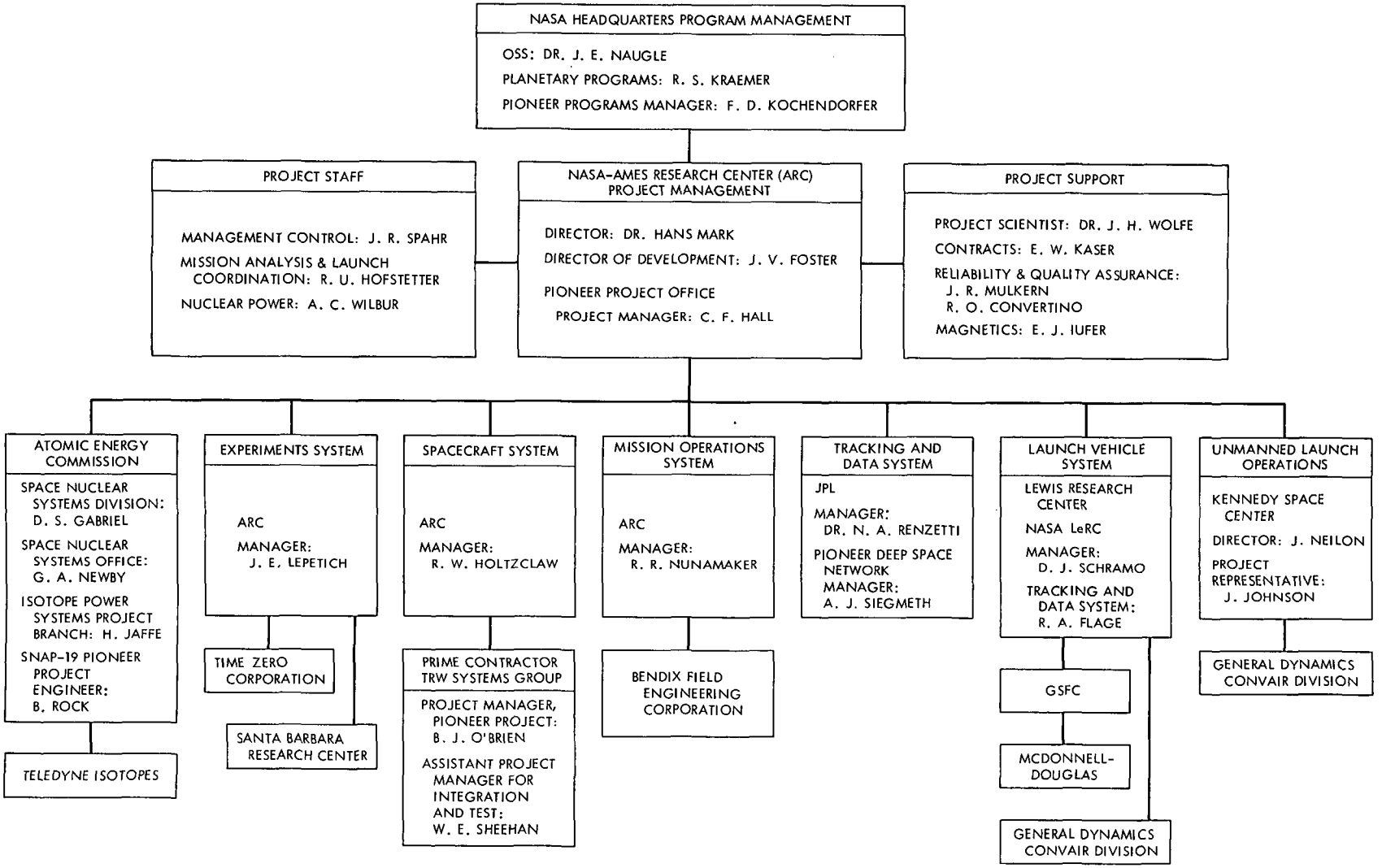

Fig. 1. *Pioneer F* and G Program Management Team

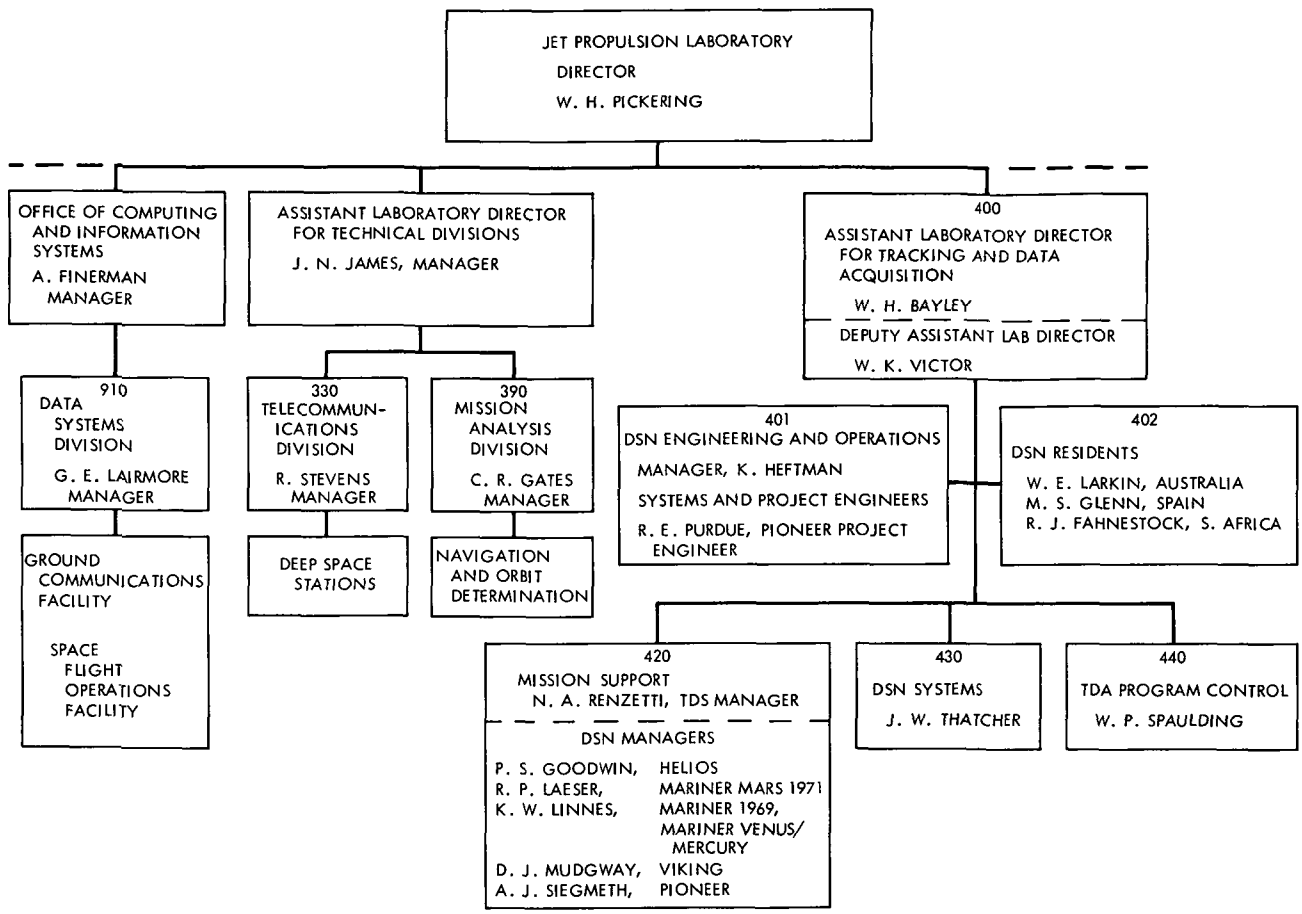

Fig. 2. JPL divisions engaged in tracking and data acquisition support of *Pioneers F and G*

Helios Mission Support

P. S. Goodwin
Mission Support Office

Project Helios is a cooperative U.S./West German space effort. Two unmanned solar-orbiting spacecraft are planned to be launched: the first in mid-1974, and the second in late 1975. These spacecraft will follow a trajectory that brings them closer to the Sun (under 0.3 AU) than any known program to date. Using specially designed instruments, the Helios spacecraft will enter unexplored regions near the Sun in an attempt to expand mankind's knowledge of how the Sun influences life on Earth. In addition to the scientific goals, Project Helios presents many challenging technological problems—none the least of which is to design a spacecraft which will endure 16 times the amount of heat from the Sun (at 0.25 AU) than is normally received on Earth. In addition, the spacecraft reaches its closest approach to the Sun (perihelion) in only 90 days after launch. These and other facets of this unique mission were described in Volumes II through VI of this series. Volume VII treated the JPL/TDS activities during the Sixth Helios Joint Working Group Meeting held at Oberpfaffenhofen, West Germany, October 20 to 27, 1971. This article covers the DSN Helios activities since that date.

I. Introduction

The previous article (Ref. 1) highlighted the activities of the U.S./German TDS subgroup in support of the Fifth *Helios* Joint Working Group Meeting held at Oberpfaffenhofen (near Munich), West Germany, October 20–27, 1971. As mentioned in that article, considerable progress was made—both in culminating prior efforts and in establishing a firm basis for future efforts. It is, therefore, the intent of this article to summarize the NASA–TDS activity that has transpired since the Fifth *Helios* Joint Working Group Meeting, and also to mention briefly the planning effort that is under way in anticipation of the Sixth *Helios* Joint Working Group Meeting, to be held at JPL April 26, through May 3, 1972.

II. NASA Support Plan (NSP)

One of the highlights of the Fifth *Helios* Joint Working Group Meeting was the issuance by the Project Office of the preliminary Support Instrumentation Requirements Document (SIRD). The issuance of the SIRD (even though preliminary) represented an important *Helios* Project/DSN milestone in that it defined for the first time the specific network support requirements needed by the *Helios* Project Officer in order to accomplish their mission objectives. As a result of the publication of the preliminary *Helios* SIRD, the DSN was able to initiate the planning effort leading toward a NASA Support Plan (NSP). This effort, which is still under way, will lead first to a preliminary issue of the NSP covering the support for the Deep

Space Phase. Incorporation of the Near-Earth Phase Support sections of the NSP will, of necessity, have to await the preparation of the actual launch trajectories available to Project *Helios*. Preliminary versions of the latter are not expected until late in 1972, with final versions not becoming known until after mid-1973.

DSN planning to date is based upon the assumption that DSS 11 (Pioneer DSS), DSS 42 (Weemala DSS) and DSS 62 (Cebreros DSS) 26-m subnetwork will provide the major telemetry, command, and radio-metric coverage during the *Helios* primary mission (Mission Phases I and II). In addition, it is expected that selected coverage will be provided by the DSN 64-m antenna facilities at the Goldstone and Tidbinbilla DSCCs during the first perihelion portion of the *Helios* mission. *Helios* support by the Madrid, Spain, 64-m DSN antenna facility is not presently contemplated, since the West German 100-m antenna facility at Effelsberg is expected to provide enhanced telemetry coverage from that longitude. As mentioned in previous volumes, the West German station facilities (Effelsberg and Weilheim) and the DSN will cooperate in providing the needed *Helios* support. The combination of the DSN's 26-m subnetwork and the two 64-m facilities is, however, expected to provide the majority of the tracking and data acquisition support for Project *Helios*, since the more northerly latitude of the West German Effelsberg station restricts its visibility of the *Helios* spacecraft to approximately 4 to 6 h/day—depending upon the time of year. Nonetheless, the Effelsberg antenna, due to its higher gain, is expected to provide valuable support to the *Helios* Project—especially when the spacecraft is at its maximum range from Earth (Fig. 9 of Vol. VI of this series). Nonetheless, as stated in Vol. VI, the *Helios* telecommunications link design specification is such that all primary mission objectives can be accomplished utilizing only the DSN 26-m subnetwork. Therefore, the primary emphasis within the Deep Space Phase portion of the NSP will relate to the capabilities of the DSN 26-m antenna subnetwork—i.e., DSSs 11, 42, and 61. However, all data obtained, regardless of which size DSS antenna is providing the support, will be made available to the *Helios* Mission Operations Team. The NSP is, therefore, expected to fulfill most, if not all, of the requirements set forth in the *Helios* Project SIRD.

III. Compatibility Test Planning

The first full-scale compatibility tests between the *Helios* spacecraft telecommunications system and the DSN are presently scheduled to be conducted in April–May 1972. These tests will employ the engineering model (EM) version of the *Helios* spacecraft radio system—minus the digital data handling subsystem. These tests, which are to establish basic spacecraft/DSN compatibility, have been intentionally scheduled sufficiently early in the *Helios* spacecraft development cycle to permit design modifications should any be deemed necessary subsequent to the compatibility tests. Planning effort directed toward the engineering model compatibility tests has been under way for approximately one year. It has involved both the *Helios* Spacecraft Project Office and the DSN. As of this time, both a Management Plan and a Test Plan have been published (Refs. 2 and 3). In preparation is a document covering the actual test procedures to be used during the *Helios* engineering model/DSN compatibility tests. This latter document is scheduled for publication just prior to the start of the compatibility tests in order that its information will be as current as possible. In addition, a report covering the results of the tests is planned for publication.

According to the present schedule, the EM compatibility tests will be conducted at DSS 71, Cape Kennedy, Florida. The EM transponder and its associated ground support equipment will be located either within the DSS 71 facility or in the shield room at Hangar AO, Cape Kennedy—depending upon the nature and requirements of the particular test under way at the time. For those tests conducted within DSS 71, coaxial "hard-line" connections will be made between the EM transponder and the DSS 71 station equipment. For those tests conducted with the EM transponder located within the Hangar AO shield room, RF microwave paths (operating passively on the *Helios* frequencies) will be employed to interconnect the transponder with DSS 71. In either event, computer-controlled attenuators, programmers, etc., will be employed to automate the tests cycles—with the results being presented on a standard computer line printer. This unique capability of the two DSN compatibility test facilities, DSS 71 and CTA 21, greatly reduces the time and manpower that would otherwise be required to perform these essential tests.

While the EM compatibility tests at DSS 71 represent an important Project milestone, it will not be the first time that portions of the *Helios* radio system have interfaced with the DSN. During mid-summer 1971, the *Helios* spacecraft command detector modules were laboratory-tested at JPL, and in December 1971 the newly redesigned *Helios* spacecraft receiver was similarly tested. During the latter tests, the *Helios* spacecraft receiver was connected to a spare *Mariner* spacecraft transmitter to form a complete transponder which was then patched to the

JPL CTA 21 facility for end-to-end tests. At that time, there were no indications of a serious incompatibility between the contemplated *Helios* spacecraft radio system design and the DSN. Because of this fact, both the *Helios* Project Office and the DSN are optimistic that the EM compatibility tests at DSS 71 will proceed on schedule.

IV. Action Items

As mentioned in the previous article (Ref. 1) the semi-annual *Helios* Joint Working Group meetings not only present a forum for the exchange of technical information but also establish the plans for future effort. Many of these plans result in the assignment of action items upon the various subgroup members. In this regard, the TDS subgroup has received its share of action items. A significant number of these relate to the interface between the German Space Operations Center (GSOC) at Oberpfaffenhofen and the SFOF at Pasadena since, during Mission Phase II, Project control will be in West Germany, while a majority of the tracking and data system support for *Helios* will be provided by the DSN with network control in Pasadena. During this Phase II time period, the DSN will be accumulating and forwarding in real-time, spacecraft telemetry data to Germany, and in return will be receiving from GSOC command instructions to be sent to the spacecraft. In addition, the German Effelsberg and Weilheim antenna facilities will be used to provide a portion of the tracking and data acquisition support. These factors present many interfaces which must be resolved—hence are the subject of a number of action item assignments, since the overall interface is too complicated to be treated as a single topic. The generation of responses to action items is, therefore, a continuing process requiring significant activity during the intervals between Joint Working Group Meetings.

V. Preparations for the Sixth *Helios* Joint Working Group Meeting

The Jet Propulsion Laboratory is honored to have been selected to be the host for the Sixth *Helios* Joint Working Group Meeting. These meetings, which are held semi-annually, are alternately held in the United States and in the Federal Republic of West Germany. The meetings, which last approximately one week, encompass all aspects of the *Helios* Project activities. Representatives of each experiment; the spacecraft structure, thermal, power, etc., subsystems; the launch vehicle; launch support facilities; the supporting tracking and data systems; and the Mission Operations organization participate in these meetings (Ref. 4). In all, approximately 150 to 200 people are in attendance. The Working Group Meetings open and close with General Sessions embodying all participants, the intervening period being occupied with individual and joint meetings between the aforementioned subgroup membership representing the experimenters, launch vehicle, etc. Hosting such a meeting obviously requires considerable prior preparation. Not only must adequate conference room areas be obtained, but the host committee must concern itself with such mundane matters as hotel reservations for the visitors, reserved parking areas, secretarial services, and general information pamphlets. Since the Sixth *Helios* Joint Working Group Meeting is scheduled for April 26, to May 3, 1972, JPL host committee activities have already started in preparation for this meeting. Also, technical agenda items are being formulated even though the final agendas cannot be prepared until just prior to the meeting since action item activity, etc., are continuing subjects. Nonetheless, during this reporting period, JPL preparation activity in anticipation of the forthcoming Sixth *Helios* Joint Working Group Meeting has been initiated.

VI. Conclusion

This article has only attempted to highlight some of the more significant JPL/TDS activities in support of Project *Helios* since the Fifth *Helios* Joint Working Group Meeting held in Oberpfaffenhofen, West Germany, October 20 to 27, 1971. Obviously, a considerable amount of technical detail activity also transpired during this time period, but it is beyond the scope of this article. Such information is better retained in the Project working files, at least until it appears in official interface documents. Nonetheless, from an overall Project viewpoint, the TDS has made continued and steady progress since the last Joint Working Group Meeting. The results of this progress are being reflected in the various *Helios* Spacecraft/TDS Interface Documents that are scheduled for publication in the weeks and months ahead. These and other significant factors will be treated in future articles of this series.

References

1. Goodwin, P. S., "*Helios* Mission Support," in *The Deep Space Network*, Technical Report 32-1526, Vol. VII, pp. 17–23. Jet Propulsion Laboratory, Pasadena, Calif., Feb. 15, 1972.
2. *DSN/Helios Spacecraft Telecommunications Compatibility Management Plan*, Document 613-3, Sept. 15, 1971 (JPL internal document).
3. *DSN/Helios Spacecraft Telecommunications Compatibility Test Plan*, Vol. I, Part A, Document 613-4, Jan. 15, 1972 (JPL internal document).
4. Goodwin, P. S., "*Helios* Mission Support," in *The Deep Space Network*, Technical Report 32-1526, Vol. II, p. 20. Jet Propulsion Laboratory, Pasadena, Calif., April 15, 1971.

Viking Mission Support

D. J. Mudgway
Mission Support Office

Until recently, DSN configuration intended for support of the Viking 1975 mission included the SFOF, with its Central Processing System, Mission Support Areas, and Simulation Center.

In response to the NASA Headquarters directive of October 1, 1971, the Project/DSN interface was changed to delete the SFOF from the scope of DSN responsibility. As a consequence, many existing understandings between the DSN and the Project must now be renegotiated with resulting impact on schedules, documentation, and resources.

This report identifies areas where rework is necessary and describes progress toward defining the new DSN configuration for Viking and reestablishing a mutually acceptable interface between the Project and DSN.

I. General

The DSN configuration intended for support of *Viking* has been described in detail in previous issues of this document (Refs. 1, 2). This configuration was comprised of the DSIF, GCF, and SFOF, the latter facility including the 360/75/1108 complex of computers known collectively as the Central Processing System, the Mission Support Areas with pertinent I/O and display devices, and the Simulation Center. The disposition of all these resources in support of the *Viking* 1975 mission was the responsibility of the DSN Manager for *Viking*.

In accordance with existing practice, the schedules, interface agreements, and capabilities had been negotiated with various elements of the Project and had been formally documented and approved. A Support Instrumentation Requirements Document had been prepared and delivered to the DSN, and a response in the form of a NASA Support Plan had been prepared by the DSN and reviewed in preliminary form by the Project.

In January 1972, the DSN/Flight Project interfaces were redefined in such a way as to exclude the SFOF from the areas of DSN responsibility, and to assign responsibility for SFOF support to the Office of Computing and Information Systems (OCIS). As a consequence, many of the existing understandings between the DSN and Project described in Refs. 1 and 2 are no longer valid and must therefore be renegotiated. New interfaces between both the Project and DSN, and between the DSN and OCIS must be established, and new schedules and statements of capability must be developed and documented. The more significant areas in which rework will be necessary are described in the following sections.

II. Configuration

The new DSN configuration for *Viking* is shown in conceptual form in Fig. 1. The *Viking* Mission Control Center (VMCC) includes the SFOF Central Processing System, the Mission Support Areas, and the *Viking* Simulation System, and is the joint responsibility of the OCIS and the *Viking* Flight Operations System (FOS). The Deep Space Stations include the 64-m and 26-m subnets. They transfer data to and from the VMCC via the high-speed and wideband data lines of the GCF.

Control and monitoring of Network performance, and validations of the data streams flowing between the VMCC and the DSSs will be accomplished by a separate data processing capability which will be independent of the mission computers in the SFOF. These functions may be accommodated in a Network Operations Control Facility which is in the process of being designed at this time.

The capabilities of the DSSs and GCF remain as described previously (Ref. 3), but the capability of the Network Operations Control Facility and its relationship with FOS activity, particularly in regard to the production of data records and simulation, has not yet been decided.

III. Interfaces

As mentioned above, the DSS capabilities are unchanged in the new configuration and interface agreements have been documented (Ref. 1) and formally signed off between the DSN and the *Viking* Orbiter System, and between the DSN and *Viking* Lander System. However, the interface between the VMCC and the GCF is entirely new and remains to be developed. Of particular concern in this regard is the question as yet undecided of whether responsibility for the VMCC side of the interface properly rests with OCIS or the *Viking* Flight Operations System.

IV. Schedules

The *Viking* Tracking and Data System (TDS) Level 3 Schedule is the controlling schedule for all TDS planning in support of *Viking*. A previous issue (Ref. 2) described a rather complex addition to this schedule to cover *Viking* Mission Demonstration tests in January, February and March of 1974. The SFOF support of these tests is now the responsibility of OCIS and has been deleted from the TDS schedule although support from CTA 21, DSS 12 and DSS 14 is still required from TDS.

As soon as the amended TDS Level 3 Schedule is approved, development of the lower level DSN implementation schedules will commence.

V. Documentation

As previously reported, the majority of the Project documents in which the TDS is involved have been completed although not all have been formally signed off. The principal documents in this category are:

Support Instrumentation Requirement Document

NASA Support Plan

Viking Project Specification

Viking Mission Requirements and System Design

Viking Configuration Management Plan

Viking Data Management Plan

In addition, there are a number of DSN mission-independent documents which have been used by the Project as a basis for much of its Orbiter, Lander and Flight Operations systems design.

Typical documents in this category are:

DSN/Project Interface Design Handbook

DSN/Project Interface Compatibility Test Design Handbook

All of the foregoing documents are impacted by the redefined interfaces and must be revised to reflect the new DSN responsibilities. Of these, the NSP has already been revised and is presently out for review with a June 1 goal for JPL approval and signoff. The others will follow in due course.

VI. Organization

In the past the DSN has carried out its planning and implementation function through the medium of a DSN Manager, DSN Project Engineer (PE), Capabilities Planning Team and Interface Teams. This organization was geared to the DSIF/GCF/SFOF configuration and included representatives at all levels from each of these facilities. The change in DSN responsibilities, together with the deletion of the DSN PE position, makes it necessary for the DSN to develop a new method of working with the technical support divisions.

This will undoubtedly lead to more direct working relationships between the DSN Manager and the facility representatives, and a significant reduction in the hither-to standard family of DSN mission-dependent documents.

VII. Conclusion

The recent re-definition of the DSN/Flight Project interfaces has a significant impact on previously established understandings between *Viking* and the DSN in regard to configurations, capabilities, interfaces, schedules, documentation, and interface organization.

Effort is now being directed to each of these areas in order to reestablish DSN/Project relationships as soon as possible. Progress in this direction will be reported in subsequent issues of this report.

References

1. Mudgway, D. J., "*Viking* Mission Support," in *The Deep Space Network Progress Report*, Technical Report 32-1526, Vol. V, pp. 24–28. Jet Propulsion Laboratory, Pasadena, Calif., Oct. 15, 1971.
2. Mudgway, D. J., "*Viking* Mission Support," in *The Deep Space Network Progress Report*, Technical Report 32-1526, Vol. VI, pp. 37–62. Jet Propulsion Laboratory, Pasadena, Calif., Dec. 15, 1971.
3. Mudgway, D. J., "*Viking* Mission Support" in *The Deep Space Network Progress Report*, Technical Report 32-1526, Vol. III, pp. 38–45. Jet Propulsion Laboratory, Pasadena, Calif., June 15, 1971.

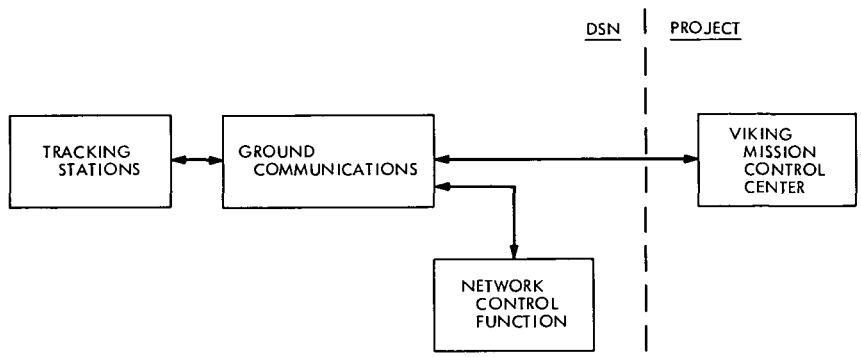

Fig. 1. DSN configuration for *Viking* (conceptual form)

Radio Science Support

K. W. Linnes
Mission Support Office

Since 1967, radio scientists have used the Deep Space Network 26- and 64-m-diameter antenna stations to investigate pulsars, to study the effect of solar corona on radio signals, and to observe radio emissions from X-ray sources. More recently, very long baseline interferometry (VLBI) techniques have been used for high-resolution studies of quasars. During the reporting period, VLBI observations were made of quasars and also of the Mariner 9 spacecraft. Support was also provided by the 64-m-diameter antenna for the measurement of cosmic background noise.

I. Introduction

The 26- and 64-m-diameter antenna stations of the DSN have been used for several years to support radio science experiments. NASA, JPL, and university scientists have used key DSN facilities whose particular and unique capabilities were required for the performance of the experiments. In order to formalize the method of selecting experiments and experimenters, a Radio Astronomy Experiment Selection (RAES) Panel was formed in 1969. Notice of availability of these facilities was placed in professional journals to inform the scientific community that they were available for limited use by qualified radio scientists (Ref. 1). No charge is made for use of the standard DSN facilities and equipment; special equipment, however, must be provided by the experimenters. A summary of all experiments conducted through December 1971 is reported in Refs. 2, 3, 4, and 5.

II. Radio Science Operations

Table 1 shows experiments supported in January and February 1972. The observations at 13 cm and 3 cm by the National Radio Astronomy Observatory (NRAO)–Cornell–Caltech group make use of the 64-m-diameter antenna at Goldstone, California (DSS 14) and the 37-m-diameter antenna at the Massachusetts Institute of Technology (MIT) Haystack Observatory. These observations have resulted in a number of articles identified in Refs. 2 and 5. Reference 6 is an article previously overlooked in these reports.

The observations by the Goddard Space Flight Center (GSFC)–JPL–MIT–University of Maryland group are a continuation of earlier work, the published results of which are identified in Refs. 2, 3, and 5. These observations resulted in the initial report of the apparent anoma-

lous expansion rate of Quasars 3C279 and 3C273 (Ref. 7). The NRAO–Cornell–Caltech group confirmed the observations. These topics were discussed at the meeting of the American Astronomical Society in San Juan, Puerto Rico, December 5–8, 1971 (Ref. 5).

Measurements of the cosmic background radiations at 3.5 cm were made by Carpenter, Gulkis, and Sato. These are the initial measurements made by this group since approval of the experiment in the September–October 1971 reporting period. Use of the 64-m-diameter antenna has been preempted by *Mariner* 9 until recently. Availability of the antenna has also permitted resumption of VLBI measurements at 13 cm using the trans-Pacific baseline between Goldstone and the 26-m-diameter antenna at Woomera, Australia. Results of previous measurements on this baseline have been published (Ref. 8). The Australian experimenters have also used the Woomera antenna in coordination with observations made from the 26-m-diameter dish near Johannesburg, South Africa. These observations on a trans-Indian Ocean baseline were made under the auspices of South African and Australian agencies under arrangements whereby they may utilize the antennas when not required for support of NASA programs.

III. RAES Panel Activities

The Radio Astronomy Experiment Selection Panel approved three experiments during the reporting period (Table 2).

IV. OSS Program Support

The DSN also provides support and use of the facilities for radio science programs of the NASA Office of Space Sciences (OSS). As reported in Ref. 4, feasibility was demonstrated in October of 1971 of tracking the *Mariner* 9 spacecraft by VLBI techniques. In the demonstration, the Goldstone 26-m Echo station and the 64-m Mars station were equipped with JPL hydrogen maser frequency systems and operated electrically independent, although with coordinated observing modes. As shown in Table 1, such observations were repeated using the 64-m-diameter antenna at Goldstone and the 26-m-diameter antenna at Woomera, Australia. The observations were made successfully and the data are now being processed.

V. NASA Radio Science Plan Support

In January, the Laboratory forwarded to the NASA Radio Science Panel inputs to the annual Radio Science Plan being formulated by the Panel. The submission included all experiments currently approved by the RAES Panel, the descriptions and requirements of all OSS Program Radio Science experiments, and, for information, the descriptions of the DSN Development activities that produce radio science data. The latter are planetary radar experiments conducted in the development of advanced high-power transmitters, improved-stability frequency systems, etc.

References

1. *Bulletin of the American Astronomical Society,* Vol. 2, No. 1, p. 177, 1970.

2. Linnes, K. W., Sato, T., and Spitzmesser, D., "Radio Science Support," in *The Deep Space Network Progress Report,* Technical Report 32-1526, Vol. III, pp. 46–51. Jet Propulsion Laboratory, Pasadena, Calif., June 15, 1971.

3. Linnes, K. W., "Radio Science Support," in *The Deep Space Network Progress Report,* Technical Report 32-1526, Vol. V, pp. 42–44. Jet Propulsion Laboratory, Pasadena, Calif., Oct. 15, 1971.

4. Linnes, K. W., "Radio Science Support," in *The Deep Space Network Progress Report,* Technical Report 32-1526, Vol. VI, pp. 43–45. Jet Propulsion Laboratory, Pasadena, Calif., Dec. 15, 1971.

5. Linnes, K. W., "Radio Science Support," in *The Deep Space Network Progress Report,* Technical Report 32-1526, Vol. VII, pp. 29–31. Jet Propulsion Laboratory, Pasadena, Calif., Feb. 15, 1972.

6. Cohen, M. H., and Shaffer, D. B., "Positions of Radio Sources from Long-Baseline Interferometry," *Astron. J.,* Vol. 76, No. 2, pp. 91–100, Mar. 1971.

7. Shapiro, I., et al., "Quasars: Millisecond of Arc Structure Revealed by Very Long Baseline Interferometry," *Science,* Vol. 172, p. 52, Apr. 2, 1971.

8. Gubbay, J. S., et al., "The Structure of P1934-63," *Astron. J.,* Vol. 76, No. 10, pp. 965–969, Dec. 1971.

Table 1. Radio science experiments involving 64- and 26-m-diameter antenna facilities

Experiment	Purpose	Experimenter	DSN facility	Date
X-band VLBI	To study the structure of extra galactic sources with improved resolution.	J. Broderick (NRAO) B. Clark (NRAO) K. Kellermann (NRAO) D. Jauncey (Cornell University) M. Cohen (Caltech) D. Shaffer (Caltech)	DSS 14 (and MIT Haystack Antenna)	Feb. 1971 Nov. 2, 1971 Feb. 5, 1972
Quasar structure by X-band VLBI	To monitor time variations and fine structure and apparent position of quasars.	T. Clark (GSFC) R. Goldstein (JPL) H. Hinteregger (MIT) C. Knight (MIT) G. Marandino (Univ. of Maryland) A. Rogers (MIT Haystack Observatory) I. Shapiro (MIT) D. Spitzmesser (JPL) A. Whitney (MIT)	DSS 14 (and MIT Haystack Antenna)	June 9 and 19, 1971 Sept. 19, 1971 Oct. 2–4, 10, 17, 1971 Jan. 4, 1972 Feb. 18, 1972
Small-scale variations in cosmic background radiation.	Search for small-scale spatial variations in the 2.7 K cosmic background radiation of 3.5 cm	R. Carpenter (Calif. State College, Los Angeles) S. Gulkis (JPL) T. Sato (JPL)	DSS 14	Jan. 10 and 11, 1972 Feb. 11, 12, and 22, 1972
Very long baseline interferometry (medium data bandwidth, S-band)	To determine angular size of radio sources	J. Gubbay (Univ. of Adelaide) A. Legg (Space Research Group, WRE) D. Robertson (Space Research Group, WRE) A. Moffett (Caltech) B. Seidel (JPL)	DSSs 14 and 41	June 12, 1971 Jan. 25, 1972 Feb. 21, 1972
Mariner 9/extra-galactic source VLBI	To locate Mariner 9 spacecraft with respect to well-known quasars at 2300 MHz.	P. MacDoran (JPL)	DSSs 14 and 41	Jan. 17, 20, and 25, 1972
Indian Ocean baseline VLBI	To study structure of selected quasars and galaxies at 2300 MHz.	G. Nicholson (National Institute of Telecommunications Research, South Africa) D. Robertson [Weapons Research Establishment (WRE), Australia]	DSS 41 (26-m) DSS 51 (26-m)	Jan. 21, 1972 Feb. 14, 1972

Table 2. Recent experiments approved by the RAES panel

Experiment	Purpose	Experimenters	DSN facility
Weak radio source observations	To measure the "confusion distribution" of weak radio sources at 2.3 GHz.	D. L. Jauncey (Cornell University) M. J. Yerbury (Cornell University) J. J. Condon (Cornell University) D. J. Spitzmesser (JPL)	64-m-diam antenna (DSS 14) at Goldstone
Transcontinental baseline VLBI	To measure transcontinental vector baselines by VLBI observation of quasars.	T. A. Clark (GSFC) H. F. Hinteregger (MIT) C. A. Knight (MIT) S. Lippincott (MIT Haystack Observatory) A. E. Rogers (MIT Haystack Observatory) I. I. Shapiro (MIT) A. R. Whitney (MIT)	64-m-diam antenna (DSS 14) at Goldstone with hydrogen maser [Also MIT Haystack 37-m-diam antenna and National Oceanic and Atmospheric Administration (NOAA) 26-m-diam antenna in Alaska]
Pulsar observations	To measure position and apparent motion of pulsars at 2.3 GHz by VLBI.	T. A. Clark (GSFC) G. S. Downs (JPL) N. C. Erickson (University of Maryland) P. E. Reichley (JPL) N. R. Vandenberg (University of Maryland)	64-m-diam antenna (DSS 14) at Goldstone. 26-m for feasibility. (Also NRAO 42-m-diam antenna at Greenbank, West Virginia)

An Analysis of Long Baseline Radio Interferometry, Part II

J. B. Thomas
Tracking and Orbit Determination Section

This report continues the analysis of the cross-correlation procedure used in long baseline radio interferometry begun in Technical Report 32-1526, Vol. VII, pp. 37–50. It is assumed that the radio signal is generated by a very distant, completely incoherent, extended source. For both digital and analog recording systems, the normalized cross-correlation function is derived in terms of noise temperature, fringe visibility, and bandpass overlap. For very strong point sources and accurate model delays, it is shown that the digital cross-correlation function becomes a sawtooth time function whose extrema and zero crossings agree with the sinusoidal cross-correlation function produced by an analog system. For weak sources, such as those common to most very long baseline interferometry measurements, the digital cross-correlation function is identical to the normalized analog cross-correlation function, except for a loss of $2/\pi$ in amplitude.

General signal/noise (S/N) expressions are derived for both the digital and the analog cross-correlation functions. For a very strong point source, the S/N ratio in a digital system can be infinitely better than the S/N ratio in an analog system at time points of maximum correlation. However, at points of weak correlation, the digital S/N ratio is $2/\pi$ smaller than the analog value. In the case of small correlated amplitude, the digital system produces a S/N ratio that is uniformly $2/\pi$ worse than the analog system ratio.

I. Introduction

In very long baseline interferometer (VLBI) measurements, the radio signal produced by a distant source is recorded simultaneously at two widely separated antennas. These recorded signals are then cross-correlated to determine correlated amplitude, as well as delay and delay rate due to path differences. An earlier report (Ref. 1) presented an analysis of long baseline interferometry that included the following topics—time delay theory, source statistics, electronic factors, and a derivation of the analog cross-correlation functions for point sources and completely incoherent, extended sources. In this report, the analog cross-correlation function is simplified by normalization and expressed in terms of noise temperature, fringe visibility, and bandpass overlap. In addition, this report considers digital recording and signal-to-noise ratios for the following reasons.

In the digital recording systems found in many VLBI systems, the voltage signal is infinitely clipped before it is

recorded. That is, each time the signal is sampled, only the sign of the voltage is recorded. Since this clipping process only preserves the zero crossings of the original analog signals, the digital cross-correlation function will deviate from the analog cross-correlation function derived in earlier work (Ref. 1). In order to assess the importance of this deviation, the digital cross-correlation procedure is investigated in the case of a completely incoherent, extended source. The statistical approach used in this analysis is based on a technique employed by Van Vleck and Middleton (Ref. 2) to investigate the *autocorrelation* of clipped Gaussian noise. Their technique is applied to the *cross-correlation* of infinitely clipped VLBI signals in order to obtain the digital cross-correlation function.

A signal/noise (S/N) analysis has been performed for two reasons. First, source brightness measurements are often based on the S/N values observed in VLBI experiments. In the case of infinite clipping, brightness measurements must depend to some extent on S/N expressions since all absolute amplitude information is lost in the clipping process. Second, estimates of the measurement precision for time delay and delay rate can be calculated on the basis of the S/N ratios for the cross-correlation function. For these reasons S/N expressions have been derived for both the analog and digital cross-correlation functions.

II. Normalized Cross-Correlation Function

In this section, the analog cross-correlation function for an extended source is simplified by a normalization process that introduces noise temperature and fringe visibility. We first derive expressions for the mean-square noise and signal voltages. These expressions are then used to normalize the cross-correlation function in terms of noise temperatures.

As indicated in previous work (Ref. 1), the voltage due to an extended source recorded at antenna j may be represented as the sum of a signal term and a noise term as follows:

$$V_j(t) = \int_{\hat{\mathbf{k}}} \int_0^\infty G_j(y_j)\,\kappa_j\,A(\hat{\mathbf{k}},\omega)\,e^{i\alpha_j}\,d\omega\,d\Omega + \text{c.c.} + \int_0^\infty G_j(y_j)\,H_j(\omega)\,e^{i\theta_j}\,d\omega + \text{c.c.} \qquad (1)$$

where

$$y_j = \omega(1 - \hat{\mathbf{k}}\cdot\mathbf{x}_j/c)$$

$$\alpha_j = (\omega - \omega_j)\,t - \omega\hat{\mathbf{k}}\cdot\dot{\mathbf{x}}_j/c - \omega\tau_j + \phi_j$$

$$\theta_j = (\omega - \omega_j)\,t - \omega\tau_j + \phi_j$$

The quantity $A(\hat{\mathbf{k}},\omega)$ is the Fourier amplitude of the wave received from direction $\hat{\mathbf{k}}$ at frequency ω. Note that the signal term consists of a superposition of waves received from all parts of the source ($\hat{\mathbf{k}}$ integral) over all allowed frequencies (ω integral). The quantity $d\Omega$ represents a differential solid angle centered at $\hat{\mathbf{k}}$. The function G_j is the effective bandpass filter with an argument y_j that accounts for doppler shifting. The quantity ω_j is the effective mixing frequency, ϕ_j is the instrumental phase shift, and τ_j is the instrumental delay. The vector $\mathbf{x}_j$ is the position of station j, and c is the speed of light. We have assumed the antenna pattern is large compared to the source size and may therefore be neglected. More discussion of Eq. (1) is given in Ref. 1. This expression differs from the reference in two ways. First, the noise term has been represented in terms of its frequency components $H_j(\omega)$. In this representation, it has been assumed, without loss of generality, that all instrumental noise is effectively added at the first stage of amplification. This noise term will also include all background radio noise. Second, a factor κ_j has been included in order to separately account for antenna factors such as aperture and efficiency in the conversion from electrical field to voltage.

In order to calculate the mean-square voltages, we must know the average values of random products such as $A(k,\omega)\,A^*(k',\omega')$. If we assume that the source is completely incoherent, an ensemble average of the signal components is given by the expressions (Ref. 1)

$$\left.\begin{aligned} &\langle A(\hat{\mathbf{k}},\omega)\,A^*(\hat{\mathbf{k}}',\omega')\rangle = S_D(\hat{\mathbf{k}},\omega)\,\delta(\omega-\omega')\,\delta(\hat{\mathbf{k}}-\hat{\mathbf{k}}') \\ &\langle A(\hat{\mathbf{k}},\omega)\,A(\hat{\mathbf{k}}',\omega')\rangle = 0 \qquad \text{for } \omega \text{ and } \omega' > 0 \end{aligned}\right\} \qquad (2)$$

where $S_D(\hat{\mathbf{k}},\omega)$ is the spectral power from direction $\hat{\mathbf{k}}$ and $\delta(z)$ is the Dirac delta function. That is, radio waves emitted by different areas of the source are uncorrelated. Furthermore, noise waves emitted by a given area of the source are stationary and therefore possess uncorrelated frequency components (Ref. 1). We will also assume that the system noise is stationary, so that

$$\left.\begin{aligned} &\langle H_j(\omega)\,H_j^*(\omega')\rangle = N_j(\omega)\,\delta(\omega-\omega') \\ &\langle H_j(\omega)\,H_j(\omega')\rangle = 0 \qquad \text{for } \omega' \text{ and } \omega > 0 \end{aligned}\right\} \qquad (3)$$

where $N_j(\omega)$ is the power spectrum of the system noise at station j.

Under these assumptions, it is readily shown that an ensemble average of the square of the voltage is given by the expression

$$\langle V_j^2\rangle = \langle V_{S_j}^2\rangle + \langle V_{N_j}^2\rangle \qquad (4)$$

where

$$\langle V_{S_j}^2 \rangle = 2 \int_0^\infty \int_{\hat{\mathbf{k}}} |G_j(y_j)|^2 \kappa_j^2 S_D(\hat{\mathbf{k}}, \omega)\, d\Omega\, d\omega \tag{5}$$

and

$$\langle V_{N_j}^2 \rangle = 2 \int_0^\infty |G_j(\omega)|^2 N_j(\omega)\, d\omega \tag{6}$$

In analogy with the derivation of the cross-correlation function in Ref. 1, the cross terms between uncorrelated components have disappeared. As one would expect, the average signal power is given by the power received in the passband (ω integral) from all parts of the source ($\hat{\mathbf{k}}$ integral).

We may define the total spectral power of the source as the integral

$$S_p(\omega) = \int_{\hat{\mathbf{k}}} S_D(\hat{\mathbf{k}}, \omega)\, d\Omega \tag{7}$$

so that the mean-square signal becomes

$$\langle V_{S_j}^2 \rangle = 2 \int_0^\infty |G_j(\tilde{y}_j)|^2 \kappa_j^2 S_p(\omega)\, d\omega \tag{8}$$

We have neglected the insignificant doppler shift variations (<0.01 Hz) in y_j across the source and have chosen the source center to evaluate the doppler term $\hat{\mathbf{k}} \cdot \dot{\mathbf{x}}_j$ in the argument of the bandpass filter.

If both stations possess a square effective bandpass of width W and height $|G_j|$, and if the power spectra of the signal S_p and noise N_j are flat in the region of the bandpass, we obtain

$$\langle V_{S_j}^2 \rangle = 4\pi |G_j|^2 \kappa_j^2 S_p W \tag{9}$$

$$\langle V_{N_j}^2 \rangle = 4\pi |G_j|^2 N_j W \tag{10}$$

The analog cross-correlation function for a completely incoherent, extended source is given by the expression (Ref. 1)

$$\langle V_1(t)\, V_2(t + \tau_m) \rangle = \exp\{i[(\omega_2 - \omega_1)t + \omega_2 \tau_m + \phi]\} \times \int_0^\infty R(u, v, \omega)\, G_1(\tilde{y}_1)\, G_2^*(\tilde{y}_2) \exp(i\omega\Delta\tau)\, d\omega + \text{c.c.} \tag{11}$$

where

$$\tilde{y}_1 = \omega(1 - \hat{\mathbf{k}}_a \cdot \dot{\mathbf{x}}_1/c)$$

$$\tilde{y}_2 = \omega(1 - \hat{\mathbf{k}}_a \cdot \dot{\mathbf{x}}_2/c)$$

$$\Delta\tau = \tau_g + \tau_e - \tau_m$$

In addition, the brightness transform is defined by the expression

$$R(u, v, \omega) \equiv \int_{-\infty}^{\infty} \int_{-\infty}^{\infty} S_D(\beta, \gamma, \omega) \exp\{2\pi i [u(\beta - \beta_a) + v(\gamma - \gamma_a)]\}\, d\beta\, d\gamma \tag{12}$$

where

$$u \equiv \left.\frac{\partial \hat{\mathbf{k}}}{\partial \beta}\right|_a \cdot \mathbf{B}_r/\lambda$$

$$v \equiv \left.\frac{\partial \hat{\mathbf{k}}}{\partial \gamma}\right|_a \cdot \mathbf{B}_r/\lambda$$

$$\lambda = 2\pi c/\omega$$

The brightness transform determines the self-interference of the extended source by summing the point-source interferometer response over the total area of the source, using the source center as a zero-phase reference. The variables β and γ are two direction parameters chosen to describe the direction vector $\hat{\mathbf{k}}$. (In VLBI work, γ is usually declination δ, while β is right ascension multiplied times the cosine of the declination of the source center or $\alpha \cos \delta_a$.) The subscript a on γ, β, and $\hat{\mathbf{k}}$ refers to the source center where $\hat{\mathbf{k}}_a = \hat{\mathbf{k}}(\gamma_a, \beta_a)$. The quantity τ_g is the geometric delay, τ_e is the instrumental delay, and τ_m is the model delay. In these expressions, the following factors are evaluated at the center of the source $\hat{\mathbf{k}}_a$—the geometric time delay τ_g; the $\hat{\mathbf{k}}$ partials in u, v; and the doppler shifts in $\tilde{y}_j$. The vector $\mathbf{B}_r$ is the retarded baseline, and λ is the RF wavelength. (For more detail concerning definitions and the derivation of this result, see Ref. 1.)

Note that the brightness transform for a "zero-length" baseline gives

$$R(0, 0, \omega) = \int_{-\infty}^{\infty} \int_{-\infty}^{\infty} S_D(\beta, \gamma, \omega)\, d\Omega = S_p(\omega) \tag{13}$$

where S_p is the total spectral power of the source. The fringe visibility, which is defined by the expression

$$\gamma_v(u, v, \omega) = \frac{|R(u, v, \omega)|}{R(0, 0, \omega)} = \frac{|R(u, v, \omega)|}{S_p(\omega)} \tag{14}$$

measures the "correlated flux" in terms of the total flux. That is, the fringe visibility is the fractional amplitude that remains after self-interference. Note that γ_v equals one for a point source.

For unsymmetrical brightness distributions $S_D(\beta, \gamma, \omega)$, one must be careful when assigning an effective source center. For example, consider a source that consists of a broad diffuse disk-shaped background with a point-source at one edge. For a short baseline with weak resolution, the effective center will be approximately equal to the centroid of the total brightness distribution. For long baselines that totally resolve the diffuse component, the effective source center becomes the point-source location. In present VLBI measurements, this effect is generally not observed since instrumental and transmission media uncertainties in time delay measurements lead to source location errors that are several times greater than the interferometer resolution. For example, typical source location errors are of the order of 0.01 arc sec, while resolution is of the order of 0.001 arc sec for intercontinental baselines.

In general, both the magnitude and phase of the brightness transform depend on u, v, and ω. In the following work, we will assume that all parts of the source emit a flat power spectrum in the region of the passband. This means that the explicit frequency variation in $R(u, v, \omega)$ may be neglected in the ω integration in Eq. (11) if we make the explicit frequency ω equal to the bandpass center. In addition to this explicit frequency dependence, the variables u and v depend implicitly on ω. In the following derivation, we will assume this implicit frequency dependence is negligible over the passband for both the amplitude and phase of the brightness transform. That is, we will assume that R may be removed from the integral if we evaluate ω, u, and v at ω_0, the bandpass center frequency. The approximation is justified by the fact that the frequency typically changes about one part in 10^3 or 10^4 in integrating over the bandpass. For most brightness distributions, this approximation is very accurate. For example, in the case of diffuse, yet compact distributions, it can be shown that the fractional amplitude change will be of the order of 10^{-3} and the phase change of the order of 0.0001 cycle if the fractional frequency change is 10^{-3}. Both of these changes may presently be neglected in the ω integral.

If we express the brightness transform in terms of its real and imaginary parts,

$$R(u, v, \omega) = |R(u, v, \omega)| \exp[i\phi_R(u, v, \omega)] \tag{15}$$

the cross-correlation function becomes

$$\langle V_1(t) V_2(t + \tau_m)\rangle = \exp\{i[(\omega_2 - \omega_1)t + \omega_2 \tau_m + \phi + \phi_R]\}$$

$$\times |R(u_0, v_0, \omega_0)| \int_0^\infty G_1(\widetilde{y_1}) G_2(\widetilde{y_2}) \exp(i\omega\Delta\tau)\, d\omega \tag{16}$$

where we have evaluated R and ϕ_R at the bandpass center and removed them from the integral. If we now assume that both stations possess a square bandpass filter of height $|G_j|$ and width W, we can perform the frequency integration in Eq. (16) to obtain (Ref. 1)

$$\langle V_1(t) V_2(t + \tau_m)\rangle =$$

$$4\pi \kappa_1 \kappa_2 |G_1|\, |G_2|\, \gamma_v S_p W_D \frac{\sin \pi W_D \Delta\tau}{\pi W_D \Delta\tau} \cos\phi_f \tag{17}$$

where

$$\phi_f \equiv (\omega_2 - \omega_1)t + \omega_2 \tau_m + \omega_0 \Delta\tau + \phi + \phi_R$$

In this expression, W_D is the bandpass overlap after doppler shifting. The bandpass center ω_0 is the centroid of the bandpass product. In addition, $|R|$, the magnitude of the brightness transform, has been replaced by the fringe visibility γ_v and the total power spectrum S_p as indicated in Eq. (14). Both γ_v and S_p are evaluated at the bandpass center (ω_0, u_0, v_0).

The normalized cross-correlation function will be defined by the expression

$$r(t, \tau_m) = \frac{\langle V_1(t) V_2(t + \tau_m)\rangle}{\sqrt{\langle V_1^2\rangle \langle V_2^2\rangle}} \tag{18}$$

With this definition and Eqs. (9), (10), and (17), the normalized cross-correlation function becomes

$$r(t, \tau_m) = \gamma_v \sqrt{\frac{\langle V_{S_1}^2\rangle \langle V_{S_2}^2\rangle}{\langle V_1^2\rangle \langle V_2^2\rangle}} \frac{W_D}{W} \frac{\sin \pi W_D \Delta\tau}{\pi W_D \Delta\tau} \cos\phi_f \tag{19}$$

The last expression may be simplified by the concept of noise temperature. The system temperature (Ref. 3) for antenna j will satisfy the relation

$$T_j = \frac{p_j}{W} \langle V_j^2\rangle \tag{20}$$

while the signal temperature will be given by

$$T_{s_j} = \frac{p_j}{W} \langle V_{s_j}^2 \rangle \tag{21}$$

The quantity p_j is a proportionality constant whose magnitude will depend on the amplifier gains at station j. The actual value for p_j will not be of importance, since we are only interested in ratios of noise power and signal power. With the aid of Eqs. (20) and (21), the normalized cross-correlation function becomes

$$r(t, \tau_m) = \gamma_v \sqrt{\frac{T_{S_1} T_{S_2}}{T_1 T_2}} \frac{W_D}{W} \frac{\sin \pi W_D \Delta\tau}{\pi W_D \Delta\tau} \cos \phi_f \tag{22}$$

where

$$\phi_f = (\omega_2 - \omega_1) t + \omega_2 \tau_m + \omega_0 \Delta\tau + \phi + \phi_R$$

Thus, the normalized interferometer response to an extended source consists of the following factors. The geometric mean of the noise temperature ratios accounts for signal-to-noise factors. The bandpass overlap factor, W_D/W, accounts for power lost due to imperfect passband alignment. As discussed in Ref. 1, the $(\sin x)/x$ delay function indicates the accuracy with which the two signals have been aligned and peaks for zero delay error ($\Delta\tau = 0$). The fast fringes, $\cos \phi_f$, express the average overall phase behavior of the cross-correlated signals. The fringe visibility γ_v accounts for power lost due to self-interference of the extended sources.

Techniques for measuring system temperature are routinely employed at DSN stations. Note that the system temperatures, T_1 and T_2, in Eq. (20) are a sum of the instrumental noise temperature, the background radio noise temperature, and the total radio signal T_{s_j}. DSN instrumental noise temperatures are typically between 18 and 40°K and are due mainly to receiver noise. Background radio noise depends on sky temperature and elevation angle, but generally is less than 30°K for DSN antennas. Recent experimental results indicate that approximate values for signal temperature may be calculated by means of the expression

$$T_{s_j} \approx 0.0002\, S A_j \tag{23}$$

where T_{s_j} is the signal temperature in °K, S is the total source strength in flux units,[1] and A_j is the area of antenna j in meters. However, exact values for signal temperature may deviate from this expression because of differences in antenna and receiver efficiencies. The signal temperature for a 1-flux-unit source at DSS 14 (64-m-antenna) is approximately 0.65°K at S-band.

[1] 1 flux unit = 10^{-26} W/m²Hz.

III. Digital Cross-Correlation Function

In this section, an expression is derived for the cross-correlation function produced by infinitely clipped signals. The derivation is an application of a technique devised by Van Vleck and Middleton (Ref. 2) to analyze the *autocorrelation* of clipped noise. This section shows their derivation can be applied to the *cross-correlation* problem found in VLBI work.

Define the normalized voltage $X(t)$ for station 1 by the relation

$$X(t) = \frac{V_1(t)}{\sqrt{\langle V_1^2 \rangle}} \tag{24}$$

and the normalized voltage $Y(t)$ for station 2 by the relation

$$Y(t) = \frac{V_2(t)}{\sqrt{\langle V_2^2 \rangle}} \tag{25}$$

The normalized cross-correlation function for analog signals is then given by the expression

$$r(t, \tau_m) \equiv \frac{\langle V_1(t)\, V_2(t + \tau_m) \rangle}{\sqrt{\langle V_1^2 \rangle \langle V_2^2 \rangle}} = \langle X(t)\, Y(t + \tau_m) \rangle \tag{26}$$

As indicated in Eq. (1), the voltage at each station may be represented as the sum of integrals of random noise and signal components. Suppose that the components $A(\hat{\mathbf{k}}, \omega)$ and $H_j(\omega)$ are normally distributed. Since the voltages are then a linear combination of normally distributed random variables, their joint probability distribution (Ref. 2) will be given by the following normalized bivariate Gaussian distribution:

$$P(X, Y) = \frac{1}{2\pi (1 - r^2)^{1/2}} \exp\left[- \frac{(X^2 + Y^2 - 2rXY)}{2(1 - r^2)} \right] \tag{27}$$

where, for conciseness, we have used the abbreviated notation

$$X = X(t), \qquad Y = Y(t + \tau_m)$$

and

$$r = r(t, \tau_m) = \langle XY \rangle$$

Suppose that, for a particular recording system, the voltage signal is subjected to amplitude distortion so that the recorded amplitude is $f(X)$ instead of X. If this recording system is deployed at both antennas, the cross-correlation function will be given by the expression

$$R(t, \tau_m) = \langle f(X) f(Y) \rangle = \int_{-\infty}^{\infty} \int_{-\infty}^{\infty} f(X) f(Y) P(X, Y) \, dX dY \tag{28}$$

In the case of extreme clipping, we have the distortion function

$$\begin{aligned} f(X) = f_c(X) &= +1, \quad X > 0 \\ &= -1, \quad X < 0 \end{aligned} \tag{29}$$

For this distortion, Eq. (28) may be integrated (Ref. 2) to give the digital cross-correlation function r_c.

$$\begin{aligned} r_c(t, \tau_m) &= \int_{-\infty}^{\infty} \int_{-\infty}^{\infty} f_c(X) f_c(Y) P(X, Y) \, dX dY \\ &= \frac{2}{\pi} \sin^{-1} [r(t, \tau_m)] \end{aligned} \tag{30}$$

Thus, after defining the content, statistics, and normalization of the voltage signals, the derivation of the digital cross-correlation function duplicates the technique employed by Van Vleck and Middleton (Ref. 2). However, in the present work, the correlation functions depend on time in addition to the model delay. The appearance of a time dependence is due to the fact that the VLBI procedure is a cross-correlation process, rather than the autocorrelation process in Ref. 2. Furthermore, the voltage signals and the normalization process involve both the radio signal and the additive noise. Note that this result, Eq. (30), is quite general, since it only assumes that the signals, X and Y, are sums of Gaussian random variables. In particular, the result is valid for both extended sources and point sources.

In particular cases, the digital cross-correlation function assumes a simpler form. First, suppose that the radio signals are very weak ($T_{s_j} << T_j$) or that the correlated flux is very small ($\gamma_v << 1$). (In typical VLBI work, the amplitude of the normalized cross-correlation function falls in the range 0.1 to 0.001.) In either case, the normalized cross-correlation function r is small compared to one, so that Eqs. (22) and (30) give

$$\begin{aligned} r_c(t, \tau_m) &\approx \frac{2}{\pi} r(t, \tau_m) \\ &= \frac{2}{\pi} \gamma_v \sqrt{\frac{T_{s_1} T_{s_2}}{T_1 T_2}} \frac{W_D}{W} \frac{\sin \pi W_D \Delta\tau}{\pi W_D \Delta\tau} \cos \phi_f \end{aligned} \tag{31}$$

Thus, in the case of small correlated amplitude, the normalized digital cross-correlation function is identical to the sinusoidal analog cross-correlation function, except for a loss of $2/\pi$ in amplitude. Schematic examples of the normalized analog and digital cross-correlation functions are shown in Fig. 1a. In this and following examples, we utilize the fact that the fringe frequency $\dot{\phi}_f$ is almost constant over small time intervals.

In the limit of a very strong point source, the system temperature is equal to the signal temperature ($T_j = T_{s_j}$). If, in addition, the bandpass alignment is perfect ($W_D = W$) and the model delay is very accurate ($\Delta\tau << 1/W$), the analog cross-correlation function, Eq. (22), becomes

$$r(t, \tau_m) = \sin \lambda_p \tag{32}$$

where

$$\lambda_p = \frac{\pi}{2} - (\omega_2 - \omega_1) t - \omega_2 \tau_m - \omega_0 \Delta\tau - \phi - \phi_R$$

The normalized digital cross-correlation function for strong signals then becomes

$$\begin{aligned} r_c(t, \tau_m) &= \frac{2}{\pi} \sin^{-1} [r(t, \tau_m)] \\ &= \frac{2}{\pi} \tilde{\lambda}_p \end{aligned} \tag{33}$$

where

$$\tilde{\lambda}_p = \sin^{-1} [\sin \lambda_p] \tag{34}$$

In the expression for $\tilde{\lambda}_p$, the sine inversion ambiguity is uniquely resolved as follows. Since the digital cross-correlation function r_c must be less than one in magnitude, $\tilde{\lambda}_p$ must lie between $-\pi/2$ and $+\pi/2$. Thus, given a value for λ_p, only one value for $\tilde{\lambda}_p$ is less than $\pi/2$ in magnitude and satisfies the equation $\sin \lambda_p = \sin \tilde{\lambda}_p$. A schematic plot of the analog cross-correlation function for a very strong point source is shown in Fig. 2a, while the corresponding digital cross-correlation function is shown in Fig. 3a. Note that the digital cross-correlation function consists of a sawtooth curve rather than the sinusoidal function associated with analog recording. However, the extrema and zero crossings of the digital system occur at the same time points found with the analog system. For this reason, the frequency characteristics of the digital cross-correlation function are the same as those found in the analog case if we neglect harmonics higher than the first.

IV. Signal-to-Noise Analysis

In this section, expressions are derived for the S/N ratios associated with the cross-correlation functions produced by both analog and digital recording systems. This S/N analysis is valid for both point sources and extended sources.

In the case of analog recording, the rms noise on the cross-correlation function is given by the expression

$$\sigma_r^2 = \langle (XY - r)^2 \rangle = \iint (XY - r)^2 P(X, Y)\, dXdY$$

$$= \iint X^2 Y^2 P(X, Y)\, dXdY - r^2 \qquad (35)$$

where $P(X, Y)$ is given by Eq. (27). The last integration is assisted by the transformation

$$X' = X$$

$$Y' = \frac{(Y - rX)}{(1 - r^2)^{1/2}} \qquad (36)$$

which gives

$$\sigma_r = \sqrt{1 + r^2} \qquad (37)$$

In the case of digital recording, the rms noise on the cross-correlation function is given by

$$\sigma_{r_c}^2 = \langle [f_c(X) f_c(Y) - r_c]^2 \rangle$$

$$= \iint [f_c(X) f_c(Y) - r_c]^2 P(X, Y)\, dXdY \qquad (38)$$

which is easily integrated to give

$$\sigma_{r_c} = \sqrt{1 - r_c^2} \qquad (39)$$

The S/N ratio for the analog case is therefore given by the expression

$$\left.\frac{S}{N}\right|_a = \frac{r}{\sigma_r} = \frac{r}{\sqrt{1 + r^2}} \qquad (40)$$

where r is the normalized analog cross-correlation function. For digital recording, the S/N ratio is given by

$$\left.\frac{S}{N}\right|_c = \frac{r_c}{\sigma_{r_c}} = \frac{r_c}{\sqrt{1 - r_c^2}} \qquad (41)$$

where

$$r_c = \frac{2}{\pi} \sin^{-1} r$$

For small correlated amplitude, the S/N ratios assume simple forms. In this limit, we have $r << 1$ and $r_c << 1$, so that

$$\sigma_{r_c} = \sigma_r \approx 1 \qquad (42)$$

and

$$r_c = \frac{2}{\pi} r \qquad (43)$$

The S/N ratios in Eqs. (40) and (41) become

$$\left.\frac{S}{N}\right|_a = r(t, \tau_m) \qquad (44)$$

for analog recording and

$$\left.\frac{S}{N}\right|_c = \frac{2}{\pi} r(t, \tau_m) \qquad (45)$$

for digital recording. Thus, for small correlated amplitude, one would uniformly lose a factor of $2/\pi$ in signal-to-noise by using digital recording instead of analog recording. This fact has been mentioned in various VLBI papers. Schematic examples of the digital and analog cross-correlation functions and their rms noise are shown in Figs. 1a and 1b for the case of small correlated amplitude.

For the case of very strong point radio sources, plots of the cross-correlation function and its rms noise are shown in Fig. 2 for analog recording and in Fig. 3 for digital recording. Note that, for analog recording, the maximum S/N ratio is $1/\sqrt{2}$ due to self-noise. For digital recording, the S/N ratio goes to infinity at time points of maximum correlation. The zero noise at these points may be explained by considering the autocorrelation of infinitely clipped noise. When the autocorrelation signals are perfectly aligned ($\tau = 0$), the product of the clipped voltages is always $+1$ [$(+1)(+1)$ or $(-1)(-1)$] with no noise. At points of weak correlation, the digital S/N is $2/\pi$ smaller than the analog S/N.

V. Summary

The analog cross-correlation function is normalized and expressed in terms of noise temperature, fringe visibility, and bandpass overlap for rectangular filters.

By defining the content, statistics, and normalization of the VLBI signals, the Van Vleck derivation is used to determine the digital cross-correlation function in terms of the normalized analog cross-correlation function. For very strong point sources, a digital recording system generates a sawtooth cross-correlation function in place of the sinusoidal function produced by an analog system. For small correlated amplitude, the digital cross-correlation function is identical to the normalized analog cross-correlation function, except for a loss of $2/\pi$ in amplitude.

General expressions for signal-to-noise ratios are derived for the analog and digital cross-correlation functions. When a very strong point source is recorded with a digital system, the S/N ratio is infinite at time points of maximum correlation, while, at points of weak correlation, the S/N ratio is $2/\pi$ smaller than that for the analog case. In addition, the S/N ratio for an analog system is, at most, only $1/\sqrt{2}$ due to self-noise. For small correlated amplitude, the S/N ratio for a digital system is uniformly $2/\pi$ smaller than the analog S/N ratio.

References

1. Thomas, J. B., "An Analysis of Long Baseline Radio Interferometry," *The Deep Space Network: Progress Report for November and December 1971*, Technical Report 32-1526, Vol. VII, pp. 37–50. Jet Propulsion Laboratory, Pasadena, Calif., Feb. 15, 1972.
2. Van Vleck, J. H., and Middleton, D., "The Spectrum of Clipped Noise," *Proc. IEEE*, Vol. 54, No. 1, 1966.
3. Kraus, J. D., *Radio Astronomy*. McGraw-Hill, New York, 1966.

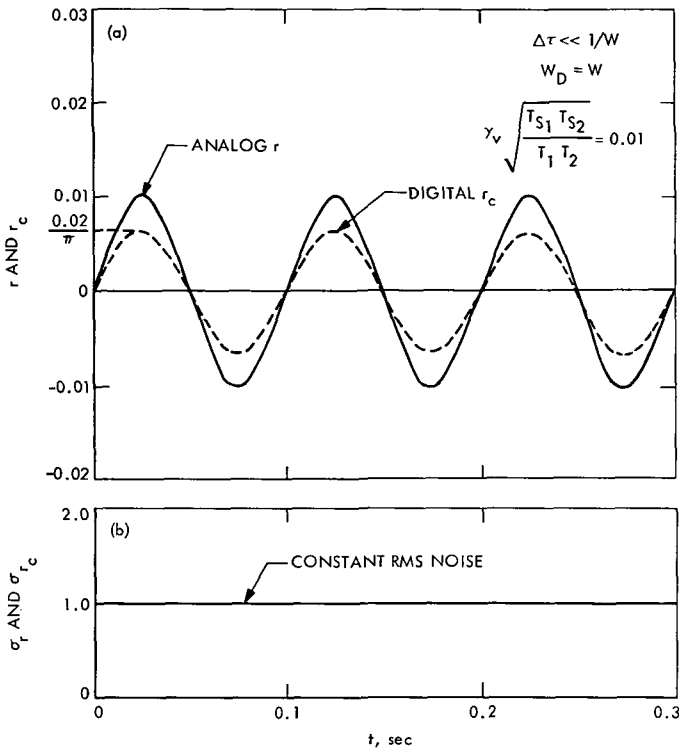

Fig. 1. (a) Normalized analog and digital cross-correlation functions for the case of small correlated amplitude, (b) rms noise on cross-correlation functions of (a)

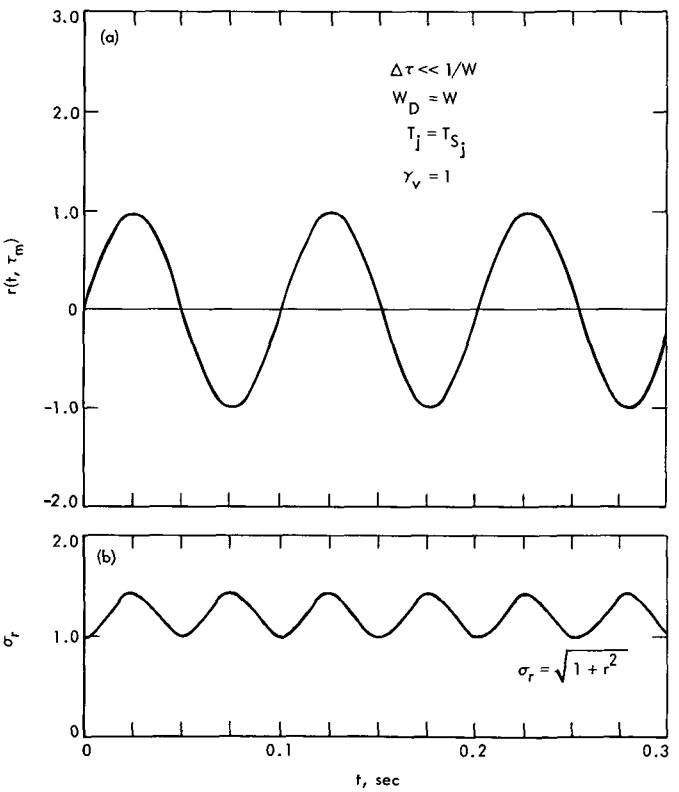

Fig. 2. (a) Normalized analog cross-correlation function for a very strong point source, (b) rms noise on cross-correlation function of (a)

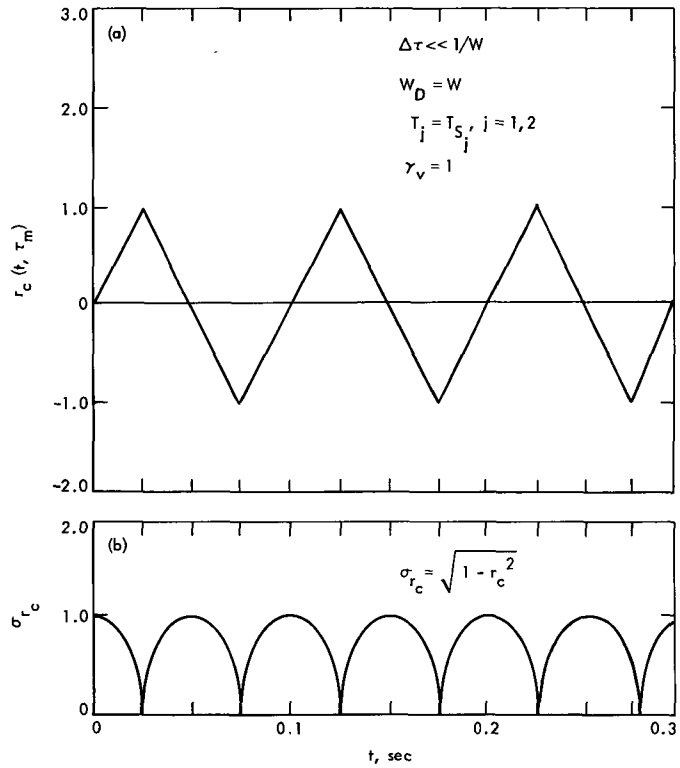

Fig. 3. (a) Normalized digital cross-correlation function for a very strong point source, (b) rms noise on cross-correlation function of (a)

The Translation of the Tropospheric Zenith Range Effect From a Radiosonde Balloon Site to a Tracking Station

K. L. Thuleen and V. J. Ondrasik
Tracking and Orbit Determination Section

The temporal behavior of the wet tropospheric zenith range effect, $\Delta\rho_z(w)$, over the radiosonde balloon sites at Edwards AFB and Yucca Flats, Nevada, was compared. The $\Delta\rho_z(w)$ over the balloon site may be translated to a nearby tracking station for use in performing tropospheric navigational error analysis studies and for developing models, incorporating seasonal variations, to be used for the tropospheric calibration of radio metric data. The daily variations in $\Delta\rho_z(w)$ appear to prohibit the use of radiosonde balloon data for the daily calibration of radio metric data.

I. Introduction

One of the error sources which corrupts range and doppler data, and thereby degrades navigational capabilities, is the troposphere. To determine the amount of this tropospheric-induced degradation, and also to improve the tropospheric model used for calibrations, it is very valuable to examine the temporal behavior of the tropospheric zenith range effect, $\Delta\rho_z$. References 1 and 2 examined the variability of $\Delta\rho_z$ throughout 1967 and 1968 by using radiosonde balloon data obtained from the radiosonde balloon site closest to each tracking station complex. Implicit in these studies was the assumption that the behavior of $\Delta\rho_z$ over the radiosonde balloon site is representative of the $\Delta\rho_z$ behavior over the tracking station. This article attempts to evaluate this assumption by comparing the behavior of $\Delta\rho_z$ over Yucca Flats, Nevada, and over Edwards AFB, California, during 1967. These two radiosonde balloon sites were chosen because the Goldstone tracking complex lies between them, as shown in Fig. 1. The comparison of the Yucca Flats- and Edwards AFB-generated values of $\Delta\rho_z$ shows that the gross features of the time behavior of $\Delta\rho_z$ may be translated from one station to the other for use in accuracy analysis studies or in the development of a tropospheric model involving seasonal variations as described in Ref. 2. Unfortunately the comparison also seems to show that the behavior of $\Delta\rho_z$ over the two sites is different enough to prevent use of the data gathered at a radiosonde balloon site to make daily calibrations of the radio metric data.

II. Zenith Range Effect

Using the methods described in Ref. 1, the tropospheric zenith range effect can be computed from atmospheric pressure, temperature, and humidity data obtained from radiosonde balloon measurements. The total tropospheric range effect $\Delta\rho_z$ is the sum of a dry portion, $\Delta\rho_z(d)$, and

a wet portion, $\Delta\rho_z(w)$. Since the dry portion can be computed very accurately (1%) from surface pressure measurements, only the results involving $\Delta\rho_z(w)$ will be considered.

The radiosonde balloon data used in this study was obtained with the help of Mr. Richard Davis and Mr. Larry Snelson of the National Climatic Center in Asheville, North Carolina, and Capt. George Frederick, USAF.

Figure 2 shows the behavior of $\Delta\rho_z(w)$ over Edwards AFB during 1967 and over Yucca Flats for the first nine months of 1967 computed from radiosonde balloon data which went up to 24,384 m (80,000 ft). The last three months of the Yucca Flats' $\Delta\rho_z(w)$ in Fig. 2 was computed from radiosonde balloon data which went up to 6096 m (20,000 ft) and the wet model described in Ref. 2. To ease the comparison of the gross features of the time behavior of $\Delta\rho_z(w)$ over Edwards AFB and Yucca Flats, the monthly averages and standard deviations, σ, were computed and are shown in Fig. 3. For convenience the Edwards AFB and Yucca Flats monthly averages are overlaid in Fig. 4. An examination of Figs. 2, 3, and 4 shows that the gross time behavior of $\Delta\rho_z(w)$ computed from the Edwards AFB data is very similar to the same quantity computed from the Yucca Flats data. For example, the standard deviation of the difference between the Edwards AFB and Yucca Flats monthly averages of $\Delta\rho_z$ is only 1½ cm. Using the procedure described in Ref. 1, this number can be shown to give an equivalent error in the distance of the tracking station off the spin axis of 8 cm.

Because the time behavior of $\Delta\rho_z(w)$ is grossly the same for the two stations, it appears that radiosonde data taken from a nearby balloon site may be successfully used to perform the following two tasks:

(1) Determine spacecraft navigational errors generated by variations in the tropospheric zenith range effect and refractivity profile (see Ref. 3).

(2) Develop tropospheric models, which incorporate seasonal trends, to calibrate radio metric data.

In an attempt to determine the fine structure similarity of the temporal behavior of $\Delta\rho_z$, the Edwards AFB and Yucca Flats values are overlaid for the months of July and August in Fig. 5. It is difficult to obtain a measure of how much the daily variations in $\Delta\rho_z(w)$ at Yucca Flats reflect the daily variations in $\Delta\rho_z(w)$ at Edwards AFB, and vice versa, because the measurements were generally not made at the same time of day. However, at first glance, it appears that the differences between the Edwards AFB and Yucca Flats values of $\Delta\rho_z(w)$, at nearly the same time, appear to be approximately the same size as the variation of $\Delta\rho_z(w)$ about its monthly average. If this is generally true, it will not be advantageous to use data taken from radiosonde balloon sites to make daily tropospheric calibrations of the radio metric data.

III. Summary and Conclusions

The temporal behavior of the wet zenith range effect, $\Delta\rho_z(w)$, over the radiosonde balloon sites at Edwards AFB and Yucca Flats, Nevada, were compared during 1967. The gross behavior of $\Delta\rho_z(w)$ over the two sites is very similar. This similarity enables the radiosonde balloon data to be used effectively in performing tropospheric navigational error analysis studies and developing models, incorporating seasonal variations, to be used to make tropospheric calibrations of radio data. Unfortunately, it appears that the daily variations in $\Delta\rho_z(w)$ are such that they cannot be translated from the balloon site to the tracking station for the daily calibration of radio metric data.

This study suffers from the fact that only 1967 data for Edwards AFB and Yucca Flats have been examined. It is doubtful that an examination of data obtained during different years or from different stations would modify the conclusions which have been stated regarding the gross features of the temporal behavior of $\Delta\rho_z(w)$. However, if the question of using radiosonde balloon data to make daily calibrations of radio metric data is being addressed, it will be necessary to make use of data taken from other balloon sites, and for different years.

References

1. Ondrasik, V. J., and Thuleen, K. L., "Variations in the Zenith Tropospheric Range Effect Computed From Radiosonde Balloon Data," in *The Deep Space Network*, Space Programs Summary 37-65, Vol. II, pp. 25–35. Jet Propulsion Laboratory, Pasadena, Calif., Sept. 30, 1970.

2. Thuleen, K. L., and Ondrasik, V. J., "The Repetition of Seasonal Variations in the Tropospheric Zenith Range Effect," in *The Deep Space Network Progress Report*, Technical Report 32-1526, Vol. VI, pp. 83–98. Jet Propulsion Laboratory, Pasadena, Calif., Dec. 15, 1971.

3. Miller, L. F., Ondrasik, V. J., and Chao, C. C., "A Cursory Examination of the Sensitivity of the Tropospheric Range and Doppler Effects to the Shape of the Refractivity Profile," in *The Deep Space Network Progress Report*, Technical Report 32-1526, Vol. I, pp. 22–30. Jet Propulsion Laboratory, Pasadena, Calif., Feb. 15, 1971.

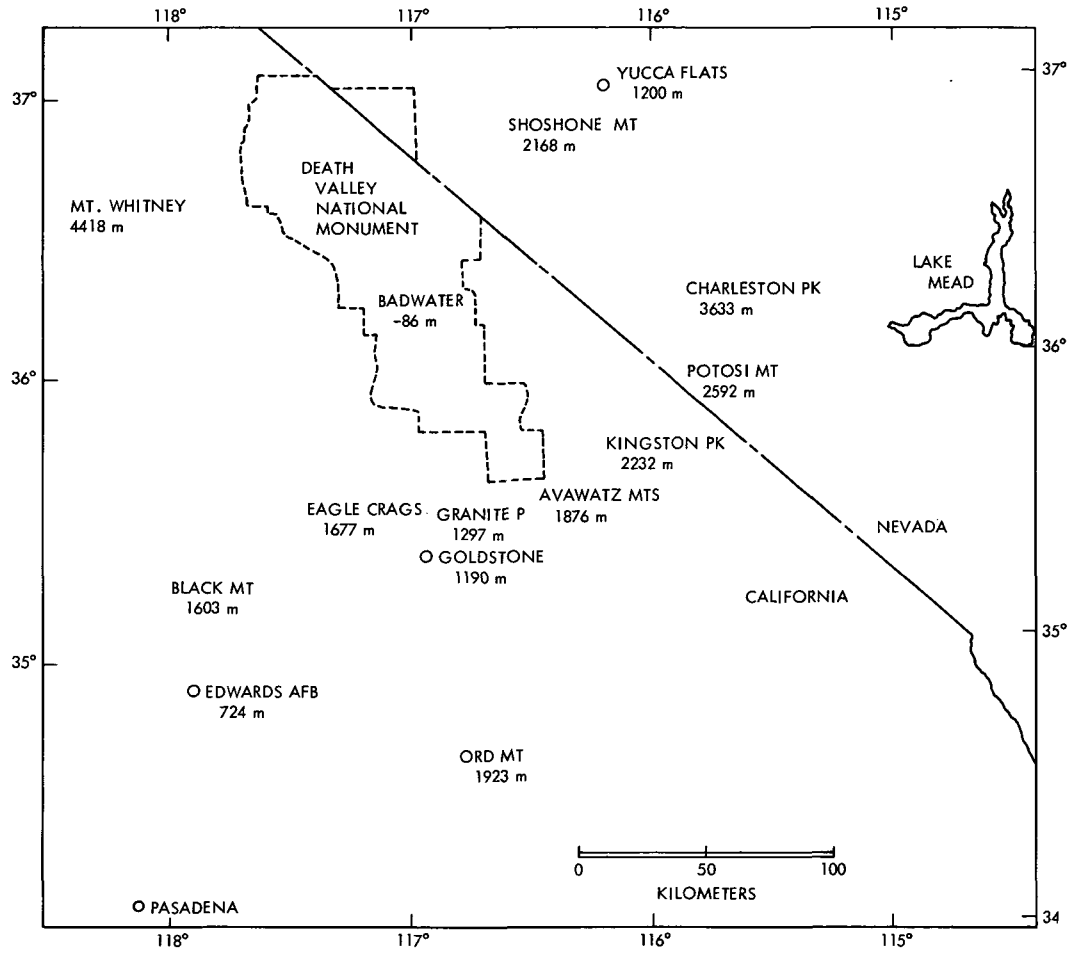

Fig. 1. Relative locations of Edwards AFB, Goldstone, and Yucca Flats

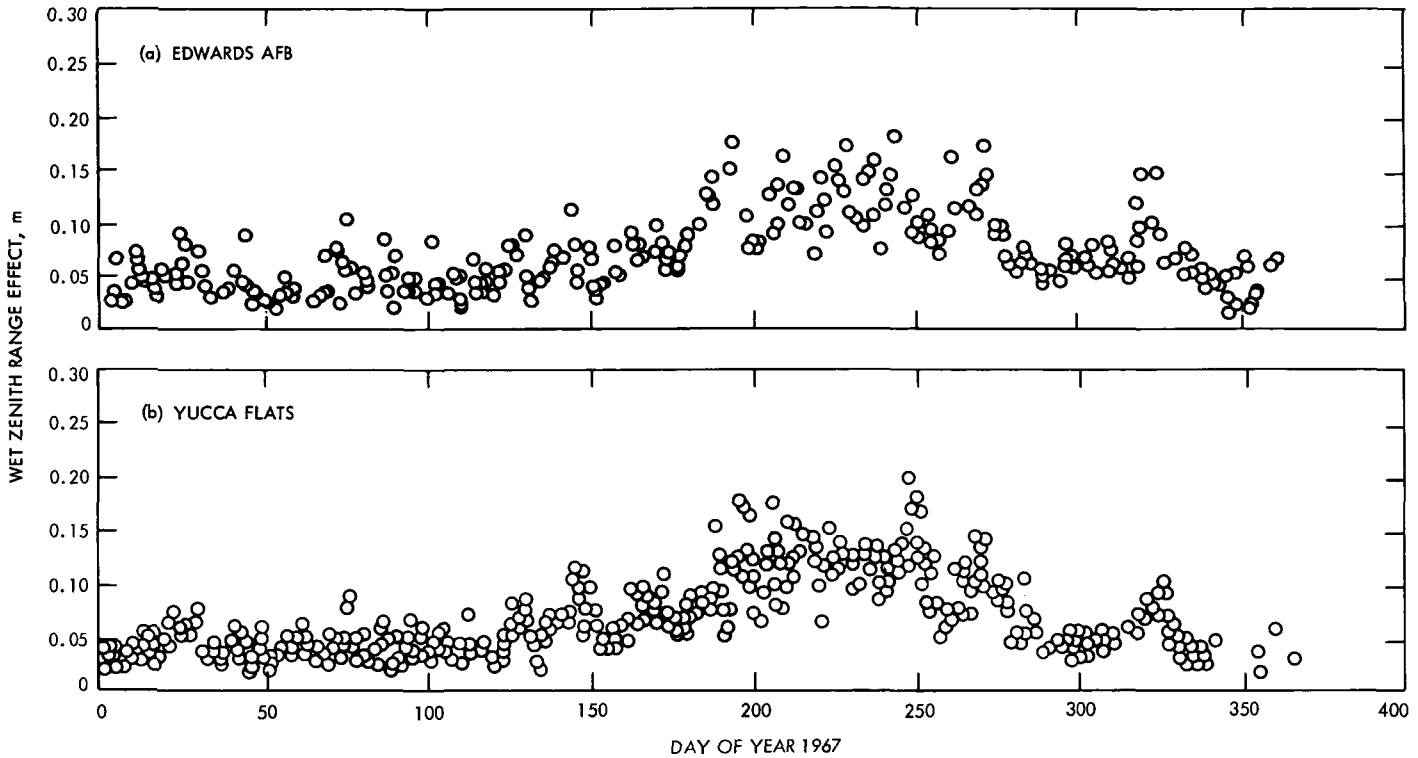

Fig. 2. Wet zenith range effect over Edwards AFB and Yucca Flats during 1967

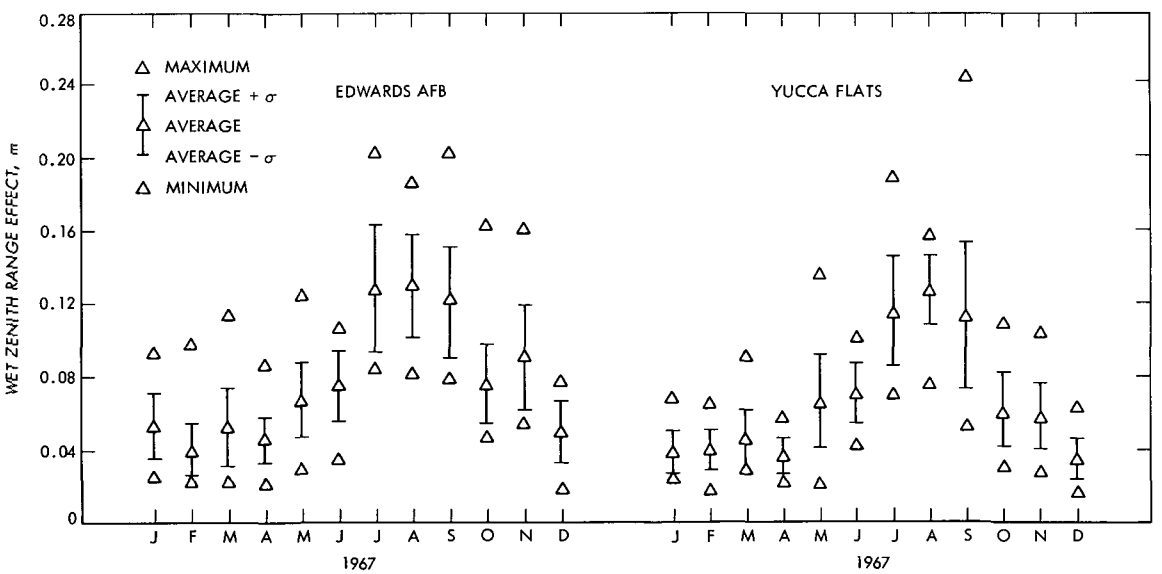

Fig. 3. Monthly averages and standard deviations of wet zenith range effects over Edwards AFB and Yucca Flats during 1967

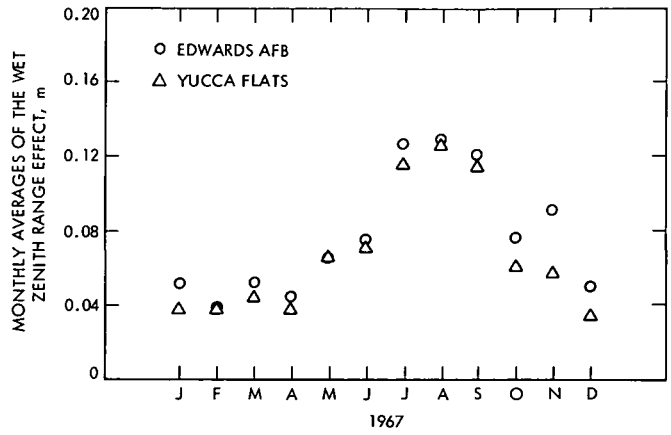

Fig. 4. Comparison of the Edwards AFB and Yucca Flats monthly averages of the wet zenith range effect during 1967

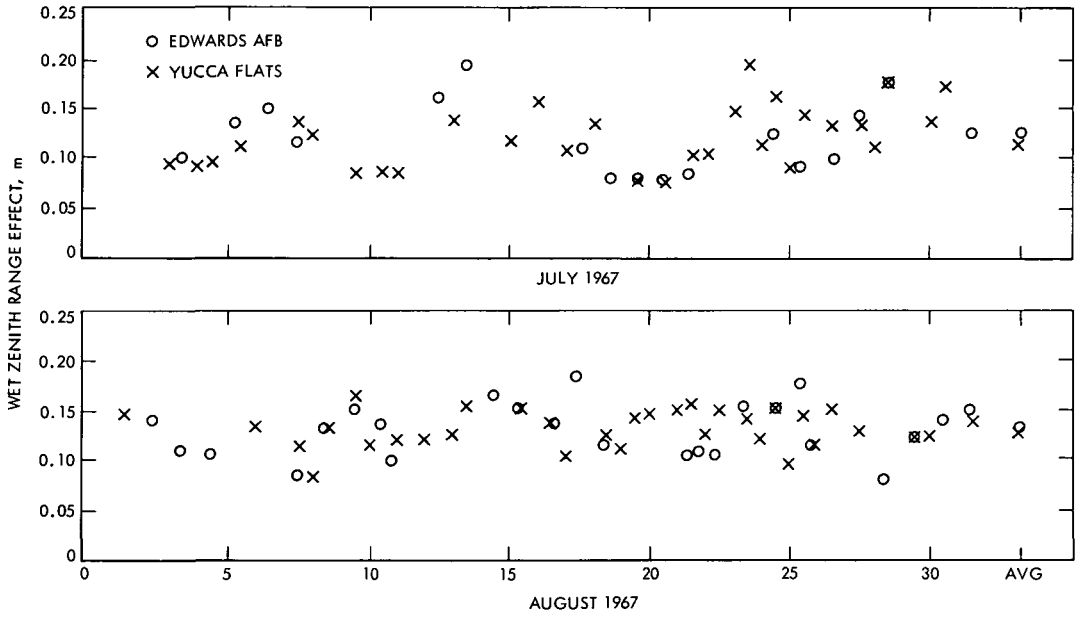

Fig. 5. Wet zenith range effect over Edwards AFB and Yucca Flats during July and August 1967

On Modeling Continuous Accelerations as Piecewise Constant Functions

R. K. Russell and D. W. Curkendall
Tracking and Orbit Determination Section

Random, non-gravitational forces acting on the spacecraft in an unpredictable manner have long been identified as a major limitation in using DSN radio data to deduce the state of the spacecraft and predict its subsequent motion. An important aspect of properly handling the non-gravitational forces is determining when their presence affects the data to an extent and in a manner that cannot be modeled accurately within the limitations of the batch filtering orbit determination procedures. This is relevant in its own right but is also important in regard to the proper configuration of the operational sequential filters. The design of these filters is such that the data is segregated into a series of batches. Between batches, stochastic elements are assumed to enter, and any or all of the parameters subject to solution can change at that time. Within any one batch, however, every parameter is assumed constant, and, within that batch, the data is treated exactly as it is treated in the classical least squares problem. In the limit as batch size reduces to a single data point, this machinery becomes identical to the point sequential filter widely discussed in the literature. To reduce the computational complexity of the operational sequential filters, however, it is desirable to keep the batch sizes as large as possible. Determining this bound in the presence of what is viewed as a continuously varying force model becomes the focus of this article.

I. Introduction

Random, non-gravitational forces acting on the spacecraft in an unpredictable manner have long been identified as a major limitation in using DSN radio data to deduce the state of the spacecraft and predict its subsequent motion (Refs. 1 and 2). Two major approaches have evolved for reducing the accuracy penalty paid for a given level of uncalibrated force involvement:

(1) Employ the net in a dual station tracking mode, taking two- and three-way doppler simultaneously. By explicitly differencing the simultaneous data, the geocentric spacecraft motion, which includes the effects of the forces and is common to both data points being received, is removed. If the stations are separated adequately, the difference of the two topocentric motions, which does not involve the random forces, is significant and can be used to determine the position of the probe. This notion of obtaining what has been termed quasi very long baseline interferometry (QVLBI) data is treated extensively by Ondrasik and Rourke (Refs. 3 and 4).

(2) Model the forces as a formal stochastic process and include this model explicitly in the filtering equations used for data processing; i.e., employ some sort of sequential filter.

These approaches are by no means mutually exclusive. In many applications, the explicit differencing operation mentioned may incur too severe a penalty in itself, because by so doing, the information inherent in the probe's geocentric motion is irretrievably lost. The existence of these forces, especially when they are present at the low levels achievable with current generation ballistic spacecraft ($<10^{-9}$ m/s^2), "clouds" the geocentric information. It does not, however, obliterate it. We are hopeful that the combination of taking simultaneous two- and three-way data and presenting these data to a sequential filter which adequately models the spacecraft forces will:

(1) Permit the inherent benefits of the QVLBI data just described to be obtained.

(2) Simultaneously enable a rather accurate reconstruction of the clouding force profile, which in turn permits the orbit determination process to capitalize on the information inherent in the long arc behavior of the probe.

An important aspect of properly handling the non-gravitational forces is determining when their presence affects the data to an extent and in a manner that cannot be modeled accurately within the limitations of the batch filtering orbit determination procedures. This is relevant in its own right but is also important in regard to the proper configuration of the operational sequential filters. The design of these filters (Ref. 5) is such that the data is segregated into a series of batches. Between batches, stochastic elements are assumed to enter and any or all of the parameters subject to solution can change at that time. Within any one batch, however, every parameter is assumed constant and, within that batch, the data is treated exactly as it is treated in the classical least squares problem. In the limit as batch size reduces to a single data point, this machinery becomes identical to the point sequential filter widely discussed in the literature (see, for example, Ref. 6, Chapter 12).

To reduce the computational complexity of the operational sequential filters, however, it is desirable to keep the batch sizes as large as possible. Determining this bound in the presence of what is viewed as a continuously varying force model becomes the focus of this article. The problem is illustrated in Fig. 1, which shows a continuously varying acceleration record along with a piecewise constant representation of that function. As shown, the approximation $\hat{a}$ is allowed to change its value once every time unit. Whether this is appropriate must await a quantitative criterion.

II. Analysis

In order to create the needed criterion, Fig. 2a shows an expanded version of the first portion of the acceleration function of Fig. 1. This time we inspect the adequacy of a single, constant representation of this portion of the wave. Since the primary damage done by the stochastic forces is caused by the effects on the data (rather than direct changes of the spacecraft state) and a primary data type is doppler, it is natural to focus on the ability of the constant acceleration to produce a model velocity which tracks the actual velocity being induced. This is shown in Fig. 2b. We suggest the following criterion:

> The interval chosen over which to hold the acceleration constant should be small enough so that the rms velocity departure between the actual and resulting modeled velocity can be kept to 10^{-5} m/s or smaller.

The numerical value chosen in this criterion is the same used throughout the formulation of the Orbit Determination Program; i.e., the software model should be accurate enough to model the doppler observables to the 10^{-5} m/s accuracy level. Stated mathematically, the mean squared residual, SOS, is

$$\mathrm{SOS} = \frac{1}{T}\int_0^T [v(t) - \hat{a}t]^2\, dt \tag{1}$$

In order to minimize Eq. (1), the following condition must be satisfied:

$$\frac{\partial \mathrm{SOS}}{\partial a} = \frac{1}{T}\int_0^T 2\,[v(t) - \hat{a}t]\,[-t]\, dt = 0 \tag{2}$$

which implies

$$\hat{a} = \frac{3}{T^3}\int_0^T tv(t)\, dt \tag{3}$$

The interval T must be chosen without specific knowledge of what $v(t)$ really is. The best that can be hoped for is that a reasonable *a priori* model of the random process for the non-gravitational forces can be obtained. The numerical criterion must be viewed with respect to the average SOS obtained from all possible acceleration functions drawn from the population of the process. Assume

that the process is stationary, exponentially correlated with known standard deviation σ_a and correlation time τ. That is,

$$E[a(t_1)\,a(t_2)] = \sigma_a^2 e^{-|t_1-t_2|/\tau} \tag{4}$$

The statistical description of the related velocity process,

$$v(t) = \int_0^t a(\rho)\,d\rho$$

is therefore

$$E[v(t_1)\,v(t_2)] = \int_0^{t_1}\int_0^{t_2} \sigma_a^2 e^{-|\rho-\eta|/\tau}\,d\rho\,d\eta \tag{5}$$

which can be integrated to yield

$$E[v(t_1)\,v(t_2)] = \begin{cases} \sigma_a^2\tau^2\left[\left(2\dfrac{t_2}{\tau}-1\right) + e^{-t_1/\tau} + e^{-t_2/\tau} - e^{-(t_1-t_2)/\tau}\right]; & t_2 \leq t_1 \\ \sigma_a^2\tau^2\left[\left(2\dfrac{t_1}{\tau}-1\right) + e^{-t_1/\tau} + e^{-t_2/\tau} - e^{-(t_2-t_1)/\tau}\right]; & t_1 \leq t_2 \end{cases} \tag{6}$$

Using Eq. (3), the expected value of the (minimum) SOS can be written

$$E[\mathrm{SOS}] = E\left[\frac{1}{T}\int_0^T v^2(t)\,dt - \frac{3}{T^4}\int_0^T\int_0^T v(\rho)\,v(\eta)\,\rho\eta\,d\rho\,d\eta\right] \tag{7}$$

After substitution of Eq. (6) into Eq. (7) and laborious algebraic detail, Eq. (7) can be shown to be

$$E[\mathrm{SOS}] = \frac{\sigma_a^2\tau}{T}\left[\left\{4\tau^2 - \frac{5}{4}\tau T + \frac{T^2}{5} + \frac{6\tau^5}{T^3} - \frac{6\tau^3}{T}\right\} + \left\{\tau^2 - \frac{6\tau^5}{T^3} - \frac{6\tau^4}{T^2} + \frac{3\tau^3}{T}\right\} e^{-T/\tau}\right] \tag{8}$$

Letting $\alpha = \tau/T$, this equation may be rewritten as

$$E[\mathrm{SOS}] = \sigma_a^2\tau T\left[\left\{6\alpha^5 - 6\alpha^3 + 4\alpha^2 - \frac{5}{4}\alpha + \frac{1}{5}\right\} - \alpha^2\{6\alpha^3 + 6\alpha^2 - 3\alpha - 1\}\,e^{-1/\alpha}\right] \tag{9}$$

If $T >> \tau$, then Eq. (9) reduces to

$$E[\mathrm{SOS}] \simeq \sigma_a^2\frac{\tau T}{5}; \qquad (\alpha \text{ small}) \tag{10}$$

If $\tau > T$, then Eq. (9) becomes a very poor way to compute $E[\mathrm{SOS}]$ as it is extremely ill-conditioned. If the exponential in Eq. (9) is expanded through eighth order and terms are grouped appropriately, it can be reduced to

$$E[\mathrm{SOS}] \simeq \sigma_a^2\frac{T^3}{\tau}\left[\frac{1}{105} - \frac{1}{320\alpha} + \frac{1}{1512\alpha^2} + 0\left(\frac{1}{\alpha^3}\right)\right]; \qquad (\alpha \text{ large}) \tag{11}$$

which is very well-conditioned for $\tau > T$.

From formulas (10) and (11), it can be seen that

(1) $E[\mathrm{SOS}] \to 0$ as $\tau \to \infty$

(2) $E[\mathrm{SOS}] \to 0$ as $\tau \to 0$

This behavior is entirely reasonable due to the fact that

(1) As $\tau \to \infty$, the acceleration process becomes a bias for which the non-stochastic model can effectively track.

(2) As $\tau \to 0$, the $E[v^2(t)] \to 0$ (see Eq. 6) which implies that the velocity error due to such an acceleration process vanishes as the correlation time goes to zero.

III. Results

To observe the behavior of the expected value of the normalized sum of squares, a few details are required. First, the size of σ_a is needed. For typical missions this may be assumed to be

$$\sigma_a = 10^{-12}\ \mathrm{km/s^2} = 10^{-9}\ \mathrm{m/s^2} \tag{12}$$

Secondly, in order to scale the results in a meaningful way, it is desirable that the residual error due to the

modeling be less than our stated criterion of 10^{-5} m/s. Denoting this value as e_0, let

$$\sigma_{a_s} = \frac{\sigma_a}{e_0} \tag{13}$$

In this case the scaled σ_a, σ_{a_s} will be

$$\sigma_{a_s} = 10^{-4}/s \tag{14}$$

Using this value for σ_a in formulas (9) and (11) results in E [SOS] being a dimensionless quantity, which should be less than unity if the above criterion of error is to be met. Figure 3 displays the square root of E [SOS] as a function of the correlation time τ for a family of values of the batch size T. Examination of this figure shows that if τ were equal to 5 days, as a typical example, then the batch size T would have to be 2 days or less to meet the error criterion. This also implies that a strict batch filter would begin to experience some difficulty after processing this amount of data. If, however, τ were 50 days, then T could at most be 4 days, which is somewhat surprising. This tends to indicate that the general rule-of-thumb procedure of having the batch size be some fixed fraction of the correlation time (such as 1/3) is not at all valid for a large range of values of τ.

Figure 4 displays the same information as Fig. 3; however, here the square root of E [SOS] is shown as a function of T for a family of values of τ.

As an example of how to use the charts for other circumstances, suppose the random acceleration magnitude was characteristic of solar electric missions, that is, was three orders of magnitude larger than the assumed ballistic levels of 10^{-9} m/s^2. In this case the unity level of the $\sqrt{E\,[\mathrm{SOS}]}$ would move downward 3 cycles, or reside at the bottom of the chart. Extrapolating the $\tau = 2d$ curve of Fig. 4 backwards yields that the intersection with the abscissa occurs at approximately $T = 20$ min.

The results of this analysis, displayed in these figures, should prove to be a useful aid in determining optimal batch sizes when some idea of the correlation time and error bound exists.

It should be mentioned, however, that this analysis is presented under the assumption of a single batch. The analysis for multiple batches proved far too formidable to complete. It is felt, however, that the single batch analysis should give sufficiently accurate results to serve as a useful guide.

References

1. Curkendall, D. W., et al., "The Effects of Random Accelerations on Estimation Accuracy with Applications to the Mariner 1969 Relativity Experiment," *Proceedings of the Conference on Experimental Tests of Gravitation Theories*, California Institute of Technology, Pasadena, California, November 11–13, 1970.

2. Gordon, H. J., et al., *The Mariner VI and VII Flight Paths and Their Determination from Tracking Data*, Technical Memorandum 33-469, Section II-B-6. Jet Propulsion Laboratory, Pasadena, Calif., Dec. 1, 1970.

3. Ondrasik, V. J., and Rourke, K. H., "Application of New Radio Tracking Data Types to Critical Spacecraft Navigation Problems," in *JPL Quarterly Technical Review*, Vol. 1, No. 4, pp. 116–132. Jet Propulsion Laboratory, Pasadena, Calif., Jan. 1972.

4. Rourke, K. H., and Ondrasik, V. J., "Improved Navigation Capability Utilizing Two-Station Tracking Techniques for a Low-Declination Distant Spacecraft," in *The Deep Space Network Progress Report*, Technical Report 32-1526, Vol. VII, pp. 51–60. Jet Propulsion Laboratory, Pasadena, Calif., Feb. 15, 1972.

5. Jordan, J. F., and Boggs, D., *Formulas for the Implementation of the Forward Batch-Sequential Square-Root Filter in the SATODP*, TM 391-142, Dec. 8, 1970 (JPL internal document).

6. Bryson, A. E., and Ho, Y., *Applied Optimal Control.* Blaisdell Publishing Company, Waltham, Mass., 1969.

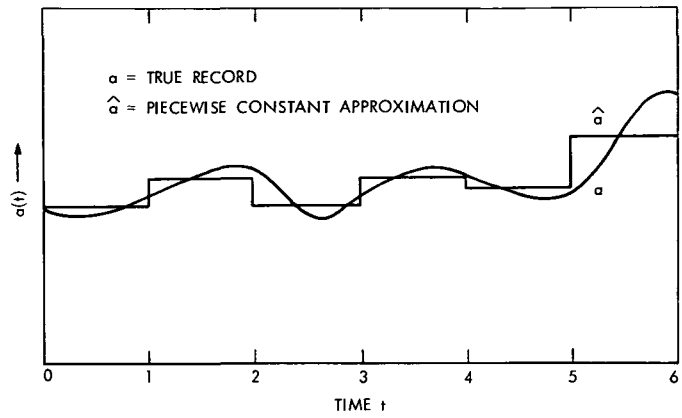

Fig. 1. Modeling a continuous record with a piecewise constant

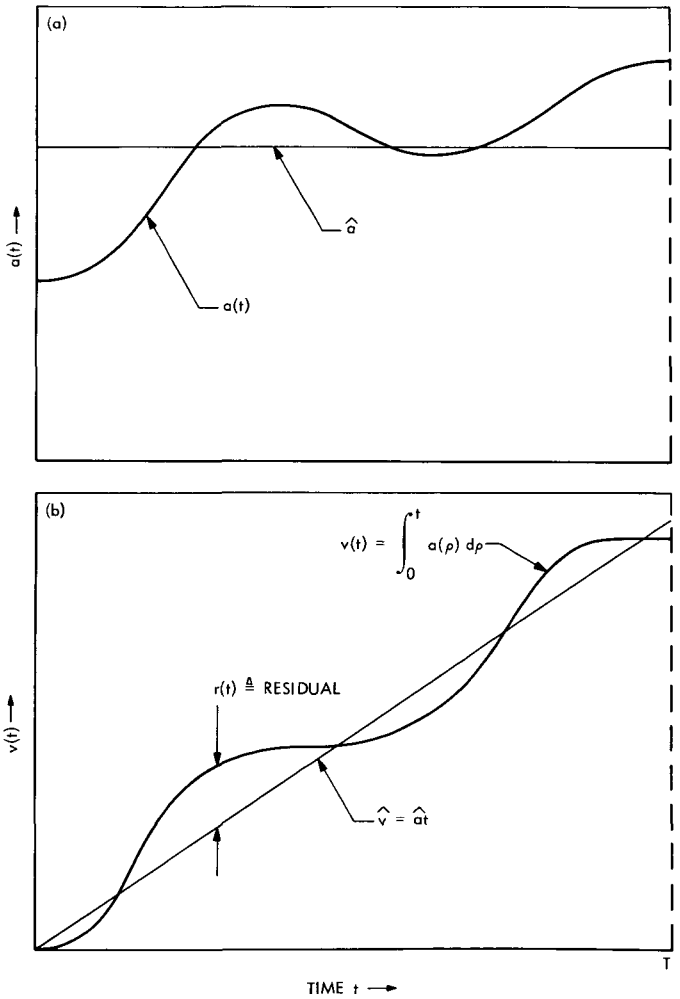

Fig. 2. First interval of Fig. 1 with velocity coordinate also displayed

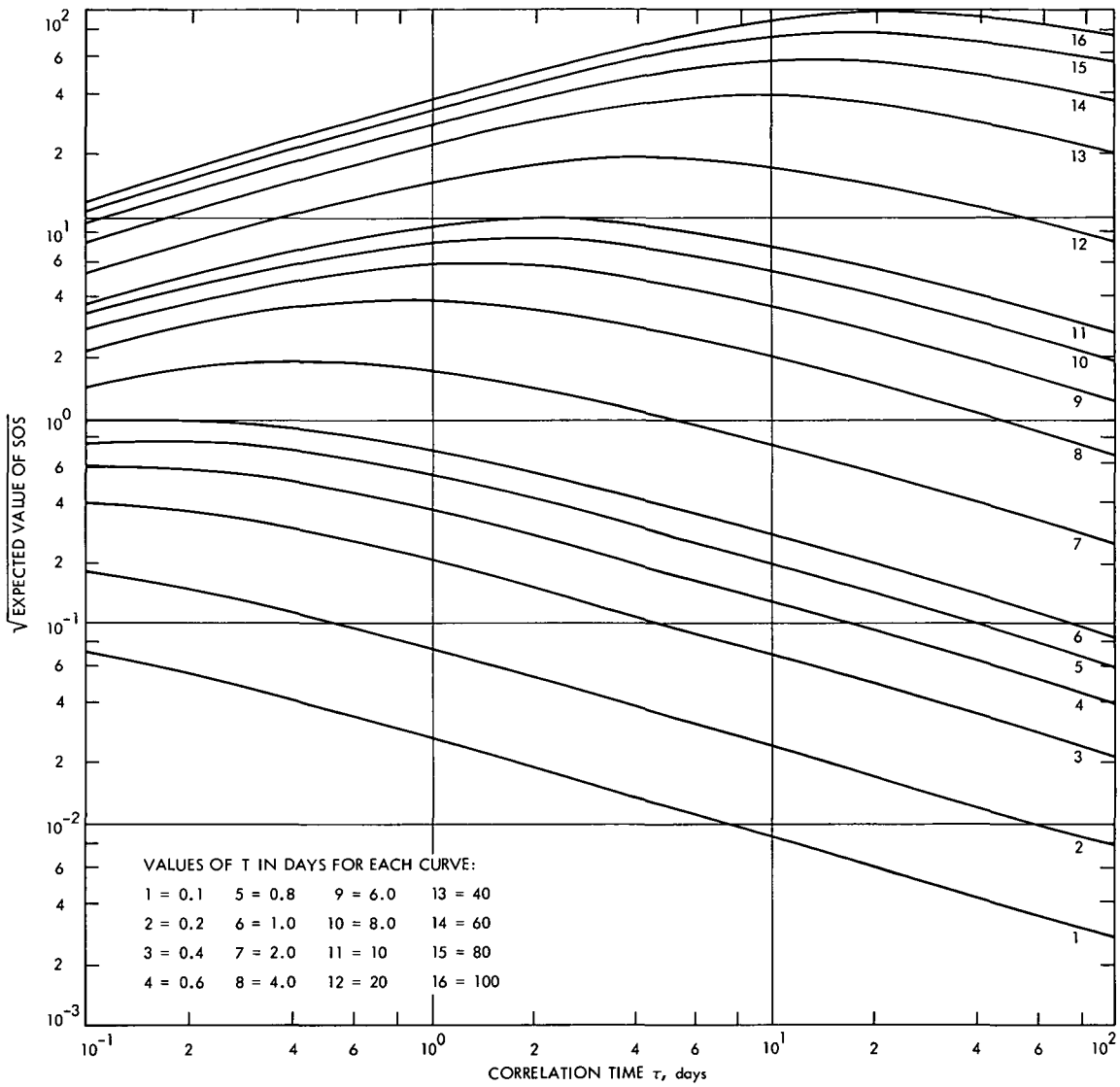

Fig. 3. The square root of *E* [SOS] as a function of correlation time for various batch sizes

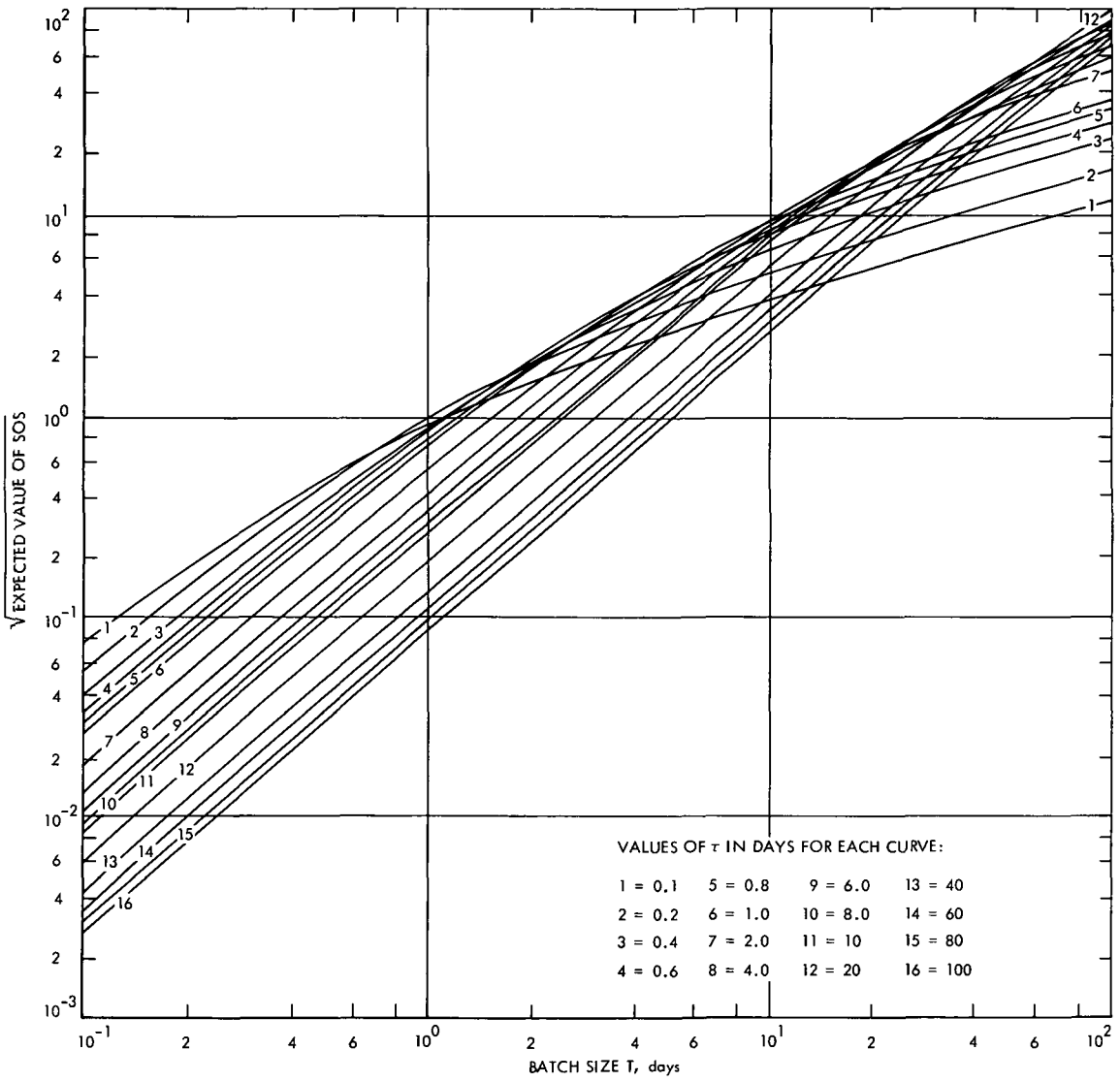

Fig. 4. The square root of *E* [SOS] as a function of batch size for various correlation times

S- and X-Band RF Feed System

P. D. Potter
Communications Elements Research Section

To support the Mariner 1973 X-band experiment, it will be necessary to implement a dual-frequency microwave feed system for the DSS 14 64-m antenna. This system must be capable of simultaneous low noise reception at S- and X-bands and high power transmission at S-band. To fulfill this requirement, a particularly attractive approach, the reflex feed system, is being implemented. The system makes simultaneous use of both an X-band feedcone and one of the S-band feedcones. By a system of two reflectors, one of which is dichroic, the effective S-band phase center is translated from its normal position in the S-band feedhorn to a new point which very nearly coincides with the X-band feedhorn phase center. Thus, during simultaneous S- and X-band operation, the antenna subreflector optics are aligned with the X-band feedcone position. This article describes the analytical techniques used to design and analyze the feed system, as well as preliminary results from scale model tests.

I. Introduction

A cross-sectional view of the reflex feed system[1] geometry is shown to scale in Fig. 1. The system is comprised of four basic components: the S-band feedhorn centrally located in its feedcone, an ellipsoidal reflector, a planar dichroic reflector, and the X-band feedhorn centrally located in its feedcone. By reciprocity, the operation of the reflex feed is the same in the receiving mode as in the transmitting mode; for simplicity, Fig. 1 shows only the transmitting mode. For S-band operation, from a geometrical optics standpoint, radiated energy from one of the ellipsoid foci f_1 is focused to the point f_2. As shown in Fig. 1, however, the system is not large compared to a wavelength. Because of this consideration and the fact that the S-band feedhorn does not represent a point source, the radiated energy from the ellipsoid is actually found to focus to a small region centered at the point C. This energy is then redirected by the planar reflector to the antenna subreflector. By the principle of images, this redirected radiation appears to emanate from the point F_X, which is the far-field phase center of the X-band feedhorn and also coincides with one of the subreflector foci. To permit simultaneous X-band operation, the central region of the planar reflector is perforated with an array of X-band slots, thereby making the reflector essentially transparent to X-band but reflective to S-band.

A preliminary design for the dichroic plate has been extensively tested and previously described (Ref. 2). Although this design has acceptable performance, a continuing effort is in progress to study the S- and X-band performance as a function of the plate thickness and the detailed slot design.

[1]A brief description of the reflex feed system is given in Ref. 1.

II. Analytical Techniques Used for Design and Analysis

An existing scattering program (Ref. 3) was modified[2] to accept general quadratic scattering surfaces and was utilized to calculate the far-field radiation patterns of the S-band horn and ellipsoidal reflector combination. This program was thus used to study and optimize the ellipsoid geometry in order to produce a scattered radiation pattern very similar to the radiation pattern of the horn by itself. The horn pattern has been previously optimized for correct subreflector illumination. The phase of the ellipsoid scattered fields was used to locate the point C (Fig. 1) for a practical overall geometry.

Unlike present and past DSS 14 feed systems, the reflex feed does not have physical rotational symmetry about the axis of symmetry of the antenna subreflector. For this reason, the reflex feed radiation pattern does not exhibit the high level of pattern symmetry which the horns have. To investigate the magnitude of the resulting antenna gain degradation due to this effect, spherical wave techniques were utilized. In the spherical wave method, a radiation pattern is expanded in a series of orthogonal waves which have a known mathematical dependence on the polar angle θ, the azimuthal angle ϕ and the radius R. The details of spherical wave analysis are well documented in the literature (Refs. 3, 4, and 5) and will not be repeated here.

The azimuthal dependence of the feed radiation is represented as a Fourier series as follows:

$$E_\theta(\theta,\phi,R) = \sum_{m=1}^{M} E_{\theta me}(\theta,R)\sin(m\phi) \quad \text{(EVEN)} + \sum_{m=0}^{M} E_{\theta mo}(\theta,R)\cos(m\phi) \quad \text{(ODD)} \tag{1}$$

$$E_\phi(\theta,\phi,R) = \sum_{m=0}^{M} E_{\phi me}(\theta,R)\cos(m\phi) \quad \text{(EVEN)} + \sum_{m=1}^{M} E_{\phi mo}(\theta,R)\sin(m\phi) \quad \text{(ODD)} \tag{2}$$

In Eqs. (1) and (2), $E_\theta(\theta,\phi,R)$ and $E_\phi(\theta,\phi,R)$ are given radiation patterns to be represented as a truncated Fourier series. It is easily shown (Ref. 6) that only the $m = 1$ components of the pattern contribute to the antenna gain. Energy contained in $m \neq 1$ components represents a degradation of antenna gain and, also, in the receive mode, a possible source of system noise temperature degradation. Figure 2 shows the form of the component radiation patterns for the first four m dependences.

A new computer program was developed to compute the azimuthal component patterns as given by Eqs. (1) and (2). The input to this program is a group of radiation patterns which may be either experimental or obtained from the previously described scattering program. The program output is a series of polar patterns for each m index up to M, together with the total powers in each of the m-component patterns. This program was first utilized to analyze the ellipsoid scattered fields. The resulting modal power distribution is shown in Fig. 3. As would be expected from the geometry shown in Fig. 1 and the patterns shown in Fig. 2, the dominant extraneous energy is in the $m = 0$ and $m = 2$ modes. The gain degradation factor of 0.10 dB from pattern asymmetry is considered acceptable.

To calculate the scattered fields from the flat plate, the $m = 0$ and 2 patterns were first expanded in spherical polar modes (Ref. 3) about the point C. The resulting mode coefficients were then utilized in the scattering program (Ref. 3) to calculate the scattered fields from the flat plate.

III. Comparison of Computed and Measured Data

Since the reflex feed design is based on a series of computer programs which are novel in some respects, it was necessary to experimentally validate the design by scale model testing. Three 1/7-scale model ellipsoid designs have been tested in the JPL Mesa Antenna Range anechoic chamber. The three designs differed in the beamwidth of scattered fields: the first two bracketing, and the final being essentially the same as the standard feedhorn. Figures 4 and 5 show the excellent agreement between the computed and measured elipsoid patterns, thus validating the scattering program design. For these patterns the feedhorn was polarized perpendicular to the plane of Fig. 1. Patterns taken with the orthogonal polarization were essentially identical.

Scale model patterns were also taken of the complete feed including the flat plate (planar reflector); these are compared with the computed patterns in Figs. 6 and 7. The computational technique was that described in *Section II*, above, using the $m = 0$, 1, and 2 pattern components. A comparison of these two figures with Figs. 4 and 5 shows that, even though the planar reflector is relatively small, it behaves very nearly as predicted by image

[2]Private communication from R. A. Norman, JPL Communications Elements Research Section.

theory. By resolution of the flat plate scattered patterns into m-component patterns, it was also determined that reflection from the flat plate does not significantly change the energy distribution between the m modes, i.e., orthogonality is maintained.

IV. Present Efforts

Several efforts are presently being pursued by the Communications Elements Research Section. Reduction and analysis of scale model data for the third and final ellipsoid design is in progress. Additional scale model tests are being undertaken in which the relative geometry of the four reflex feed component parts is perturbed and the effect on system performance is evaluated. Both experimental and analytical data on the power dissipation/temperature profile of the ellipsoid and flat plate under high power S-band transmission are being developed. Further tests and calculations of the dichroic plate design are being undertaken for optimization of the slot configuration.

References

1. Katow, M., "S- and X-Band RF Feed System," in *The Deep Space Network Progress Report*, Technical Report 32-1526, Vol. VI, pp. 139–141. Jet Propulsion Laboratory, Pasadena, Calif., Dec. 15, 1971.
2. Woo, R., "A Low-Loss Circularly Polarized Dichroic Plate," in *1971 G-AP International Symposium Digest*, pp. 149–152, Sept. 22-24, 1971.
3. Ludwig, A. C., *Calculation of Scattered Patterns From Asymmetrical Reflectors*, Technical Report 32-1430. Jet Propulsion Laboratory, Pasadena, Calif., Feb. 15, 1970.
4. Potter, P. D., "Application of Spherical Wave Theory to Cassegrainian-Fed Paraboloids," *IEEE Trans. Ant. Prop.*, Vol. AP-15, No. 6, pp 727–736, Nov. 1967.
5. Ludwig, A. C., "Near-Field Far-Field Transformations Using Spherical-Wave Expansions," *IEEE Trans. Ant. Prop.*, Vol. AP-19, No. 2, pp. 214–220, Mar. 1971.
6. Rusch, W. V. T., and Potter, P. D., *Analysis of Reflector Antennas*, pp. 78–81. Academic Press, New York, 1970.

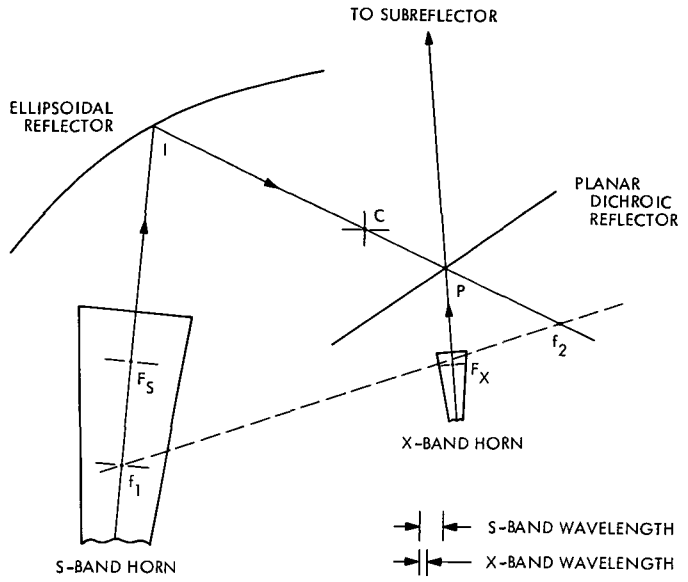

Fig. 1. Reflex feed system

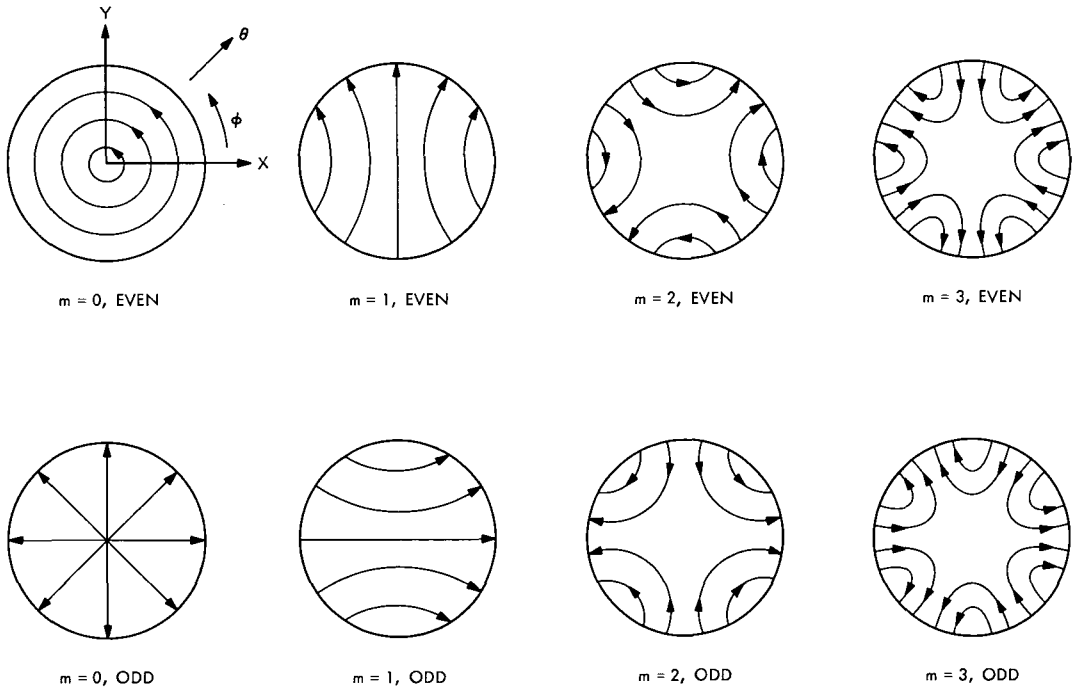

Fig. 2. Physical interpretation of *m* dependence

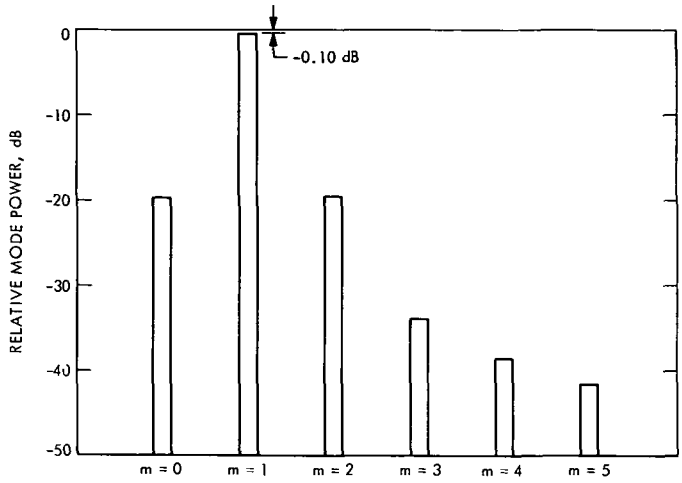

Fig. 3. Ellipsoid pattern azimuthal mode power

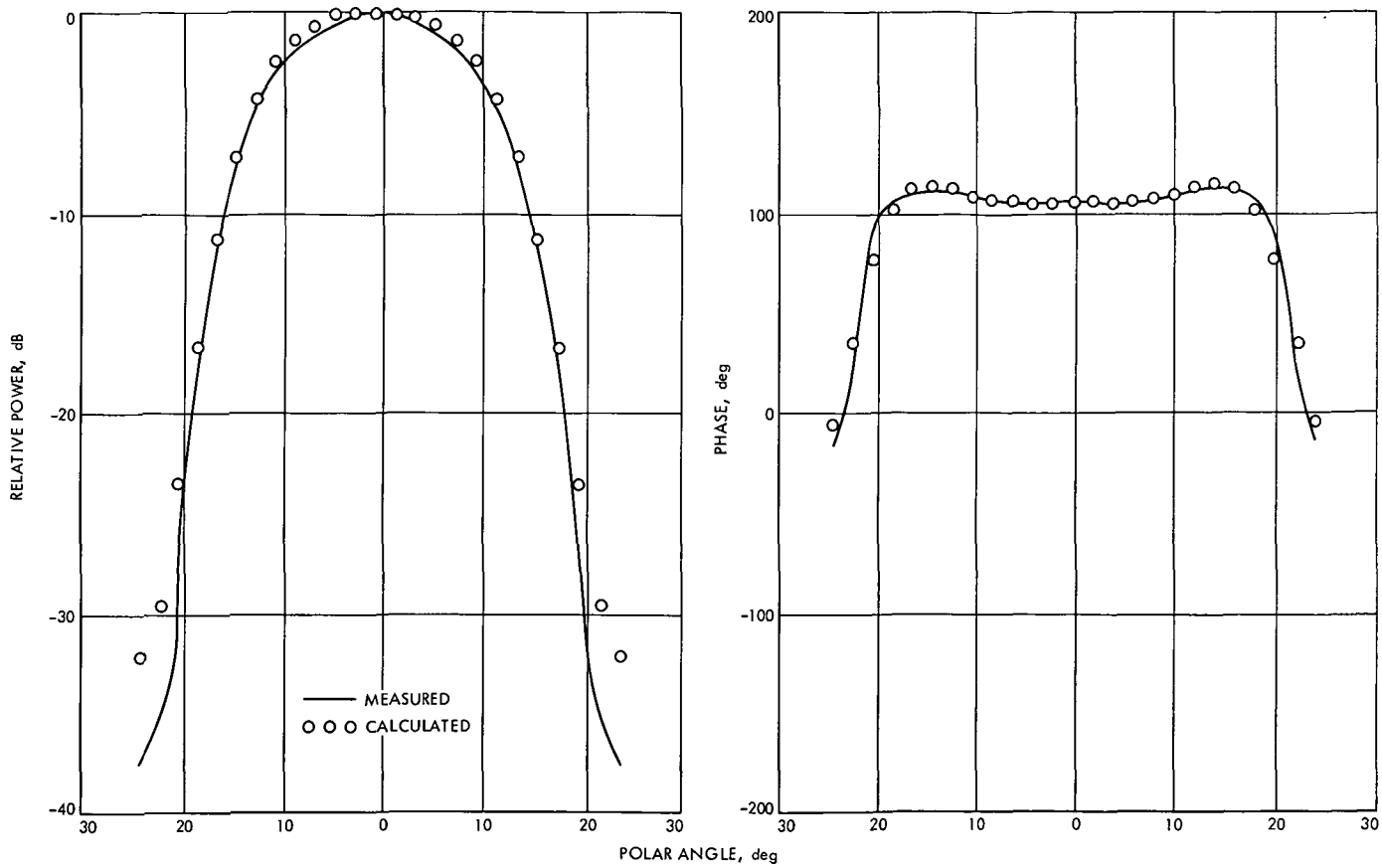

Fig. 4. E-plane ellipsoid patterns, design 1

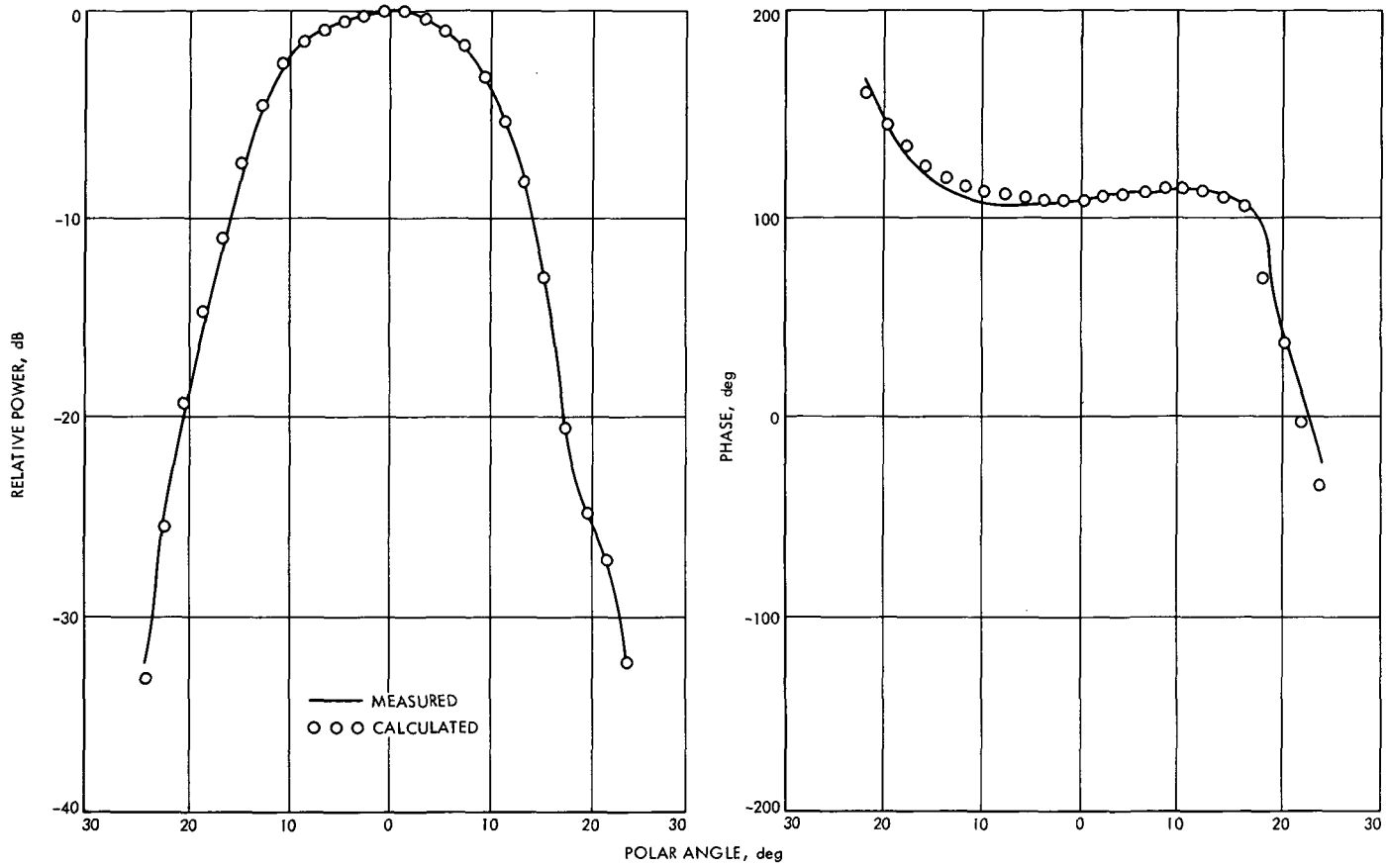

Fig. 5. H-plane ellipsoid patterns, design 1

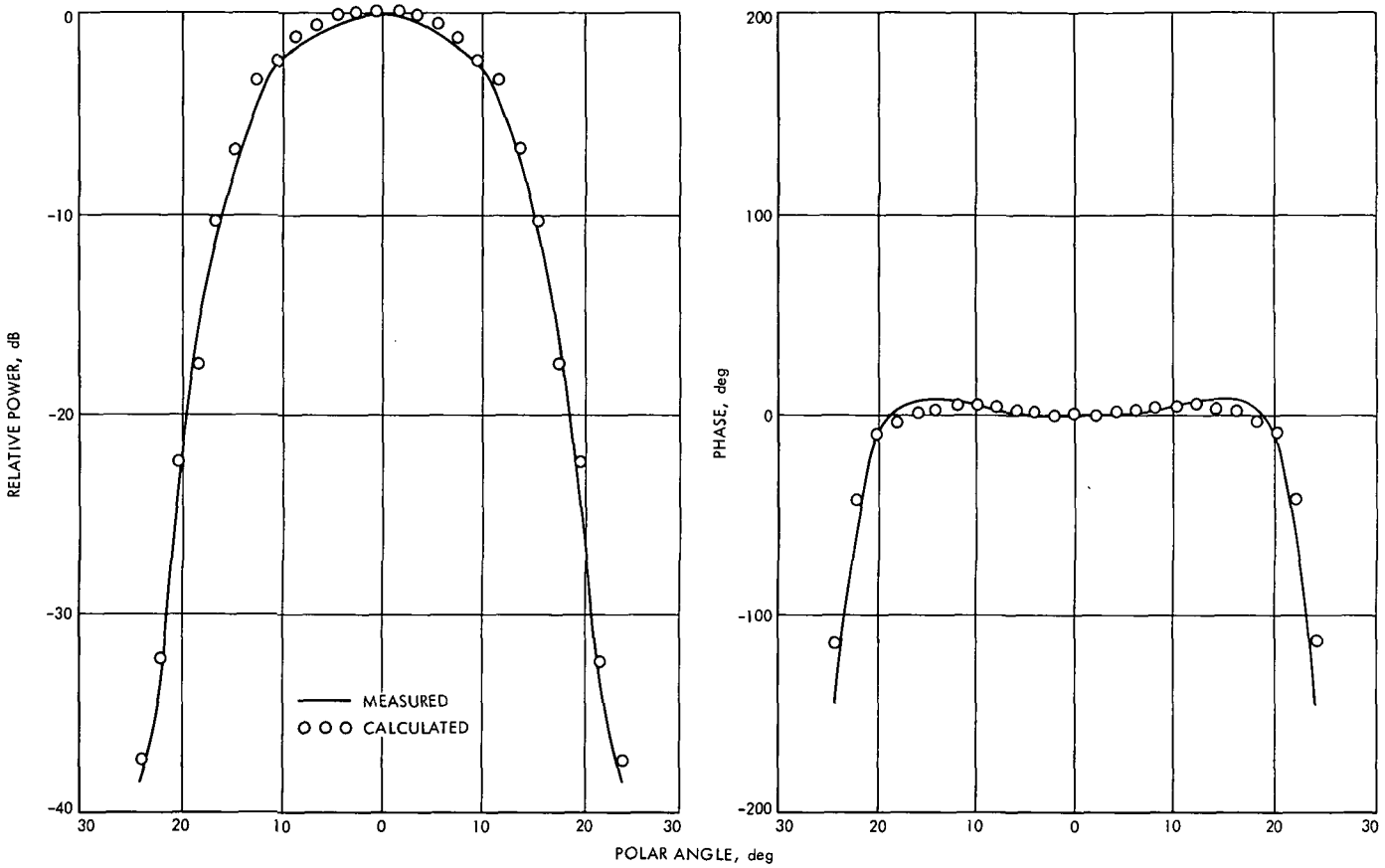

Fig. 6. E-plane flat plate patterns, design 1

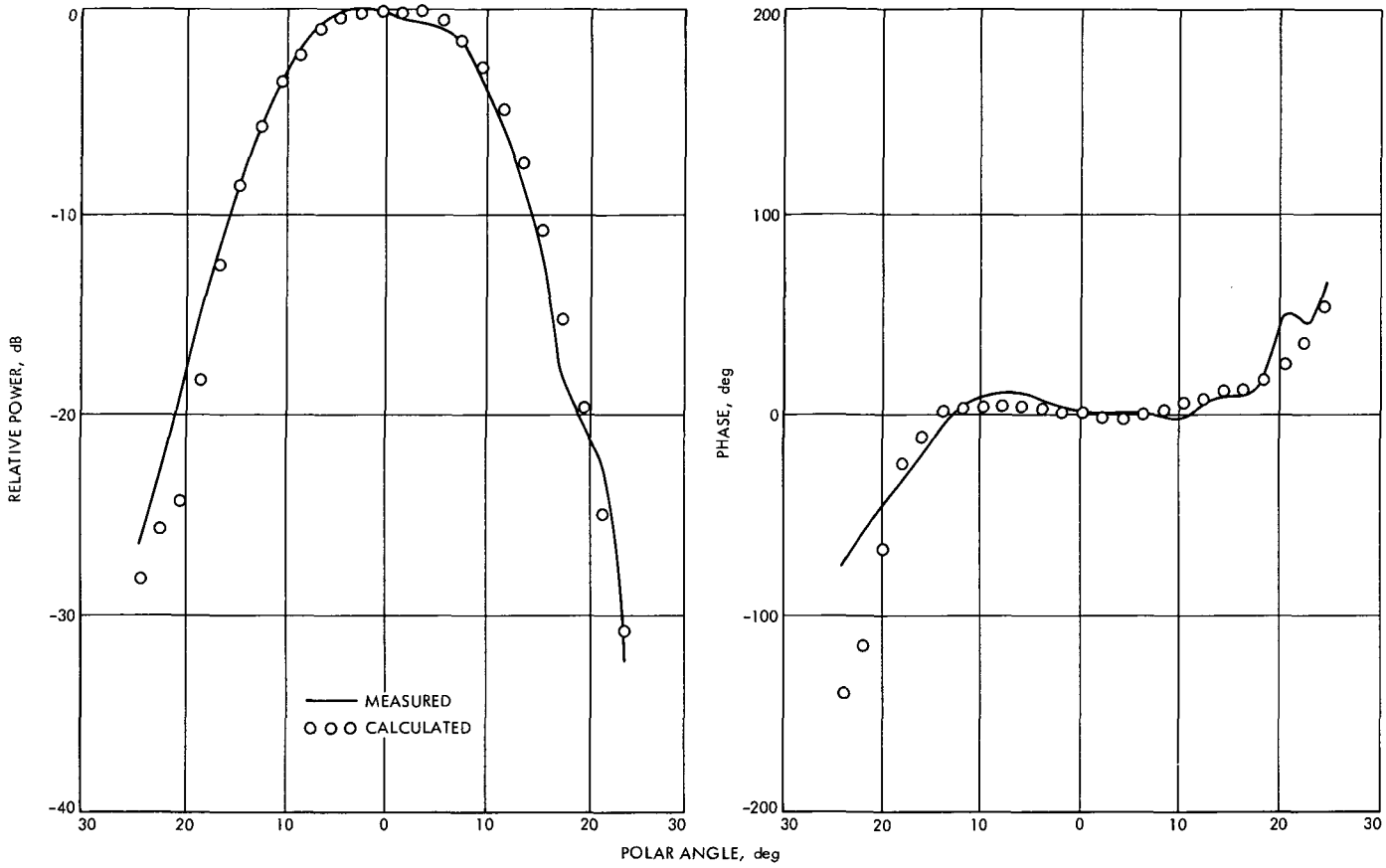

Fig. 7. H-plane flat plate patterns, design 1

Improved RF Calibration Techniques: System Operating Noise Temperature Calibrations

M. S. Reid
Communications Elements Research Section

System operating noise temperatures and other calibration data of the S-band research operational (SRO) cone at DSS 13 and the tricone system at DSS 14 are reported for the period October 1, 1971 through January 31, 1972. During this reporting period the tricone system consisted of the polarization diversity S-band (PDS) cone, the S-band megawatt transmit (SMT) cone, and the multifrequency X- and K-band (MXK) cone. S-band calibration data for various configuration modes of the PDS and SMT cones are reported as well as X-band calibration data for the MXK cone.

The system operating noise temperature performance of the low noise research cones at the Goldstone Deep Space Communications Complex is reported for the period October 1, 1971 (day 274) through January 31, 1972 (day 31). Most of the operating noise temperature calibrations were performed with the ambient termination technique[1] (Ref. 1). Measurements made with an aperture load are indicated in Table 1. System temperature calibrations were made on the following cones:

(1) S-band research operational (SRO) cone at DSS 13.

(2) Polarization diversity S-band (PDS) cone at DSS 14.

(3) S-band megawatt transmit (SMT) cone at DSS 14.

(4) Multifrequency X- and K-band (MXK) cone at DSS 14.

The averaged operating noise temperature calibrations for the SRO cone at DSS 13, and other calibration data, are summarized in Table 2. Maser serial number 96S2 was

[1]Most of the measurements were taken by DSS 13 (Venus) and DSS 14 (Mars) personnel.

in operation on the 26-m-diameter antenna at DSS 13 up to January 25, 1972. On this date, the maser was replaced by one with a superconducting magnet (maser serial number 96S5). Table 2 shows calibration data prior to January 25 with 96S2, as well as data that were taken between January 25 and 31 with 96S5. Measurements made with the maser (96S2) connected to the gain standard horn at 2278.5 MHz are also shown in Table 2.

Averaged operating noise temperature calibrations, and other calibration data, are presented in Table 1 for the tricone system at DSS 14. The tricone configuration for this reporting period consists of the PDS, SMT, and MXK cones. Maser serial number 80S1, which is located in the 3A section, can be switched into either the PDS system or the SMT system. Calibrations made with this maser are tabulated under the cone into which the maser was switched for those measurements. The *new low-noise path* is an additional receive-only mode which bypasses the 2100-MHz transmit band notch filter. Insufficient measurements have been made to make a good comparison with the original low-noise path. Measurements made with an aperture load on the SMT cone agree well with the data from the ambient load technique, as shown in Table 1. The focused MXK cone data were taken with the subreflector correctly positioned on the X-band main horn, while the defocused data were taken with the subreflector positioned on either the PDS or the SMT cones.

The calibration data were reduced with JPL computer program number 5841000, CTS20B. Measurement errors of each data point average are recorded under the appropriate number in the tables. The indicated errors are the standard deviation of the individual measurements and of the means, respectively. They do not include instrumentation systematic errors. The averages were computed using only data with:

(1) Antenna at zenith.

(2) Clear weather.

(3) No RF spur in the receiver passband.

(4) Standard deviation of computed operating noise temperature due to measurement dispersion less than 0.15 K.

Figure 1 is a plot of system operating noise temperature of the maser connected to the gain standard horn (DSS 13) as a function of time in day numbers. The frequency was 2278.5 MHz and the maser was 96S2. Figure 2 is a plot of system operating noise temperature of the SRO cone at 2278.5 MHz as a function of time in day numbers. The date when the superconducting magnet was installed is indicated. Figure 3 is a similar plot of the SRO cone at 2388 MHz. In all figures in this article, data that satisfy the four conditions stated above are plotted as solid circles or triangles while data that fail one or more conditions are plotted as open circles or triangles.

Figures 4 and 5, respectively, are plots of the system operating noise temperatures of the SMT cone using the 3A section maser (80S1) and the SMT cone maser (96S4), both at 2295 MHz. Each graph contains data taken by both the ambient load technique and the aperture load technique. No distinction is made between the two methods in the figures.

System operating noise temperatures of the PDS cone, both low-noise path and diplexed, are plotted in Fig. 6 as a function of time in day numbers. In all cases the frequency is 2296 MHz. Although these data were taken using the ambient termination method, most of them were not reduced by the above CTS20B computer program. These data are single Y-factor numbers, made with the antenna at zenith but with no regard for weather conditions, which were reported into Operational Data Control (SFOF) as part of the daily track report.

Figure 7 is a plot of system operating noise temperatures of the MXK cone at 8415 MHz. Focused data are plotted as circles and defocused data as triangles.

Reference

1. Stelzried, C. T., "Operating Noise-Temperature Calibrations of Low-Noise Receiving Systems," *Microwave J.*, Vol. 14, No. 6, pp. 41–48, June 1971.

Table 1. System operating noise temperature calibrations of the PDS, SMT, and MXK cones on the 64-m-diameter antenna at DSS 14

Cone	Configuration or measuring technique	Frequency, MHz	Maser serial number	Maser gain, dB	Follow-up receiver contribution, K	System operating noise temperature, K
PDS	Low-noise path	2296	80S1 (3A section)	40.2 1 measurement	0.07 1 measurement	25.1 ±0.06 1 measurement
PDS	Low-noise path	2296	96S3	52.4 ±1.39/0.57 4 measurements	0.03 ±0.005/0.002 4 measurements	19.4 ±0.52/0.29 4 measurements
PDS	New low-noise path	2296	80S1 (3A section)	37.9 1 measurement	0.05 1 measurement	24.0 ±0.16 1 measurement
PDS	New low-noise path	2296	96S3	51.9 ±0.14/0.10 2 measurements	0.03 ±0.002/0.001 2 measurements	19.6 ±0.87/0.62 2 measurements
PDS	Diplexed	2296	80S1 (3A section)	40.3 1 measurement	0.07 1 measurement	30.8 ±0.02 1 measurement
PDS	Diplexed	2296	96S3	51.7 1 measurement	0.03 1 measurement	22.9 ±0.38 1 measurement
SMT	Aperture load	2295	80S1 (3A section)	38.1 ±0.14/0.10 2 measurements	0.06 ±0.001/0.0006 2 measurements	25.8 ±0.06/0.04 2 measurements
SMT	Aperture load	2295	96S4	48.1 ±0.06/0.03 4 measurements	0.17 ±0.007/0.003 4 measurements	15.9 ±0.11/0.06 4 measurements
SMT	Ambient load	2295	80S1 (3A section)	38.0 ±0.17/0.06 9 measurements	0.06 ±0.006/0.002 9 measurements	25.4 ±0.50/0.15 9 measurements
SMT	Ambient load	2295	96S4	48.5 ±1.11/0.24 20 measurements	0.16 ±0.03/0.01 20 measurements	15.4 ±0.26/0.06 20 measurements
MXK	Focused	8415	150X1	No measurements	0.54 ±0.53/0.27 4 measurements	23.3 ±0.90/0.44 4 measurements
MXK	Defocused	8415	150X1	No measurements	1.3 ±0.75/0.33 5 measurements	30.5 ±1.5/0.67 5 measurements

Table 2. System operating noise temperature calibrations of the SRO cone and the gain standard horn on the 26-m-diameter antenna at DSS 13

Maser serial number	9652				9655		
Frequency, MHz	2278.5		2295	2388	2278.5	2295	2388
	Gain standard horn	SRO cone					
Maser gain, dB	46.9 ±2.51/1.02 6 measurements	46.7 ±3.07/0.55 31 measurements	50.2 ±1.81/0.74 6 measurements	36.6 ±1.10/0.16 47 measurements	No measurements	No measurements	32.5 ±0.07/0.05 2 measurements
Follow-up receiver contribution, K	0.12 ±0.08/0.03 6 measurements	0.11 ±0.05/0.01 31 measurements	0.05 ±0.02/0.01 6 measurements	0.54 ±0.07/0.01 31 measurements	0.17 ±0.01/0.006 5 measurements	0.24 1 measurement	1.1 ±0.04/0.03 2 measurements
System operating noise temperature, K	26.2 ±1.86/0.75 6 measurements	17.2 ±0.63/0.11 31 measurements	17.0 ±0.84/0.40 6 measurements	17.8 ±0.72/0.13 31 measurements	15.2 ±0.29/0.14 5 measurements	15.0 ±0.01 1 measurement	16.9 ±0.65/0.45 2 measurements

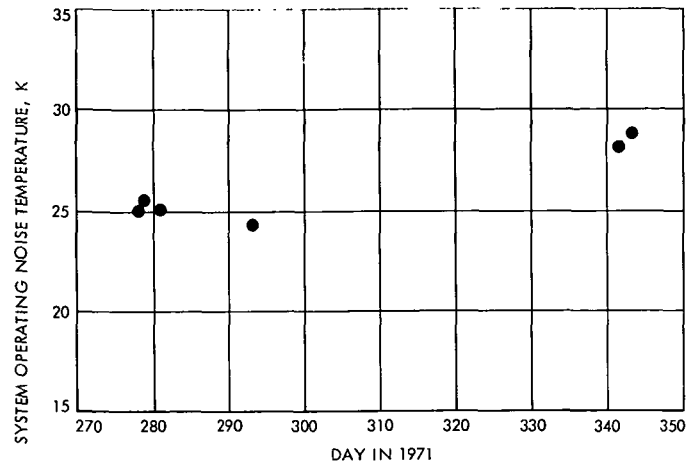

Fig. 1. System operating noise temperatures with the 96S2 maser connected to the gain standard horn at 2278.5 MHz; 26-m-diam antenna at DSS 13

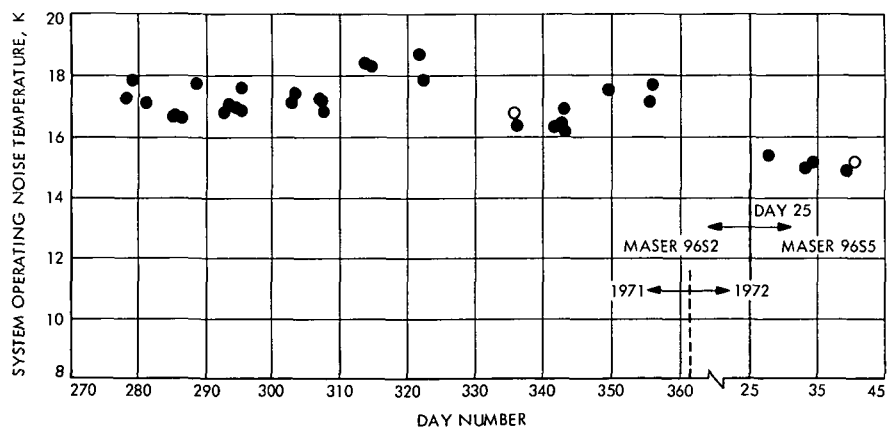

Fig. 2. System operating noise temperatures of the SRO cone at 2278.5 MHz; 26-m-diam antenna at DSS 13

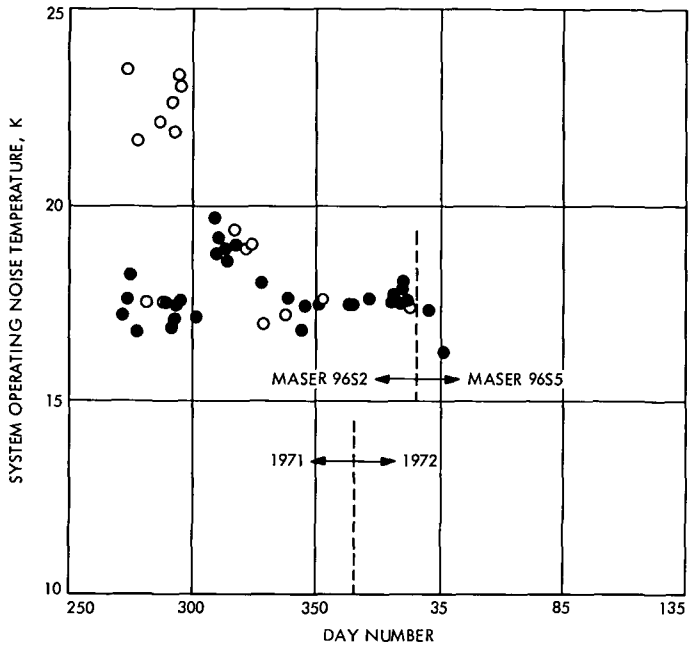

Fig. 3. System operating noise temperatures of the SRO cone at 2388 MHz; 26-m-diam antenna at DSS 13

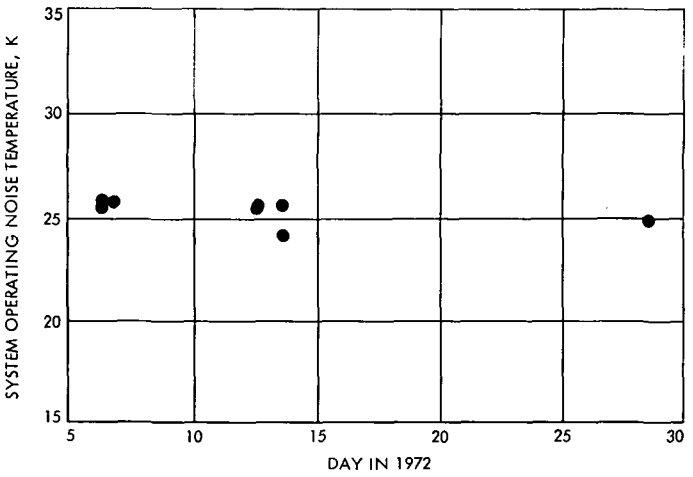

Fig. 4. System operating noise temperatures of the SMT cone at 2295 MHz; maser serial number 80S1 (3A section); 64-m-diam antenna at DSS 14

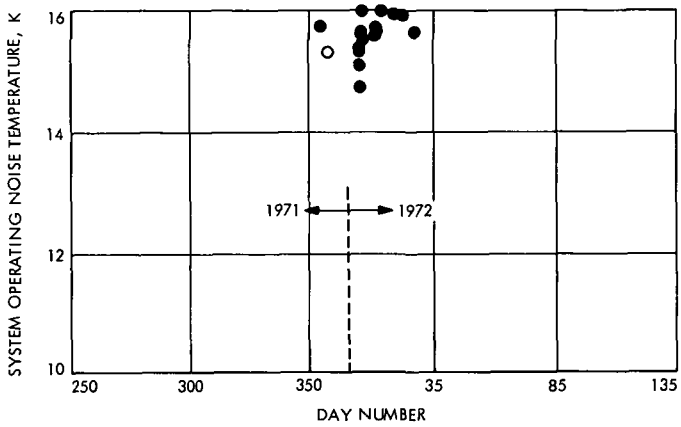

Fig. 5. System operating noise temperatures of the SMT cone at 2295 MHz; maser serial number 96S4 (SMT cone maser); 64-m-diam antenna at DSS 14

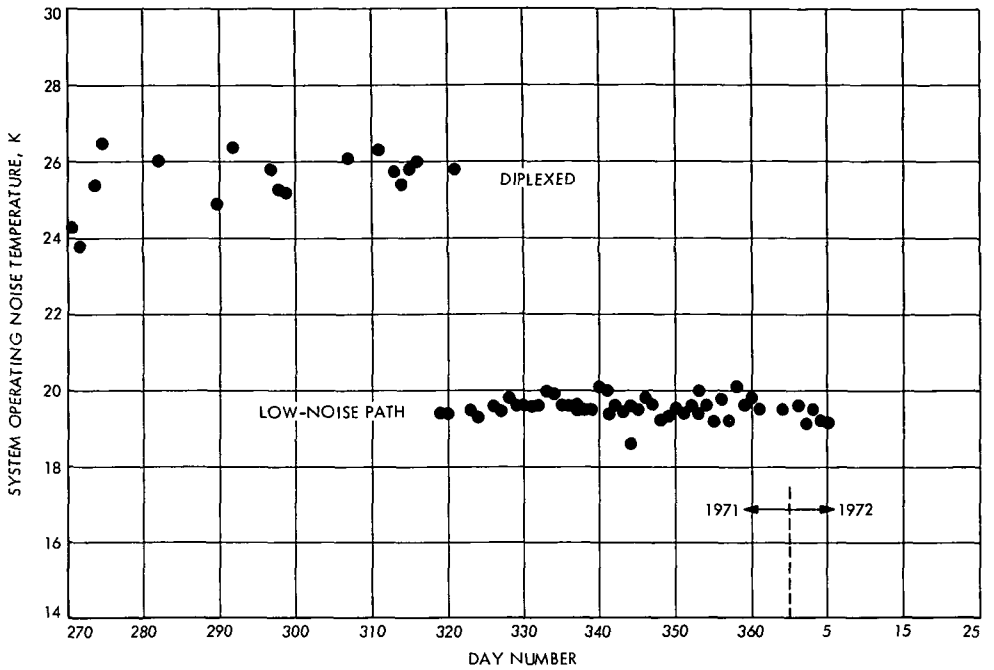

Fig. 6. System operating noise temperatures of the PDS cone at 2296 MHz; maser serial number 9653; diplexed and low-noise path; 64-m-diam antenna at DSS 14

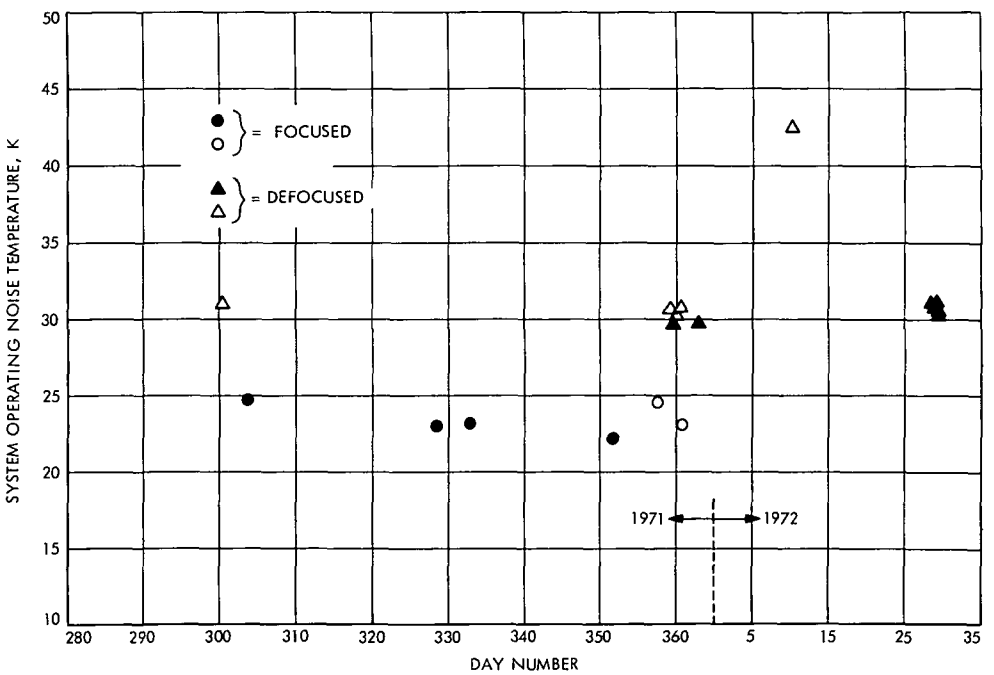

Fig. 7. System operating noise temperatures of the MXK cone at 8415 MHz; maser serial number 150X1; 64-m-diam antenna at DSS 14

DSN Research and Technology Support

E. B. Jackson
R. F. Systems Development Section

Major activities in support of the Deep Space Network research and technology program performed at both the Venus Deep Space Station and the Microwave Test Facility during the last two months are presented. Progress and performance summaries are given in the following areas: pulsar reception, mu ranging from DSS 14, tricone assembly and testing, precision antenna gain measurements on the 26-m antenna weak-source observations of various radio sources, very long baseline interferometry in cooperation with National Radio Astronomy Observatory, dual carrier measurements, noise and intermodulation experiments, clock synchronization transmissions, and various maintenance activities.

During the two months ending February 15, 1972 the Development Support Group (Section 335) was engaged in the following activities.

I. DSS 13 Activities

A. In Support of Section 331

1. Pulsars. The Venus DSS continues to devote approximately 23 h/wk to the observation of pulsars. Information obtained includes pulse-to-pulse spacing, pulse time of arrival, and pulse shape. The program observes twenty-two of the approximately fifty known pulsars. The pulsars observed during the two-month period ending February 15, 1972 are tabulated in Table 1 with their coordinates.

2. SDS 930 installation at DSS 14. In preparation for performing mu-ranging at DSS 14, the Development Support Group installed at DSS 14, in Room 201 on the second floor of the 64-m antenna pedestal, the SDS 930 which was used at the Echo DSS for off-line program support. With the additional installation of the communications buffer from the DSS 13 SDS 930, and the other specialized hardware required, successful mu-ranging of the *Mariner 9* spacecraft has been performed. We will continue to provide maintenance support on this machine in order to assure success of the celestial mechanics experiment with *Mariner 9*.

B. In Support of Section 332

1. Tricone support structure (TCSS). With the installation of interior waveguide plumbing and installation of the S-band polarization diversity feed cone atop the TCSS, high-power testing could commence. Extensive testing was done with the standard DSN 20-kW transmitter and, after some waveguide cleaning, smoothing, and removal of manufacturing debris, 400 kW was successfully attained and held for an 8-h period. Extensive measurements were made of the total system temperature during these tests in order to measure the expected weak signal performance of the cone in 400-kW diplexed operation. After full testing

was completed, the harmonic filter was replaced with one of a slightly different design. It was also successful in handling the power, and the total system temperature showed a decrease, possibly due to different manufacturing techniques, which result in a physically cleaner filter in the radio-frequency path in the new filter.

After completion of the high-power testing, the SPD cone was removed and shipped overseas to DSS 42A, the TCSS was disassembled and shipped to DSS 42A, and the TCSS destined for DSS 61A was assembled on the DSS 13 test pad. Interior components, waveguide, and a feed cone have been installed atop this unit, with testing proceeding on schedule.

C. In Support of Section 333

1. Precision antenna gain measurements. In continuing the project to perform an accurate measurement of the gain of the 26-m antenna at DSS 13, the comparison standard gain horn was relocated to the periphery of the antenna and extensive measurements were made by Section 333 personnel of the impedance match between the antenna feedhorn, the subreflector, and the maser. Measurements continue to be made of Cygnus A and *Apollo* lunar surface experiments package (ALSEP) to obtain comparison data between the gain of the antenna and the gain of the standard gain horn.

2. Weak-source observations. Extensive time has been devoted to this activity by both Section 333 and Development Support Group personnel. A semiautomated data taking technique has been developed, with long periods of stability measurements and technique validation being accomplished with the maser terminated in the antenna feedhorn and the antenna at various fixed positions. Substantial amounts of data have also been taken on various radio sources, in particular 3C48, 3C123, 3C218, 3C270, 3C353, Cygnus A, and the Moon.

3. Very long baseline interferometer (pulsars). In cooperation with the National Radio Astronomy Observatory (Green Bank, Maryland), a very long baseline interferometer experiment was performed involving observation of 38 pulsars and reference sources at 2295 MHz. The data was taken from the receiver as wideband noise and recorded with a digital tape recorder at a bandwidth of 325 kHz. Table 2 tabulates, with their position coordinates, the pulsars and reference sources which were jointly observed in this experiment. Fringes have been observed on the reference sources and source diameters are now being computed.

4. Maser instability. Most of the measurements made by DSS 13 require that the maser have very good stability. In the early part of December, the S-band maser developed a periodic gain instability. It steadily worsened until, on January 9, 1972, the instability had a peak-to-peak variation of 0.88 dB, with a repetition rate of once per 26 min, in a very periodic fashion. These changes are depicted in Fig. 1, which is a chart recording of the noise power output from the maser instrumentation system. Extensive troubleshooting did not uncover the cause of this regular instability, and a new developmental maser with a superconducting magnet was installed on January 24, 1972. Although some minor instability problems manifested themselves with this new maser, they have been corrected and the system is now operating. System performance with this new maser is given in Table 3 at the three frequencies at which most work is done at DSS 13.

D. In Support of Section 335

1. 100-kW dual-carrier experiments. In preparation for the *Viking* Project, which will require communicating with two spacecraft, measurements were made on a 100-kW transmitter excited with two simultaneous carriers. Measurements were made with balanced carriers (10 to 20 kW per carrier) and unbalanced carriers (50 and 10 kW) and in the frequency domain of the resulting intermodulation products and their relative amplitudes.

2. Effects of snow on 26-meter antenna. Several inches of snow fell during the holiday season and, since the antenna had been left in the zenith position, the surface was partially covered with snow. Measurements were made of total system temperature and then a radio star was tracked and data recorded on apparent source temperature and boresight error for later study to see what effect partial snow cover had on beam direction. These measurements continued until the snow was basically all gone from the antenna surface.

3. Servo performance measurements with PN codes. Maintaining an antenna/servo system in optimum adjustment requires some knowledge of the system's transfer function, so a simple technique for measurement of the antenna's response is desirable. By impressing a small ($\pm$0.050 deg) error signal generated by a 255 state PN code onto the normal smooth rate tracking input, the antenna's response to an impulse function input can be determined without the stresses that would be associated with actually inputting an impulse. The only requirement is that the individual PN states be short with respect to

the antenna response time. The changes in the antenna position readouts are then correlated with the input PN for all possible delays, and the resulting correlation function as a function of delay allows observation of the antenna response to an impulse function. Figure 2 is the result of one such measurement, made on the elevation axis, in high-speed mode. Note the classical underdamped appearance, basically what one would expect from the high-speed mode which is not ordinarily used for tracking. The horizontal axis is 0.5 s per division, while the vertical axis is in arbitrary units, depending upon correlation time. These measurements are discussed at greater length elsewhere in this issue.

E. In Support of Section 337

1. Clock synchronization transmissions. Routine transmission of clock synchronization signals continued, using the Moon as a reflector. These transmissions were made to DSSs 14, 41, 42, 51, 62, and United States Naval Observatory at a power of 100 kW on a five-day week schedule. During a particularly cold period the water-cooling system fractured, and since it could not be drained, the heat exchanger core was damaged by freezing. A new core, with a design change to allow gravity draining of the coolant, has been installed and no further damage from freezing is expected.

The interface between the SDS-910 computer used for clock synchronization control and the programmed oscillator used for frequency generation failed when power was turned off during the weekend shutdown period. This has been repaired and modified so that power-off conditions will not cause any future troubles. Additionally, when an attempt was made to use a new 50-MHz reference generator, the receiving stations were unable to obtain correlation. This difficulty was traced to excessive noise on the 50-MHz reference caused by high power supply ripple from the central frequency synthesizer. Repairs are under way.

The 400-Hz motor generator, located in the transmitter control area in Building G-58, has been removed and power is now being furnished by an externally installed generator which was removed from Building G-51. Cross connections were made so that one generator now furnishes power to G-51, G-58, and G-53, thus freeing the previously used generator to be relocated to the 26-m area to aid in tricone testing.

To aid in smooth tracking of the Moon, the 9-m antenna has been rebalanced by the removal of approximately 498 kg of lead from various parts of the structure. The removal of this lead is counterbalanced by the weight of the various electronic components installed in the electronics room.

II. Microwave Test Facility Activities

A. In Support of Section 332

1. Tricone. Extensive machine shop support continues to be furnished to the tricone project. Fabrication of bracketry, waveguide spacers, etc., has been quite heavy. Additionally, major modifications were performed on the transmitter mounting drill jig as well as doing major precision redrilling three times as requirements changed. The angle requirements on this rework were quite stringent.

B. In Support of Section 335

1. Transmitter development. The continued modification and development of the 100- and 20-kW transmitters at DSS 13 require special high-voltage connector work, bracketry, waveguide adapters, etc. Extensive machine shop support has been given in this area. Additionally, construction of a flow monitor panel and design and fabrication of a voltage crowbar for the clock synchronization transmitter is under way.

2. Noise and intermodulation testing. In cooperation with personnel from the Goddard Space Flight Center, experiments have been ongoing to determine the causes of noise generation and what effects various waveguide pressurizing gases have on this noise. Special test jigs with needle points to produce arcing, carefully lapped flanges for flatness, and other special fixtures have been fabricated and used in this investigation. Sulphur hexafluoride (SF_6) has proven to suppress minor arcing and noise production and more experiments are planned. Both 20-kW transmitters, operating into a combiner, have been utilized in these experiments to investigate noise and intermodulation production.

Table 1. Pulsars currently being observed at DSS 13

Pulsar	Sidereal hour-angle	Declination
0031	351.834	352.497
0301	314.563	19.367
0329	307.314	54.482
0525	278.253	21.986
0628	262.577	331.438
0736	245.599	319.375
0823	233.728	26.722
0833	231.415	314.929
1133	186.368	16.011
1237	170.423	25.045
1604	118.550	359.555
1642	109.164	356.750
1706	103.039	343.350
1749	92.221	331.891
1818	85.169	355.591
1911	71.915	355.250
1929	67.291	10.926
1933	66.384	16.210
2021	54.606	51.765
2045	48.267	343.618
2111	41.882	46.684
2218	25.209	47.769

Table 2. Pulsars and reference sources, with positions, jointly observed with NRAO

Source	Right ascension, deg	Declination, deg
3C279	193.688	−05.640
3C273	186.925	02.204
3C274	187.358	12.536
0Q208	211.471	28.656
DA406	243.158	34.271
3C345	250.504	39.857
3C371	271.758	69.816
VR422201	330.383	42.145
3C418	309.438	51.222
PSR1929	292.725	10.930
0U080	297.179	8.042
3C409	303.313	23.488
1821 + 10	275.658	10.721
3C424	311.704	6.971
NRA0 530	262.867	−13.064
1741 − 03	258.904	−3.838
2128 − 12	322.513	−12.239
2134 + 00	323.792	0.566
2127 + 04	322.288	4.914
3C84	49.496	41.416
CP0329	52.725	54.483
NRA0 150	59.371	50.895
3C91	53.929	50.664
0607 − 15	92.113	−15.710
0704 − 23	106.367	−23.166
0J297	134.863	−28.020
0814 − 35	123.783	−35.506
PSR0833	128.608	−45.077
0807 − 38	122.158	−39.005
0843 − 33	131.021	−33.718
1055 + 01	164.271	1.714
CP0950	147.929	8.060
0K290	148.821	25.387
CP1133	173.658	15.999
1116 + 12	169.371	12.718
1148 − 00	177.329	−0.245

Table 3. Performance of DSS 13 development S-band maser with superconducting magnet

Frequency, MHz	Gain, dB	Total zenith system Temperature, K
2278	44.8	17.8
2295	43.6	16.3
2388	32.4	17.8

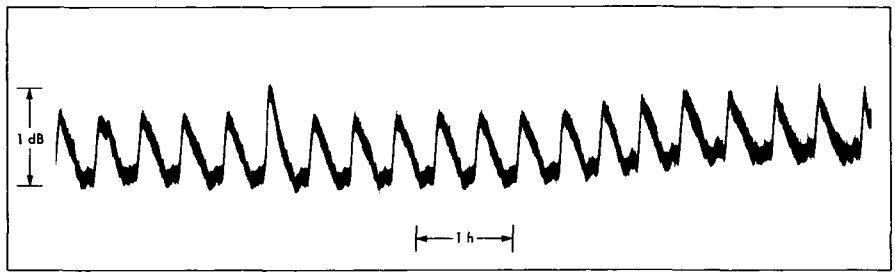

Fig. 1. Periodic gain instability in DSS 13 S-band maser

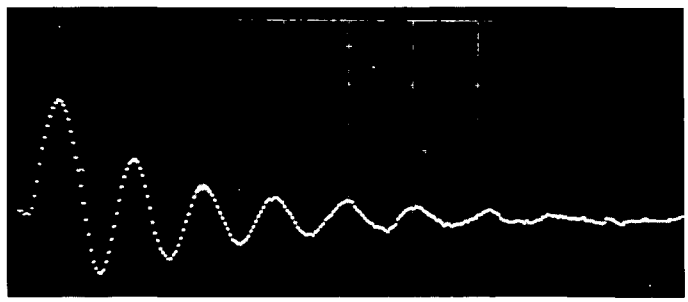

Fig. 2. Elevation response (high-speed), 26-m antenna

Antenna Drive System Performance Evaluation Using PN Codes

R. M. Gosline, E. B. Jackson, and J. C. Campbell
R. F. Systems Development Section

A maintenance tool for quick and easy evaluation of the performance of an antenna drive system is described and preliminary results are given. The technique uses a PN code as a system input signal and correlates the system output with all possible states of the input PN code. The resulting correlation function has the same shape as the system response to an impulse input and can be considered in the same way. A program description, block diagrams, and some system response curves are given.

I. Introduction

Proper maintenance and adjustment of any system requires a suitable technique of performance measurement so that troubleshooting can be performed and the results of component changes evaluated. Existing techniques for measuring the performance of the 26-m antenna drive and positioning system took too long for easy utilization as a routine maintenance and adjustment aid. Initial testing of a method of performance evaluation by using PN codes as an input signal has been done and the results will be briefly described herein.

The 26-m antenna at DSS 13 is an elevation-over-azimuth mount using hydraulic motors for positioning in both axes. The azimuth axis is driven by a conventional "bull" gear arrangement through four drive units. The elevation axis is driven by two recirculating ball screws. These drives give the antenna a capability of slewing at better than 4 deg/s in either axis, in high-speed mode. Either axis can also be driven in low-speed mode at the operator's discretion and this is the mode usually used for tracking.

The servo system is of the "zero velocity error" type and moves the antenna by electrically controlling, with servo valves, the flow of hydraulic fluid to the hydraulic motors in response to signals input into the appropriate points. Figure 1 is a block diagram of the azimuth and elevation system showing the various feedback loops, gear units, hydraulic motors, etc. The system utilizes three feedback loops to achieve maximum stability and smooth tracking.

In normal tracking, signals are input into the position loop, causing the antenna to move in the direction required to drive the input signal to zero. The rate loop, which receives signals from the "dc tachometers" driven by the hydraulic motors, senses rate changes and provides

damping for the position loop. The valve drivers that operate the servo valves receive a linearizing signal from the current feedback loop which senses valve current. Properly adjusted, the system is capable of smooth tracking with essentially zero position error.

In order to effect this proper adjustment, the system response must be measured. This is conventionally done by use of a servo network analyzer, although useful data can be obtained by exciting the system with an approximation of an impulse. However, the first method is too time consuming for routine maintenance application, and the second puts undesired stresses on the system if the approximation of an impulse is good.

A properly constructed pseudo-noise (PN) sequence can be used as the system input and obtain the same information as would be obtained if the system were actually excited by an impulse input (Refs. 1, 2). The only requirement is that the PN digit period be short with respect to the servo response time and the code length be long enough to allow complete observation of the system response. If the amplitude of the PN code is kept small, the perturbations of the system will be quite small, and normal operation can be maintained while measurement of the response is under way.

The complexity of the system, as seen from Fig. 1, is such that modeling is extremely difficult; so the values of the various elements of the PN code could not be selected with great confidence in advance. For this reason, plus the availability of an already interfaced SDS-930 digital computer, it was decided to use software to generate the PN code, effect the required correlation, integrate the resulting correlation function, and display the results. This would enable easy modification of any parameter without the expense of building any hardware until the technique had been fully investigated. To further aid in ease of effecting changes, the computer program was written in real-time Fortran with machine language instructions for the high-speed loops.

II. Technique Description

A 255-state PN code, with bilevel states of ± 1 was chosen, with a basic digit period of 20 ms, variable in multiples of 20 ms. This provides a minimum code period of 5.1 s, with multiples of this period available for use with systems which are slow to stabilize. The PN code is generated and stored only once, when the program is initially loaded. By incrementation of a "pointer" cell and proper addressing, the PN code can be shifted and all delays obtained without actually moving the PN bits in computer memory. The program provides the following control functions and parameter variable inputs: (1) PN code amplitude in degrees, (2) digit period multiplier, (3) position and rate offset inputs, (4) clearing of correlator and accumulator, and (5) data output to magnetic tape, line printer, or plotter. A functional block diagram of the construction is depicted in Fig. 2. Bear in mind that all code generation, correlation, and integration (accumulation) are done by software, and the only additional hardware required is the oscilloscope display. (A Tektronix 585 was used, but almost any oscilloscope could be used.)

The monitor section of the program provides for entering various parameters, and scales the integrator data for the oscilloscope display. It also provides for selection of either azimuth or elevation axis for evaluation, and read-in of previously recorded data. (As a precautionary measure, all input parameters are tested for proper range before acceptance, since the antenna is under slave control.) The functional part of the program, under interrupt control, increments the position rate, increments the PN code clock, demodulates, limits, correlates with all possible PN delays, integrates the correlation function, and outputs the data to an oscilloscope display for observation by the operator.

III. Initial Results

Thus far, we have only been testing the suitability of our "tool" and have not made any changes in the servo system with the exception of those front panel adjustments commonly made by the operator. Figures 3, 4, and 5 are typical of the response patterns obtained with input conditions as summarized in Table 1. For a given set of conditions, the patterns are quite repeatable and suggest that the antenna drive system is not optimum in either adjustment or design. Remember that the system under evaluation includes the servo electronics, hydraulics, antenna structure, angle encoders, servo repeater, and computer (all items shown in Fig. 1). In future work we plan to investigate these various sections in more detail.

IV. Conclusions

Using perturbing amplitudes as small as 0.010 deg, we have established that a properly designed PN code, utilized as a system input and then correlated with the system output for all possible states of the input PN code, will produce a correlation function whose shape is identical to the shape of the system response to an impulse utilized as an input.

Initial observation of our results indicates that the 26-m antenna drive system is not optimum, but additional measurements are necessary before the effects of system changes can be evaluated. The technique offers definite promise as a maintenance tool, since all of the DSN stations have computers which are used as antenna drive signal sources. Future work will be directed toward achievement of a simple maintenance tool with simple procedures for servo-system adjustment toward optimum response for the tracking performance desired.

References

1. Towill, D. R., and Lamb, J. D., "Pseudo-Random Signals Test Nonlinear Controls," *Cont. Eng.*, Nov. 1970, pp. 59–63.
2. Dack, D., "System Identification by On-Line Correlation," *Cont. Eng.*, March 1970, pp. 64–70.

Table 1. Input parameters

Figure	Axis	Rate, deg/s	PN amplitude, deg	Digit period, ms	Code length, s	Servo speed
3	Elev	−0.02	0.01	40	10.2	Low
4	Elev	−0.1	0.01	20	5.1	High
5	Azimuth	0.05	0.05	20	5.1	High

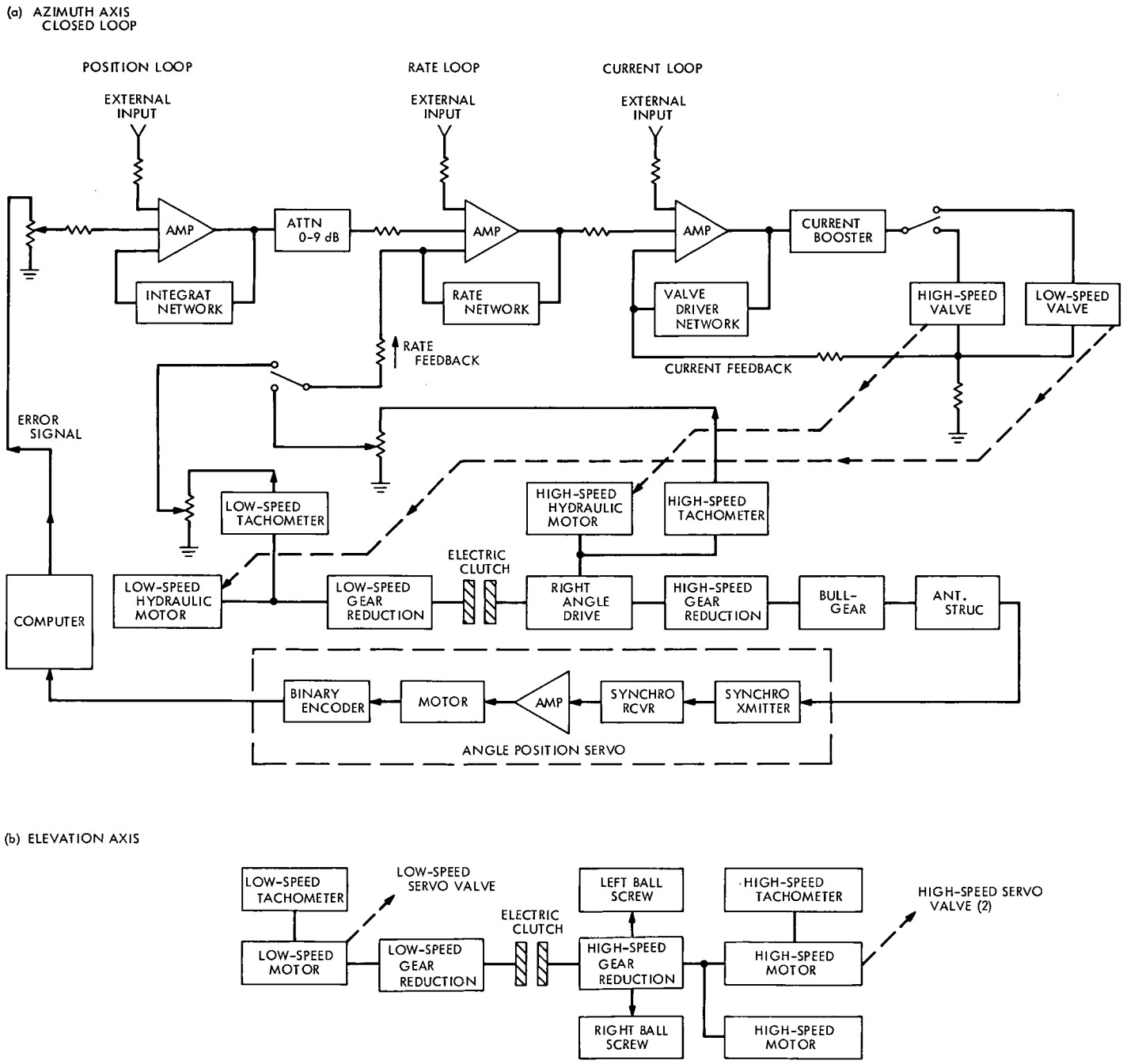

Fig. 1. Functional block diagram, 26-m antenna servo system: (a) azimuth (closed loop), (b) elevation axis

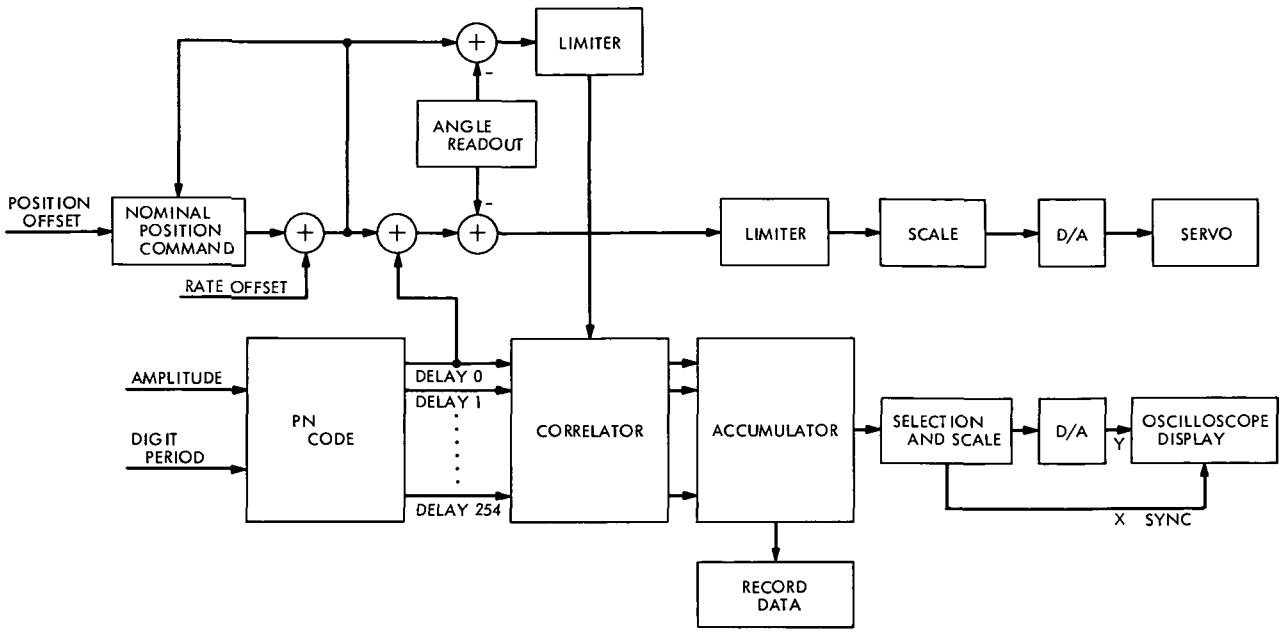

Fig. 2. Functional diagram, antenna drive system evaluation by PN code

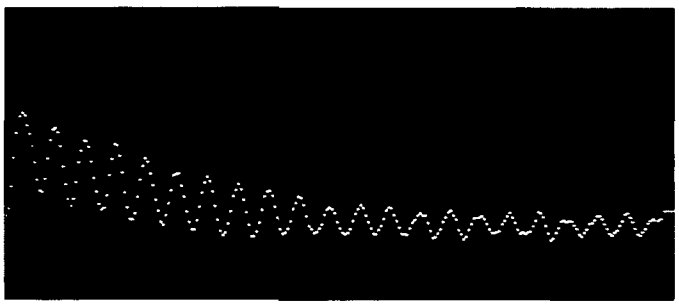

Fig. 3. Elevation axis, low-speed mode, 26-m antenna, Venus DSS

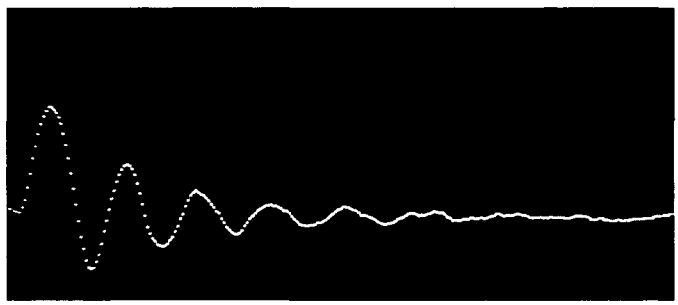

Fig. 4. Elevation axis, high-speed mode, 26-m antenna, Venus DSS

Fig. 5. Azimuth axis, low-speed mode, 26-m antenna, Venus DSS

SOFTWARE: A General-Purpose External Function for PDP-11 BASIC

E. C. Oakley
R. F. Systems Development Section

This article describes a new tool to dramatically simplify the test and software development phases in computer-controllable subsystems for the DSN. This tool does not add to the endless computer language proliferation, but instead adds dimension to a well-established, high-level, moderately sophisticated language to enable simplified control of minicomputer peripherals. Some of its versatility is demonstrated by programs used to aid its own implementation in hardware exercisers.

I. Introduction

The DSN is being called upon to provide multi-mission support capability with a minimum of down-time and spacecraft data loss due to system reconfiguration. The speed and accuracy required dictate that the subsystems involved be computer-controllable.

The general-purpose minicomputer is ideal for the test and control of such subsystems by providing the speed, versatility, and availability to be solely dedicated to the controlling task. The minicomputer generally has less memory available than larger computers, usually requiring that assembly-language programming be employed to realize best core utilization.

Assembly-language programming (Ref. 1) is a formidable obstacle to the speedy development of computer-controllable hardware (Ref. 2), because of the portion of time required for software development. Frequent program changes necessitate long edit/assembly cycles.

A high-level interpretive programming language, such as BASIC, offers the hardware designer a software environment providing ease of editing with immediate "RUN" capability. Helpful error diagnostics are supplied, and programming errors can rarely reach "self-destruct" proportions. Higher-level languages usually do not provide for control of nonstandard external peripherals. BASIC (Refs. 3 and 4), as implemented for the Digital Equipment Corp. PDP-11 (Ref. 5), does provide for a user-designed external function (EXF) to perform a specified operation.

II. Design

A general-purpose EXF has been written for BASIC in PDP-11 assembly language (Fig. 1 and Ref. 6), and uses 48_{10} words of core. It can move data to and from any peripheral device located along the PDP-11 Unibus. This includes analog-to-digital converters (ADCs), digital-to-analog converters (DACs), the general-purpose interface DR-11A, plus all the standard peripherals including the core memory itself.

The EXF call in BASIC user-programs consists of a parenthetical expression, such as:

(LINE #) LET X = EXF (A,D,M)

OR

(LINE #) PRINT EXF (A,D,M)

OR

(LINE #) IF EXF (A,D,M) >X THEN STOP

The expression contains three arguments separated by commas, any one of which may be numbers, assigned-variable letters (with or without subscripts), or zero (Ø), but all arguments must always be present. The first argument, A, is the decimal ADDRESS of the location to be accessed. The second argument, D, is the decimal value of the DATA to be moved. The third argument, M, is the command MODE of the function to be performed on the data. M's value may equal +1 for the LOAD mode, −1 for the READ mode, or Ø for an optional special mode function to be described in later paragraphs.

For the first EXF call cited (LINE #) LET X = EXF (A,D,M), the variable X will assume the decimal value of data at the address being accessed. This means that the second argument (DATA field) of an EXF call to READ an address will normally be zero (Ø) since the decimal value of the data will be returned to BASIC and be assigned to the variable X, as follows:

(LINE #) LET X = EXF (A,Ø,−1)

The ADDRESS field argument A must be an even number so that even addresses (whole words) will be accessed. An attempt to access data at odd addresses (upper bytes) will cause a fatal error, and EXF will not return control to the BASIC interpreter.

Data arbitrarily loaded into core locations occupied by EXF, BASIC, its user area, or stack may cause them to be destroyed, although careful, deliberate modification of BASIC or EXF core locations by using EXF calls under program control can yield considerable expansion of BASIC's capabilities.

Decimal address and data values are restricted by the 16-bit word size to integers in two's-complement form in the range ±32767.

The software interface for the EXF in BASIC is defined mainly in Chapter 8 of Ref. 3.

EXF is fully re-entrant. That is, a statement which requires the call to be re-entered before the first call is complete:

(LINE #) LET X = EXF (A1, EXF (A2,Ø,−1), +1)

will fetch (READ) data from one peripheral, and immediately output (LOAD) it into a second peripheral with minimum interpreter execution time.

III. Applications

The EXF conditional expression

(LINE #) IF EXF (A,D,M) <>X THEN STOP

could be used to test the value of a status word (input to a DR-11A general-purpose interface) from a typical DSN subsystem. As an example, assume that the value of the correct status for the subsystem is X = 25732, and a test of the input DR-11A reveals a mismatch; an alarm can then be sounded by continuously ringing the teletype bell as follows:

```
1ØØ LET S = −8188: REM − DR-11A AT LOC. 16ØØØ4[8].
11Ø IF EXF (S,Ø,−1) <>25732 THEN PRINT "": GOTO 11Ø
12Ø REM − CTRL/G (BELL) BETWEEN QUOTES IN
13Ø REM − LINE 11Ø; ALARM
```

By subtraction, the improper status bit can be detected, a diagnostic message printed to alert the user, and corrective action initiated to re-zero the errant phase shifter:

```
11Ø IF 25732-EXF (S,Ø,−1) = 8 THEN GOTO 2ØØ
.
.
.
2ØØ PRINT "PHASE SHIFTER TO BE RE-ZEROED..."
```

```
21Ø REM–RE-ZEROING ROUTINE FOLLOWS:
22Ø
.
.
.
```

Figure 2 shows a program for exercising the digital step attenuator (Ref. 2) of the Ranging Demodulator Assembly. It is used for generating time-linear control ramps and steps to aid in the test of attenuator parameters such as monotonicity and phase shift. Instructions are printed to direct the user, and convenient pauses are introduced to allow instrumentation range changes to properly display the results on a strip-chart recorder, as measured by a vector voltmeter.

Figure 3 shows a BASIC-EXF program for taking voltage measurements with the Digital Equipment Corp. ADØ1-D analog-to-digital converter. The program assembles a control word from Channel and Gain data input by the user. This peripheral control technique is straightforward, requiring separate EXF statements for initiating ADØ1-D conversion, testing for 'DONE' and then reading the data buffer.

If the user requires more program execution speed than this straightforward method can yield, an interesting alternative is available. EXF can be used to append a short Assembly-Language driver to the BASIC user program to improve peripheral handling speed by several orders of magnitude. This is accomplished by first writing the Assembly-Language program and then converting the octal machine instructions to decimal values. These values are entered into the BASIC user program as DATA statement elements. These data are loaded into the Loader core area (which is otherwise totally unavailable to BASIC), by using the EXF(A,D,+1) LOAD mode. During program execution, these machine instructions are then branched-to by using the EXF(A,D,Ø) ZERO mode, yielding about a thousand-fold increase in execution speed for servicing the desired peripheral. Figure 4 shows such a program which will cycle the ADØ1-D analog-to-digital converter at a much higher rate than the straightforward program shown in Fig. 3.

Using the technique just described, Fig. 5 shows a program for providing power-fail protection for any BASIC user program. In this case, the power-fail-save machine-language routine is branched-to only when the computer hardware detects that a power-down or subsequent power-up condition exists. This software routine will prevent catastrophic execution of a DSN subsystem test or control program, saving the user much time required for system re-initialization. Of course, the user must not HALT the processor at the console front panel.

IV. Concluding Remarks

EXF greatly simplifies input–output programming tasks, within BASIC's language environment. Examples of techniques for implementing programs for the test and control of DSN subsystems have been shown. EXF can add much flexibility to ordinary computational BASIC programs not requiring peripheral control capability.

References

1. *PDP-11 Paper Tape Software Programming Handbook*, DEC-11-GGPA-D. Digital Equipment Corporation, Maynard, Mass., June 1970.
2. Oakley, E. C., "Digital Step Attenuator," in *The Deep Space Network Progress Report*, Technical Report 32-1526, Vol. III, pp. 211–214. Jet Propulsion Laboratory, Pasadena, Calif., June 15, 1971.
3. *PDP-11 BASIC Programming Manual*, DEC-11-AJPB-D. Digital Equipment Corporation, Maynard, Mass., Dec. 1970.
4. Knight, D., and Scott, J., *Listing of PDP-11 BASIC V00A*, DEC-11-AJPB-LA. Digital Equipment Corporation, Maynard, Mass., Nov. 5, 1970.
5. *PDP-11 Handbook*, Second Edition, No. AJ0. Digital Equipment Corporation, Maynard, Mass., 1969.
6. Program Assembly Listing, External Function for PDP-11 BASIC, JPL sketch No. B137631.

```
; PDP-11 BASIC EXTERNAL FUNCTION.  2-7-72.
; USES 96 BYTES (48 WORDS) OF CORE.
; FORM:   EXF(ARG1,ARG2,ARG3)
; ARG1 IS THE ADDRESS TO BE ACCESSED
; ARG2 IS THE DATA
; ARG3 IS THE FUNCTION TO BE PERFORMED.  CODES ARE:
;       -1 = READ
;        1 = LOAD
;        0 = SPECIAL.  LOADED BY USER WITH BASIC USING
;            EXF 1 (LOAD).  MUST BEGIN AT 37500 AND
;            END WITH 'BR FIN' TO LOCATION 37440.
        R0=%0
        R1=%1
        R2=%2
        R3=%3
        R4=%4
        SP=%6; STACK POINTER
        FLT=104436  ; BASIC INTERNAL ROUTINE
        FIX=104440  ; BASIC INTERNAL ROUTINE
        EVAL=104536 ; BASIC INTERNAL ROUTINE
        .=50; TRAP LOC. FOR EXF STARTING ADDRESS
        .WORD FX
        .=37342; STARTING ADDRESS FOR EXF ROUTINE
FX:     MOV R2,-(SP); SAVE DATA IN REGISTERS
        MOV R3,-(SP)
        MOV R4,-(SP)
        MOV (R0)+,R2; PREPARE TO CONVERT TO INTEGER
        MOV (R0)+,R3
        MOV (R0),R4
        FIX; CONVERT 3-WORD FPN TO SWI
        MOV R0,-(SP); STORE ADDRESS ON STACK
        CLR -(SP); INDICATE ARG BEING INTERPRETED
LOOP:   INCB R1; PAST COMMA (POINTER TO STRING IN R1)
        EVAL; BEGINS AT (R1), RESULT IN R2, R3, R4
        FIX; CONVERT 3-WORD FPN TO SWI
        MOV R1,R2; MOVE 'EVAL' SCAN POINTER TO R2
        TST (SP)+; TEST ARG COUNTER ON STACK
        BGT ARG3; BRANCH IF FUNCTION ARGUMENT
        MOV R0,ARG2; STORE DECIMAL INTEGER VALUE OF DATA
        INC -(SP); INCREMENT ARG COUNTER ON STACK
        BR LOOP; LOOP BACK FOR NEXT ARGUMENT
ARG3:   TST R0; TEST FUNCTION CODE.
        BMI READ; IF FUNCTION CODE IS NEGATIVE
        BEQ 37500; IF FUNCTION CODE IS ZERO
LOAD:   MOV ARG2,@(SP); DATA IN ARG2 TO ADDR IN ARG1
        MOV @(SP)+,R1; MOVE TO R1 TO CONVERT TO FPN
        BR FIN
READ:   MOV @(SP)+,ARG2; CONTENT OF ADDR IN ARG1 TO ARG2
        MOV ARG2,R1; FOR CONVERSION TO FLOATING POINT
FIN:    MOV #ARG2,R0; NEED A CORE ADDRESS FOR FLT
        MOV R2,-(SP); SAVE 'EVAL' SCAN POINTER ON STACK
        FLT; REFLOAT THE RESULT -- SWI TO FPN
        MOV (SP)+,R1; RESTORE 'EVAL' SCAN POINTER
        MOV (SP)+,R4; POP STACK TO RESTORE REGISTERS
        MOV (SP)+,R3
        MOV (SP)+,R2
        MOV -(R0),-(SP); STACK RESULT TO OUTPUT TO BASIC
        MOV -(R0),-(SP)
        MOV -(R0),-(SP)
        JMP 52; RETURN TO BASIC INTERPRETER
ARG2:   0,0,0; DATA / FLT STORAGE
        .END 52
```

Fig. 1. BASIC-EXF program assembly listing

```
LIST

1 REM--DIGITAL ATTENUATOR EXERCISER.  2-14-72.
5 REM--THIS PROGRAM CONTROLS AN 8-BIT DIGITAL ATTENUATOR THROUGH
10 REM--A DR-11A INTERFACE AT LOCATION 160002[8] (-8190[10]).
20 PRINT: PRINT "<*> DIGITAL ATTENUATOR CONTROL PROGRAM <*>": PRINT
045 PRINT "DO YOU DESIRE TO EXERCISE THE ATTENUATOR BY:"
050 PRINT ,"(KEY 1) AUTO-RAMP FOR PHASE/CONFIRMATION CHECK;"
055 PRINT ,"(KEY 2) AUTO-RAMP WITH HALTS AT FIVE EQUAL POINTS"
060 PRINT ,"         (TO CHANGE VOLTMETER RANGE) FOR CHECKING"
065 PRINT ,"         MONOTONICITY;"
070 PRINT ,"(KEY 3) AUTO MAJOR STEP;"
075 PRINT ,"(KEY 4) MANUAL STEPPING;";
080 INPUT D: IF D=1 THEN 100
082 IF D=2 THEN 200
085 IF D=3 THEN 300
090 IF D=4 THEN 400
095 PRINT "TRY AGAIN...1,2,3 OR 4!";: GOTO 080
100 LET C=EXF(-8190,0,1): REM--SET TO MIN. INS. LOSS.
105 PRINT "AUTO-RAMP (PHASE/CONFIRM).  RETURN WHEN READY...";: INPUT H
110 FOR B=1 TO 255: LET C=EXF(-8190,B,1)
115 LET T=5: REM--RAMP RUNS 64 SECS.
120 LET T=T-1: IF T>0 THEN 120
125 IF B=C THEN 155
130 PRINT: PRINT "" "CONFIRM LOST AT STEP" B "(" B/5 "DB. )"
135 REM--FIVE CTRL/G'S (BELL) BETWEEN FIRST QUOTES IN LINE 130.
155 NEXT B
160 LET C=EXF(-8190,0,1): REM--SET TO MIN. INS. LOSS.
165 PRINT "RAMP IS COMPLETE.  CONFIRM IS CORRECT, EXCEPT AS NOTED."
170 PRINT: GOTO 080
200 LET C=EXF(-8190,0,1): REM--SET TO MIN. INS. LOSS.
205 PRINT "HALTING AUTO-RAMP.  RETURN WHEN READY...";: INPUT H
210 LET A=0.2
215 FOR K= 1 TO 5
220 FOR A= A TO A+10 STEP 0.2
225 LET C=EXF(-8190,A*5,1)
228 LET T=10: REM--ONE-FIFTH RAMP RUNS 1 MIN., 29 SECS.
232 LET T=T-1: IF T>0 THEN 232
235 NEXT A
240 PRINT: PRINT "CHANGE VOLTMETER -10 DB.  RETURN WHEN READY...";
245 INPUT H: LET A= A+0.2: NEXT K
250 PRINT "RAMP IS COMPLETE.": PRINT: GOTO 080
300 LET C=EXF(-8190,0,1): REM--SET TO MIN. INS. LOSS.
305 PRINT "AUTO MAJOR STEP.  RETURN WHEN READY...";: INPUT H
310 FOR Q= 0 TO 7
315 PRINT EXF(-8190,2↑Q,1)
320 LET T=150: REM--EACH STEP RUNS 9.2 SECS.
325 LET T=T-1: IF T>0 THEN 325
335 NEXT Q
340 LET C=EXF(-8190,0,1): REM--SET TO MIN. INS. LOSS.
350 PRINT "RAMP IS COMPLETE.": PRINT: GOTO 080
400 PRINT "WHAT IS THE DESIRED ATTENUATION (A) IN DECIBELS?"
405 PRINT "(RESTRICT RANGE FROM 0.0 TO 51.0 DB. IN 0.2 DB. STEPS.)"
410 PRINT "A=";: INPUT A: PRINT "  ";
415 IF A<51.2 THEN 450
420 LET A=A-51
425 IF A>51 THEN 420
450 LET C=EXF(-8190,A*5,1)
455 PRINT C/5 "DB. CONFIRMED."
460 GOTO 410
8191 END
READY
```

Fig. 2. Digital attenuator exerciser program

```
LIST

001 REM--DATE OF THIS REVISION IS 12-6-71.
050 PRINT
060 PRINT "ADC1-D ANALOG-TO-DIGITAL CONVERTER EXERCISER."
070 PRINT "AVERAGES TEN READINGS.": PRINT
095 PRINT "SELECT CHANNEL (0 TO 15), AND GAIN (1,2,4 OR 8);"
100 PRINT "INPUT IN THIS FORM--   C,G"
110 INPUT C,G
120 IF INT(C)>15 THEN GOTO 95
130 IF C<0 THEN GOTO 110
140 LET B=INT(C)*256
210 IF G=1 THEN GOTO 260
220 IF G=2 THEN GOTO 260
230 IF G=4 THEN GOTO 260
240 IF G=8 THEN GOTO 260
250 GOTO 95
260 IF G=1 THEN LET A=0
270 IF G=2 THEN LET A=8
280 IF G=4 THEN LET A=16
290 IF G=8 THEN LET A=24
300 LET Y=0
350 FOR N=1 TO 10
400 GOSUB 1050
450 LET Y=Y+V
500 NEXT N
550 LET V=Y/10: REM--AVERAGE OF 10 READINGS.
700 IF G<3 THEN PRINT INT(V*100+.5)/100 "VOLTS": PRINT
800 IF G>3 THEN PRINT INT(V*1000+.5)/1000 "VOLTS": PRINT
900 REM--ROUND-OFF TO PROPER SIGNIFICANCE.
1000 GOTO 110
1040 REM
1050 LET X=EXF(-520,A+B+1,1)
1060 REM--LOAD ADC C&SR WITH GAIN, CHANNEL AND START.
1100 IF (EXF(-520,0,-1))<128 THEN 1100
1110 REM--TEST ADC ERROR AND DONE BITS.
1120 LET D=EXF(-518,0,-1)
1130 REM--READ ADC DATA REGISTER.
1200 LET V=D*9.765625E-3/G
1210 REM--RESCALE AND PROPORTION DATUM.
1220 RETURN
1230 END
READY
```

Fig. 3. Analog-to-digital converter exerciser program (slow)

```
LIST

1 REM--AD01-D EXERCISER WITH EXF0.  3-6-72.
10 PRINT: GOTO 8000
60 PRINT "AD01-D ANALOG-TO-DIGITAL CONVERTER EXERCISER.": PRINT
70 PRINT "AVERAGE HOW MANY READINGS";: INPUT Q
95 PRINT "SELECT CHANNEL (0 TO 15), AND GAIN (1,2,4 OR 8);"
100 PRINT "INPUT IN THIS FORM ";
110 PRINT "(C,G)";: INPUT C,G
120 IF INT(C)>15 THEN 95
130 IF C<0 THEN 95
140 LET B=INT(C)*256
210 IF G=1 THEN GOTO 260
220 IF G=2 THEN GOTO 260
230 IF G=4 THEN GOTO 260
240 IF G=8 THEN GOTO 260
250 GOTO 95
260 IF G=1 THEN LET A=0
270 IF G=2 THEN LET A=8
280 IF G=4 THEN LET A=16
290 IF G=8 THEN LET A=24
300 LET Y=0: LET D=A+B+1
350 FOR N=1 TO Q: LET Y=Y+EXF(D,0,0): NEXT N
600 LET V=Y*9.765625E-3/(G*N)
650 REM--RESCALE, PROPORTION, AVERAGE DATA.
700 IF G<3 THEN PRINT INT(V*100+.5)/100 "VOLTS": PRINT
800 IF G>3 THEN PRINT INT(V*1000+.5)/1000 "VOLTS": PRINT
900 REM--ROUND-OFF TO PROPER SIGNIFICANCE.
1000 GOTO 110
6192 DATA 5559,-16716,-29705,-16720,1277,7617,-16724,488
8000 FOR A=16192 TO 16206 STEP 2: READ D
8050 LET X=EXF(A,D,1): NEXT A: REM--LOAD EXF0 PROGRAM.
8100 GOTO 60
8191 END
READY
```

Fig. 4. Analog-to-digital converter exerciser program (fast)

```
LIST

1 REM--BASIC-EXF POWER-FAIL HANDLER.  2-16-72.
10 PRINT "POWER-FAIL HANDLER WILL NOW BE LOADED...": PRINT
100 LET X=EXF(20,16328,1): REM--LOAD POWER-FAIL TRAP VECTOR.
200 FOR A=16328 TO 16382 STEP 2
300 READ D
400 LET X=EXF(A,D,1): REM--LOAD MACHINE INSTRUCTIONS.
500 NEXT A
1000 PRINT "THE POWER-FAIL HANDLER IS NOW LOADED."
1010 PRINT "YOUR BASIC USER PROGRAM MAY NOW BE READ-IN"
1020 PRINT "USING THE 'OLD' COMMAND, AND IT WILL BE"
1030 PRINT "PROTECTED FROM POWER FAILURE.": PRINT
1040 PRINT "THE BASIC USER PROGRAM WILL BE RETAINED IN"
1050 PRINT "CORE, AND NOT BE DESTROYED WHEN THE MACHINE IS"
1060 PRINT "TURNED-OFF, PROVIDED THAT THE MACHINE HAS NOT"
1070 PRINT "BEEN HALT-ED AT THE CONSOLE.": PRINT
6328 DATA 4134, 4198
6332 DATA 4262, 4326
6336 DATA 4390, 4454
6340 DATA 4535, 38
6344 DATA 5623, 16352
6348 DATA -16330, 0
6352 DATA 2560, 2688
6356 DATA -31490, 7622
6360 DATA 20, 5509
6364 DATA 5508, 5507
6368 DATA 5506, 5505
6372 DATA 5504, 5623
6376 DATA 16328, -16360
6380 DATA 2, 0
8191 END
READY
```

Fig. 5. Power-fail-save program

Manufacturing Engineering of Surface Panels for the 64-m Antennas

J. Justiss, W. Kissane, and M. S. Katow
DSIF Engineering Section

The procurement of two 64-m antennas for the overseas deep space stations was authorized with new vendors. These changes engendered new procedures to insure quality manufacturing of the surface panels for maximum RF performance. The new checking procedures are described including the mathematical formulations and functional aspects of the checking fixtures. A computer program was developed to solve the parameters. Notes on the computing of arc lengths along the parabolic curve are included.

I. Introduction

One of the major factors affecting the RF performance of the 64-m antennas is the accuracy of the contoured shape of the surface panels for the paraboloidal primary reflector. The change in the vendor for the surface panels for the overseas antennas and the use of new methods of checking the contour tolerances imposed the generation of new procedures to insure quality control. Independent checks on the shop procedures and the checking algorithms were considered advisable because of the importance of obtaining the specified accuracy tolerances.

The overall problem is first reviewed, followed by functional descriptions of the checking tools and fixtures and a schematic procedure of their use. The mathematical algorithm used is then described including some notes on the calculation of arc lengths along a parabola.

II. Program Description

The paraboloidal reflective surface of the 64-m antenna consists of 552 separate surface panels separated by 3.3-mm (0.125 in.) to 9.9-mm (0.38 in.) gaps and individually secured to the top chord of the reflector structure by screw-type adjustable means accessible from the reflective surface side. By use of an accurate angle-measuring theodolite and targets at known arc distances from the vertex of the paraboloid, the corners of the panels can be accurately positioned in a paraboloidal shape. It follows that the contoured surfaces of the individual surfaces must be checked for manufacturing accuracies in reference to these targeted positions. This was done by using contour checking fixtures which, in turn, must be checked by master measurements.

The distortions from the paraboloid, one per 645 cm^2 (100 $in.^2$) of surface, are measured normal to the zero plane determined by the four corners of the panels where the optical targets for the theodolites are located. These distortions are analyzed for the root-mean-square value not to exceed 1.52 mm (0.06 in.) rms. After all the panels are measured, specifications allowed a calculation of the mean and the standard variation about the mean surface from all of the distortion data. This value was set not to exceed 0.89 mm (0.035 in.) rms in the specifications. The actual value attained for the overseas antenna was 0.76 mm (0.030 in.) rms.

Figure 1 shows a perspective view of a typical panel surface outlined on the side edges by equally spaced radial planes $OZP'Q'$ and $OZP''Q''$ by the azimuth angle intervals of 2 times Ψ angles. The top and bottom edges are intersection lines of the paraboloid and the two cylindrical surfaces of RAD_{IN} and RAD_{OUT} radii. In practice, the intersection points of the cylinders, the paraboloid, and the radial planes (P', P'', Q', and Q'') were used to determine the corners of the panel surface and straight cuts of the developed flat surfaces formed the eventual edges. The surface of a panel could also be considered as an equally divided part of a frustum of a paraboloid. Dependent on the panels' distances to the symmetric axis, each frustum segment was divided by 48 or 96 equally spaced radial planes.

III. Contoured Surface Checking Fixture

To avoid the third-dimensional problems, it was logical to use as a measuring base a two-dimensional template that rotates about the symmetric axis of the paraboloid. This was done, as shown on Fig. 2, by providing on the panel holding fixture two flat surfaces which are perpendicular to the symmetric axis and intersect points P and Q of the parabola. The checking template or the transducer beam as finally evolved was located to the holding fixture by the two planes and pins R and S. By locating the holes for these pins in the flat planes at the same radii, the transducer beam was effectively rotated about the symmetric axis of the paraboloid. This checking system has been successfully used by antenna manufacturers. Figure 3 shows a photograph of the actual checking fixture in use.

The template shape replaced by transducer points provides a fast, accurate, and permanent printout record of the readings for each radial position checked. Figure 4 shows the method of zeroing the transducers using the calibration rods.

The panels are located in the fixture by stops on the top surfaces above the panels' mounting points on the antenna itself and at the lower-end edge. Pneumatic pressure applied by cylinders holds the panels in place as transducer beam readings are made.

IV. Formulation Data

A. Paraboloidal Surface

The working points of the surface panels are P', P'', Q', Q'', (Fig. 1) on the parabola and define the chords $P'Q'$ and $P''Q''$. We have the problem: (1) of finding the distance between the chord and the normal distance to the parabola as shown on Figure 5, and (2) of finding the distance between the plane $P''Q''$ that is normal to the XZ plane and the surface of the paraboloid. The plane $P''Q''$ on Fig. 5 would be the same as plane $P'P''Q'Q''$ of Fig. 1.

It is obvious that direct solution of the normal distance is available by transforming the coordinate axis to coincide with either the chord or the plane.

The equation defining the circular paraboloid is (Ref. 1)

$$Z = b_3 + b_4 x + b_5 y + b_9 (x^2 + y^2) \tag{1}$$

For an on-axis paraboloid, the equation reduces to

$$Z = b_9 (x^2 + y^2)$$

where

$$b_9 = \frac{1}{4F}$$

$$F = \text{focal length} \tag{2}$$

By substituting the transformation equations limited to the X and Z parameters

$$X = X' \cos\theta - Y' \sin\theta + X_0$$

$$Z = X' \sin\theta + Z' \cos\theta + Z_0$$

into Eq. (2), we get

$$X' \sin\theta + Z' \cos\theta + Z_0 = b_9 [(X' \cos\theta - Z' \sin\theta + X_0)^2 + Y^2]$$

which reduces to

$$(-b_9 \sin^2\theta)(Z')^2 + (2X' b_9 \sin\theta \cos\theta + 2X_0 b_9 \sin\theta + \cos\theta) Z' + (Z_0 + X' \sin\theta - b_9 Y^2 - b_9 (X')^2 \cos^2\theta - b_9 X^2 - 2X' X_0 b_9 \cos\theta) = 0$$

Thus, Z' or the normal distance between the plane and the paraboloid is computed by the quadratic formula

$$Z' = \frac{-B \pm \sqrt{B^2 - 4AC}}{2A}$$

where

$$A(Z')^2 + BZ' + C = 0$$

and the negative result is output from the program.

B. Arc Length

The arc length along the parabola is used as a parameter for field measuring of distortions with theodolite angles as previously described. Two different formulations for computing the arc lengths may be of interest for checking purposes:

(1) Equation (2) reduces to

$$Z = \frac{1}{4F} x^2$$

for a parabola, and using

$$ds^2 = dx^2 + dy^2 \text{ and } s = ds$$

where s = arc length, after integrating, the solution is

$$s = \frac{X}{2}\sqrt{1 + \frac{1}{4F^2}X^2} + F \ln\left(\frac{X}{2F} + \sqrt{1 + \frac{1}{4F^2}X^2}\right)$$

(2) The arc length is also equal to

$$S = D\left[1 + \frac{2}{3}M^2 - \frac{2}{5}M^4 + \cdots\right] \text{ (from Ref. 2)}$$

D = diameter of the antenna

$$M = \frac{X}{Z}$$

Since the number of terms supplied in the reference did not provide sufficient precision in the answer, the Numerical Analysis Group of the Computation and Analysis Section was the source of the following equation, which checked with the 8-digit accuracy of the answer from Eq. (1) for the 64-m antenna values, using the double-precision mathematics of the 1108 computer:

$$S = D\Big[1 + \frac{2}{3}M^2 - \frac{2}{5}M^4 + 4/7\,M^6 - 10/9\,M^8 + 28/11\,M^{10} - 84/13\,M^{12} + 264/15\,M^{14} - 858/17\,M^{16} + 2860/19\,M^{18}\Big] \quad (3)$$

It should be noted that the series converges only for $M < 0.375$, and close to this value the convergence will be very slow. The value of M for the 64-m antenna is 0.295.

References

1. Lawson, C. L., "Paraboloid Fitting to Minimize Pathlength Error," in *Supporting Research and Advanced Development*, Space Programs Summary 37-32, Vol. IV, pp. 22–24. Jet Propulsion Laboratory, Pasadena, Calif., April 30, 1965.
2. Hudson, R. G., *The Engineers' Manual*, Second Edition. John Wiley & Sons, Inc., New York, August 1945.

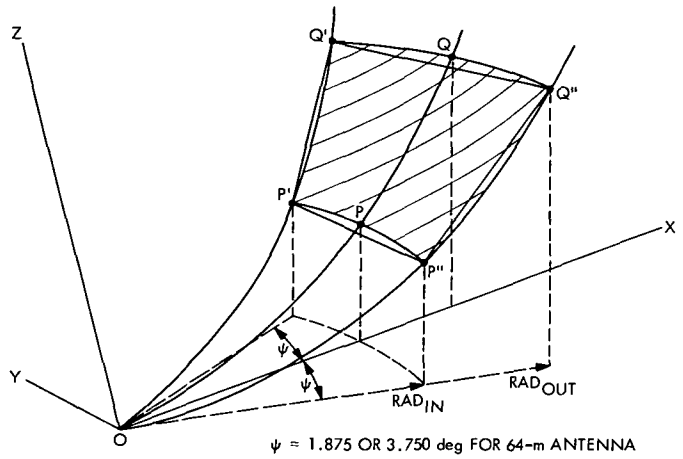

Fig. 1. Perspective view of a panel surface

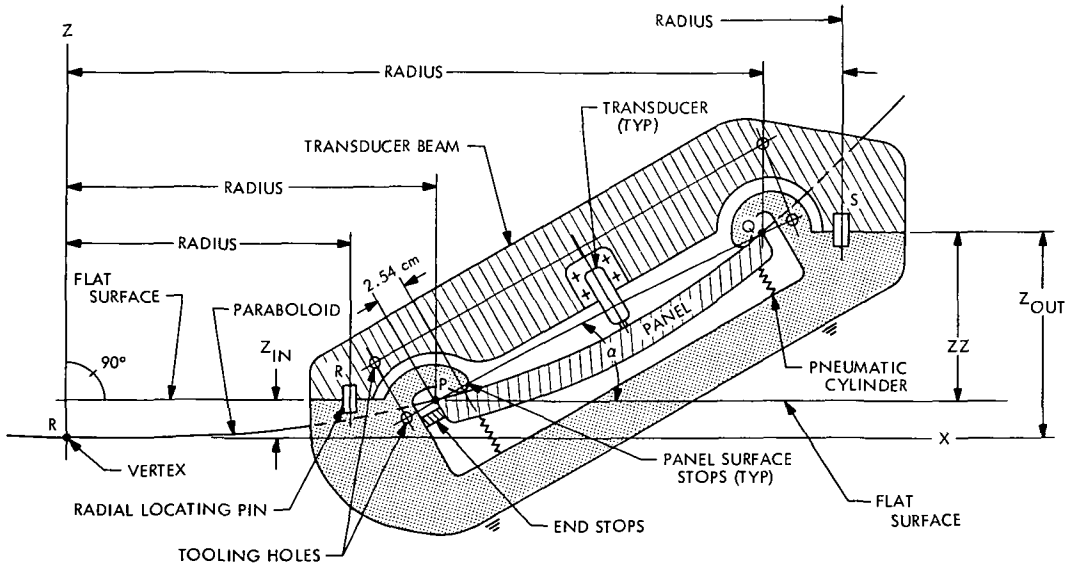

Fig. 2. Surface panel contour checking fixture side elevation view

Fig. 3. Contour checking fixture

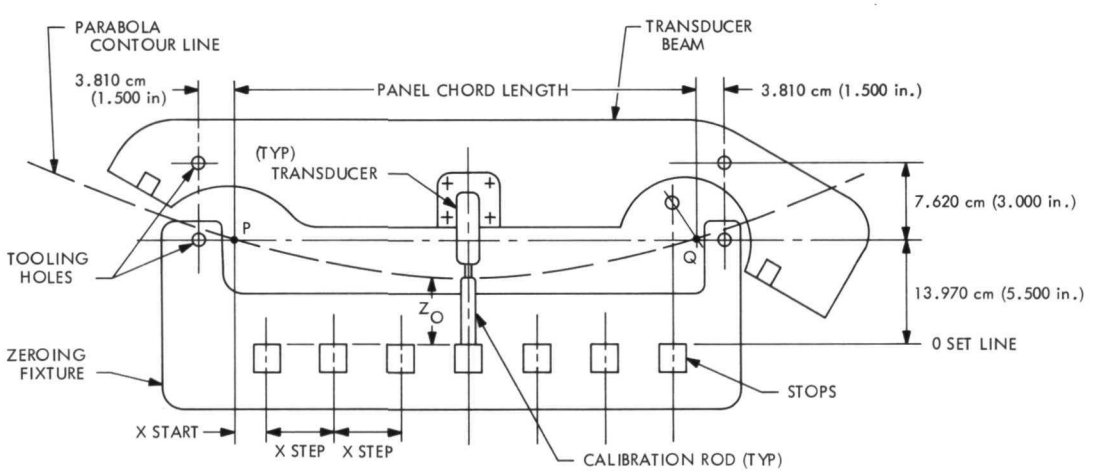

Fig. 4. Transducer zeroing fixture

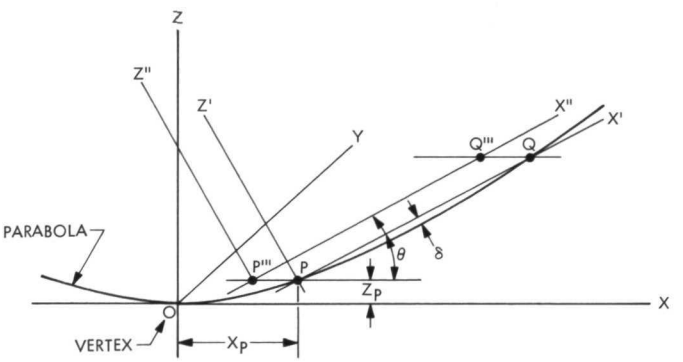

Fig. 5. Coordinate transformation scheme

100-kW X-Band Transmitter for FTS

J. R. Paluka
R.F. Systems Development Section

During the month of July 1971 a 100-kW X-band transmitter was installed on the Venus Deep Space Station's 9-m antenna. This transmitter replaces the experimental 25-kW transmitter formerly used at this station to transmit timing signals via the Moon to five other tracking stations in the Deep Space Network. Primary results of this change are an improved signal-to-noise ratio, higher reliability, and a change from the experimental frequency of 8.450 GHz to the operational frequency of 7.1495 GHz.

I. Introduction

The frequency-time synchronization (FTS) network underwent a scheduled shutdown during the month of July 1971. During this period the 8.450-GHz 25-kW transmitter was removed from the DSS 13 9-m antenna and replaced by a newly designed 7.1495-GHz 100-kW transmitter.

The purpose of the 100-kW X-band transmitter is to broadcast frequency-timing signals, using the Moon as a passive reflector, to five other stations in the Deep Space Network (DSN) as well as the U.S. Naval Observatory in Washington, D.C. The five DSN stations which form a part of this one-way link are located at Goldstone, California (DSS 14), Madrid, Spain (DSS 61), Johannesburg, South Africa (DSS 51), Woomera, Australia (DSS 41), and Weemala, Australia (DSS 42).

A block diagram of the 100-kW X-band transmitter is shown in Fig. 1. This transmitter utilizes some components of the experimental 25-kW X-band transmitter. Those components which were utilized from the older transmitter are the 500-kW motor-generator, the vacuum disconnect switches, the high-voltage transformer, the rectifier, the choke and the local and remote control racks. All other components are new.

A description of the overall FTS system can be found in Refs. 1, 2. A description of the receiving antennas of the forementioned stations is given in Ref. 3.

II. Antenna-Mounted Equipment

A view of the modified 9-m antenna is shown in Fig. 2. All of the transmitter equipment now mounted on the

antenna is new. These units include the buffer amplifier, klystron assembly, the heat exchanger, water manifold, and control instrumentation.

A. Buffer Amplifier

Except for its beam supply, the buffer amplifier shown in Fig. 1 is a self-contained antenna-mounted unit. In addition to power amplification, it performs the following functions in the transmitter: provides a means of remotely varying the drive to the 100-kW klystron, provides a method of quickly ($<10\,\mu s$) removing drive from the 100-kW klystron when arcs occur in the klystron or in other waveguide components, and provides a test point for monitoring drive power. The minimum drive power to the buffer amplifier is +17 dB, and its nominal output is +30 dBmW (1 W).

B. Klystron Assembly

The 100-kW klystron assembly consists of a VA-879G klystron, a VA-1949A focus magnet, body and collector current sensors, filament transformer, and a cathode cooling fan. This assembly is capable of delivering 100-kW average power continuously and under certain limited test conditions can deliver 150 kW. The klystron is tunable between 7100 and 7200 MHz, and the present operating frequency is 7149.9 MHz.

C. Water Manifold

The water manifold distributes the cooling water to the body, collector, and magnet of the klystron; to the RF water load; and to the waveguide. Additionally it serves to control and monitor the pressure and flow rates to each of these distribution points.

D. Control Instrumentation

The antenna-mounted control instrumentation provides limited local control of the transmitter, and provides monitoring of the forward, reflected, and drive power of the klystron assembly. Other functions it houses are the vacion pump power supply and the arc detector circuits. All of these functions are sent from this instrumentation to the ground-based local-control console and the remote-control console.

E. Water-to-Air Heat Exchanger

All of the previously discussed equipment is located in the electronics room of the antenna. This room is located directly below the vertex of the reflector and within the elevation (bull) gear of the 9-m antenna. This room is visible in Fig. 2, which shows the modified 9-m antenna.

Also visible in Fig. 2 is the new heat exchanger which is on the antenna alidade. It was necessary to place the heat exchanger on the alidade, rather than on the ground as it was in the old transmitter, to avoid problems of bringing the water lines through the cable wrapup.

A pure water system was necessary for the VA-879G klystron rather than an ethylene-glycol solution. Winterization is provided by heaters in the surge tank which, together with the pumps, are controlled by outside air temperature.

Other major components of the heat exchanger are the two 29,840 W (40-hp) pumps, two 7460 W (10-hp), 1.22-m (48-in.) fans and an eight-layer-deep core. Weight of the entire heat exchanger system is 66,150 kg (30,000 lb).

The heat exchanger is capable of dissipating 490 kW of heat at ambient air temperature of 32.2°C (90°F) and below, and 340 kW of heat at ambient air temperature of 51.5°C (125°F) and below. This latter condition is the amount of heat dissipated when the transmitter is supplying 100 kW into the RF water load. Normal flow rate is 0.0884 m^3/s (140 gal/m).

III. Ground-Mounted Equipment

Major transmitter units mounted on the ground are the beam power supply, the local-control console and the remote-control console.

A. Beam Power Supply

The beam power supply is located in proximity to the base of the antenna. This supply is a modification of the beam supply of the old transmitter. Modifications include additional protective circuits for the power supply and a crowbar for klystron protection. The function of the crowbar is to quickly ($<10\,\mu s$) remove both RF drive and beam voltage from the klystron in the event of arcing within the klystron or waveguide components or in the event of excessive reflected power back into the klystron. Should either event occur, the crowbar opens three vacuum switches to disconnect the output of the 500-kW motor generator set and fires an ignitron to discharge the beam supply output through a resistor to ground. Simultaneously with this action the crowbar also closes (50-dB isolation)

two crystal switches in the buffer amplifier to remove RF drive to the klystron. Maximum output of the beam supply is 48.6 kV and 10 A.

B. Local and Remote Control Consoles

The local and remote consoles each provide for complete control of the transmitter. The local console is in a building about 30 m from the antenna, and the remote console is in the operations building of DSS 13. These units are similar to the configuration used for the old 25-kW transmitter.

IV. System Testing

System testing is now under way. Good data correlation has been achieved at all receiving DSN stations. The reported signal-to-noise ratio is now in excess of 10 dB at all receiving stations. Signal-to-noise ratios using the old system normally ran between 6 to 8 dB. This improvement is particularly significant, because the old receiving system had a noise figure between 7 and 8 dB. This increase in noise figure is a result of changing from a tunnel diode to a crystal mixer in the receiver first stage. This change was a tradeoff for improved reliability.

References

1. Higa, W. H., "Time Synchronization via Lunar Radar," accepted for publication in the *Proceedings of the IEEE*, May 1972.
2. Coffin, R. C., Emerson, R. F., and Smith, J. R., "Time Synchronization System," in *The Deep Space Network*, Space Programs Summary 37-45, Vol. III, pp. 72–75. Jet Propulsion Laboratory, Pasadena, Calif., May 31, 1967.
3. Kron, M., "Four-Foot HA-Dec Time-Synchronization Antenna Mount," in *The Deep Space Network*, Space Programs Summary 37-46, Vol. III, pp. 109–113. Jet Propulsion Laboratory, Pasadena, Calif., July 31, 1967.

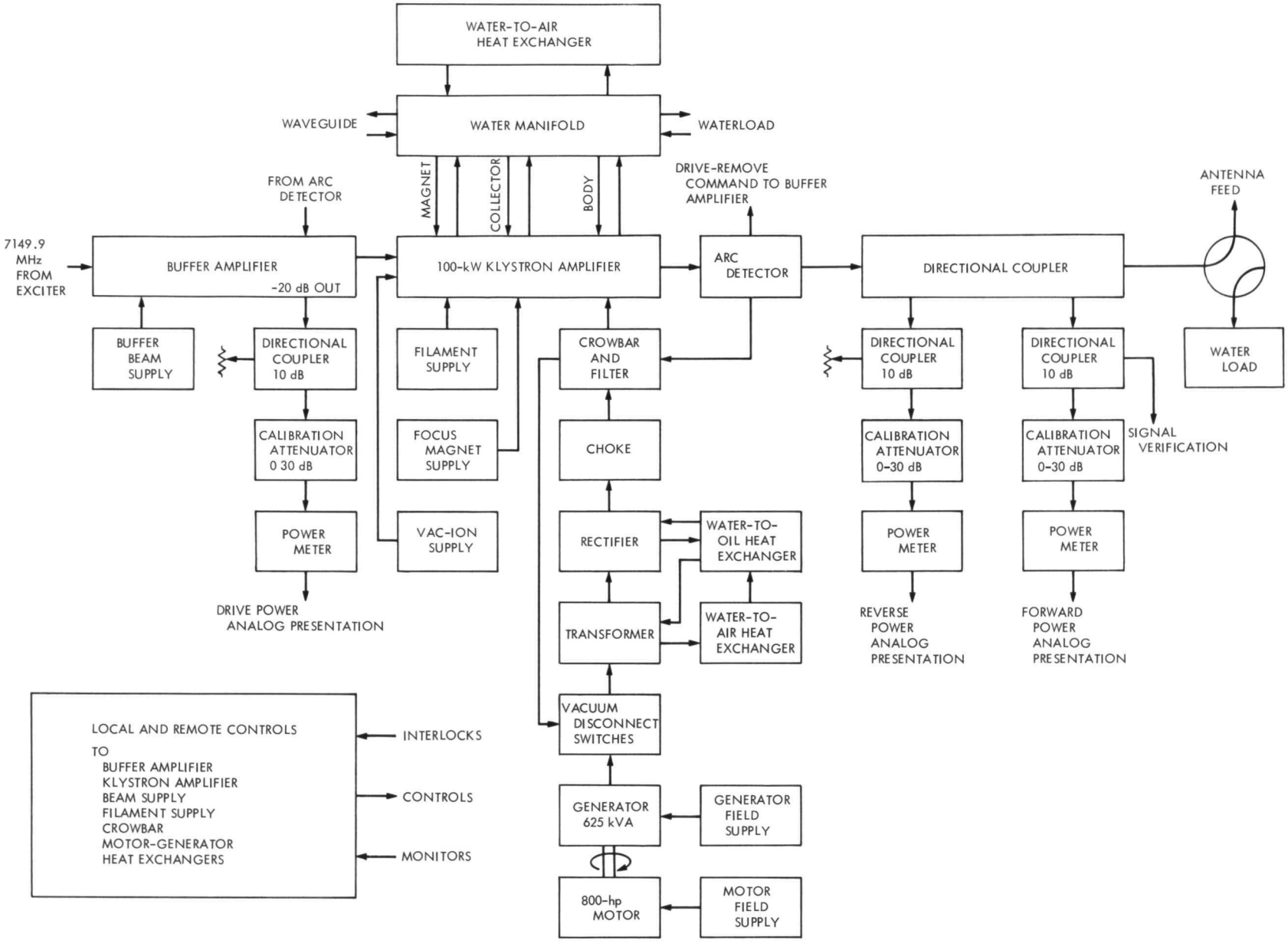

Fig. 1. Block diagram of 100-kW X-band transmitter

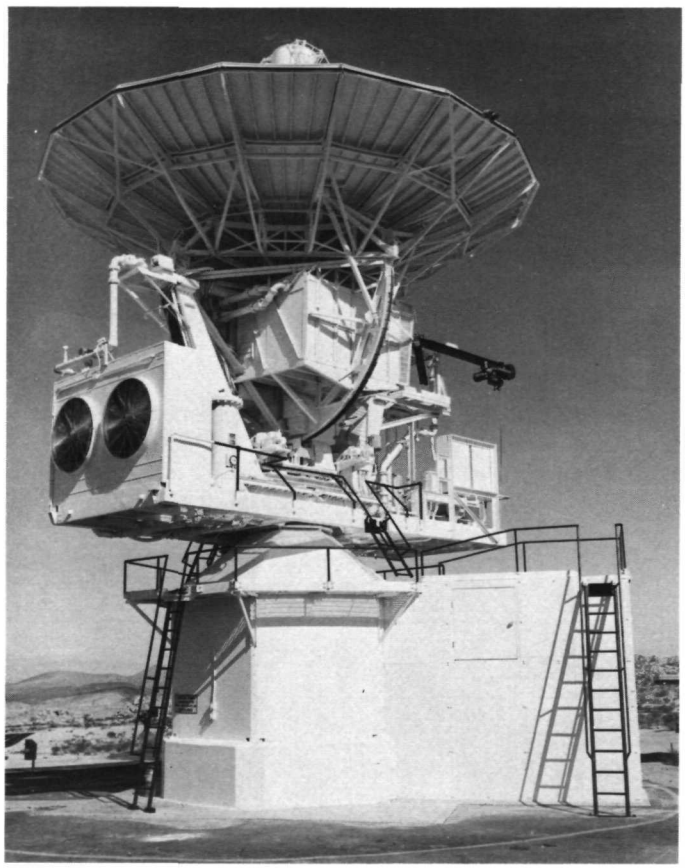

Fig. 2. View of modified 9-m antenna

Third-Order Phase-Locked Loop Perspectives

D. W. Brown
R.F. Systems Development Section

Analysis and practical application of third-order phase-lock design have been sporadic, compared with the second-order, in both the servomechanism and telecommunication fields. The attractiveness of minimal tracking errors resulting from near "perfect" third-order filtering (three true integrators) has been largely offset by undesirable acquisition properties and to some extent by a dearth of analysis of this configuration. A useful approach, both in viewpoint and in design, is to consider the prevalent "imperfect" second-order and third-order configurations for what they are—namely, loops with one integrator augmented by one or two lag time constants, so proportioned with respect to loop gain as to approximate the closed-loop response of true second- and third-order configurations, while manifesting a controlled (but not infinite) improvement in tracking performance over the first-order loop. This article seeks to apply this approach to the existing work in third-order analysis, and to emphasize the principal effects, both positive and negative, of the relative proportioning of loop gain and time constants, with a view toward practical exploitation of the best features of these loop configurations.

I. Introduction

Many works on phase-locked loops commence with first-order, progress to second-order, touch upon third-order, and then revert to an extensive treatment of second-order loops. While true that the latter is the most prevalent application, it seems clear that this sequence and depth of analysis are, in part, due to the fact that exact mathematical models exist for the first-order loop and quite adequate, but approximate, models exist for the second-order loop; and only tentative optimizations have appeared for the third-order loops. The word "tentative" is used here to imply that while there have existed theoretically optimum designs (Ref. 1) for the tracking of input signals of specified characteristics, they may have lacked acceptable acquisition or stability properties over a range of input signal-to-noise ratios.

One of the more recent and detailed treatments (Ref. 2) of third-order loops appears to have made a significant step in overcoming these detrimental characteristics by evolving new optimization criteria. Whether by design or circumstance, this treatment by Tausworthe and Crow (Ref. 2) is closely structured to a "parallel" loop filter—that is, one which sums the output of a single-pole filter with that of a double-pole filter. This, coupled with the notation adopted, lends itself admirably to the switched second-to-

third order or "hybrid" application, as well as to a "straight" third-order design in which it is of interest to compare performance with that of the loop which results from the single-pole filter path only.

The purpose of this article is to apply the results and exactitude of the referenced work to a more conventional configuration by establishing an equivalence of the loop configurations and a somewhat re-oriented notation. This article will concern itself specifically with the optimum design and application of the third-order loop confronted with a variable signal level. Fortuitously, this condition is virtually sufficient to establish the equivalence mentioned above. Therefore, this treatment will be equally applicable to both configurations. A further purpose is to summarize and extend the analysis to include optimum investment of the third-order characteristic and to establish a direct comparison with second-order tracking performance given the same circuit technology.

II. The General Transfer Function

Consider the phase-locked loop whose open-loop transfer function is

$$G(s) = \frac{G}{s}\frac{(1+T_2 s)(1+T_4 s)}{(1+T_1 s)(1+T_3 s)} \tag{1}$$

This loop has been considered (Ref. 3) with intuitive time constant scaling, but represents the form for which we seek a more rigorous and detailed analysis. Let us now proceed to develop a specific notation and optimization, borrowing heavily from Tausworthe (Refs. 2 and 4) and Hoffman (Ref. 5).

Tausworthe's parallel filter open-loop model is of the form

$$G'(s) = \frac{AK}{s}F(s)$$

$$= \frac{AK}{s}\left[\frac{1+\tau_2 s}{1+\tau_1 s} + \frac{1}{(1+\tau_1 s)(\delta+\tau_3 s)}\right] \tag{2}$$

with the following definitions:

$$\left.\begin{aligned} k &= \tau_2/\tau_3 \\ \epsilon &= \tau_2/\tau_1 \\ r &= AK\tau_2^2/\tau_1 \\ AK &= \text{open-loop gain at zero frequency (second-order path)} \\ \frac{AK}{\delta} &= \text{open-loop gain at zero frequency (third-order path)} \end{aligned}\right\} \tag{3}$$

An optimum value for k has been established for which the loop will be unconditionally stable for all higher values of signal level, that is, for $r \geqq r_0$ (design point). This value is 1/4, subject to the restriction that the third-order lag time constant (τ_3/δ) be much larger than the lead compensation (τ_2). This restriction is directly analogous to the usual second-order assumption of $\tau_2/\tau_1 = \epsilon << 1$.

III. Establishing Equivalence

Rewrite Eq. (2):

$$G'(s) = \frac{AK}{s}\left[\frac{1+\tau_2 s}{1+\tau_1 s} + \frac{1}{(1+\tau_1 s)(\delta+\tau_3 s)}\right]$$

and, with a little manipulation,

$$G'(s) = \frac{AK}{s}\left(\frac{1+\delta}{\delta}\right) \times \left[\frac{1+\left(\frac{\delta}{1+\delta}\right)(\tau_2+\tau_3/\delta)\,s + \left(\frac{\delta}{1+\delta}\right)\frac{\tau_2\tau_3}{\delta}s^2}{(1+\tau_1 s)(1+\tau_3/\delta\, s)}\right] \tag{4}$$

The numerator is factorable with negative real roots, provided $\delta << 1$ and

$$\delta^2\left(\tau_2 + \frac{\tau_3}{\delta}\right)^2 = 4\tau_2\tau_3 \tag{5}$$

Examination of Eq. (4) reveals τ_1 and τ_3/δ to be the lag time constants, and τ_2 and τ_3 to be the approximate lead time constants and, therefore, δ represents the approximate lead–lag ratio, thus justifying the $\delta << 1$ approximation for moderate-to-high-performance loops. By similar reasoning,

$$\tau_2 + \frac{\tau_3}{\delta} \approx \frac{\tau_3}{\delta}$$

and Eq. (5) becomes

$$\tau_3^2 = 4\tau_2\tau_3$$

$$\frac{\tau_2}{\tau_3} = k = \frac{1}{4}$$

Thus, we find the necessary condition for cascaded equivalence to be identical to the aforementioned criterion for stability versus signal level, namely, $k = 1/4$. A term-by-term comparison of Eqs. (1) and (4), that is, setting $G(s) = G'(s)$, now yields

$$
\left.
\begin{aligned}
G &= AK\left(\frac{1+\delta}{\delta}\right) \approx \frac{AK}{\delta} \\
T_1 &= \tau_1 \\
T_3 &= \frac{\tau_3}{\delta} \\
T_2 T_4 &= \frac{\tau_2 \tau_3}{1+\delta} \approx \tau_2 \tau_3 \\
T_2 + T_4 &= \frac{\delta \tau_2 + \tau_3}{1+\delta} \approx \tau_3
\end{aligned}
\right\} \quad (6)
$$

and, setting $\tau_2/\tau_3 = 1/4$,

$$
\left.
\begin{aligned}
\frac{T_2 T_4}{(T_2+T_4)^2} &= \frac{1}{4} \\
T_2 = T_4 &= \frac{\tau_3}{2} = 2\tau_2
\end{aligned}
\right\}
$$

The open-loop transfer function may now be written as

$$
G(s) = \frac{G}{s}\left[\frac{(1+T_2 s)^2}{(1+T_1 s)(1+T_3 s)}\right] \quad (7)
$$

with relations (3) restated in terms of Eq. (7):

$$
\left.
\begin{aligned}
\epsilon &= \frac{T_2}{2T_1} \\
\frac{\delta}{4} &= \frac{T_2}{2T_3} \\
r &= \frac{G}{2}\frac{T_2^3}{T_1 T_3}
\end{aligned}
\right\} \quad (8)
$$

A word about approximations is perhaps in order at this point. The two measures of "imperfection" of the circuit "integrators" (ϵ and δk or $\delta/4$) will, for clarity, be taken as much less than unity, but never assumed to be zero. Indeed, the design "management" of these two small quantities (and related loop gain) constitutes a significant set of design tradeoffs. Therefore, only the first-order effects of ϵ and δ will usually be considered.[1]

The definitions and equivalences of (3) and (6) are summarized in Appendix A. The identities and subsequent definitions based upon Eq. (7) are listed in Appendix B.

In order to establish the design point (minimum) value of the loop-gain-related variable, r, consider the closed-loop transfer function

$$
H(s) = \frac{1 + 2T_2 s + T_2^2 s^2}{1 + \left(1 + \frac{1}{2GT_2}\right)2T_2 s + \left(1 + \frac{T_1 + T_3}{GT_2^2}\right)T_2^2 s^2 + \frac{T_1 T_3}{G} s^3} \quad (9)
$$

or

$$
H(s) \approx \frac{1 + 2T_2 s + T_2^2 s^2}{1 + 2T_2 s + T_2^2 s^2 + \frac{T_1 T_3}{G} s^3}
$$

Tausworthe's criterion of no underdamped roots in the interest of reliable acquisition can be applied by examining the characteristic equation, obtained by substitution:

$$
s^3 + \frac{2r}{T_2} s^2 + \frac{4r}{T_2^2} s + \frac{2r}{T_2^3} = 0
$$

A standard test for no imaginary roots reveals that

$$
r \geqq r_0 = \frac{27}{8} \quad (10)
$$

As with the second-order loop, performance will be a function of r/r_0, since

$$
G = \frac{r}{r_0} G_0
$$

[1]For instance, the relations in (8) result from approximations in the establishment of equivalence and r could be written more exactly as

$$
r = \frac{G}{2(1+\delta)}\frac{T_2^3}{T_1 T_3}
$$

On the other hand, one can take the view that once the equivalence and related optimizations have been established, relations in (8) become exact definitions for the cascade configuration. In fact, unpublished notes have *defined* a quantity

$$
q = \frac{GT_2^3}{T_1 T_3}
$$

yielding the equivalence relation

$$
q = 2r(1+\delta) \approx 2r
$$

In the material that follows, G and r will usually be written as such for generality; however, $r_0 = 27/8$ will be implicitly assumed, especially in the next section dealing with approximations of comparative performance.

IV. Design Considerations

A. Definitions

We have now expended two of our five degrees of freedom[2]—that is, ratio of leads (function of k) and (design point) damping, $r = r_0$. Before investigating further the properties of the third-order loop, let us define:

$$\omega_1 = G \tag{11}$$

$$\omega_2 = \left(\frac{G}{T_1 + T_3}\right)^{1/2} \tag{12}$$

$$\omega_3 = \left(\frac{G}{T_1 T_3}\right)^{1/3} \tag{13}$$

By standard operations on Eq. (9), we see that ω_1 relates to (steady-state) phase error due to frequency offset and ω_2^2 to phase error due to a frequency ramp. Referring to Fig. 1, we see that ω_3 is the radian frequency at which the open-loop transfer function would pass through unity gain were it not for the lead compensation, T_2. As such, ω_3 bears a close relationship to the bandwidth of the closed-loop response.

The distinctive advantage of the third-order over second-order loop lies in the ability to set ω_2 greater than ω_3. In the second-order loop, ω_2, or as usually written, $\omega_n \simeq (G/\tau_1)^{1/2}$, represents both the closed-loop bandwidth and the reciprocal root of the ramp error coefficient.

B. Performance Factor

Let us define a performance factor, F, corresponding to the italicized statement above; that is,

$$F = \frac{\omega_2}{\omega_3}$$

$$F^6 = \left(\frac{G}{T_1 + T_3}\right)^3 \left(\frac{T_1 T_3}{G}\right)^2 = \frac{GT_1 \left(\frac{T_3}{T_1}\right)^2}{\left(1 + \frac{T_3}{T_1}\right)^3} \tag{14}$$

[2]Physically represented by G, T_1, T_2, T_3, T_4.

or, alternatively,

$$F^6 = \frac{G\sqrt{T_1 T_3}\left(\frac{T_3}{T_1}\right)^{3/2}}{\left(1 + \frac{T_3}{T_1}\right)^3}$$

$$F^2 = \frac{(G\sqrt{T_1 T_3})^{1/3}\left(\frac{T_3}{T_1}\right)^{1/2}}{\left(1 + \frac{T_3}{T_1}\right)} \tag{15}$$

We now find that given constant gain and bandwidth, and therefore constant $G\sqrt{T_1 T_3}$, F is maximized when

$$T_3 = T_1 \qquad \text{or} \qquad \frac{4\epsilon}{\delta} = 1$$

resulting in

$$F^2_{\text{opt}} = \frac{(GT_1)^{1/3}}{2} = \frac{(2r)^{1/3}}{4\epsilon} \tag{16}$$

The conclusions here are that (1) for any given bandwidth and gain, the ramp error will be minimized when $T_1 = T_3$ (equal lags), and (2) the $G\sqrt{T_1 T_3}$ or GT_1 product is a measure of "how much third-order characteristic" is embodied in the design.

Now, let us generalize upon this result. As defined above, $F = \omega_2/\omega_3$ is a measure of third-order performance, but is based upon the $\epsilon, \delta << 1$ simplification. While this is a useful design assumption in many cases, a more general definition of F is

$$F_x = \frac{\text{Reciprocal root of ramp error coefficient}}{\text{Open-loop (undamped) unity gain frequency}} = \frac{\omega_2}{\omega_x}$$

The previously used expression for the numerator,

$$\omega_2 = \left[\frac{G}{T_1 + T_3}\right]^{1/2}$$

can be seen to be applicable over the full range of $0 \leqq T_3/T_1 \leqq \infty$. On the other hand, the denominator of F_x may be obtained by setting the absolute value of Eq. (7) to unity, yielding

$$\left(\frac{T_1 T_3}{G}\right)^2 \omega_x^6 + \left[\left(\frac{T_1 + T_3}{G}\right)^2 - \frac{2T_1 T_3}{G^2}\right]\omega_x^4 + \frac{\omega_x^2}{G^2} = 1$$

The solution of this expression for ω_x is not conveniently expressible over the full range of T_3/T_1. However, it will be stated without proof that whereas the unity gain frequency ω_x equals ω_3 for moderate ratios of T_3/T_1, ω_x approaches $[G/T_1]^{1/2}$ or $[G/T_3]^{1/2}$ as T_3/T_1 approaches zero or infinity, respectively, and that

$$F_x^2 = \frac{\omega_2^2}{\omega_x^2} \approx 1 + \frac{\omega_2^2}{\omega_3^2} \tag{17}$$

Now consider a second-order loop of fixed G and T_1, augmented by T_3 as T_3/T_1 increases from zero to infinity.

From Eqs. (14) and (17), we can now write

$$F_x^2 = 1 + \frac{(GT_1)^{1/3}\left(\frac{T_3}{T_1}\right)^{2/3}}{\left(1 + \frac{T_3}{T_1}\right)} \tag{18}$$

This expression is plotted with GT_1 as a parameter in Fig. 2. This presentation offers an insight to the effect of T_3: As it increases (relative to T_1) from zero, it represents the typical "extra time constant" (Ref. 6) in a second-order loop until it becomes a stability "problem" in the transitional region, where it increases over $1/\omega_n$ to bring about a third-order characteristic. As T_3/T_1 eventually exceeds GT_1, the loop reverts to one of second order, now with T_3 as the principal time constant and T_1 in the role of "extra."

The asymmetry of the curves results from the situation chosen for illustration, i.e., constant G and T_1. If we now fix our attention near $T_3/T_1 = 1$ and ask: "How does the performance vary with T_3/T_1, given a constant gain and closed-loop bandwidth," we get

$$F_x^2 = 1 + \frac{(G\sqrt{T_1T_3})^{1/3}\left(\frac{T_3}{T_1}\right)^{1/2}}{\left(1 + \frac{T_3}{T_1}\right)} \tag{19}$$

as plotted in Fig. 3.

Consider now the time constant required by a second-order loop compared to a third-order design, again holding constant the gain and closed-loop bandwidth. By setting $\omega_n = \omega_3$,

$$\frac{G}{\tau_{1_{2nd}}} = \left(\frac{G}{T_1T_3}\right)^{2/3}$$

$$\frac{\tau_{1_{2nd}}}{\sqrt{T_1T_3}} = (G\sqrt{T_1T_3})^{1/3}$$

or, if we set $T_3 = T_1$,

$$\frac{\tau_{1_{2nd}}}{T_1} = (GT_1)^{1/3} = 2F_{opt}^2$$

or, in terms of second-order measure,

$$\frac{\tau_{1_{2nd}}}{T_1} = (G\tau_1)^{3/4}$$

Since the GT_1 product is always a large number (see Fig. 1 and Appendix B), we find that the ω_2/ω_3 performance advantage is accompanied by a reduction in required time constant for the case under consideration ($\omega_n = \omega_3$ and $G = G$). The inverse statement of this effect (i.e., maintaining constant gain and time constant, third-order design offers narrower bandwidth) appears later in the section dealing with steady-state error.

It must be noted that because ω_3 has been chosen as representative of closed-loop bandwidth in the definition of F, Figs. 2 and 3 and the equations of this paragraph implicitly set $r = r_0 << F_{opt}$. For this reason, numerical application of this paragraph is not generally warranted for $G > G_0$.

C. Design Conclusions

The titles "Normalized ramp performance" for Figs. 2 and 3 arise through squaring the original definition of F_x above and by noting that for the second-order loop, $\omega_x = \omega_2 = \omega_n$. In other words, F_x^2 or ω_2^2/ω_x^2 may be considered as either the ratio of ramp performance for the two loop orders or, alternatively, as a measure of third-order ramp performance normalized to bandwidth.

Indeed, as F_x approaches unity, by definition, second-order performance prevails; similarly, as F_x approaches infinity, an "ideal" third-order loop is manifested, with infinitesimal steady-state errors. But extremely large values of loop gain and/or time constant are neither practically achievable nor necessarily desirable from an overall performance standpoint.

In summary, then, with or without the exact optimization of $T_1 = T_3$ (it is difficult to envision a circumstance where this should not be applied), the fifth degree of freedom[3] consists of "modulating" the GT_1 product with respect to bandwidth selection in achieving a compromise

[3]As noted earlier, the ratio of leads and damping have been considered established; we may now consider T_1 versus T_3 and closed-loop bandwidth the third and fourth degrees, respectively.

between steady-state tracking errors and problems of design and performance associated with high GT_1. Some of these performance characteristics will be examined in the next section.

V. Performance Characteristics[4]

A. Closed-Loop Frequency Response

Referring back to the approximate form of Eq. (9), and to the design point value of r given in Eq. (10), we may write

$$H(j\omega) = \frac{1 - \omega^2 T_2^2 + j2\omega T_2}{1 - \omega^2 T_2^2 + j\left(2\omega T_2 - \frac{4}{27}\omega^3 T_2^3\right)} \tag{20}$$

and the loop error

$$1 - H(j\omega) = \frac{-j\frac{4}{27}\omega^3 T_2^3}{1 - \omega^2 T_2^2 + j\left(2\omega T_2 - \frac{4}{27}\omega^3 T_2^3\right)} \tag{21}$$

The absolute values of these functions have been plotted in Fig. 4 with respect to the normalized ω/ω_3 for a third-order loop in comparison to the familiar second-order curves given as a function of ω/ω_n.

B. Loop Noise Bandwidth[5]

It has been shown that

$$2\beta_L = W_L = \frac{r}{2\tau_2}\left[\frac{r-k+1}{r-k}\right]$$

which may be rewritten in the cascade notation as

$$2\beta_L = W_L = \frac{r}{T_2}\left(\frac{4r+3}{4r-1}\right) \tag{22}$$

$$2\beta_{L_0} = W_{L_0} = \frac{891}{200T_2}, \qquad \text{given } r = r_0 = \frac{27}{8}$$

or, in terms of $\omega_3 = (G/T_1T_3)^{1/3}$:

$$2\beta_L = W_L = \left(\frac{r^2}{2}\right)^{1/3}\left(\frac{G}{T_1T_3}\right)^{1/3}\left(\frac{4r+3}{4r-1}\right) \tag{23}$$

$$2\beta_{L_0} = W_{L_0} = \frac{297}{100}\frac{\omega_{3_0}}{(2)^{1/3}} \approx 2.36\,\omega_{3_0}$$

For the second-order loop, we have

$$2\beta_L = W_L = \frac{r+1}{2\tau_2} \tag{24}$$

$$2\beta_L = W_L = \frac{r+1}{2\sqrt{r}}\left(\frac{G}{\tau_1}\right)^{1/2} \tag{25}$$

$$2\beta_{L_0} = W_{L_0} = \frac{3}{2\tau_2} \approx 1.06\,\omega_{n_0}, \qquad \text{given } r = r_0 = 2$$

C. Steady-State Error

The steady-state error in response to an input of $\Omega(t)$ instantaneous frequency offset and Λ_0 rate of change of frequency is given by

$$\Phi_{ss} = \frac{\Omega(t)}{G} + \Lambda_0\frac{T_1 + T_3}{G}$$

or, in the case of $T_3 = T_1$,

$$\Phi_{ss} = \frac{\Omega(t)}{G} + \Lambda_0\frac{2T_1}{G} = \frac{\Omega(t)}{G} + \frac{\Lambda_0}{\omega_3^2} \tag{26}$$

For the second-order loop,

$$\Phi_{ss} = \frac{\Omega(t)}{G} + \Lambda_0\frac{\tau_1}{G} = \frac{\Omega(t)}{G} + \frac{\Lambda_0}{\omega_n^2} \tag{27}$$

Comparing these two expressions, we can formulate another second-to-third-order loop comparison as follows. Given a second-order loop design of G, τ_1 and appropriate damping, a third-order loop may be formed by halving the τ_1 filter and placing the halves in series as T_1 and T_3,[6] maintaining the same G and readjusting the damping; the resulting third-order loop will have exactly the same steady-state phase error due to offset and ramp as the given loop and will have a noise bandwidth approximately $1/F_{\text{opt}}$ times narrower.

D. Acquisition Range

For the ideal (no hardware biases or nonlinearities) noiseless case, it has been shown that the maximum frequency pull-in range is given by

$$\Omega_0 \leq \frac{r}{\tau_2}\left[\frac{2\tau_1}{\tau_2}\left(\frac{1+\delta}{\delta}\right)\right]^{1/2}$$

[4]Unless otherwise specified, ϵ and $\delta/4$ are assumed to be much less than unity, but greater than zero. Also, the equivalences of Eq. (6) apply throughout.

[5]β_L and W_L are in hertz; all other frequencies are in radians/second.

[6]Conservation of time constant $T_1 + T_3 = \tau_1$, while probably not a usual design concept, is of economic as well as mathematical consequence.

which, for third-order, $\delta << 1$ and $T_1 = T_3$, reduces to

$$\Omega_0 \leqq \frac{\sqrt{2}r}{T_2\epsilon} = \frac{2\sqrt{r}}{T_2}\sqrt{GT_2} \tag{28}$$

and, for second-order, $\delta >> 1$, yields

$$\Omega_0 \leqq \frac{\sqrt{2}r}{\tau_2\sqrt{\epsilon}} = \frac{\sqrt{2r}}{\tau_2}\sqrt{G\tau_2} \tag{29}$$

In terms of gain (G) and bandwidth ($1/\tau_2$ or $1/T_2$), we find that pull-in ranges for the second- and third-order loops are comparable and yet there is a difference of $\epsilon^{1/2}$ in terms of bandwidth only ($1/\tau_2$ or $1/T_2$). This arises from the fact that for the $T_1 = T_3$ third-order loop, G is proportional to ϵ^{-2}, whereas for the second-order, G varies as ϵ^{-1}. This effect can also be observed for steady-state error. That is, for a given bandwidth, second-order step error varies as ϵ^{-1} and ramp error as ϵ^0, while third-order step error varies as ϵ^{-2} and ramp error as $\epsilon^{-1/2}$, even though Eqs. (26) and (27) are essentially identical as expressed in terms of G and τ_1 or T_1. Obviously, extreme care must be exercised in the drawing of comparative conclusions. These relationships result directly through application of the identities of Appendix B. Appendix C attempts to catalog these relationships by relating the orders-of-magnitude, in terms of ϵ and of G, of second- and third-order performance.

Returning to acquisition, unpublished work of Tausworthe shows that in the presence of hardware drift referred to phase error, θ_d, expressed in radians, pull-in from one side is not simply reduced in range in proportion to $\theta_d G$, but is conditional upon initial conditions of the acquisition process, unless

$$|\theta_d| < \sqrt{2}\epsilon$$

for the $T_1 = T_3$ third-order loop. So, while for negligible θ_d, pull-in range will be enhanced as $\epsilon, \delta \to 0$, the existence of a finite θ_d will bound the useful ϵ, δ unless circumstances of acquisition (initial conditions) are well controlled.

E. Design Limitations

We have found that, in general, performance characteristics of tracking loops are all enhanced as $\epsilon, \delta \to 0$, either in the secondary sense of validation of approximations or in the primary sense of steady-state tracking errors. However, in the paragraph above, we encountered a limitation. Other considerations of practical implementations which are negative attributes of high-gain designs include:

(1) Cost and resistance shunting (leakage) of large capacitors and of extremely high-gain operational amplifier configurations.

(2) Unpredictability of performance under conditions of leakage versus time, environment, and hardware sample. This can be partially overcome through the use of compensating circuit configurations, such as with capacitance in an operational feedback configuration, gain and time constant are equally affected by shunting, thus yielding a constant G/T ratio and consequent stabilization of some aspects of performance.

(3) Design difficulties related to saturation of operational amplifiers and VCOs.

(4) Acquisition uncertainties due to input noise and hardware drift.

(5) Operational limitations resulting from combinations of the above.

Since these limitations are so dependent upon specific circuit technologies and configurations, as well as particular performance applications, it would be virtually impossible to offer any comprehensive analytical treatment of these effects. Rather, the approach here has been an attempt to clarify the performance through the perspectives and relationships established earlier and summarized in Appendix C, thus allowing the designer to choose an appropriate loop order and gain to just satisfy his performance objectives while realizing a tolerable set of "negative" effects.

F. Acquisition Strategies

While considering closed-loop (tracking) performance, it may have been noted that the two extra degrees of freedom (T_3 and T_4) available in third-order loop design were spent early, in the interest of stability and minimization of ramp error ($T_1 = T_2$ and $T_3 = T_4$). To put it more directly, third-order design and second-order design both reduce to a choice of loop gain and bandwidth. This rationale assumes that the established values of design point damping are beyond question for the variable signal level tracking loop. Actually, for the third-order design, the criterion of critical damping at design point ($r_0 = 27/8$), in the interest of reliable acquisition, may be a bit conservative. As with the second-order practice of $r_0 = 2$, one could design for a slight underdamping at design point and still realize unconditional stability at all higher signal levels. While rigorously related mathematically (see Appendices A and B and Refs. 2 and 4), the significance of a given value of r_0 in each loop order is somewhat different. It has been pointed out that more analysis in this area may be enlightening.

Assuming now that all the foregoing has established a tracking design, there are two commonly used strategies of acquisition taken together or separately that alter the loop (additional external aids such as frequency sweeping will not be considered here). Firstly, one can seek to control the initial conditions—commonly implemented and referred to as either "open" or "shorted" loop. Extra care must be exercised here for third-order design due to the existence of twice as many repositories for initial charge as in the more familiar second-order design. And secondly, one may choose to modify one or more of the five loop parameters to enhance pull-in range or time and/or to reduce (until lock is achieved) the effect of a hardware imperfection. Several strategies that have been used in second-order applications are:

(1) Reduce τ_1 and τ_2, constant gain and ϵ.

(2) Reduce τ_1, constant gain and τ_2.

(3) Reduce τ_1 and τ_2, constant gain and r.

The first reduces acquisition time but doesn't affect acquisition range; the second does both, and the third is a completely new bandwidth design, etc.

Now, to consider additional possibilities for the third order, a switched second-to-third-order loop strategy is possible; also, gain switching with or without time constant switching has been utilized to some extent. To illustrate the complexity of the problem, one can readily imagine a circumstance wherein one would face a dilemma in loop gain: Considerations of pull-in time or range might seem to demand an increased gain during acquisition and yet this might invoke problems related to initial conditions and equipment drift (θ_d). The answer in a given situation might lie in switching one or more time constants in addition to or instead of loop gain. Here, again, the relationships of Appendix C may provide the insight to achieve a workable strategy. The significant point is that, with several degrees of freedom available (criteria established for optimum tracking performance are not necessarily applicable during acquisition), the difference, for instance, in a linear and a square root dependence may offer the answer to a given situation.

VI. Concluding Remarks

Partial conclusions have been drawn as the discussion and analysis proceeded above. Suffice it to say here that it is hoped that this treatment has provided a "feel" for the characteristics and relationships of the third-order loop, not only in an absolute sense, but in relation to second-order characteristics. And, perhaps most importantly, some of the stigma of operational unreliability of this device has hopefully been removed through demonstration that a number of undesirable acquisition and design characteristics tend to result not from the loop order but from the application of excessive loop gain in the guise of more "perfect" low-pass "integrators."

In summary, third-order design can offer (other things equal) reduced time constant requirement, narrower closed-loop bandwidth, reduced tracking errors or combinations of these with slight increase in complexity over typical high-performance second-order designs.

References

1. Viterbi, A. J., *Principles of Coherent Communication*, p. 66. McGraw-Hill Book Co., Inc., New York, 1966.

2. Tausworthe, R. C., and Crow, R. B., *Practical Design of Third-Order Phase-Locked Loops*, Report 900-450, Apr. 27, 1971 (JPL internal document).

3. Gardner, F. M., *Phaselock Techniques*, p. 15. John Wiley & Sons, Inc., New York, 1966.

4. Tausworthe, R. C., *Theory and Practical Design of Phase-Locked Receivers*, Technical Report 32-819. Jet Propulsion Laboratory, Pasadena, Calif., Feb. 15, 1966.

5. Hoffman, L. A., *Receiver Design and the Phase-Lock Loop*. The Aerospace Corporation, El Segundo, Calif., May 1963.

6. Rechtin, E., *Design of Phase-Lock Oscillator Circuits*, Section Report No. 8-566, Feb. 7, 1957 (JPL internal document).

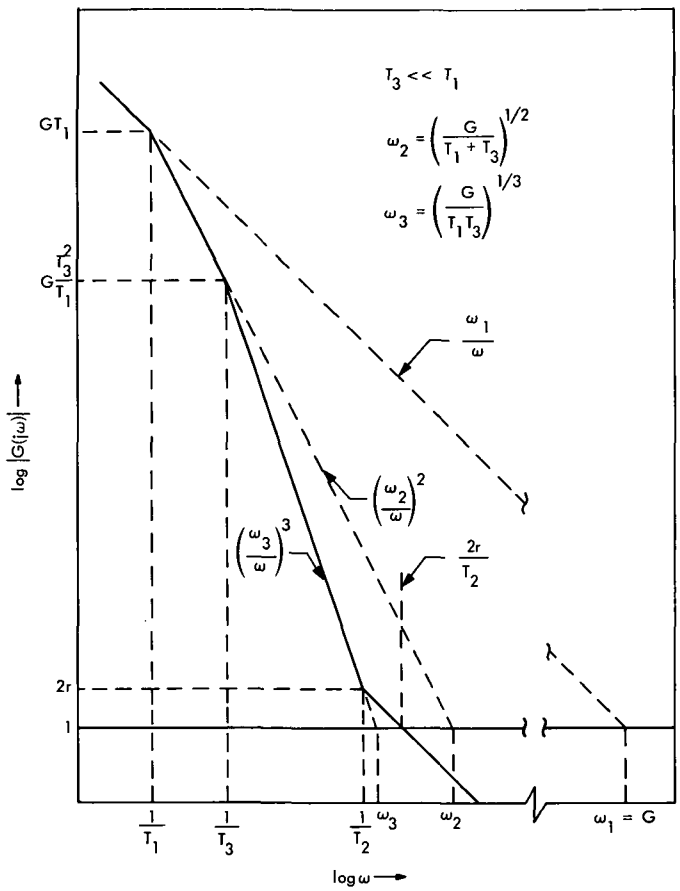

Fig. 1. Idealized open-loop frequency response

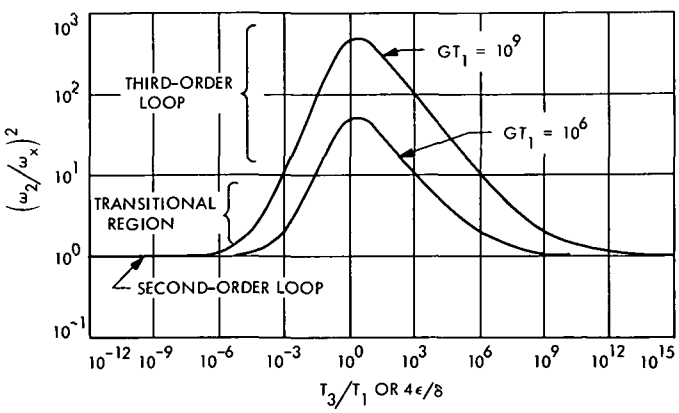

Fig. 2. Normalized ramp performance (fixed G and T_1)

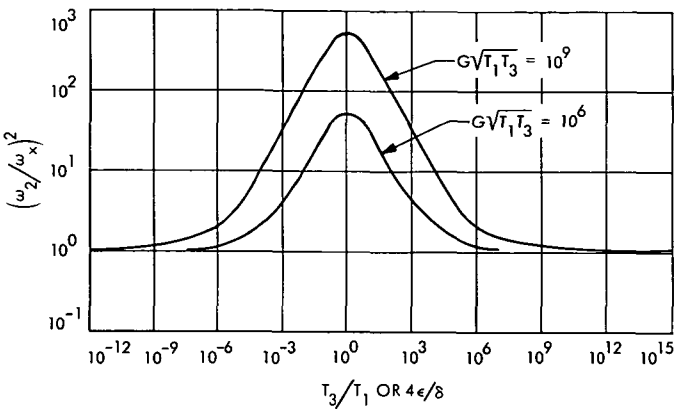

Fig. 3. Normalized ramp performance (fixed G and bandwidth)

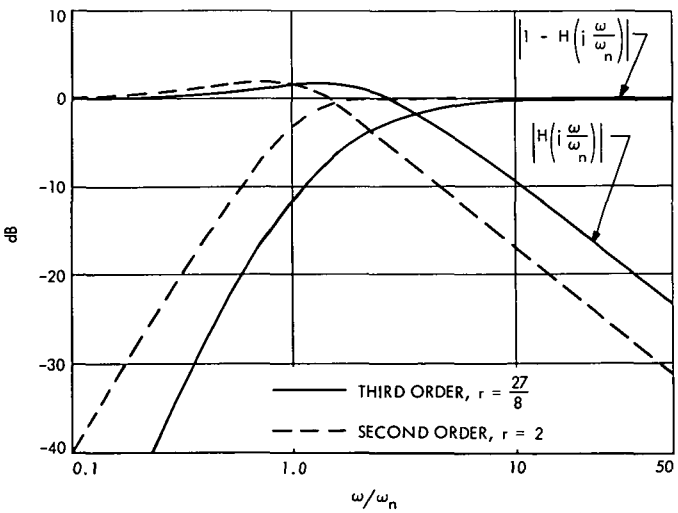

Fig. 4. Closed-loop frequency response

Appendix A

Summary of Definitions and Equivalences

Definitions (from Refs. 2 and 4)

$k = \tau_2/\tau_3$

$\epsilon = \tau_2/\tau_1$

$r = AK\tau_2^2/\tau_1$

AK = Open-loop gain of second-order portion of "parallel" configuration at zero frequency

$\frac{AK}{\delta}$ = Open-loop gain of third-order portion of "parallel" configuration at zero frequency

Equivalences (given $k = 1/4$ and $\delta << 1$)

$$G = AK\left(\frac{1+\delta}{\delta}\right) \approx \frac{AK}{\delta}$$

$T_1 = \tau_1$

$T_2 \approx \frac{\tau_3}{2} = 2\tau_2$

$T_3 = \frac{\tau_3}{\delta}$

$T_4 = T_2$

Appendix B

Summary of Derived Identities and Definitions

Basic Identities

$$\epsilon = \frac{T_2}{2T_1}$$

$$\delta = \frac{2T_2}{T_3}$$

$$r = \frac{G}{2}\frac{T_2^3}{T_1 T_3}$$

Derived Identities

	General	$T_3 = T_1$
$\frac{T_3}{T_1} = \frac{4\epsilon}{\delta}$	⟶	1
$GT_1 = \frac{r}{\delta\epsilon^2}$	⟶	$\frac{r}{4\epsilon^3}$
$GT_2 = \frac{2r}{\delta\epsilon}$	⟶	$\frac{r}{2\epsilon^2}$
$\frac{2r}{T_2} = \epsilon\delta G$	⟶	$4\epsilon^2 G$
$G\sqrt{T_1 T_3} = \frac{2r}{(\delta\epsilon)^{3/2}}$	⟶	$\frac{r}{4\epsilon^3}$

Supplemental Definitions

$\omega_1 = G$ = Reciprocal step (frequency) error coefficient

$\omega_2 = \left[\frac{G}{T_1 + T_3}\right]^{1/2}$ = Reciprocal square root of ramp (frequency) error coefficient

$\omega_3 = \left[\frac{G}{T_1 T_3}\right]^{1/3}$ = Natural (undamped) frequency

$\omega_n = \left[\frac{G}{T_1}\right]^{1/2}$ = Natural (undamped) frequency *and* reciprocal square root of ramp (frequency) error coefficient for *second*-order loop

ω_x = Open loop (undamped) unity gain frequency; equal to ω_3 for third-order and to ω_2 or ω_n for second-order loop

$F = \frac{\omega_2}{\omega_3}$ = A performance factor relating ramp error to closed-loop bandwidth

$F_x = \frac{\omega_2}{\omega_x}$ = A generalization of F for any δ from zero to infinity, holding $\epsilon << 1$

Appendix C

Characteristics Versus G Versus Gain, Given $T_1 = T_3, 1 < r < 10$

This figure is perhaps best interpreted as an order-of-magnitude conversion chart for ϵ and G for each loop order. The $T_2 \approx \tau_2$ normalization and notes allow superposition of the principal characteristics.

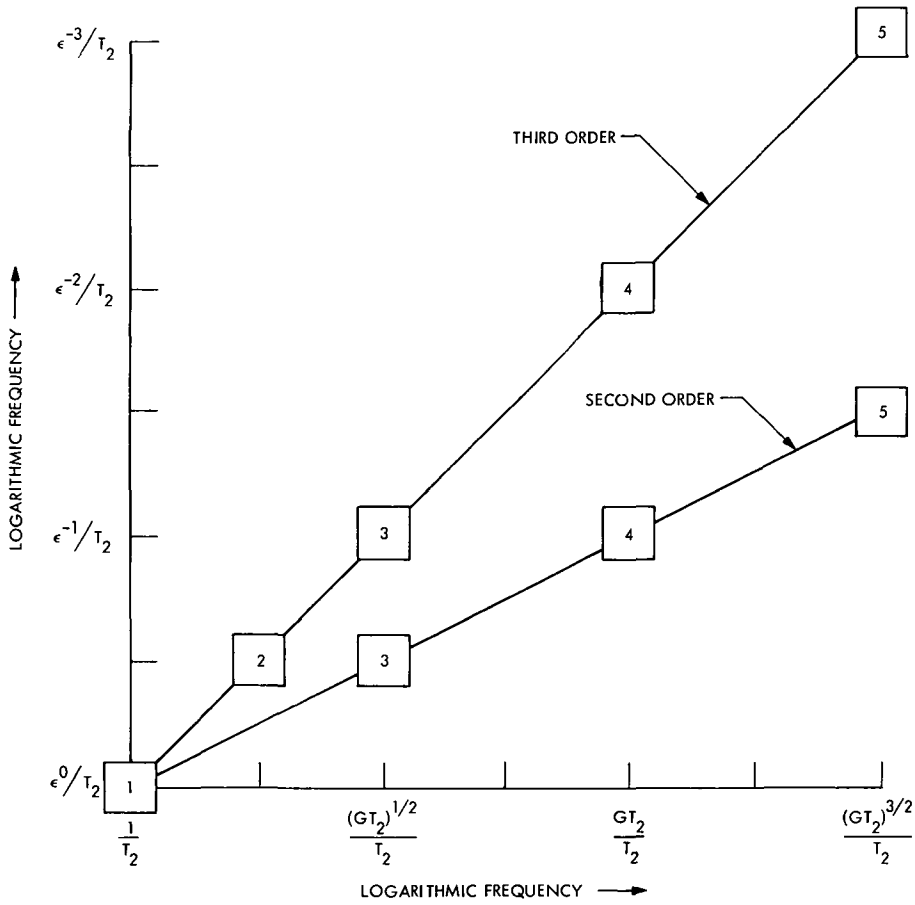

1 BANDWIDTH, BOTH ORDERS; RECIPROCAL ROOT RAMP COEFFICIENT, SECOND ORDER

2 RECIPROCAL ROOT RAMP COEFFICIENT, THIRD ORDER

3 MAXIMUM PULL-IN RANGE, BOTH ORDERS

4 RECIPROCAL STEP ERROR COEFFICIENT, BOTH ORDERS

5 $(GT_2)^{3/2} \approx GT_1$ (THIRD ORDER) $\approx (G\tau_1)^{3/4}$ (SECOND ORDER)

DSN Programmed Oscillator Development

M. R. Wick
R.F. Systems Development Section

This article describes the development of a programmed oscillator utilizing a Dana Laboratory Digiphase synthesizer Model 7010-S-179. A brief description of the synthesizer characteristics and the technique for digital control is given. With this synthesizer, the programmed oscillator has the capability to be controlled at rates and ranges required for tracking outer-planet probes and yet provide the resolution and stability required for narrow-loop bandwidth receivers.

I. Introduction

The development of a new technique to program frequency using a Dana Laboratory Model 7020-103 Digiphase synthesizer was described in Ref. 1. The engineering model that was built demonstrated the feasibility of using this technique. However, to provide the capability required for the DSN, an improved synthesizer, Model 7010-S-179, was developed by Dana Laboratory. This article describes the increased capability of the new synthesizer and the assembly developed to control it.

II. Synthesizer

The increased capability of the Model 7010-S-179 synthesizer (Fig. 1) is shown in Table 1. Each of these items is discussed in more detail below.

A. Frequency Resolution

Model 7020-103 (Ref. 2) by itself provides frequency resolution of 1 Hz. However, fractional-hertz resolution was obtained with this synthesizer in the remote control mode. This capability was described in Ref. 1. The Model 7010-S-179 (Ref. 3) incorporates fractional-hertz resolution with local control to 10^{-6} decade. The inclusion of fractional-hertz resolution in the synthesizer eliminates the need to use the rate multiplier technique described in Ref. 1 to externally generate fractional-hertz control.

B. Phase Increments

In Model 7020-103, the numbers in each decade, down to the 10-Hz decade, are sampled by the loop each 10 μsec. An increase of one digit in the 10-Hz decade during one of these sample periods would then be an incremental change in phase of $(2\pi)(1)(10)(10^{-5})$ or $2\pi \times 10^{-4}$ rad. This represents about an 8-deg incremental change in phase at X-band in the Block 4 receiver–exciter. The Model 7010-S-179 synthesizer has been modified to sample down to the 1-Hz decade (Fig. 2). This modification then reduces the incremental phase change at X-band to less than 1 deg.

C. Long-Term Phase Stability

Two modifications to the synthesizer have been developed to improve the long-term phase stability. First, the temperature stability of the components in the digital

loop have been improved; second, the input reference frequency has been changed from 5 to 50 MHz. Utilizing 50-MHz permits the use of a simpler and more stable mechanization for the generation of the 100-kHz clock. Both these changes have improved the stability by an order of magnitude.

D. Input Reference Standard

The 50-MHz reference standard now being used is the most stable reference available from the hydrogen maser. The use of this reference improves the total system stability directly and the synthesizer stability indirectly as mentioned in Sect. C. above.

E. Output Frequency Monitor

Monitoring outputs that indicate whether or not the synthesizer is responding correctly to the programmed input have been provided in Model 7010-S-179. This is described in more detail later.

III. Control Assembly

First, the Model 7010-S-179 synthesizer will be examined. The output frequency is determined by the input BCD number into each of the decades from 10^7 to 10^{-6}. This number can be selected from the front panel switches in the local control mode or from an external device in the remote control mode (Fig. 2). This input number is sampled once each 10 μsec, the sampling interval being controlled by the 100-kHz clock. The sampling occurs during one-half of each clock cycle, while the other half of each cycle is reserved for number changes (Ref. 1). This is illustrated in the timing diagram (see Fig. 6), which shows the number changes occurring during the half cycle when the 100-kHz clock is low. Since number changes must be synchronized with the clock, the synthesizer can only be used in the remote control mode when the frequency is programmed.

Next, consider the digital loop within the synthesizer. The reference numbers for the loop control are obtained from the 10^0 to 10^7 decades. Since these numbers are sampled 10^5 times per second, when the number in the 10^0 decade is increased by one during one of these sampling periods, it represents an incremental change in the output of the synthesizer of $2\pi \times 10^{-5}$ rad (<1 deg at X-band). When the number in the 10^0 decade is incremented during one of the sampling periods and retained at this higher number, then the incremental change is still $2\pi \times 10^{-5}$ rad, but the frequency has been increased by 1 Hz. Incrementing the reference number once each second and retaining this increased value would then provide a frequency change at a rate of 1 Hz/sec. Pursuing this one step further, when the number in the 10^0 decade is increased by one each sampling period and retained, the incremental changes are still only $2\pi \times 10^{-5}$ rad each, but the frequency changes at a rate of 10^5 Hz/sec. Using this technique, frequency changes at a rate of 10^5 Hz/sec at the synthesizer output can be obtained with incremental changes of less than 1 deg at X-band. Since incrementing the frequency at each sample period results in a frequency rate of 10^5 Hz/sec, lower rates can be generated by increasing the frequency less often than each sample period.

To compute frequency numbers for each 10-μsec interval and insert these numbers into the synthesizer is beyond the capability of a computer. The control assembly, therefore, has been developed to provide this capability. Since doppler frequency changes are relatively slow, the program can be divided into linear segments, each much greater than 10 μsec long. The computer can then calculate these linear frequency rates ($\dot{F}$), and the control unit provides the logic circuitry necessary to convert these frequency rates to synthesizer control input numbers for each 10-μsec sample interval.

To illustrate the methods of obtaining fractional-hertz control and of generating a linear frequency ramp, consider the following simplified mathematical model (Fig. 3): The input reference phase ($\Delta\phi_{\text{ref}}$) to the loop can be expressed as

$$\Delta\phi_{\text{synth}} = \Delta\phi_{\text{ref}} = \Delta\phi_0 + \sum_{i=1}^{n} \Delta\phi_i$$

where

$\Delta\phi_0$ = initial phase

$\Delta\phi_i$ = incremental change in phase

n = number of incremental changes

However, the initial phase and incremental phase changes are

$$\Delta\phi_0 = F_0 \Delta t_i$$

$$\Delta\phi_i = \Delta F_i \, \Delta t_i$$

where

F_0 = initial frequency

ΔF_i = incremental change in frequency

Δt_i = time period between increments (10 μsec)

Then

$$\Delta\phi_{\text{synth}} = \Delta\phi_{\text{ref}} = \sum_{i=1}^{n} F_0 \Delta t_i + \Delta F_i \, \Delta t_i$$

This is accomplished in the following manner: The initial frequency (F_0) and the frequency ramp ($\dot{F}$) numbers are inserted into the control unit. The frequency ramp, or incremental frequency changes, are accumulated and combined with the initial frequency at clock intervals. The combined frequency numbers are then inserted into the synthesizer at these same clock intervals. Within the synthesizer, the frequency numbers are then accumulated at the 100-kHz clock rate to provide the phase reference for the digital loop.

To illustrate the phase tracking response of the synthesizer to an incremental frequency step, consider a step change of 1 Hz applied to the simplified model of Fig. 3. (It is assumed the loop is initially in a steady-state condition prior to the frequency change.) This results in an additional reference phase increment $\Delta\phi_{\text{ref}}$ equal to $2\pi \times 10^{-5}$ rad. The loop output phase response $\Delta\phi\,(t)_{\text{synth}}$ for that of the model of Fig. 3 is as follows:

$$\Delta\phi\,(s)_{\text{synth}} = \left(\frac{K_T}{N}\right) \frac{1 + \tau s}{s^2 + \frac{K_T}{N}\tau s + \frac{K_T}{N}} \left(\frac{\Delta\phi_{\text{ref}}}{s}\right)$$

Loop parameters of the model are:

$K_T = K_A K_V K_D$ = open-loop gain

K_A = loop amplifier gain $\cong 500$

$\frac{K_D}{N}$ = phase detector gain $\cong 5.8$ V/rad

K_V = VCO gain $\cong 2\pi \times 10^6$ rad/sec/V

N = 500 for this example

τ = loop time constant (165 μsec)

δ = loop damping factor (assumed = 0.707)

The time response $\mathcal{L}^{-1}\,[\Delta\phi\,(s)_{\text{synth}}]$ is as follows:

$$\Delta\phi\,(t)_{\text{synth}} = \left[1 - \epsilon^{-\alpha t}\left(\cos\omega_D t + \frac{\alpha}{\omega_D}\sin\omega_D t\right)\right]\Delta\phi_{\text{ref}}$$

where

$$\alpha = \delta\sqrt{K_T/N}$$

$$\omega_D = \sqrt{\frac{K_T}{N} - \alpha^2}$$

For this example,

$$\alpha \cong 6060$$

$$\omega_D \cong 6060 \text{ rad/sec}$$

The time response $\Delta\phi\,(t)_{\text{synth}}$ is shown in Fig. 4. Note that the synthesizer VCO output phase settles to that resulting from the new programmed frequency $F_0 + 1$ Hz within approximately 1000 μsec.

Although a time lag occurs, the synthesizer VCO must track the input reference phase generated by integration of the frequency control number. If no further frequency increments are applied, the loop phase tracking error settles to less than that value defined by the sample rate, since the loop is corrected at that rate. Going one step further, if the frequency is incremented by 1 Hz every clock period, the synthesizer output lags the computed reference phase by approximately 0.001 rad. This corresponds to a sweep rate of 100,000 Hz/sec. When the frequency ramp is removed, the output phase of the synthesizer converges with that of the reference phase computed and settles to that value within approximately 1000 μsec.

The frequency ramp is generated in the control assembly, as derived from manually selected or computer-generated rate control numbers. The functional units which accomplish this task are described individually below.

A. Frequency Control Register

Frequency BCD format is sent to the synthesizer from the frequency control register each clock cycle (10 μsec) (Fig. 5). The frequency information stored in this register is the algebraic sum of two inputs: the initial frequency and the incremental/decremental change in frequency. The initial frequency BCD information for each decade from 10^{-6} to 10^{7} is sent to the register either from the manual control select switches of the control assembly or from the computer. The incremental change in frequency is derived from the rate accumulator and is furnished to one of the 10^{-5} to 10^{-1} decades, depending on the rate of frequency change. To provide the capability of incrementing or decrementing the frequency, the frequency control register consists of decade UP/DOWN counters. Polarity information is received by the register along with an output pulse from the rate accumulator. The polarity selected determines whether the pulse from the rate accumulator will increase or decrease the frequency number in the frequency control register.

B. Rate Accumulator

The rate accumulator integrates the selected five-significant-figure rate number and produces a pulse rate output equal to the rate number. The output pulses increment the frequency control register in fractional-Hz increments, as determined by the decade of operation (Table 2). Similar to the frequency control inputs, the rate control numbers can be derived from manual BCD selectors or the computer. The five significant figures used are based on the clock rate (100 kHz). This means that 1 to 99,999 pulses each second as selected are generated over the 100,000 10-μsec sample periods (1-sec interval). This method of generating the frequency ramp approximates a smooth function, since the incremental step changes never exceed $2\pi \times 10^{-5}$ rad and the pulses are approximately evenly spaced over the 1-sec period.

To accommodate all known tracking requirements, five ranges are available. The range selected is identified by the position of the decimal point in the range rate manual control select switch or corresponding display. Although the frequency control resolution (Table 2) is reduced by a factor of 10 operating in the next higher range, the synthesizer control loop incremental step changes are still maintained at the minimum size of $2\pi \times 10^{-5}$ rad.

Generating the pulse to update the frequency control register is accomplished by using a BCD adder and an accumulator register to sum and accumulate the selected BCD rate every 10 μsec (Fig. 6). This is accomplished in the following manner: The input frequency rate number ($\dot{F}$) is stored in the rate register. These numbers are sampled each 10 μsec in sequence, as shown in the timing diagram. The timing diagram shows the timing pulses used in sampling these numbers. Pulse T1 enables the least-significant BCD number to be added to its related previous value stored in the accumulator register. The result of the add operation is stored as the new value along with any carry which may have resulted. This value is then shifted, and the next higher significant digit is sampled. The process continues until all five rate numbers are sampled to complete a full add cycle. Note that a full add cycle occurs within 2.5 μsec. A carry resulting from the most-significant number addition is the output pulse desired. This pulse then increments or decrements the proper frequency control register decade as listed in Table 2.

C. Acquisition Sweep

For an application such as acquisition, it is desirable to have the capability of triangular sweep. This capability is included in the control unit and provides a frequency sweep between predetermined upper and lower limits. Fig. 7 is a simplified diagram showing the frequency control register compared with the upper or lower stored limit, as determined by the polarity. When the digital comparator logic senses equality, a signal is sent to the polarity control logic to momentarily clear and stop the rate accumulator, force a polarity reversal, and then enable the rate accumulator to continue. Limits are selectable over the operating range of the synthesizer with resolution of 10^{-4} Hz. The figure is shown with rate range 1 selected.

D. Monitoring

It is necessary to verify that the output frequency of the synthesizer agrees with the input program. The output frequency cannot be counted directly to the accuracy required; therefore, it is necessary to use indirect means of monitoring (Fig. 8). The alternative used is to verify that the programmed frequency numbers (monitor 1) are being entered into the synthesizer and that the synthesizer loop remains locked. The control assembly includes the capability to read and store the synthesizer phase computer BCD codes (loop control inputs) at the station 1-sec tick (monitor 2). These values can, in turn, be sent to the computer for comparison with the predicted values. The synthesizer loop phase detector output is also monitored. Failure of the synthesizer VCO to track the phase computer is signaled by a digital pulse indicating the loop phase error has exceeded normal operating limits (monitor 3).

E. Controls and Displays

As mentioned previously, the synthesizer can be controlled remotely in the manual mode, although the primary remote mode is computer-controlled. The manual capability is included for operator control as a backup mode and for local checkout and fault localization when it is not desirable or possible to use the computer. Controls for the manual mode of operation are located on the front panel of the control assembly (Fig. 9). Commands to display or enter selections are dialed up on a coded selector switch, and the display or load pushbutton is enabled. In the load (enter) mode, the operator depresses the enabled load pushbutton, which stores the related BCD digital codes from the front panel selector switches. In the read mode, the display pushbutton is enabled, resulting in the selected display of frequency or sweep limits and GMT time or rate, as indicated on the command selector switch. The synthesizer control frequency displayed is that value present at the last station 1-sec tick.

Sweep rates entered are transferred to control latches at the next station 1-sec tick. Sweep ON/OFF and polarity selected are also transferred to control latches on the next station 1-sec tick. Sweep controls consist of RUN (ON/OFF), SWP (ON/OFF), and POLARITY (+/−). SWP ON enables the triangular sweep in frequency by enabling a polarity reversal when the preselected upper frequency limit and lower frequency limits are reached. This provides selection of a sweep window for automatic acquisition. RUN ON enables the rate accumulator operation producing the sweep rate (Hz/sec) selected and loaded in the rate control register. In the RUN mode, i.e., SWP OFF, the limits are disabled, inhibiting automatic polarity reversal. This is the doppler tracking mode.

An additional manual control will be added to the programmed oscillator control to allow the operator to preset sweep commands to be initiated at a desired GMT time. The selected rate and polarity will be initiated when station GMT time matches the stored value at the station tick.

F. Computer Interface

Data transfer to and from the programmed oscillator (PO) is in 8-bit bytes. Command and PO ID codes are sent first for register addressing in the PO, with data bytes following. Fig. 10a is a simplified diagram of the interface.

Data transmitted to the PO are stored in latches, and the latches are sampled on the station 1-sec tick in order to produce frequency corrections synchronous with the station clock. In the "tracking mode" (SWP OFF), the commands to load the frequency control register control decades and the rate control register control decades and the commands to initiate RUN are decoded, and corresponding data are transferred to latches. The registers that control the synthesizer are then loaded from these latches at the next 1-sec tick. Commands to stop a sweep are instantaneous (within 1 μsec after command is received).

Data transmitted to the computer are stored in latches and transferred one byte at a time (8 bits). The computer program sends a "read" command, which specifies the data requested and the number of bytes associated with the data. These data will be valid for the time tag related to the last 1-sec station tick.

Received 8-bit bytes, containing two BCD control codes each, are received sequentially from the computer and steered to storage latches in the PO, based on the value of a byte counter. The following is a description of the byte counter used for steering the data (8-bit bytes) to the addressed storage latch in the PO control registers (Fig. 10b).

The byte control word is a 3-bit code that sets the byte counter to the specified initial starting state. The counter output BCD code is decoded to the equivalent decimal value, thus enabling one of the 7 lines used for steering the subsequently occurring data strobe to the appropriate storage latch. For each successive value of the counter during multiple byte transfers, 8 bits are stored. The byte counter value is forced down 1 count with each 8-bit byte transfer, as signaled by a response RSP followed by a data ready RDY cycle of the interface control signals.

The first 8-bit byte received from the computer interface is the byte control word. This byte control word is stored in the byte counter in accordance with the number of data bytes to follow. The RCV/XMT control logic generates the data strobe, which is, in turn, steered by the successive value of the byte counter as it decrements by 1 for each data byte transferred. This is shown in the timing diagram of Fig. 11.

Data transfer can be terminated with the byte counter forced to zero (0), as accomplished by removing the computer stimulus (STC). Thus, any one of the byte latches may be addressed individually as well as sequentially. In this instance, the byte counter is set to the value desired with a data transfer of one byte following. After the RSP signal is received, the STC signal is removed to terminate transfer.

A typical data transfer from the computer to the PO is as follows: The computer transmits a coded command with the PO unit ID code concurrent with a computer stimulus (STC). The command is one of the 15 commands to load or read PO registers. This command is sent in BCD code on the 8 bi-directional data lines (4 bits containing command and 4 bits containing unit ID). If the unit ID is correct, the PO responds with a response to the stimulus (STC) and stores the command. The decoded command results in an enabling signal to the set of latches that are to receive data. In the case of a read command, transmit gates are enabled.

As a result of the response signal sent to the computer interface, the computer loads the interface lines with the byte count associated with the number of 8-bit bytes to follow and sets the data RDY bit. The byte control word

is recognized as such by the PO by a byte control code sent on the function lines C8 and C9. The byte control code enables a strobe to load the byte counter. The RSP signal is removed upon detection of the RDY signal. Subsequent byte transfers are coded as data bytes on C8 and C9 and occur with each successive cycle of RSP → RDY → $\overline{\text{RSP}}$ → $\overline{\text{RDY}}$ until the byte counter has decremented to zero, as illustrated in the timing diagram (Fig. 11).

IV. Packaging

The control assembly hardware is mounted in a 19.5-in. cabinet chassis that occupies 5.5 in. of panel space (Fig. 9). The front panel contains controls that are used in the manual control mode, as well as numeric displays used in either the manual or the computer control mode. Two LED numeric displays are used, one containing 14 digits and the other containing 6 digits. The 14-digit display reads out on command, either manually or from the computer, the upper and lower frequency sweep limits and the frequency input to the synthesizer from the control unit at a 1-sec sample rate. The 6-digit displays read out on command GMT or frequency sweep rate.

Fig. 9 shows the control assembly with the top cover removed. The compartment with the louvered cover contains the power supplies. Two rows of digital subassemblies can be seen. Wire wrap plug-in subassemblies are used to divide the control logic into separate functional elements and still provide high-density packaging. The use of functional subassemblies simplifies maintenance by reducing field troubleshooting to subassembly substitution until the defective plug-in is determined. One of the digital control plug-in cards is shown in Fig. 12 with the integrated circuits and with a plastic cover to protect the wire wrap pins from damage during handling.

V. Concluding Remarks

A PO has been developed that has the capability to be controlled at rates and ranges required for tracking outer-planet probes and yet provide the resolution and stability required for narrow-loop bandwidth receivers. This PO is being used in the Block 4 receiver–exciter, as well as in the exciter for the time sync. At the present time, the time sync is operational, and the PO is performing as predicted.

References

1. Wick, M. R., "Programmed Oscillator Development," *The Deep Space Network*, Space Programs Summary 37-66, Vol. II, pp. 127–132, Nov. 30, 1970.
2. Gillette, G. C., "The Digiphase Synthesizer," *Freq. Technol.*, Vol. I, No. 8, Aug. 1969.
3. *Dana Model 7010-S-179 Digiphase Frequency Synthesizer*, Dana Laboratory Publication 980428-S-179, July 1971.

Table 1. Synthesizer capability

Characteristic	Model	
	7020-103	7010-S-179
Frequency resolution, Hz	1	10^{-6}
Phase increments, 2π rad	10^{-4}	10^{-5}
Long-term phase stability, deg phase/°C	10.0	0.1
Input reference standard	5	50
Output frequency monitor available	No	Yes

Table 2. Rate accumulator ranges

Range	Control register decade	Range rate, Hz/s
1	10^{-5}	0.00001– 0.99999
2	10^{-4}	0.0001 – 9.9999
3	10^{-3}	0.001 – 99.999
4	10^{-2}	0.01 – 999.99
5	10^{-1}	0.1 –9999.9

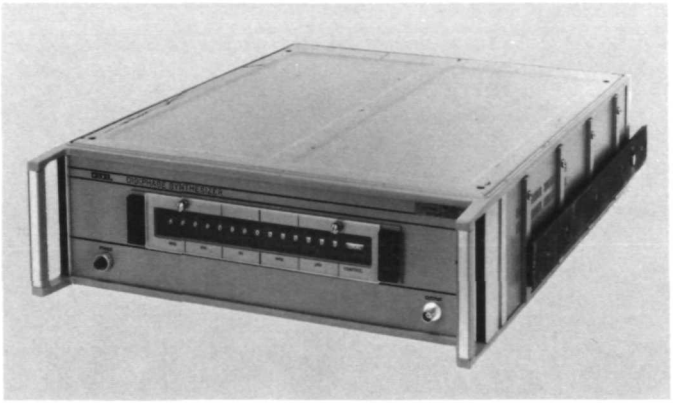

Fig. 1. Dana 7010-S-179 Digiphase frequency synthesizer

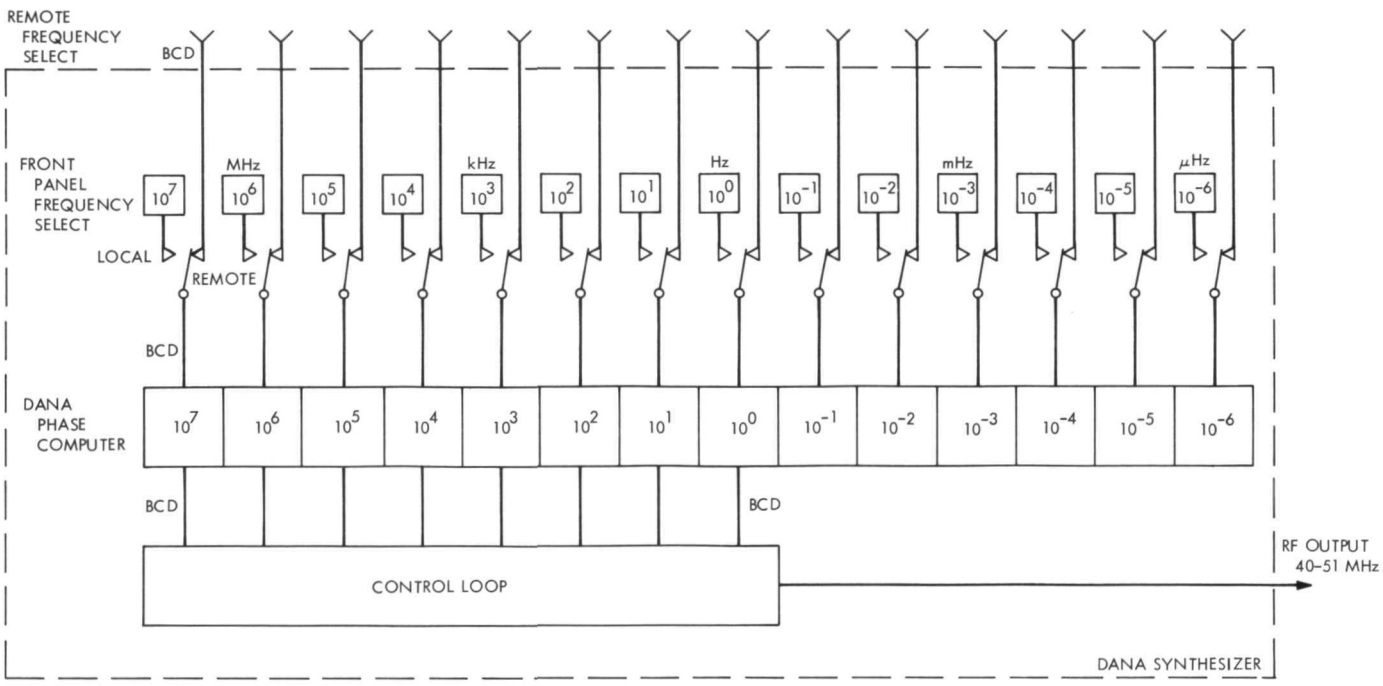

Fig. 2. Dana synthesizer control

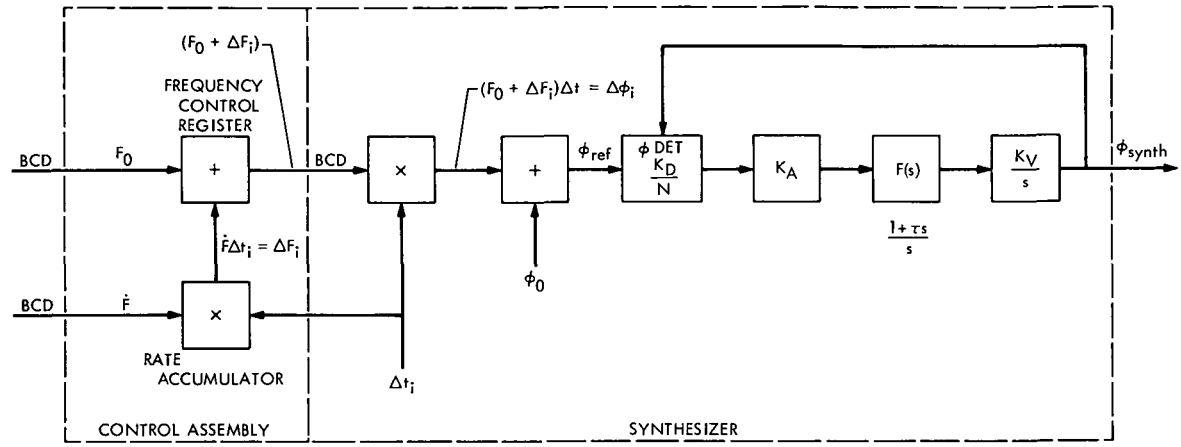

Fig. 3. Dana loop digital control

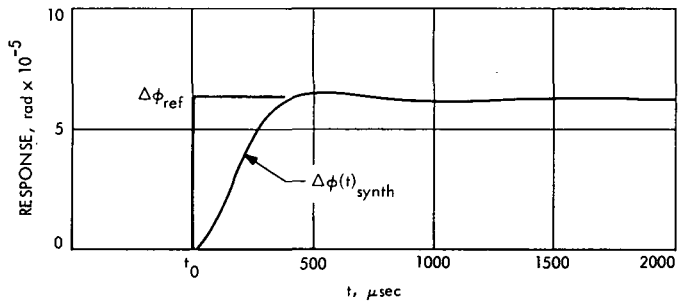

Fig. 4. Synthesizer model output response

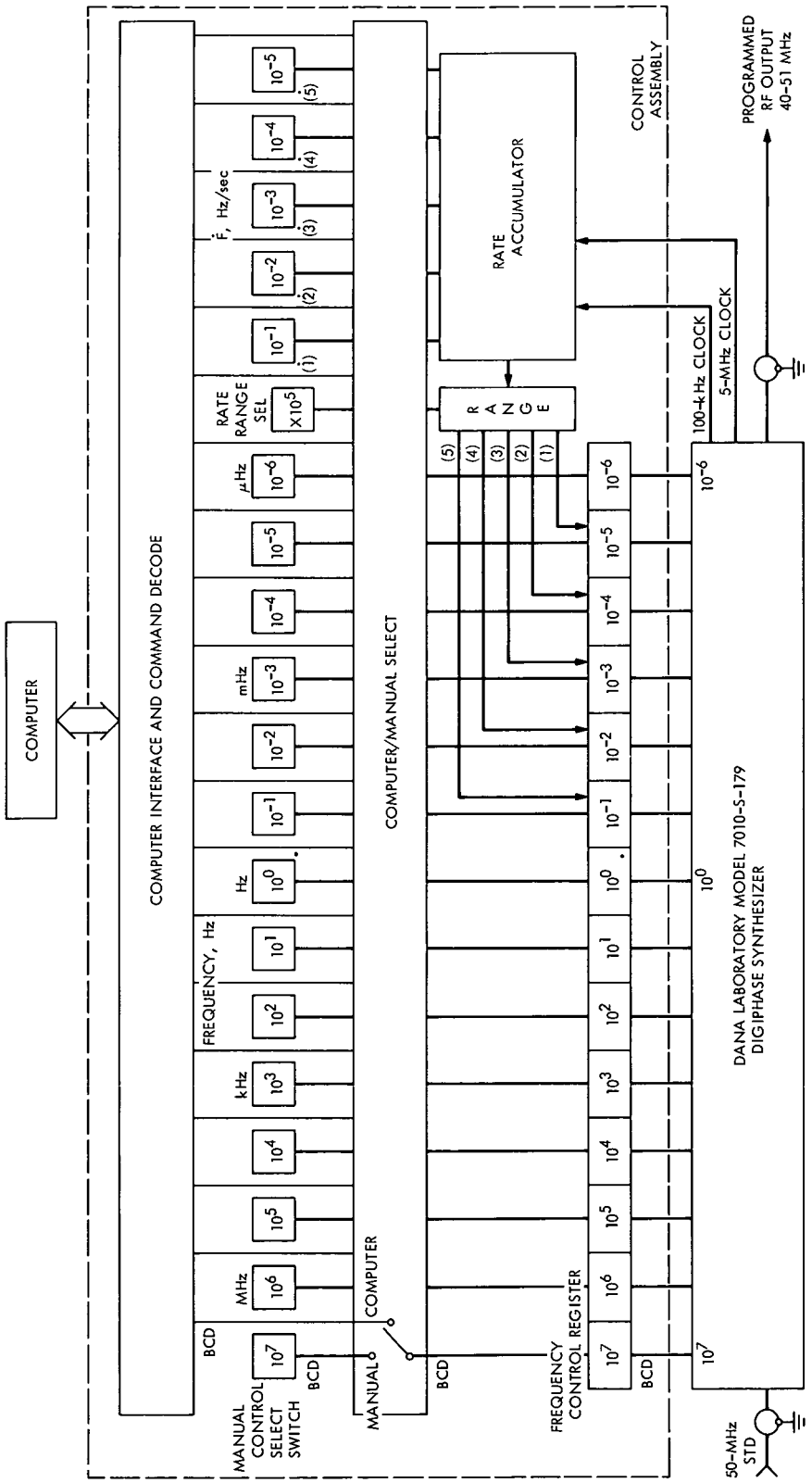

Fig. 5. Control assembly

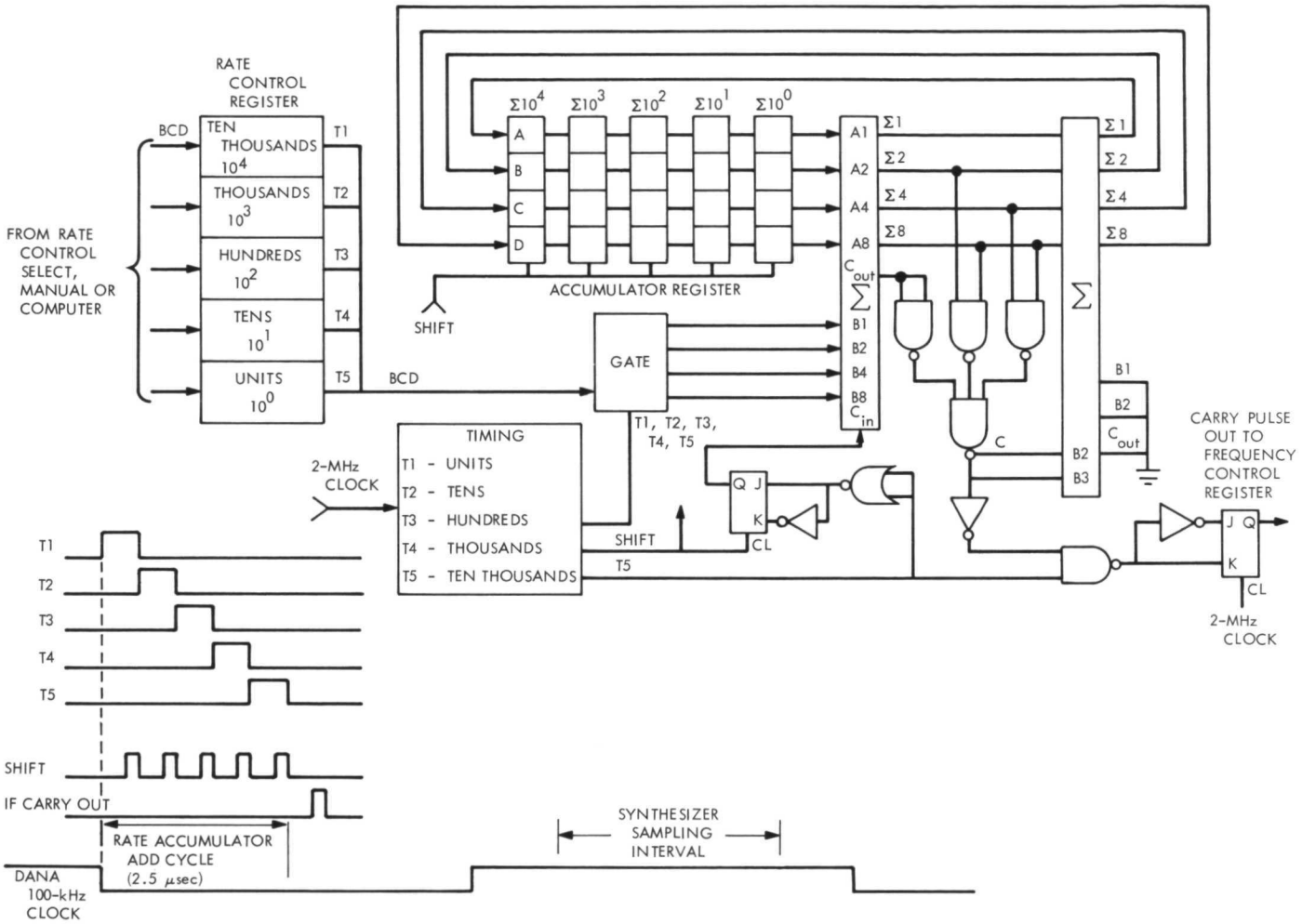

Fig. 6. Rate accumulator

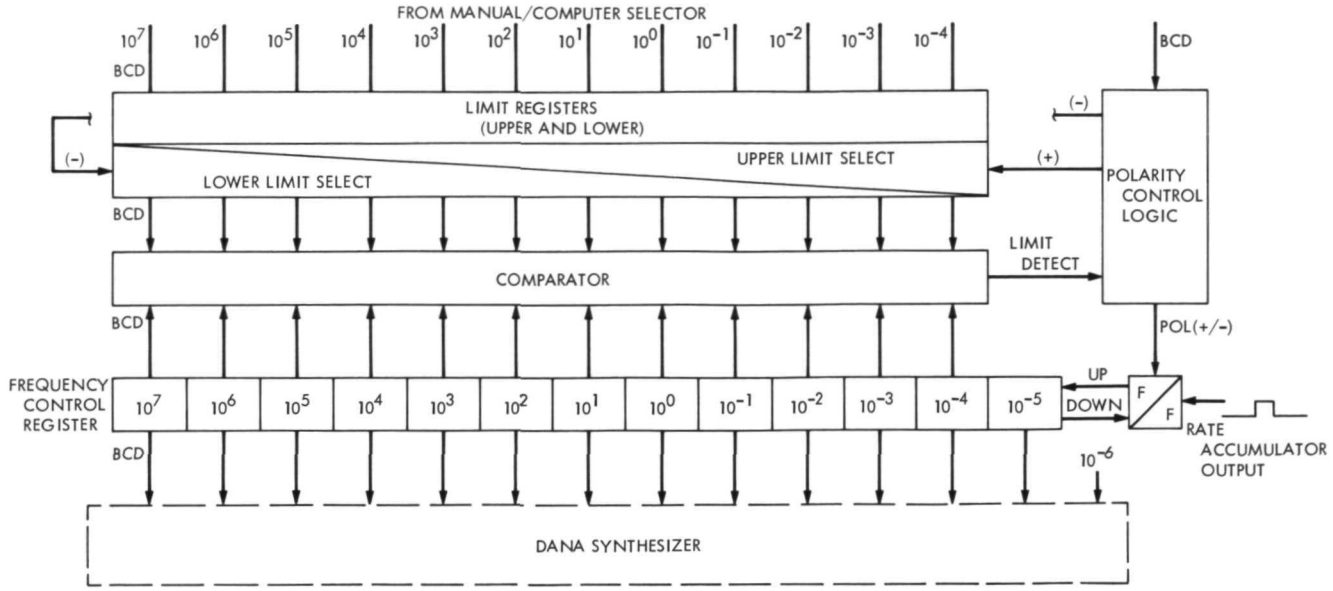

Fig. 7. Acquisition sweep control

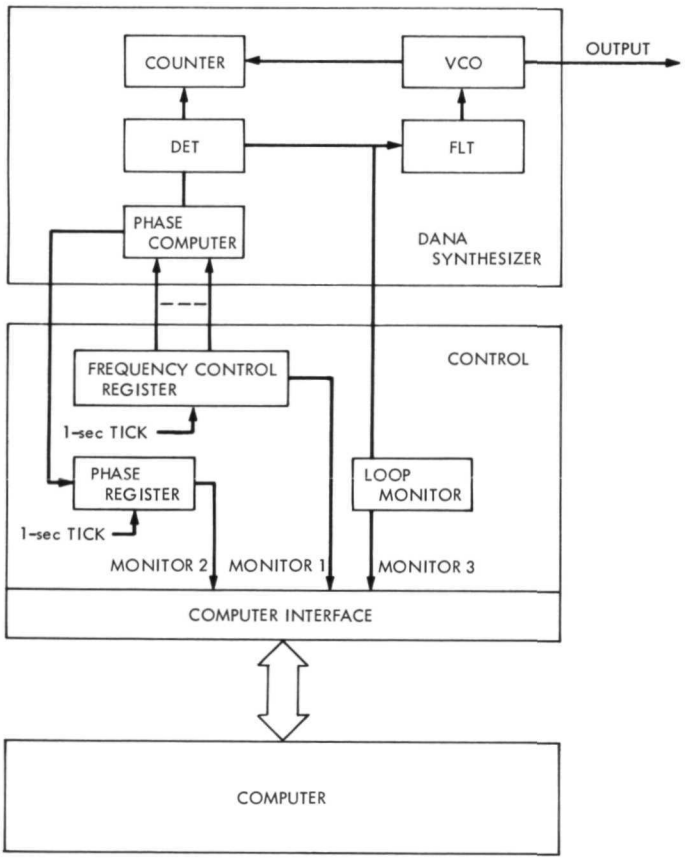

Fig. 8. Digital control assembly

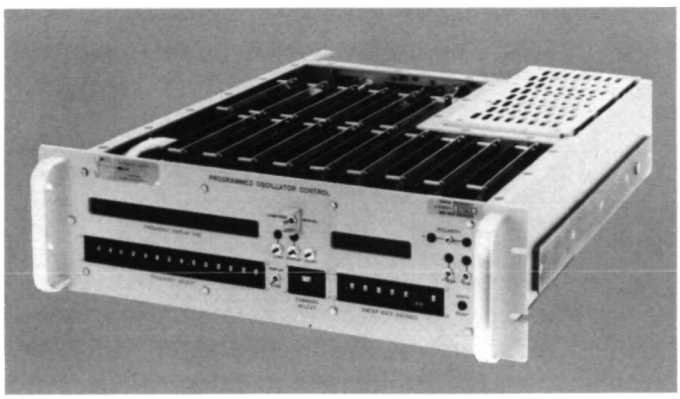

Fig. 9. Frequency monitor

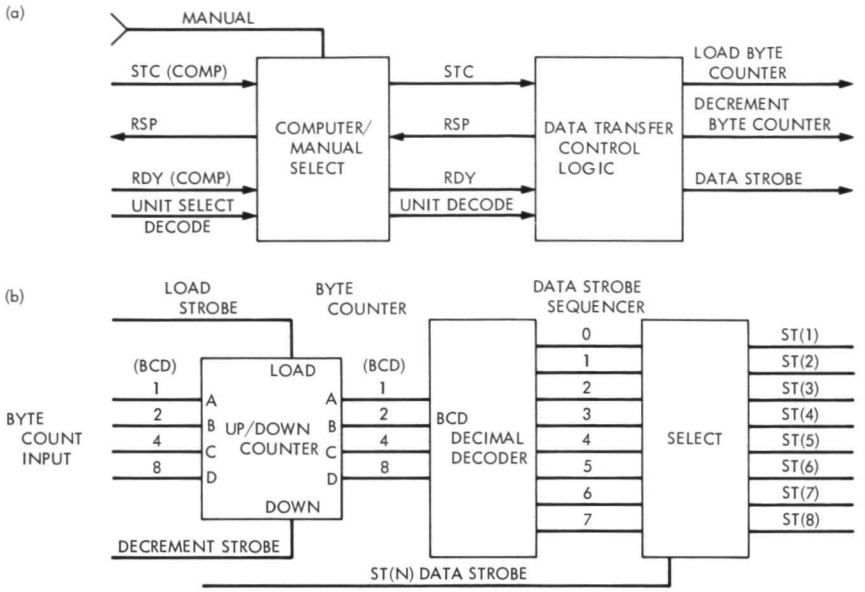

Fig. 10. Computer interface

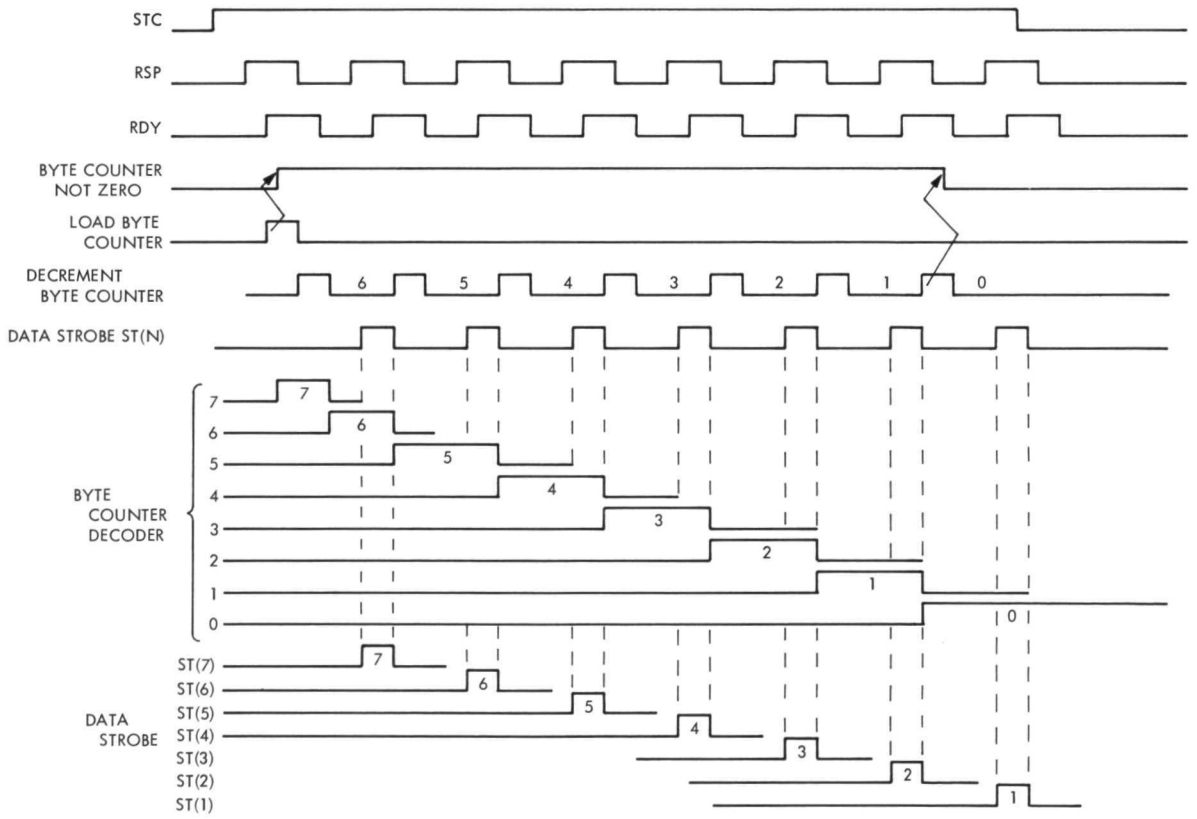

Fig. 11. Timing diagram for computer interface

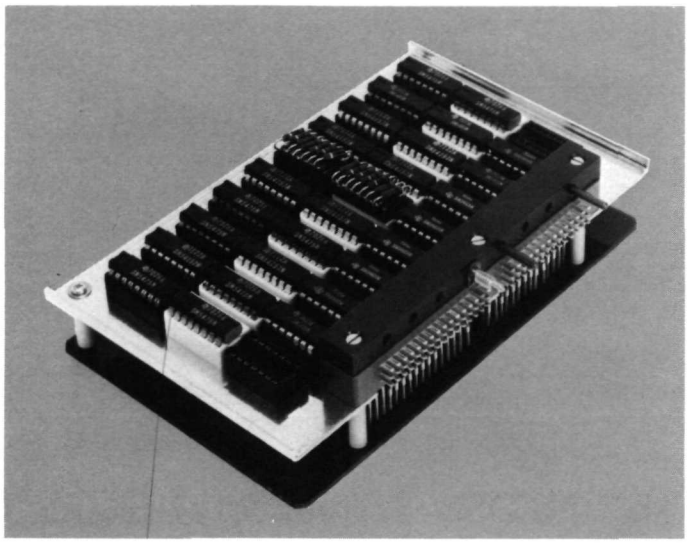

Fig. 12. Digital control plug-in card

Integration of the DSN Sequence of Events Generator

C. L. Morgan
DSN Engineering and Operations Section

This article reviews the concept, function, implementation, and operational status of the DSN sequence of events generator. The supporting software resides in IBM 360-75 as a part of the real-time mission support software system. The program title is "Sequence of Events Generator."

I. Introduction

The DSN sequence of events (SOE) is a part of the network allocation subsystem and provides a baseline sequence for use by the DSN operations and analysis functions in conducting minute-to-minute DSN operations. In the past, sequences of events were cumbersome, hand-manipulated manuscripts generated to support only critical phases of mission activity.

The software package used five years ago by the Lunar Orbiter Project to generate SOEs was the basis of the original SOE program. This program was nearly as cumbersome as the hand-generated method, since all events had to be coded for card punching. These data cards were then time ordered by hand prior to being input to the program. The program resided in the IBM 7094 and provided the capability of sequence numbering, page numbering, and adding titles to output pages.

The change from the old IBM 44/94 flight support system to the newer IBM 360-75s provided the time required to design a functional sequence of events program.

The Software Requirements Document (SRD) for the initial version of the Sequence of Events (SEG) program was issued in March, 1970. The SRD for the second and final version was issued in January, 1971.

II. Function

The new SEG provides a broad data base accumulated from all project and DSN user requirements. DSN, project, or combined sequences are generated using selective sort routines.

The sequence of events provides data which is sensitive to the nearest second. This timing accuracy was neces-

sary to reflect optimum spacecraft command transmission times as well as routine operational times such as view periods, two way transfers, etc.

Using a subsequence library designed into SEG, redundant, time-sequenced events can be cataloged and retrieved at will using a single input "trigger" card. Any number of special sequence sets can be implemented into the library to reduce input time and the redundant coding of cards.

Using file management techniques, many sequences may be written using different file names. These files may then be outputed individually, selectively merged, or as a large master SOE. High-speed transmission files for remote location may be created on either magnetic tape, disk pack, or both.

Any internal file containing input format, time-ordered input format or output format can be dumped to magnetic tape or disk pack for later restoration and use. Communications with SEG are through the 2260 I/O system and punched cards.

III. Implementation

It was determined that production of sequence of events would be the responsibility of the DSN scheduling group. Forms design, implementation, and program operation were hampered to some extent by the absence of documentation on SEG program capabilities.

Many times, unexpected program changes or "bugs" would appear in new versions of the software causing the redesign of input forms, cards or sometimes both to maintain communications with the program.

The current model of SEG meets the requirements set forth in the SRD dated January, 1971 with few exceptions. This model was documented and scheduled with sufficient visibility to allow revised forms and subsequence card libraries to be prepared prior to its implementation and inclusion in the operational software system.

IV. Operational Status

The DSN scheduling personnel are fully trained and are currently producing a sequence of events for DSN Operations on a daily basis. A weekly SOE is being generated which basically parallels the DSN 7-Day Schedule. This sequence provides the base data for the daily sequences. DSN Document 890-20 "Deep Space Network-Oriented Sequence of Events Generator User's Manual" has been published to provide a guide to users in operating the program at its peak efficiency.

The sequence of events generator has been fully integrated into the DSN scheduling subsystem. A sequence of events can be created for any user as specified in the *Standard Operating and User Procedures*. The daily sequence of events used by DSN operations has proved to be a valuable tool in conducting operations efficiently under any condition of loading.

SEG is a multi-user program. Present daily sequences are created by merging DSN-unique data with project sequence files from earlier runs. The master sequence is then selectively sorted to meet required support for that day.

References

1. Rung, R., *Software Requirements Document–Sequence of Events Generator,* IOM A01-1347, January 5, 1971 (JPL internal document).
2. Morgan, C. L., *Requirements for the Generation of the DSN Sequence of Events,* DSN SOP 842-20 (20-306) Aug. 1, 1971 (JPL internal document).
3. Morgan, C. L., *Request and Submittal for DSN Sequence of Events,* DSN SUP 846-48 (60-206) Nov. 15, 1971 (JPL internal document).
4. Morgan, C. L., *Deep Space Network-Oriented Sequence of Events User's Manual,* DSN Document 890-20, February 1, 1972 (JPL internal document).

DSN Frequency and Time Scale Change From UTC to IAT or New UTC

J. Curtright
DSIF Operations Section

By international agreement, the UTC time scale was changed to parallel that of the atomic (A.1) scale. The new time scale is called New UTC 1972 or International Atomic Time (IAT). This change in time scale made it necessary to change the frequency and time standards at all Deep Space Instrumentation Facility stations. The existing offset of UTC from A.1 time was removed from the oscillators, and all clocks were retarded approximately 107,600 μsec. This article covers the background material leading to the change, problems dealt with during the planning for it, and the procedures used to implement the change.

I. Introduction

Since 1967, the second has been defined in terms of an atomic transition; however, time scales in general continued to be derived from the rotation period of the Earth. Since the rotation speed of the Earth is slowly decreasing, a discrepancy existed because the atomic second is constant in relation to the Earth-rotation-derived second. This discrepancy between related and measurable quantities resulted in an international agreement to a compromise time scale based on the atomic transition of the element cesium. The time scale called Coordinated Universal Time (UTC) was agreed to under the auspices of the International Radio Consultative Committee, with maintenance assigned to the International Bureau of Time (BIH). The UTC time scale operated at a frequency offset of -300×10^{-10} from the cesium (A.1) scale so that it would correspond more closely to time derived from the rotation of the Earth.

UTC, although offset from atomic time, is not exactly synchronous with Earth-rotation-derived time. The Earth's rotation not only is slowing down, but is decreasing in rotational speed at a varying rate. Because of the lack of exact correspondence between UTC and other time scales (UT, A.1, ET, etc.), periodic corrections were sent by time-keeping laboratories located throughout the world to the various users of precision time. Both radio (WWV, NSS, etc.) and mail corrections were made available to the users, depending on the urgency of their requirements.

Over the past few years, several offset or frequency adjustments were made to UT scales. This effort was troublesome to users requiring long-term constant scales. UTC was never known in real time and had to be solved for after the fact or predicted. Some agencies could afford the delay in the solution of the time errors, but users such as astronomers and deep space tracking networks could not.

To avoid disadvantages in trying to keep up with the old UTC, the DSIF changed its frequency offset on or about 00:00:00 GMT, January 1, 1972. The new UTC scale now in use operates with no frequency offset from the A.1 scale. New UTC time intervals are exactly 1 sec in duration, but offset in time about 10 sec from the A.1 scale.

II. Timing Subsystem Configuration

All DSIF stations, with the exception of DSS 71 and CTA 21, have atomic oscillators as frequency sources for their timing systems. The oscillators include two Varian rubidium gas types and one Hewlett-Packard rubidium type. Three stations in the DSIF also have available hydrogen masers that are used for MSFN experiments. The rubidium oscillators have a long-term stability specification of 1×10^{-11}, which, if measured at 1 MHz, indicates ± 0.864 Hz/day or approximately 1 μsec in time.

Time signals at each of the DSIF stations are generated by connecting a 1-MHz sine wave obtained from the atomic oscillators to a shaping network that converts them to square waves. The square waves are fed to a digital divider network that divides the 1-MHz input by 10^6. The resultant 1 pulse/sec (1 pps) is used to drive a digital counter that adds the pulses; the adding circuits are configured to operate as a digital clock. Additional circuits in the clock interpret the accumulated sum and provide outputs for visual display units, which continuously indicate the time of day to the second.

Adjustment circuits are provided within the clock to allow the setting of the clock to any calibrating source providing a 1-MHz signal. By using the adjustments available, it is possible to set the clock to within 1 μsec of the calibrating source. With the clock set to the source oscillator, time outputs are provided with an accuracy equal to that of the oscillator, which in the case of the DSIF is 1 μsec/day.

By tracking standard radio time sources at VLF frequencies, phase differences between the DSIF oscillators and the input of primary time-keeping laboratories can be detected. This daily phase comparison provides an accurate determination of how fast or slow the DSIF oscillators are running. All of the sources of time and frequency used in the DSIF are traceable to the National Bureau of Standards (NBS) and/or the U.S. Naval Observatory (USNO). (The NBS is the agency responsible for frequency, and the USNO is responsible for time in the United States.)

III. Change Preparation

Many detailed requirements were established during the first few months following the decision to change the DSIF from old UTC to new UTC. Major items dealt with included:

(1) Equipment in use or required.

(2) Non-interference with tracking.

(3) Preventing loss of epoch while obtaining correct differential and offset (from old UTC).

(4) Attaining maximum cumulative error of < 20 μsec between stations.

(5) Best time for change.

IV. Equipment Required

The first decision made was that the DSIF should replace the Varian Model V4700 rubidium oscillators. The V4700 oscillators had been in the network for well over 8 yr and were approaching their calculated life expectancy. Failure data indicated the units needed increasing amounts of service; some were so old and repair-ridden that repairs were excessively costly. To update the old type oscillators, a new gas cell was required at a high initial cost. In addition, the update work would have to be done at the DSIF Maintenance Facility because the factory agreed only to furnish the new cells.

The second type of rubidium oscillator used in the DSIF, the Varian Model R20, was considered good for a few more years, since these oscillators are only 4–5 yr old and in much better condition than their predecessor, the V4700. The R20s are equipped with a time increment changer, which allows frequency changes to be made by installing a different crystal in the synthesizer. The cost of the new crystals was minimal and warranted keeping this model and updating it to the new frequency.

A new type of rubidium oscillator, the Hewlett-Packard Model 5065A, was selected to replace the V4700. Enough units were purchased to supply one to each tracking station and place one spare at the complex level, i.e., Goldstone, Spain, and Australia. The HP5065A is equipped with a feature that allows changing frequency by simply setting thumb wheel adjustments in the synthesizer and adjusting the trim of the crystal. The entire change process takes less than 5 min to complete and can be done without powering down the oscillators or the clocks. The quick-change capability enabled stations to reset their clocks with microsecond recovery to the new epoch guaranteed.

V. Time Change Parameters

With the starting and ending configurations defined for each station in the DSIF, the next problem was to find the precise frequency change (rate) required and what time scale changes, if any, were to be made. Through coordination with the USNO and the NBS, a precise rate definition was generated and a precise time offset established. The general rules were defined as follows: (1) The frequency offset or rate will be 300×10^{-10} from old UTC; (2) the time offset will be 107,600 μsec at 00:00:00 GMT, January 1, 1972; and (3) the net result will indicate new UTC parallel to A.1, but retarded by 10 sec (Fig. 1).

VI. Equipment Change

The new rubidium HP5065A oscillators were checked for proper operation at the DSIF Maintenance Facility (DMF) before being shipped to the stations in the DSIF. A procedure was also developed so that the 300×10^{-10} change could be made smoothly and with a minimum effort at the station level. Each HP5065A oscillator was shipped to the station with an adjustment procedure, proper settings for old UTC, and proper settings for new UTC included in the package.

After the HP5065As were received by the station, the Model R20 rubidium oscillators were called in to the DMF for time-increment-changer update and frequency change. The R20 units were returned to the stations set on the new UTC rate. Stations were asked to plug the units in to insure operation and to keep power on until the time change was to take place. The new HP5065A and the updated R20s were sent to all stations between October and December, 1971.

VII. Project Interface

The date selected for the change to new UTC coincided with the relatively critical orbit determination period of the *Mariner* Mars 1971 mission. To avoid interfering with station tracking requirements, it was decided that change parameters spanning a period of 30 hr would be supplied to the stations. The period between -10 hr to $+20$ hr from 00:00:00 GMT, January 1, 1972, was designated as the time to make the adjustments. Since the entire change, including verification of the results, required 2.5 hr or less to complete, the stations had more than adequate time to accomplish the task. The ground rules used to determine when the change would start were: If spacecraft tracking started prior to and continued through 00:00:00 GMT, January 1, 1972, old UTC would be used for that tracking pass; if tracking started after 00:00:00 GMT, January 1, 1972, new UTC would be used for that pass.

VIII. Document Support

Procedures were written for the three station configurations existing in the DSIF. Since the three stations at Goldstone (DSSs 11, 12, and 14) are each configured differently, the three procedures were all validated at Goldstone prior to their release. The general sequence of the change in time and frequency was accomplished as follows:

(1) Maintain old UTC GMT with the oscillator that was to be removed from the configuration (the V4700) and an offline clock (time code generator).

(2) Adjust frequency of new oscillator (or maser) to the new UTC rate by adjusting the unit's synthesizer to a predetermined number.

(3) Retard clocks that are being run by the new UTC oscillators by the predetermined number of microseconds (Fig. 2 or 3).

(4) Monitor both rates to insure that proper convergence between old UTC and new UTC of 108 μsec/hr was established correctly.

(5) Disconnect old UTC oscillator from system and replace with new UTC oscillator (HP5065A) to complete the procedure.

All stations in the network followed the procedure perfectly, and subsequent checks with portable clocks and Operational Time Synchronization (lunar bounce of radar) indicated that the stations performed the change within $\pm 1 \times 10^{-11}$ in frequency and ± 5 μsec in time synchronization. Reports from all stations through their respective DSN projects showed no degradation in data and no lost data; actually, the change was so flawless that there was no indication from the projects that the change was detected.

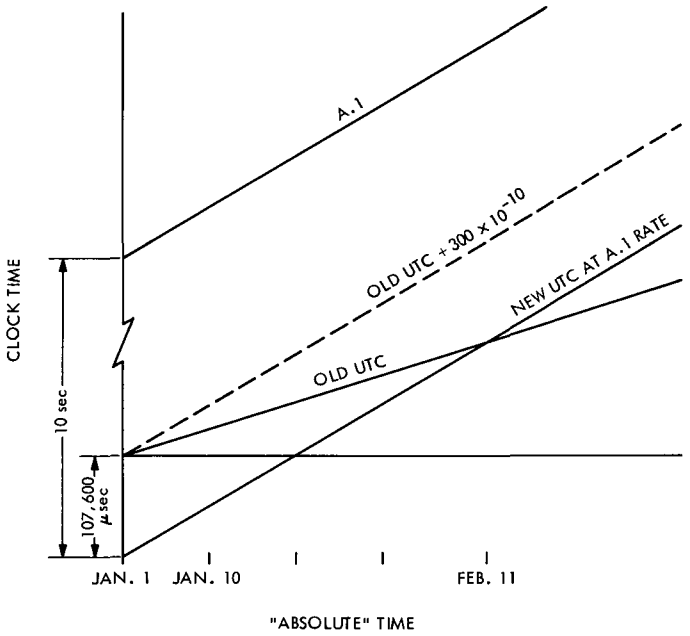

Fig. 1. Old/new UTC comparison

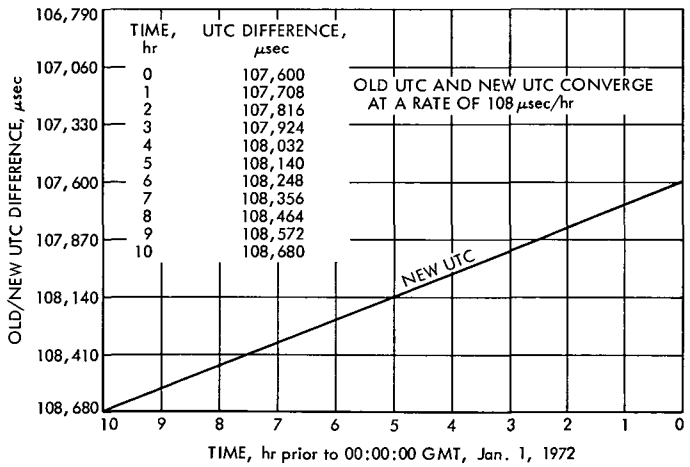

Fig. 2. Difference between old/new UTC with time: 0–10 hr prior to 00:00:00 GMT, Jan. 1, 1972

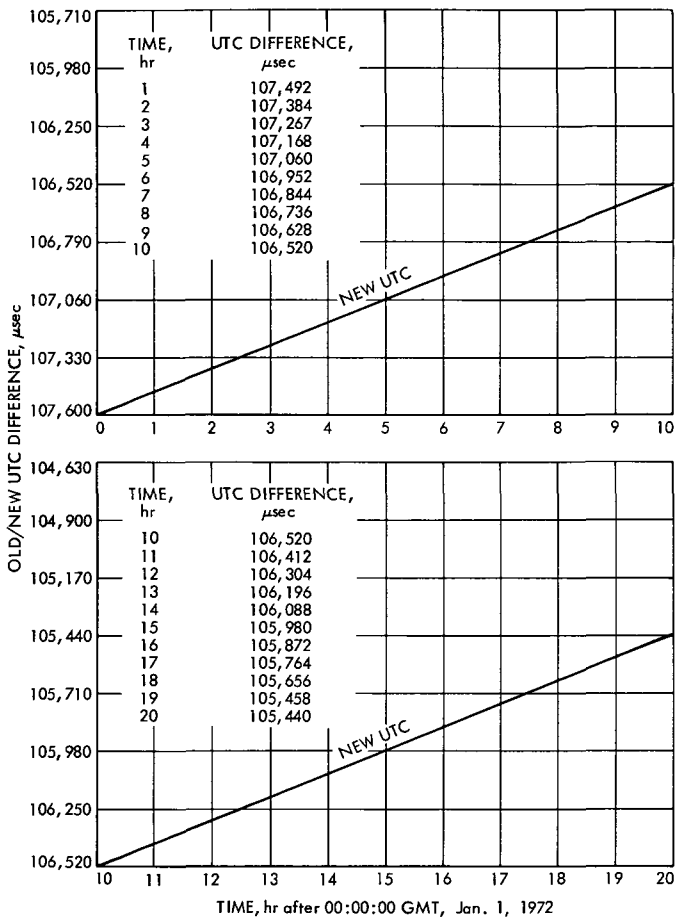

Fig. 3. Difference between old/new UTC with time: 0–20 hr after 00:00:00 GMT, Jan. 1, 1972

Angle Tracking Analysis and Test Development for the Integrated Stations

G. D. Barnes
DSIF Operations Section

An analysis and test development have been completed for the integrated tracking system. An antenna servo model was developed and its transfer function and gain constants are presented. The model was used to simulate the response of the antenna for the autotrack and program modes. These simulation results are compared with the data collected at the Pioneer site and the differences between the two modes are shown. Antenna response data for the integrated servo system are compared with the Echo site response data and DSIF servo specification curves. The servo specification curves are shown to be unrealistic for either the standard or integrated angle tracking systems.

I. Introduction

The integrated site tracking systems (DSSs 11, 42, and 61) have been analyzed and modeled. From the analysis, test software and procedures have been developed. The analysis and test design were done with two goals in mind. First, the test was used to evaluate the equipment just coming into service. Secondly, the same test will serve as a tool for regular maintenance and prepass countdown tests. In order to achieve these goals, several tasks were undertaken.

First, documentation was collected on the Angle Tracking System. This documentation was studied and from this the system was broken down into functional blocks. From these functional blocks, a model was developed, and simulations were conducted. Since the performance specifications for the antenna servo system were either nonexistent or vague, the model was used to establish realistic, definitive performance specifications.

An XDS 910 computer program was developed to monitor the response of the antenna servo system to a step input. This program was essentially a modification of the software that was written for the standard 26-m-diameter antenna sites (Ref. 1). The modified program is different from the original 26-m test program in that it does not command the antenna, and that it receives the antenna position from the high-speed data line instead of directly from the angle encoders. Except for these two differences, the sampling program is the same for both the standard DSIF sites and the integrated sites.

A secondary task was undertaken which complemented the previously mentioned efforts. The test program for the integrated site tracking system can output a paper tape that contains the antenna response to a step input as measured by the angle encoders. A program was written that writes the paper tape on a magnetic tape for processing by the UNIVAC 1108. The processing program has the same processing routines as the test program and also contains routines for plotting the various types of data. In this way angle servo data from the various sites can be processed and compared.

II. Angle Tracking Analysis and Model

A detailed angle tracking model was developed for the integrated sites. The model was developed under the assumption that the response of the angle tracking system was dominated by the servo electronics and inertia and friction of the antenna assembly. A functional block diagram of the servo system is shown in Fig. 1.

The isolation amplifier converts all input voltages to represent 10 volts/degree. This amplifier accepts input from the antenna position programmer or Magic "T" assembly of the antenna as well as manual commands. The isolation amplifier outputs to the position integrator.

The position integrator is a variable filter that determines how high a frequency will be allowed to affect the servo electronics. The frequency filtering is determined by the bandwidth selection switch located on the servo control console. This low-pass filter has as its cutoff frequencies 1.0, 0.5, 0.25, and 0.12 Hz. The position integrator outputs to the rate error junction which inputs to the rate integrator.

The rate integrator is the true integrator of the servo electronics. It is the location of the integrator, following the rate error junction, that makes the integrated servo electronics noticeably different from the standard DSIF servo electronics. The location of the integrator gives the integrated servo electronics more stability since the rate feedback loop will have better control over low-frequency poles. The output of the rate integrator is applied to the antenna through the servo valve, motor, and gear reducers.

The antenna characteristics block represents the most difficult part of the model. It was quickly determined that it would be too difficult to model the mechanical dynamics of the antenna in detail because of the complexity involved. Therefore, the mechanical characteristics model was developed with a pole that is determined by the antenna inertia to antenna friction ratio. A gain constant and zero were added, with the help of a root locus program. When this representation of the antenna dynamics was added to the model, the response then closely matched that of the actual antenna response. Figure 2 shows a detailed block diagram of the servo system and the *Appendix* gives the transfer functions and units of gain that were developed for the simulations.

III. Results From DSS 11

Tests were performed at DSS 11. The data from these tests were compared to the simulated data, data from DSS 12, and DSIF servo specifications. In addition a comparison was made between the servo modes at DSS 11. Figure 3 is a comparison of a DSIF step response servo specification (DOA-1146-DTL) to a standard and integrated station servo step response (DSS 12 and DSS 11, respectively). Table 1 is a comparison of several performance parameters for a standard and integrated station. It can be seen from Fig. 3 and Table 1 that, for approximately equal noise bandwidths, the integrated servo out performs the standard servo in all categories. This superior performance is due mainly to the fact that the integrator was moved inside the rate loop.

Figure 3 shows that although the integrated servo out performs the standard, it does not meet or out perform the DSIF response specification curve, with the exceptions of overshoot and settling time. The DSIF response specification curve represents a system that has much more gain than either the integrated or standard tracking systems have exhibited. Thus, the DSIF servo system response specifications are not realistic, and they should be changed so that station personnel will have realistic specifications to guide them in the operation and maintenance of the antenna servo systems.

The antenna was tested in both the autotrack and program modes. The autotrack uses the antenna's magic "T" and error channels in the receivers to determine the error signal for the servo electronics. Error signals in the program mode are determined through digital hardware in the Antenna Position Programmer (APP). This is accomplished by the APP by reading the angle encoders, subtracting this angle from a commanded angle and applying the difference, through D/A converters, to the servo electronics. It can be seen that there is a noticeable difference between the two modes (see Fig. 4). The simulations show (Figs. 5 and 6) that the autotrack or APP mode can be

simulated by varying the gain of the servo electronics. This apparent difference in system gain is tentatively being attributed to a higher gain of the receiver.

IV. Summary

A model test software and test procedure have been developed for the integrated tracking stations. These are being used as acceptance tests as each of the integrated stations becomes operational. Later, when the stations become operational, the test procedure and program will be used to determine system performance and prepass readiness. In order to help with determination of realistic operating parameters, data will be collected from each of the integrated tracking stations and comparison made between the stations. There are plans to add angle jitter analysis and error coefficient calculations to the test program in the near future.

Reference

1. Rey, R. D., "Angle Tracking Analysis and Test Development," in *The Deep Space Network Progress Report,* Technical Report 32-1526, Vol. VI, pp. 170–187. Jet Propulsion Laboratory, Pasadena, Calif., Dec. 15, 1971.

Table 1. Comparison of servo system step response for the integrated and standard stations[a]

DSS	BW setting, Hz	Gain setting	Overshoot, %	Settling time, s	Rise time, s	Delay time, s	Noise BW, Hz	−3-dB BW, Hz	Gain margin, dB	Phase margin, deg
11	0.12	0	22.35	41.03	9.00	7.68	0.04908	0.03689	−20.67	48.95
12	0.025	5	57.01	108.92	14.88	13.68	0.04175	0.01630	−7.77	35.81

[a]BW settings of 0.12 and 0.025 are equivalent bandwidth settings for these two different systems.

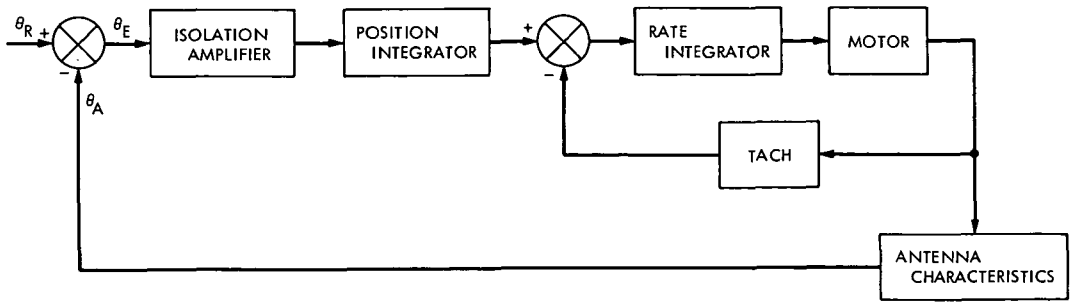

Fig. 1. Functional block diagram of the integrated servo system

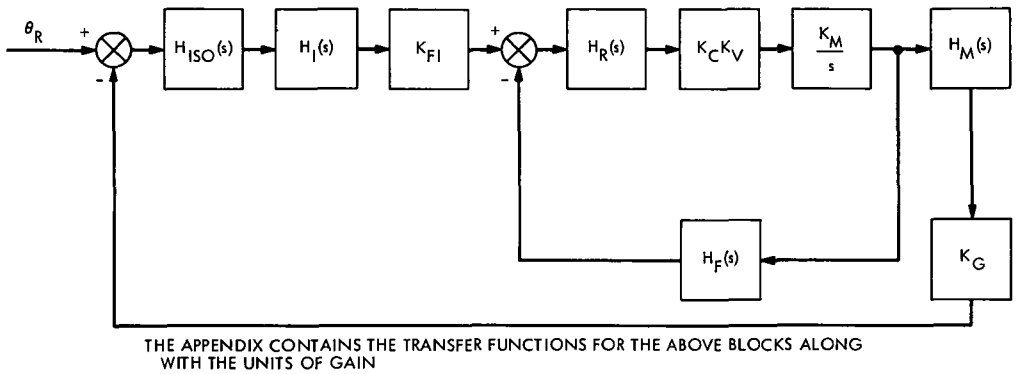

Fig. 2. Detailed block diagram for the integrated station servo system

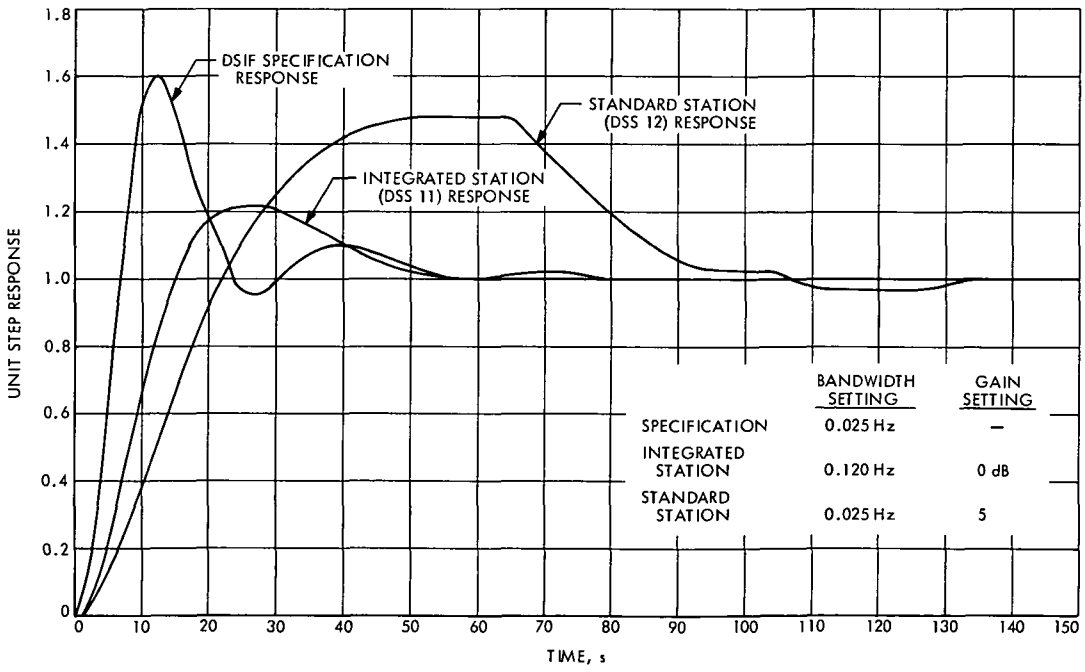

Fig. 3. Comparison of DSIF specification, standard station, and integrated station responses

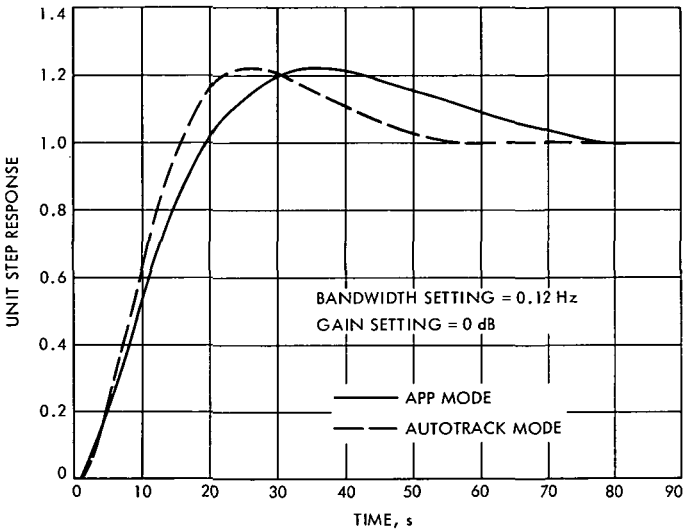

Fig. 4. Comparison of APP and autotrack modes for a step input

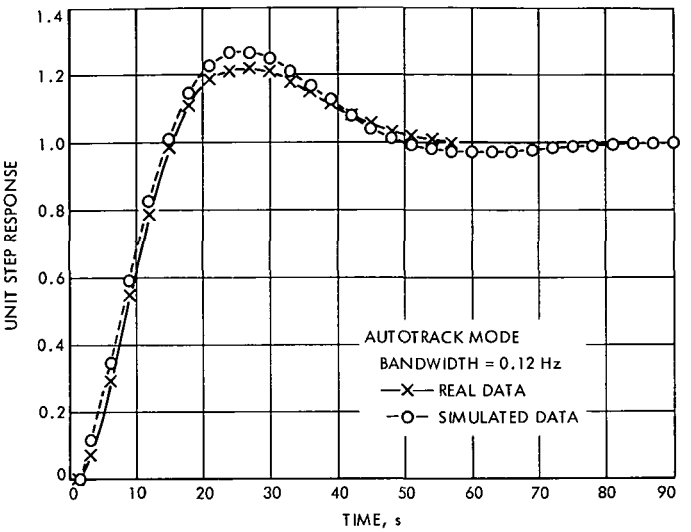

Fig. 5. Comparison of real and simulated data for autotrack mode

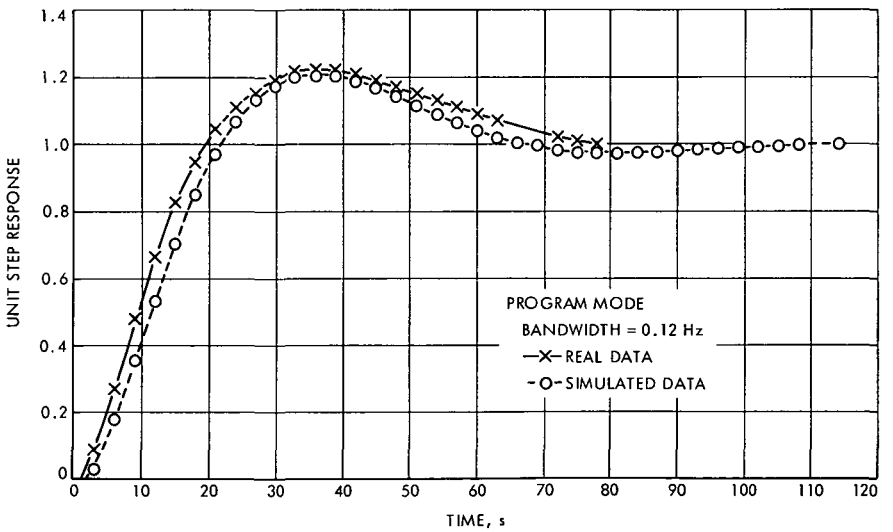

Fig. 6. Comparison of real and simulated data for program mode

Appendix
System Transfer Functions

This appendix contains circuits for the servo electronics, transfer functions for the tracking system, and values for the tracking system components. Figure A-1 is a simplified schematic of the servo electronics. The transfer functions for the servo electronics and antenna are listed below.

A. Isolation Amplifier

$$H_{ISO}(s) = \frac{A_2}{A_1} \cdot \frac{1 + sT_1}{1 + sT_2} K, \qquad \frac{\text{volts}}{\text{volt}}$$

where

$$A_1 = R_{IA8}$$

$$A_2 = \frac{R_{IA1} R_{IA13}}{R_{IA1} + R_{IA13}}$$

$$T_1 = R_{IA8} C_{IA3}$$

$$T_2 = \frac{R_{IA1} R_{IA13}}{R_{IA1} + R_{IA13}} (C_{IA1} + C_{IA2})$$

and K is the value of a voltage divider network which is controlled by the servo gain control (range: 0.5 to 0.95).

B. Position Integrator

The position integrator can be configured four ways, depending upon which bandwidth (BW) setting is selected (see Fig. A-1).

$$H_I(s) = \frac{A_I}{Z_I} \cdot \frac{1 + sT_{I2}}{1 + sT_{I3}}, \qquad \frac{\text{volts}}{\text{volt}}$$

(1) 0.12-Hz bandwidth setting

$$A_I = R_{I17} + R_{I13} + R_{I14}$$

$$Z_I = \frac{R_{I8}}{1 - \dfrac{R_{I7}}{R_{I7} + \dfrac{R_{I8} R_{I9}}{R_{I8} + R_{I9}}}}$$

$$T_{I2} = \frac{C_{I3} R_{I17} (R_{I13} + R_{I14})}{R_{I17} + R_{I13} + R_{I14}}$$

$$T_{I3} = R_{I17} (C_{I1} + C_{I2}) + (R_{I13} + R_{I14}) C_{I3} + (R_{I13} + R_{I14}) (C_{I1} + C_{I2})$$

(2) 0.25-Hz bandwidth setting

$$A_I = \frac{R_{I17}}{2}$$

$$Z_I = \frac{R_{I8}}{1 - \dfrac{R_{I7}}{R_{I7} + \dfrac{R_{I8} R_{I10}}{R_{I8} + R_{I10}}}}$$

$$T_{I2} = (R_{I13} + R_{I14}) C_{I3}$$

$$T_{I3} = \frac{R_{I17}}{2} (C_{I1} + C_{I2})$$

(3) 0.5-Hz bandwidth setting

$$A_I = \frac{R_{I17} R_{I18}}{R_{I17} + R_{I18}}$$

$$Z_I = \frac{R_{I8}}{1 - \dfrac{R_{I7}}{R_{I7} + \dfrac{R_{I8} R_{I11}}{R_{I8} + R_{I11}}}}$$

$$T_{I2} = \frac{R'_{I17} R'_{I13}}{R'_{I17} + R'_{I13}} C_{I3}$$

$$R'_{I17} = \frac{R_{I17} R_{I18}}{R_{I17} + R_{I17}}$$

$$R'_{I13} = R_{I13} + R_{I14}$$

$$T_{I3} = R'_{I17} (C_{I1} + C_{I2}) + R'_{I13} C_{I3} + R'_{I13} (C_{I1} + C_{I2})$$

(4) 1.0-Hz bandwidth setting

$$A_I = \frac{R_{I17} R_{I19}}{R_{I17} + R_{I19}} + R_{I13} + R_{I14}$$

$$Z_I = R_{I7} + R_{I8}$$

$$T_{I2} = \frac{R_{I30} R_{I31}}{R_{I30} + R_{I31}} C_{I3}$$

$$R_{I30} = \frac{R_{I17} R_{I19}}{R_{I17} + R_{I19}}$$

$$R_{I31} = R_{I13} + R_{I14}$$

$$T_{I3} = R_{I30} (C_{I1} + C_{I2}) + R_{I31} C_{I3} + R_{I31} (C_{I1} + C_{I2})$$

C. Rate Integrator

$$H_R(s) = K_R \frac{1}{s}\left(\frac{1 + sT_{R7}}{1 + sT_{R8}}\right), \qquad \frac{\text{volts}}{\text{volt}}$$

where

$$K_R = \frac{1}{B_R}$$

$$B_R = C_{R1} + C_{R3}$$

$$T_{R7} = R_{R19}C_{R1}$$

$$T_{R8} = \frac{C_{R3}C_{R1}}{C_{R1} + C_{R3}} R_{R19}$$

D. Mechanical Effects

This transfer function represents the effects of friction and inertia of the antenna structure.

$$H_M(s) = K_{MA} \frac{(1 + T_{M1}s)}{(1 + T_{M2}s)}, \qquad \frac{\text{degrees}}{\text{degree}}$$

where

T_{M1} = motor back pressure time constant

$$T_{M2} = \frac{\text{inertia of antenna}}{\text{friction of antenna}}$$

K_{MA} = hydraulic gain

E. Rate Feedback

$$H_F(s) = K_F K_T s$$

where

K_T = tachometer gain

$$K_F = \frac{1}{R_{F8} + R_{F15}}$$

F. Constant and Component Values

The values for the constants and components used in the model are listed below.

1. Isolation amplifier

$R_{IA1} = 511\,\text{k}\Omega$

$R_{IA8} = 511\,\text{k}\Omega$

$R_{IA13} = 5.6\,\text{M}\Omega$

$C_{IA1} = 0.068\,\mu\text{F}$

$C_{IA2} = 6800\,\text{pF}$

$C_{IA3} = 0.1\,\mu\text{F}$

2. Position integrator

a. 0.12-Hz bandwidth

$R_{I7} = 10\,\text{k}\Omega$

$R_{I8} = 10\,\text{k}\Omega$

$R_{I9} = 82.5\,\Omega$

$R_{I13} = 10\,\Omega$

$R_{I14} = 10\,\Omega$

$R_{I17} = 3.16\,\text{M}\Omega$

$C_{I1} = 0.01\,\mu\text{F}$

$C_{I2} = 0.1\,\mu\text{F}$

$C_{I3} = 10\,\mu\text{F}$

b. 0.25-Hz bandwidth

$R_{I7} = 10\,\text{k}\Omega$

$R_{I8} = 10\,\text{k}\Omega$

$R_{I10} = 0.348\,\Omega$

$R_{I13} = 10\,\Omega$

$R_{I14} = 10\,\Omega$

$R_{I17} = 3.16\,\text{M}\Omega$

$C_{I1} = 0.01\,\mu\text{F}$

$C_{I2} = 1\,\mu\text{F}$

$C_{I3} = 10\,\mu\text{F}$

c. 0.50-Hz bandwidth

$R_{I7} = 10\,\text{k}\Omega$

$R_{I8} = 10\,\text{k}\Omega$

$R_{I11} = 1620\,\Omega$

$R_{I13} = 10\,\Omega$

$R_{I14} = 10\,\Omega$

$R_{I17} = 3.16\,\text{M}\Omega$

$R_{I18} = 1.10\,\text{M}\Omega$

$C_{I1} = 0.01\,\mu\text{F}$

$C_{I2} = 1\,\mu\text{F}$

$C_{I3} = 10\,\mu\text{F}$

d. 1.0-Hz bandwidth

$$R_{I7} = 10\,\text{k}\Omega$$
$$R_{I8} = 10\,\text{k}\Omega$$
$$R_{I13} = 10\,\Omega$$
$$R_{I14} = 10\,\Omega$$
$$R_{I17} = 3.16\,\text{M}\Omega$$
$$R_{I19} = 464\,\text{k}\Omega$$
$$C_{I1} = 0.01\,\mu\text{F}$$
$$C_{I2} = 0.1\,\mu\text{F}$$
$$C_{I3} = 10\,\mu\text{F}$$

3. Rate integrator

$$R_{R19} = 48.7\,\text{k}\Omega$$
$$C_{R1} = 1\,\mu\text{F}$$
$$C_{R3} = 0.15\,\mu\text{F}$$

4. K_{FI} constant

$$K_{FI} = \frac{1}{R_{FI3} + R_{FI7}}$$

$$R_{FI3} = 28.7\,\text{k}\Omega$$
$$R_{FI7} = 28.7\,\text{k}\Omega$$

5. Mechanical effects

$$T_{M1} = 14 \text{ seconds}$$
$$T_{M2} = 42 \text{ seconds}$$
$$K_{MA} = 1.65 \text{ for APP mode}$$
$$K_{MA} = 2.3 \text{ for autotrack mode}$$

6. Other constants

$$K_C = 6.32 \times 10^{-3} \text{ amperes/volt}$$
$$K_V = 4055.8 \text{ cm}^3\text{/ampere-second}$$
$$K_M = 91.54 \frac{\text{degrees/second}}{\text{cm}^3}$$
$$K_G = 2.43 \times 10^6 \frac{\text{degrees}}{\text{degree}}$$
$$K_T = \frac{3.2 \text{ volts}}{1000 \text{ rpm}}$$

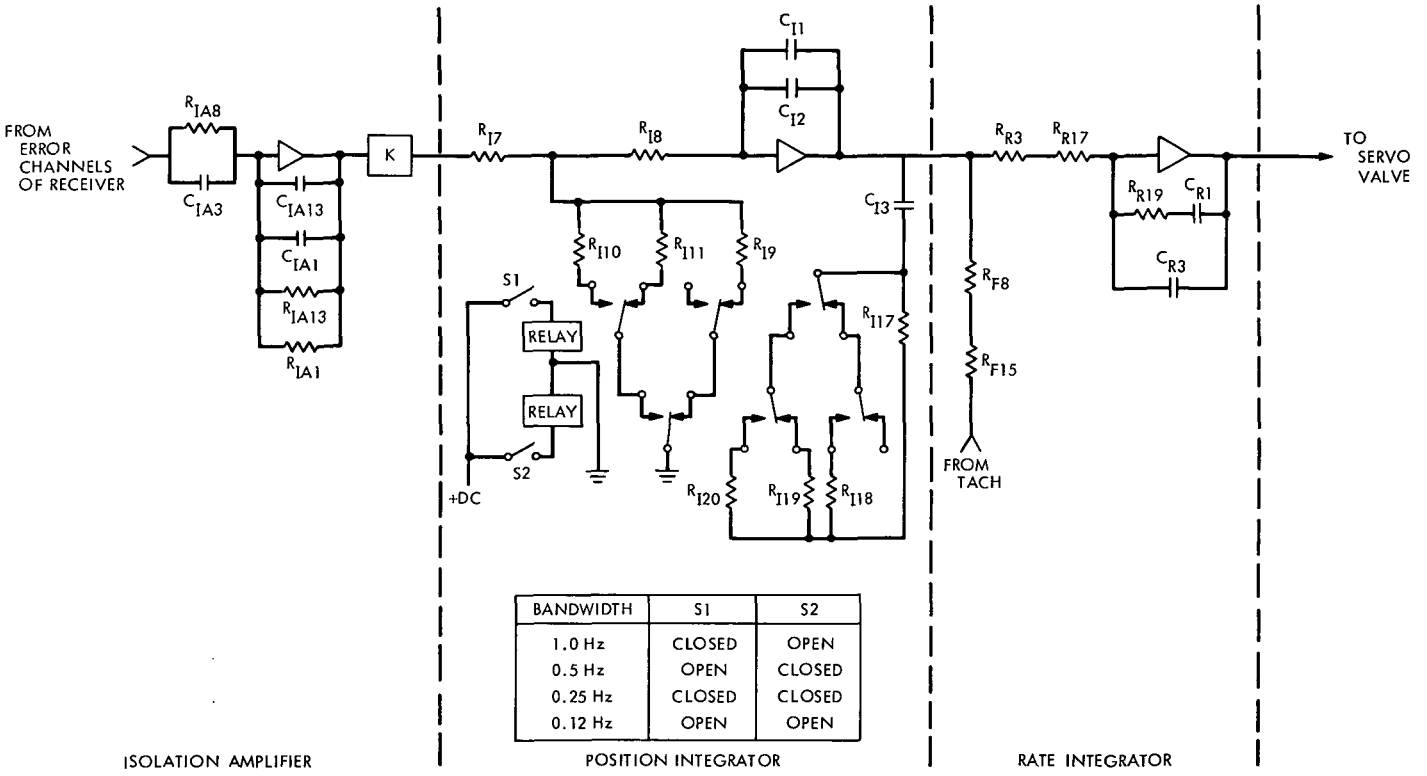

BANDWIDTH	S1	S2
1.0 Hz	CLOSED	OPEN
0.5 Hz	OPEN	CLOSED
0.25 Hz	CLOSED	CLOSED
0.12 Hz	OPEN	OPEN

Fig. A-1. Simplified schematic for the integrated servo electronics

Bibliography

Anderson, J. D., *Determination of the Masses of the Moon and Venus and the Astronomical Unit from Radio Tracking Data of the Mariner II Spacecraft.* Technical Report 32-816. Jet Propulsion Laboratory, Pasadena, Calif., July 1, 1967.

Anderson, J. D., et al., "The Radius of Venus as Determined by Planetary Radar and Mariner V Radio Tracking Data," *J. Atmos. Sci.*, pp. 1171–1174, Sept. 25, 1968.

Berman, A. L., *Tracking System Data Analysis Report, Ranger VII Final Report,* Technical Report 32-719, Jet Propulsion Laboratory, Pasadena, Calif., June 1, 1965.

Berman, A. L., *ABTRAJ—On-Site Tracking Prediction Program for Planetary Spacecraft,* Technical Memorandum 33-391. Jet Propulsion Laboratory, Pasadena, Calif., Aug. 15, 1968.

Cain, D. L., and Hamilton, T. W., *Determination of Tracking Station Locations by Doppler and Range Measurements to an Earth Satellite,* Technical Report 32-534. Jet Propulsion Laboratory, Pasadena, Calif., Feb. 1, 1964.

Carey, C. N., and Sjogren, W. L., "Gravitational Inconsistency, in the Lunar Theory: Confirmation by Radio Tracking," *Science,* Vol. 160, pp. 875, 876, Apr.–June 1968.

Curkendall, D. W., and Stephenson, R. R., "Earthbased Tracking and Orbit Determination—Backbone of the Planetary Navigation System," *Astronaut. Aeronaut.*, Vol. 7, May 1970.

Curkendall, D. W., "Planetary Navigation: The New Challenges," *Astronaut. Aeronaut.*, Vol. 7, May 1970.

Efron, L., and Solloway, C. B., *Proceedings of the Conference on Scientific Applications of Radio and Radar Tracking in the Space Program,* Technical Report 32-1475. Jet Propulsion Laboratory, Pasadena, Calif., July 1970.

Flanagan, F. M., et al., *Deep Space Network Support of the Manned Space Flight Network for Apollo: 1962–1968,* Technical Memorandum 33-452, Vol. I. Jet Propulsion Laboratory, Pasadena, Calif., July 1970.

Flanagan, F. M., et al., *Deep Space Network Support of the Manned Space Flight Network for Apollo: 1969–1970,* Technical Memorandum 33-452, Vol. II. Jet Propulsion Laboratory, Pasadena, Calif., May 1, 1971.

Fjeldbo, G., and Eshleman, V. R., "Radio Occultation Measurements and Interpretations," in *The Atmospheres of Venus and Mars,* p. 225. Gordon and Breach, Science Publishers, Inc., New York, N. Y.

Goldstein, R. M., "Radar Time-of-Flight Measurements to Venus," *Astron. J.*, Vol. 73, No. 9, Aug. 1968.

Goldstein, R. M., and Rumsey, H., Jr., "A Radar Snapshot of Venus," *Science,* Vol. 169, Sept. 1970.

Gordon, H. J., et al., *The Mariner 6 and 7 Flight Paths and Their Determination From Tracking Data,* Technical Memorandum 33-469. Jet Propulsion Laboratory, Pasadena, Calif., Dec. 1, 1970.

Bibliography (contd)

Hamilton, T. W., et al., *The Ranger IV Flight Path and Its Determination From Tracking Data,* Technical Report 32-345. Jet Propulsion Laboratory, Pasadena, Calif., Sept. 15, 1962.

Kellermann, K. I., et al., "High Resolution Observations of Compact Radio Sources at 13 Centimeters," *Astrophys. J.,* Vol. 161, pp. 803–809, Sept. 1970.

Kliore, A., "Radio Occultation Measurements of the Atmospheres of Mars and Venus," in *The Atmospheres of Venus and Mars,* p. 205. Gordon and Breach Science Publishers, Inc., New York, N. Y.

Labrum, R. G., Wong, S. K., and Reynolds, G. W., *The Surveyor V, VI, and VII Flight Paths and Their Determination from Tracking Data,* Technical Report 32-1302. Jet Propulsion Laboratory, Pasadena, Calif., Dec. 1, 1968.

Lieske, J. H., and Null, G. W., "Icarus and the Determination of Astronomical Constants," *Astron. J.,* Vol. 74, No. 2, Mar. 1969.

Lorell, J., and Sjogren, W. L., *Lunar Orbiter Data Analysis,* Technical Report 32-1220. Jet Propulsion Laboratory, Pasadena, Calif., Nov. 15, 1967.

Lorell, J., *Lunar Orbiter Gravity Analysis,* Technical Report 32-1387. Jet Propulsion Laboratory, Pasadena, Calif., June 15, 1969.

Lorell, J., et al., "Celestial Mechanics Experiment for *Mariner,*" *Icarus,* Vol. 12, Jan. 1970.

McNeal, C. E., *Ranger V Tracking Systems Data Analysis Final Report,* Technical Report 32-702. Jet Propulsion Laboratory, Pasadena, Calif., Apr. 15, 1965.

Melbourne, W. G., et al., *Constants and Related Information for Astrodynamical Calculations,* Technical Report 32-1306. Jet Propulsion Laboratory, Pasadena, Calif., July 15, 1968.

Melbourne, W. G., "Planetary Ephemerides," *Astronaut. Aeronaut.,* Vol. 7, May 1970.

Miller, L., et al., *The Atlas–Centaur VI Flight Path and Its Determination from Tracking Data,* Technical Report 32-911. Jet Propulsion Laboratory, Pasadena, Calif., Apr. 15, 1966.

Mulhall, B. D., et al., *Tracking System Analytic Calibration Activities for the Mariner Mars 1969 Mission,* Technical Report 32-1499. Jet Propulsion Laboratory, Pasadena, Calif., Nov. 15, 1970.

Mulholland, J. D., and Sjogren, W. L., *Lunar Orbiter Ranging Data,* Technical Report 32-1087. Jet Propulsion Laboratory, Pasadena, Calif., Jan. 6, 1967.

Mulholland, J. D., *Proceedings of the Symposium on Observation, Analysis, and Space Research Applications of the Lunar Motion,* Technical Report 32-1386. Jet Propulsion Laboratory, Pasadena, Calif., Apr. 1969.

Muller, P. M., and Sjogren, W. L., *Consistency of Lunar Orbiter Residuals With Trajectory and Local Gravity Effects,* Technical Report 32-1307. Jet Propulsion Laboratory, Pasadena, Calif., Sept. 1, 1968.

Muller, P. M., and Sjogren, W. L., *Lunar Mass Concentrations,* Technical Report 32-1339. Jet Propulsion Laboratory, Pasadena, Calif., Aug. 16, 1968.

Bibliography (contd)

Null, G. W., Gordon, H. J., and Tito, D. A., *Mariner IV Flight Path and its Determination From Tracking Data,* Technical Report 32-1108. Jet Propulsion Laboratory, Pasadena, Calif., Aug. 1, 1967.

O'Neil, W. J., et al., *The Surveyor III and Surveyor IV Flight Paths and Their Determination From Tracking Data,* Technical Report 32-1292. Jet Propulsion Laboratory, Pasadena, Calif., Aug. 15, 1968.

Pease, G. E., et al., *The Mariner V Flight Path and Its Determination From Tracking Data,* Technical Report 32-1363. Jet Propulsion Laboratory, Pasadena, Calif., July 1, 1969.

Renzetti, N. A., *Tracking and Data Acquisition for Ranger Missions I–V,* Technical Memorandum 33-174. Jet Propulsion Laboratory, Pasadena, Calif., July 1, 1964.

Renzetti, N. A., *Tracking and Data Acquisition for Ranger Missions VI–IX,* Technical Memorandum 33-275. Jet Propulsion Laboratory, Pasadena, Calif., Sept. 15, 1966.

Renzetti, N. A., *Tracking and Data Acquisition Support for the Mariner Venus 1962 Mission,* Technical Memorandum 33-212. Jet Propulsion Laboratory, Pasadena, Calif., July 1, 1965.

Renzetti, N. A., *Tracking and Data Acquisition Report, Mariner Mars 1964 Mission: Near-Earth Trajectory Phase,* Technical Memorandum 33-239, Vol. I. Jet Propulsion Laboratory, Pasadena, Calif., Jan. 1, 1965.

Renzetti, N. A., *Tracking and Data Acquisition Report, Mariner Mars 1964 Mission: Cruise to Post-Encounter Phase,* Technical Memorandum 33-239, Vol. II. Jet Propulsion Laboratory, Pasadena, Calif., Oct. 1, 1967.

Renzetti, N. A., *Tracking and Data Acquisition Report, Mariner Mars 1964 Mission: Extended Mission,* Technical Memorandum 33-239, Vol. III. Jet Propulsion Laboratory, Pasadena, Calif., Dec. 1, 1968.

Renzetti, N. A., *Tracking and Data System Support for Surveyor: Missions I and II,* Technical Memorandum 33-301, Vol. I. Jet Propulsion Laboratory, Pasadena, Calif., July 15, 1969.

Renzetti, N. A., *Tracking and Data System Support for Surveyor: Missions III and IV,* Technical Memorandum 33-301, Vol. II. Jet Propulsion Laboratory, Pasadena, Calif., Sept. 1, 1969.

Renzetti, N. A., *Tracking and Data System Support for Surveyor: Mission V,* Technical Memorandum 33-301, Vol. III. Jet Propulsion Laboratory, Pasadena, Calif., Dec. 1, 1969.

Renzetti, N. A., *Tracking and Data System Support for Surveyor: Mission VI,* Technical Memorandum 33-301, Vol. IV. Jet Propulsion Laboratory, Pasadena, Calif., Dec. 1, 1969.

Renzetti, N. A., *Tracking and Data System Support for Surveyor: Mission VII,* Technical Memorandum 33-301, Vol. V. Jet Propulsion Laboratory, Pasadena, Calif., Dec. 1, 1969.

Bibliography (contd)

Renzetti, N. A., *Tracking and Data System Support for the Mariner Venus 67 Mission: Planning Phase Through Midcourse Maneuver,* Technical Memorandum 33-385, Vol. I. Jet Propulsion Laboratory, Pasadena, Calif., Sept. 1, 1969.

Renzetti, N. A., *Tracking and Data System Support for the Mariner Venus 67 Mission: Midcourse Maneuver Through End of Mission,* Technical Memorandum 33-385, Vol. II. Jet Propulsion Laboratory, Pasadena, Calif., Sept. 1, 1969.

Renzetti, N. A., *Tracking and Data System Support for the Pioneer Project. Pioneer VI. Prelaunch to End of Nominal Mission,* Technical Memorandum 33-426, Vol. I. Jet Propulsion Laboratory, Pasadena, Calif., Feb. 1, 1970.

Renzetti, N. A., *Tracking and Data System Support for the Pioneer Project. Pioneer VII. Prelaunch to End of Nominal Mission,* Technical Memorandum 33-426, Vol. II. Jet Propulsion Laboratory, Pasadena, Calif., Apr. 15, 1970.

Renzetti, N. A., *Tracking and Data System Support for the Pioneer Project. Pioneer VIII. Prelaunch Through May 1968,* Technical Memorandum 33-426, Vol. III. Jet Propulsion Laboratory, Pasadena, Calif., July 15, 1970.

Renzetti, N. A., *Tracking and Data System Support for the Pioneer Project. Pioneer IX. Prelaunch Through June 1969,* Technical Memorandum 33-426, Vol. IV. Jet Propulsion Laboratory, Pasadena, Calif., Nov. 15, 1970.

Renzetti, N. A., *Tracking and Data System Support for the Pioneer Project. Pioneer VI. Extended Mission: July 1, 1966–July 1, 1969,* Technical Memorandum 33-426, Vol. V. Jet Propulsion Laboratory, Pasadena, Calif., Feb. 1, 1971.

Renzetti, N. A., *Tracking and Data System Support for the Pioneer Project. Pioneer VII. Extended Mission: February 24, 1967–July 1, 1968,* Technical Memorandum 33-426, Vol. VI. Jet Propulsion Laboratory, Pasadena, Calif., Apr. 15, 1971.

Renzetti, N. A., *Tracking and Data System Support for the Pioneer Project. Pioneer VII. Extended Mission: July 1, 1968–July 1, 1969,* Technical Memorandum 33-426, Vol. VII. Jet Propulsion Laboratory, Pasadena, Calif., Apr. 15, 1971.

Renzetti, N. A., *Tracking and Data System Support for the Pioneer Project. Pioneer VIII. Extended Mission: June 1, 1968–July 1, 1969,* Technical Memorandum 33-426, Vol. VIII. Jet Propulsion Laboratory, Pasadena, Calif., May 1, 1971.

Renzetti, N. A., *Tracking and Data System Support for the Pioneer Project. Pioneers VI–IX. Extended Missions: July 1, 1969–July 1, 1970,* Technical Memorandum 33-426, Vol. IX. Jet Propulsion Laboratory, Pasadena, Calif., Aug. 15, 1971.

Sjogren, W. L., *The Ranger III Flight Path and Its Determination From Tracking Data,* Technical Report 32-563. Jet Propulsion Laboratory, Pasadena, Calif., Sept. 15, 1965.

Sjogren, W. L., et al., *The Ranger V Flight Path and Its Determination From Tracking Data,* Technical Report 32-562. Jet Propulsion Laboratory, Pasadena, Calif., Dec. 6, 1963.

Sjogren, W. L., et al., *The Ranger VI Flight Path and Its Determination From Tracking Data,* Technical Report 32-605. Jet Propulsion Laboratory, Pasadena, Calif., Dec. 15, 1964.

Bibliography (contd)

Sjogren, W. L., et al., *Physical Constants as Determined From Radio Tracking of the Ranger Lunar Probes*, Technical Report 32-1057. Jet Propulsion Laboratory, Pasadena, Calif., Dec. 30, 1966.

Sjogren, W. L., *Proceedings of the JPL Seminar on Uncertainties in the Lunar Ephemeris*, Technical Report 32-1247. Jet Propulsion Laboratory, Pasadena, Calif., May 1, 1968.

Sjogren, W. L., "Lunar Gravity Estimate: Independent Confirmation," *J. Geophys. Res.*, Vol. 76, No. 29, Oct. 10, 1971.

Stelzried, C. T., *A Faraday Rotation Measurement of a 13-cm Signal in the Solar Corona*, Technical Report 32-1401. Jet Propulsion Laboratory, Pasadena, Calif., July 15, 1970.

Stelzried, C. T., et al., "The Quasi-Stationary Coronal Magnetic Field and Electron Density as Determined From a Faraday Rotation Experiment," *Sol. Phys.*, Vol. 14, No. 2, pp. 440–456, Oct. 1970.

Thornton, J. H., Jr., *The Surveyor I and Surveyor II Flight Paths and Their Determination From Tracking Data*, Technical Report 32-1285. Jet Propulsion Laboratory, Pasadena, Calif., Aug. 1, 1968.

Vegos, C. J., et al., *The Ranger IX Flight Path and Its Determination From Tracking Data*, Technical Report 32-767. Jet Propulsion Laboratory, Pasadena, Calif., Nov. 1, 1968.

Winn, F. B., *Selenographic Location of Surveyor VI, Surveyor VI Mission Report: Part II. Science Results*, Technical Report 32-1262. Jet Propulsion Laboratory, Pasadena, Calif., Jan. 10, 1968.

Winn, F. B., "Post Landing Tracking Data Analysis," in *Surveyor VII Mission Report: Part II. Science Results*, Technical Report 32-1264. Jet Propulsion Laboratory, Pasadena, Calif., Mar. 15, 1968.

Winn, F. B., "Post Lunar Touchdown Tracking Data Analysis," in *Surveyor Project Final Report: Part II. Science Results*, Technical Report 32-1265. Jet Propulsion Laboratory, Pasadena, Calif., June 15, 1968.

Winn, F. B., *Surveyor Posttouchdown Analyses of Tracking Data*, NASA SP-184. National Aeronautics and Space Administration, Washington, D.C., p. 369.

Wollenhaupt, W. R., et al., *The Ranger VII Flight Path and Its Determination From Tracking Data*, Technical Report 32-694. Jet Propulsion Laboratory, Pasadena, Calif., Dec. 15, 1964.

NASA — JPL — Coml., L.A., Calif.

24998

TECHNICAL REPORT STANDARD TITLE PAGE

1. Report No. 32-1526, Vol. VIII	2. Government Accession No. N72-22313	3. Recipient's Catalog No.
4. Title and Subtitle THE DEEP SPACE NETWORK PROGRESS REPORT FOR JANUARY AND FEBRUARY 1972		5. Report Date April 15, 1972 6. Performing Organization Code
7. Author(s) JPL Staff		8. Performing Organization Report No.
9. Performing Organization Name and Address JET PROPULSION LABORATORY California Institute of Technology 4800 Oak Grove Drive Pasadena, California 91103		10. Work Unit No. 11. Contract or Grant No. NAS 7-100 13. Type of Report and Period Covered Technical Report
12. Sponsoring Agency Name and Address NATIONAL AERONAUTICS AND SPACE ADMINISTRATION Washington, D.C. 20546		14. Sponsoring Agency Code

15. Supplementary Notes

16. Abstract

This report describes work performed for the JPL/NASA Deep Space Network (DSN). Progress is presented on DSN supporting research and technology, advanced development and engineering, and implementation, and DSN operations which pertain to mission-independent or multiple-mission development as well as to support of flight projects. Each issue contains a description of the functions and facilities of the DSN.

17. Key Words (Selected by Author(s))	18. Distribution Statement
Antennas and Transmission Lines Information Theory Telemetry and Command Tracking	Unclassified -- Unlimited

19. Security Classif. (of this report)	20. Security Classif. (of this page)	21. No. of Pages	22. Price
Unclassified	Unclassified	145	

HOW TO FILL OUT THE TECHNICAL REPORT STANDARD TITLE PAGE

Make items 1, 4, 5, 9, 12, and 13 agree with the corresponding information on the report cover. Use all capital letters for title (item 4). Leave items 2, 6, and 14 blank. Complete the remaining items as follows:

3. Recipient's Catalog No. Reserved for use by report recipients.

7. Author(s). Include corresponding information from the report cover. In addition, list the affiliation of an author if it differs from that of the performing organization.

8. Performing Organization Report No. Insert if performing organization wishes to assign this number.

10. Work Unit No. Use the agency-wide code (for example, 923-50-10-06-72), which uniquely identifies the work unit under which the work was authorized. Non-NASA performing organizations will leave this blank.

11. Insert the number of the contract or grant under which the report was prepared.

15. Supplementary Notes. Enter information not included elsewhere but useful, such as: Prepared in cooperation with... Translation of (or by)... Presented at conference of... To be published in...

16. Abstract. Include a brief (not to exceed 200 words) factual summary of the most significant information contained in the report. If possible, the abstract of a classified report should be unclassified. If the report contains a significant bibliography or literature survey, mention it here.

17. Key Words. Insert terms or short phrases selected by the author that identify the principal subjects covered in the report, and that are sufficiently specific and precise to be used for cataloging.

18. Distribution Statement. Enter one of the authorized statements used to denote releasability to the public or a limitation on dissemination for reasons other than security of defense information. Authorized statements are "Unclassified—Unlimited," "U. S. Government and Contractors only," "U. S. Government Agencies only," and "NASA and NASA Contractors only."

19. Security Classification (of report). NOTE: Reports carrying a security classification will require additional markings giving security and downgrading information as specified by the Security Requirements Checklist and the DoD Industrial Security Manual (DoD 5220.22-M).

20. Security Classification (of this page). NOTE: Because this page may be used in preparing announcements, bibliographies, and data banks, it should be unclassified if possible. If a classification is required, indicate separately the classification of the title and the abstract by following these items with either "(U)" for unclassified, or "(C)" or "(S)" as applicable for classified items.

21. No. of Pages. Insert the number of pages.

22. Price. Insert the price set by the Clearinghouse for Federal Scientific and Technical Information or the Government Printing Office, if known.